Vilniaus
universitetas

Aliona

Nicolenco

ELECTRODEPOSITION OF Fe-W
ALLOYS FROM ENVIRONMENTALLY-
FRIENDLY BATH AND THEIR
CHARACTERIZATION

DOCTORAL DISSERTATION

Physical sciences,
Chemistry **03P**

2018

Aliona Nicolenco | Electrodeposition of Fe-W alloys from environmentally-friendly bath and their characterization

Aliona
NICOLENCO

Electrodeposition of Fe-W alloys from environmentally-friendly bath and their characterization

DOCTORAL DISSERTATION

Physical sciences,
Chemistry (03P)

VILNIUS 2018

Scientific supervisor:
Prof., dr. Henrikas Cesiulis (Vilnius University, Physical Sciences, chemistry -03P);
Scientific consultant:
Assoc. prof., dr. Natalia Tsyntsaru (Vilnius University, Institute of Applied Physics, Physical Sciences, chemistry -03P);

Evaluation Board:
Chairman – **prof. habil. dr. Aivaras Kareiva** (Vilnius University, Physical Sciences, chemistry -03P)
Members:
dr. Eva García-Lecina (Research Institute CIDETEC, Spain, Physical Sciences, chemistry -03P);
dr. Arūnas Jagminas (Center for Physical Science and Technology, Physical Sciences, chemistry -03P).
dr. **Ieva Plikusienė** (Vilnius University, Physical Sciences, chemistry -03P);
doc. dr. Audrius Žunda (Aleksandras Stulginskis University, Mechanical Engineering – 09T);

The doctoral dissertation defense will be held on 8th of October 2018 at 2 p.m. at the public meeting of the Evaluation Board at the Kazio Daukšos auditorium (223) of the Faculty of Chemistry and Geosciences of Vilnius University. Address: Naugarduko g. 24, LT-03225, Vilnius, Lithuania, Tel.: 2193108; e-mail: aliona.nicolenco@chgf.vu.lt

The dissertation is available at the Library of Vilnius University and at the Library of FTMC, and on the Internet: *https://www.vu.lt/naujienos/ivykiu-kalendorius*

Aliona
NICOLENCO

Fe-W lydinių elektronusodinimas iš aplinkai draugiško elektrolito ir jų apibūdinimas

DAKTARO DISERTACIJA

Fiziniai mokslai,
chemija (03 P)

VILNIUS 2018

Disertacija buvo rengiama 2015 – 2018 metais Vilniaus universiteto Chemijos ir Geomokslų fakultete. Dalis eksperimentų atlikta bendradarbiaujant su Autonominiu Barselonos universitetu (Barselona, Ispanija), Kieto kūno ir medžiagų tyrimo Leibnico institutu (Drezdenas, Vokietija), CIDETEC tyrimų institutu (San Sebastianas, Ispanija), Chalmerso technologijos universitetau (Švedija) bei Fizinių mokslų ir technologijų centru (FMTC, Lietuva).

Mokslinis vadovas:
prof. dr. Henrikas Cesiulis (Vilniaus universitetas, fiziniai mokslai, chemija -03P);
Mokslinis konsultantas:
assoc. prof. dr. Natalia Tsyntsaru (Viliaus universitetas, IFA Taikomosios fizikos institutas, fiziniai mokslai, chemija -03P);

Disertacijos gynimo taryba:
Pirmininkas – **prof. habil. dr. Aivaras Kareiva** (Vilnius universitetas, fiziniai mokslai, chemija – 03P)

Nariai:
dr. Eva García-Lecina (Elektrocheminių technologijų centras CIDETEC, Ispanija, fiziniai mokslai, chemija – 03P)
dr. Arūnas Jagminas (Fizinių ir technologijos mokslų centras, fiziniai mokslai, chemija – 03P)
dr. Ieva Plikusienė (Vilnius universitetas, fiziniai mokslai, chemija – 03P)
doc. Audrius Žunda (Aleksandro Stulginskio Universitetas, mechanikos inžinerija – 09T)

Disertacija ginama viešame Gynimo tarybos posėdyje 2018 m. spalio mėn. 8 d. 14:00 val. Vilnius Universiteto Chemijos ir Geomokslų fakulteto Kazio Daukšos auditorijoje (223). Adresas: Naugarduko g.24, LT-03225, Vilnius, Lietuva, Tel.: 2193108; el. paštas aliona.nicolenco@chgf.vu.lt

Disertaciją galima peržiūrėti Vilniaus universiteto ir FTMC Chemijos instituto bibliotekose ir VU interneto svetainėje adresu:
https://www.vu.lt/naujienos/ivykiu-kalendorius

ABSTRACT

Interest in W alloys with Fe-group metals (Fe, Co, Ni) has grown continuously in recent decades because of functional properties of such alloys. These coatings exhibit a unique combination of mechanical, magnetic, and corrosion-resistance properties even at elevated temperatures. Electrochemical studies have concentrated more on Ni and Co alloys in the past, while investigation into Fe-W alloys is rather scarce. However, presently, the use of both Ni and Co is being discouraged due to environmental and health issues. Therefore, the development of new procedures for electrodeposition of Fe-based alloys as alternatives to Co and Ni ones is of particular concern. The research presented here focuses on the design of a new environmentally friendly Fe-W plating bath and the establishment of the interrelationships between the internal composition and structure of the electrodeposited alloys. Furthermore, perspectives on the sustainable application of these coatings are discussed.

In this study, particular attention is given to the development of a new glycolate-citrate Fe-W plating bath with enhanced current efficiency, based on Fe(III)-salt. The electrodeposition of Fe-W alloys is more often carried out using Fe(II)-based baths due to the higher solubility of Fe^{2+} compounds. However, the rapid oxidation of Fe^{2+} to Fe^{3+} reduces the bath lifetime and the reproducibility of the results because the electrolyte composition is changing within a short period. In addition, the electrodeposition of Fe-W alloys occurs at higher cathodic polarization than is the case with Co and Ni-W alloys, which results in a low current efficiency of the process. Several studies have aimed to synthesize Fe-W deposits from citrate-ammonia, citrate-borate, or nitrilotriacetate Fe(III)-based electrolytes. Nevertheless, the low current efficiency of the deposition remains an important issue.

The simulation of complexes distribution has been used in order to grow better understanding of the Fe-W bath chemistry and estimate the stability of the newly developed glycolate-citrate Fe(III)-based electrolyte. The bath allows Fe-W alloy coatings to be obtained with various W content, which ranges from a few percent to a maximum 25 at.% of W by changing the deposition conditions (current density, pH, temperature, and the concentration of components in electrolyte). The cathodic current efficiency increases up to 60–70 %, which is higher than that of any other previously reported Fe-W plating bath. According to Glow Discharge Optical Emission Spectroscopy analysis, the distribution of Fe and W is uniform along the coating thickness; however, a layer of oxygen-containing compounds is formed on top of the coatings.

It is commonly known that composition and structure are the key parameters determining the properties of designed materials. Therefore, in order to assess the functional properties of Fe-W alloys, samples with various tungsten contents were electrodeposited in a controlled environment. The structural changes that resulted from increasing the W content were investigated by X-ray diffraction and Mössbauer spectroscopy analyses. X-ray diffraction demonstrated that the structure of Fe-W coatings transforms from nanocrystalline to "amorphous-like" when the content of W increases from 10 at.% to 18 at.%. Moreover, due to different mobility of Fe and W atoms at 20 °C and 65 °C the structural transformations also depend on the deposition temperature, which affects the activation energy of alloy crystallization. As the W content exceeds the solubility limit in Fe at approximately 14 at.% W, the structural transition from a mixture of Fe(W) solid solution and α-Fe (nanocrystalline coatings) to a mixture of Fe_2W intermetallic phase and W(Fe) solid solution ("amorphous-like" coatings) occurs, as proven by Mössbauer spectroscopy.

These structural changes influence the magnetic and mechanical properties of Fe-W alloys. Accordingly, increasing the W content leads to a reduction of the saturation magnetization due to phase transformation; although, both nanocrystalline and "amorphous-like" Fe-W alloys exhibit a soft magnetic behavior. Furthermore, this study demonstrates that "amorphous-like" coatings containing >18% W have a rather high hardness of approximately 10 GPa (comparable to electrodeposited Co-W alloys and chromium), which is governed by direct Hall–Petch relation, that is, smaller crystallite size creates a higher volume of grain boundaries able to impede the dislocation motion, thus resulting in higher hardness values. The combination of high saturation magnetization and enhanced hardness of Fe-W alloys is suitable, for example, for high-density recording media.

Nevertheless, in some engineering applications, high hardness should be coupled with satisfactory wear and corrosion resistance, which are the major drawbacks of Fe-W alloys. To overcome these issues, Fe-W/Al_2O_3 composites were electrodeposited from the same glycolate-citrate electrolyte by adding sub-micron alumina particles. The new composite coatings have shown a superior wear resistance compared to Fe-W alloy matrix. However, the corrosion resistance of Fe-W based materials remains unenhanced due to the preferential Fe dissolution.

LIST OF ORIGINAL PAPERS

The present doctoral thesis is based on the following papers, which are referred to in the text by their Latin numerals 1-5:

Paper 1:   **A. Nicolenco**, N. Tsyntsaru, H. Cesiulis
Fe (III)-based ammonia-free bath for electrodeposition of Fe-W alloys
Journal of The Electrochemical Society 164 (2017) D590-D597

Paper 2:   **A. Nicolenco,** N. Tsyntsaru, J. Fornell, E. Pellicer, J. Reklaitis, D. Baltrunas, H. Cesiulis, J. Sort
Mapping of mechanical and magnetic properties of Fe-W alloys electrodeposited from Fe(III)-based glycolate-citrate bath
Materials and Design 139 (2018) 429–438

Paper 3:   A. Mulone, **A. Nicolenco**, V. Hoffmann, U. Klement, N. Tsyntsaru, H. Cesiulis
In-depth characterization of as-deposited and annealed Fe-W coatings electrodeposited from glycolate-citrate plating bath
Electrochimica Acta 26 (2018) 167-177

Paper 4:   A. Mulone, **A. Nicolenco**, J. Fornell, E. Pellicer, N. Tsyntsaru, H. Cesiulis, J. Sort, U. Klement
Enhanced mechanical properties and microstructural modifications in electrodeposited Fe-W alloys through designed heat treatments
Surface and Coatings Technology 350 (2018) 20–30

Paper 5:   **A. Nicolenco,** N. Tsyntsaru, T. Matijošius, S. Asadauskas, H. Cesiulis
Wear resistance of electrodeposited Fe-W alloy coatings under dry conditions and in the presence of rapeseed oil
Green Tribology 1 (2018) 17-23

AUTHOR'S CONTRIBUTIONS TO THE ORIGINAL PAPERS

Paper 1: I planned and conducted all the theoretical and experimental work, that is, the simulation of complexes distribution and thermodynamic stability lines, bath formulation, electrodeposition of coatings, SEM and XRD characterization, calculation of deposition rate, current efficiency, and partial currents distribution. The theoretical and experimental results were discussed with the co-authors.

Paper 2: I planned and conducted the major part of the experimental work, which comprised the deposition of Fe-W coatings with various W contents and their mechanical and magnetic characterization. The characterization part was accomplished during my secondment at UAB, where I performed nanoindentation tests and worked with vibrating sample magnetometer under the supervision of Professor Jordi Sort. The Mössbauer spectroscopy measurements were performed by Dr. Jonas Reklaitis (FTMC, Vilnius) and I have contributed to the evaluation of the results and their discussions.

Paper 3: I planned and conducted the electrochemical part of study: prepared Fe-W samples with required characteristics, calculated the current efficiency and discussion the possible leveling-brightening effects based on the complexes distribution. The Glow Discharge Optical Emission spectroscopy analysis was performed during my secondment at IFW institute together with Dr. Volker Hoffmann. SEM and XRD analyses were performed in collaboration with PhD student Antonio Mulone (CHALMERS). The paper was written in collaboration with co-authors.

Paper 4: I produced Fe-W samples with various W contents by means of electrodeposition. The mechanical tests were planned and discussed with co-authors and performed by PhD student Antonio Mulone. I critically reviewed the experimental data that were obtained and contributed to the writing of the manuscript.

Paper 5: I planned and conducted all the experimental work and manuscript writing. Tribological measurements were performed at FTMC (Vilnius) with PhD student Tadas Matijošius. The published article was based on discussions with the co-authors.

LIST OF SYMBOLS AND ABBREVIATIONS

α	Lattice constant
β	Equilibrium constant
Θ	Peak position on the XRD pattern
C_{dl}	Double layer capacitance
C_{ad}	Capacitance of adsorbed intermediates
CDP	Compositional depth profile
CE	Current efficiency
COF	Coefficient of friction
d	Crystallite size
DC	Direct current
E, E_r	Elastic modulus, Reduced elastic modulus
EBSD	Electron Backscattered Diffraction
E_{corr}	Corrosion potential
E_{dep}	Electrodeposition potential
EDS	Energy-dispersive X-ray Spectroscopy
EIS	Electrochemical Impedance Spectroscopy
GD-OES	Glow Discharge Optical Emission Spectroscopy
H	Hardness
H_c	Coercivity
ICP-OES	Inductively Coupled Plasma Optical Emission Spectrometry
j_{corr}	Corrosion current density
M	Magnetic moment
M_s	Saturation magnetization
OCP	Open circuit potential
PC	Pulse current
PEG	Polyethylene glycol
R_a	Average roughness
R_{ct}	Charge transfer resistance
R_{ad}	Resistance of adsorbed intermediates
R_s	Solution resistance
R_{corr}	Corrosion resistance
RO	Rapeseed oil
SAD	Selected area diffraction pattern
SEM	Scanning Electron Microscopy
TEM	Transmission Electron Microscopy
VSM	Vibrating Sample Magnetometry
XRD	X-ray Diffraction

TABLE OF CONTENTS

INTRODUCTION

Electrodeposition has been widely used since 19th century, for the fabrication of silver- and gold -plated jewelry, and consequently the initial application of this technique was limited to decorative purposes. Later, procedures for electrodepositing transition metals were developed, and electrodeposition was applied to the production of the surfaces with improved hardness, electrical and thermal conductivity, and enhanced wear and corrosion resistance. The consumption of electroplated nickel, chromium, gold, silver, zinc, and copper layers for electronics production and automotive and aerospace industry constitute the main branches that dominate in the global electroplating market [1,2]. Presently, electrodeposition remains an area of extensive research and innovation. Particular attention focuses on the electrodeposition of binary and ternary alloys and their composites, which enables the production of new materials with unique characteristics that are different from those of the individual metals [3]. Valuable applications of new electrodeposited materials continue to be developed, particularly in the fields of optimization and miniaturization of microelectronic devices, energy conversion, and applied bio-electrochemistry [4–7].

Among the various film deposition methods, electrodeposition offers several distinctive advantages in contrast to physical methods such as vacuum deposition techniques. Electrodeposition can be carried out at ambient pressure and low temperatures (below 100 °C), thus leading to simple implementation of deposition set-up, its cost-effectiveness and versatility. Moreover, the properties of deposits can be fine-tuned by the smart control of electrodeposition parameters, thus generating high demand for this technique in the fabrication of multifunctional materials at micro- and nano-scales.

Nevertheless, one of the drawbacks of electroplating is the high risks associated with the electrolytic bath composition. In fact, the metal plating industry is one of the largest consumers of toxic chemicals in the world. For instance, electrodeposition of hard chromium coatings, which are commonly used as protective coatings, involves highly carcinogenic hexavalent chromium compounds. Furthermore, a significant amount of the electroplating industry products ends up in wastewater [8]. Ni, Cd, Pb and other metal compounds have high solubility in aquatic environments, and they can thus be easily absorbed and accumulated by living organisms, leading to serious health disorders. Currently, the European Union (EU) is

11

the primary supervisory and legislative body that provides precise information on waste management and risks associated with electroplating, particularly in relation to hazardous chemicals. The use of hexavalent chromium, as well as lead, mercury, and cadmium, in materials and components placed on the market has been prohibited since 2003 according to EU directive 2000/53/EC. To address these issues, many research studies have aimed to identify environmentally friendly alternatives to established electrodeposition processes. In particular, electrodeposited Co and Ni alloys with P and W were considered as potential candidates to replace hard chromium coating due to their outstanding mechanical and corrosion properties [9,10]. Nevertheless, the production of materials containing large amounts of Co and Ni is already targeted as hazardous by recent environmental legislation. Thus, Co(II) salts has appeared in the list of "substances of high concern" since 2008 (EC 233-334-2, EC 231-589-4) due to possible carcinogenic effect (observed in animal testing). In addition, the use of metallic Ni for products that might be intended to come into direct and prolonged contact with skin is currently restricted by directives EN 1811:2011 and EN 16128:2011, since it can result in severe allergic reaction.

Notably, while the electrochemical studies in the past concentrated mainly on Ni- and Co- binary alloys, the literature available on electrodeposition of Fe-containing coatings (in particular, with W) as alternative environmentally friendly materials remains comparatively scarce. Nevertheless, iron is one of the most abundant elements in earth's crust, and the production of its compounds could meet most sustainability concerns. Currently, Fe-based alloys with Ni, Co, Pt, Nb, and Si are primarily used to produce materials for magnetic recording systems and micro-magnetic components due to the unique combination of a high saturation magnetization, high permeability, and a low coercive force [11]. However, electrodeposited iron alloys with tungsten can also possess tunable magnetic properties, as well as high hardness and remarkable thermal stability, that empower the application of these deposits as protective coatings or materials with outstanding magnetic properties free from Ni, Co, rare-earths, and noble-metals.

Despite the fact that the electrodeposition of Fe-W alloys has been studied since the 1940s and their attractive properties reported by many authors, the coatings have not attained large-scale production, primarily due to bath maintenance issues. Indeed, the electrodeposition of Fe-W alloys is more often carried out from Fe(II)-plating baths due to the higher solubility of Fe^{2+} compounds. However, the rapid oxidation of Fe^{2+} to Fe^{3+} eventually reduces the bath lifetime and reproducibility of the results because the

12

electrolyte composition is changing within a short period. Hence, the complicated maintenance of baths increases the costs associated with the personnel workload, chemicals consumption, and disposal of the waste solution. In addition, the electrodeposition of Fe-W alloys occurs at higher cathodic polarization as compared to Co- and Ni-W alloys, which results in a current efficiency of approximately 50% (in the systems with insoluble anode) [12,13]. Several studies have aimed to synthesize Fe-W deposits from citrate-ammonia, citrate-borate, or nitrilotriacetate Fe(III)-based electrolytes [14–17]. Nevertheless, the low current efficiency of Fe-W deposition remains an important issue. Furthermore, ammonia and its salts are commonly used in the bath formulation in order to increase the solubility of complexes and the buffer capacity of the plating solution. During long-term operation at elevated temperatures (60 – 80 °C), a significant portion of the ammonia can easily evaporate from the bath, thus changing the pH and alloy deposition rate. By contrast, due to improper utilization, ammonia can pollute air, soil, and water at hazardous waste sites.

The integration of sustainability into the technological progress remains an important challenge, among others, addressed to modern electrochemical society. The development and optimization of new environmentally friendly and minimally invasive electrolytic baths for production of advanced materials is necessary. Moreover, better control of the metallic growth process during electrodeposition and understanding of the fundamental phenomena involved is essential. Thus, environmentally friendly electrodeposition of Fe-W based materials presents an area of interdisciplinary research that can help to address several existing challenges and fill the gap between materials science and sustainable development.

Objectives of the study

This research focuses on the electrodeposition and assessment of nanocrystalline and amorphous-like Fe-W alloys and new Fe-W/Al_2O_3 composite coatings obtained from the environmentally friendly glycolate-citrate bath. The main research objectives are as follows:

1. To design a new aqueous plating bath for the electrodeposition of Fe-W alloys and Fe-W/Al_2O_3 composites in accordance with sustainable development, that is, avoiding the use of hazardous chemicals in the bath, increasing the electrolyte's life-time by using the thermodynamically stable Fe(III) precursor rather than Fe(II), and maximizing the current efficiency of the electrodeposition process;

2. To achieve reliable control over the composition and structure of electrodeposited Fe-W alloys and Fe-W/Al_2O_3 composite coatings by

13

variation of electrochemical conditions (pH, current density, temperature, stirring rate, and bath composition) in order to obtain alloys of various W contents and structure ranging from nanocrystalline to "amorphous-like";

3. To map the interdependencies between intrinsic (composition, structure, grain size, phase composition, and saturation magnetization) and extrinsic characteristics (hardness, wear, corrosion, and thermal resistance) of obtained coatings and unveil the perspectives on sustainable application of electrodeposited Fe-W alloys and Fe-W/Al_2O_3 composites.

Statements to be defended:

1. Elaborated environmentally friendly glycolate-citrate Fe(III)-based electrolyte is an alternative bath for electrodeposition of Fe-W alloys and Fe-W/Al_2O_3 composite coatings compared to conventional Fe(II)-based baths.

2. Designed control over the intrinsic properties (composition and structure) of electrodeposited Fe-W alloys and Fe-W/Al_2O_3 composites is a way of reasonable reorientation of their extrinsic characteristics such as hardness, wear, corrosion, and thermal resistance.

3. Fabricated materials based on Fe-W alloys possess a unique combination of structural, magnetic, mechanical, and thermal properties due to the interplay between W content, crystallite size, and crystalline structure. Thus, they can be of particular interest for the fabrication of microelectromechanical systems and hard temperature-resistant components in many applications, including the processes in which dry friction or lubrication conditions are applicable.

Organization of the text

This manuscript consists of three chapters and five appended publications. The main concepts of electrodeposition, research aims, major objectives and statements for defense were presented. The current state of knowledge on electrodeposited W alloys with Fe group metals is summarized in *chapter 1*. In *chapter 2*, the research methodology is provided along with the short description of experimental techniques used in this study and their basic principles. The experimental results of this work are discussed in *chapter 3* of this manuscript. The results are presented in a concise manner that emphasizes the most important findings of this research, while the detailed discussions are provided in appended articles. The general conclusions of the thesis followed by recommendations for future research are given.

1. STATE OF ART

This chapter provides a current state of knowledge on W alloys with Fe group metals, their synthesis, properties and applications. The attention is given to the fundamental concepts of the electrolytic bath formulation, mechanisms of induced co-deposition and evaluation of electrodeposited alloys properties in relation to their composition and structure.

1.1 W alloys with iron group metals

It is well known, that metallic tungsten is characterized by a set of unique characteristics. It has the highest melting point (T_m = 3411 °C), the highest modulus of elasticity (E = 400 GPa) and the highest hardness among the metals; it has the highest tensile strength at temperatures above 1650 °C, the lowest thermal expansion coefficient ($4.4 \cdot 10^{-6}$ /°C), as well as it exhibits excellent corrosion resistance against sulfuric, nitric, and hydrofluoric acid solutions [18,19]. Today, some of W compounds cannot be substituted in many important applications in different fields of technology. For instance, tungsten carbide is one of the most widespread W compounds, which is extensively used in cutting devices being one of the toughest, most reliable and extremely durable materials.

Iron, cobalt and nickel have proven to be excellent alloying elements for tungsten. The alloys produced by powder metallurgy and having tungsten more than ≥90 wt. % exhibit a particularly high density (~18 g/cm^3), therefore they are also known as "tungsten heavy alloys" [20]. Due to their high density the main use of sintered W alloys with Fe and Ni is fabrication of X-ray and γ-radiation shields, rigid tools for machining and fusion reactors (Fig. 1a) [19–22]. The role of alloying elements (Ni, Fe or Co) is to form a binder matrix to hold the brittle tungsten grains together and prevent fracture propagation, thus making the alloy tough and ductile even at elevated temperature. The electrodeposited W alloys with these metals present a considerable difference from those produced by physical methods. Firstly, the W content is lower (usually does not exceed 50 wt. %), the layers are thinner (up to 100 µm) and the properties are strongly depended on the deposition conditions applied. Secondly, the electrodeposition of W alloys with Fe, Co and Ni is a fascinating phenomenon by itself and many studies are conducting worldwide to understand the nature of the process.

Pure metallic tungsten cannot be electrodeposited from aqueous solutions alone due to the formation of an oxide layer on the cathode, which has a very low overvoltage for hydrogen evolution, thereby hindering the growth of the

tungsten layer. Nevertheless, tungsten can be easily co-deposited with iron group metal forming an alloy. Such phenomena Brenner in the 1940s called "induced co-deposition" [23], although the first studies dealing with electrodeposition of W alloys with Fe and Co date back to 1930s. The induced co-deposition of tungsten with iron group metals is still discussed in modern electrochemical society [24–26]. The possible mechanisms explaining this phenomenon were previously reviewed in [9,24] and are briefly introduced in the following section of this thesis.

The W content in electrodeposited binary alloys usually reaches an upper limit: 30-32 at. % with Fe and Co, and 20-25 at. % with Ni [9]. The elemental composition of an electrodeposited alloy depends on the ratio of the partial current densities of the alloy's constituents. In turn, the distribution of partial currents is influenced by a number of factors such as chemistry of the solution, total current density or applied potential, temperature, hydrodynamics and interdependencies of the rate of one metal electrodeposition to another, among others. Noticeably, the structure of W alloys with iron group metals (M-W) is very sensitive to the W content. An increase in W content leads to the gradual transition from nanocrystalline to "amorphous-like" structure, due to significant decreasing of the grain size. Thus, nanocrystalline M-W coatings have grains with few hundred nanometers size, while when the grain size falls down below 10-5 nm the structure is transformed to "amorphous-like" [27].

The alloying of iron group metals with tungsten improves their chemical, physical, and mechanical properties at both room and elevated temperatures [16,28,29]. Besides, it is possible to combine the useful properties of Fe, Ni and Co with those of the elemental W. Nanocrystalline M-W coatings with fine grains exhibit outstanding thermal stability, good mechanical properties (hardness, strength and plasticity), favorable corrosion and wear resistance, tunable magnetic characteristics. These properties make them extremely appealing materials for different industrial branches: for the fabrication of microelectromechanical systems (micro-transformers, micro-gears), sensors and recording heads for magnetic systems (Fig. 1b and d) [14,27,30–33] or other applications where aggressive conditions can exist [9]. Moreover, the possible use of M-W alloys was currently extended to the field of energy related applications. They can be applied as effective anode material for methanol oxidation [34,35] or as catalysts for hydrogen generation from water [36,37].

In addition, some of W alloys with iron group metals have the perspective to be used in some biomedical applications. The study on Fe/W composite prepared by powder metallurgy has shown that this material has good

hemocompatibility and can be used for fabrication of biodegradable coronary stent with better mechanical properties and faster degradation rate than pure iron [38]. Also, in vivo corrosion and tumor outcome has been tested using muscle-implanted tungsten heavy alloys, that is, the W-Ni-Co and W-Ni-Fe [39,40]. Implantation of W-Ni-Co pellet into the leg muscle of rat resulted in the formation of a rhabdomyosarcoma (a malignant form of cancer) around the pellet. In opposite, W-Ni-Fe alloy (as well as pure W pellet) was not cancerogenic and did not influence on the bodyweight, clinical chemistry, hematology, or urinalysis parameters of test animals at 6 months post-implantation. Recently, a novel porous Fe/Fe-W alloy scaffold resembled the structure of cancellous bone was fabricated by electrodeposition with a perspective to be used for the reparation of damaged bone tissues (Fig. 1c) [41]. In vitro cytotoxicity tests have shown that the cell viability was closely correlated with the corrosion rate of the scaffold. In addition, the pore size of the scaffold and its degradation rate could be easily controlled by electrodeposition conditions.
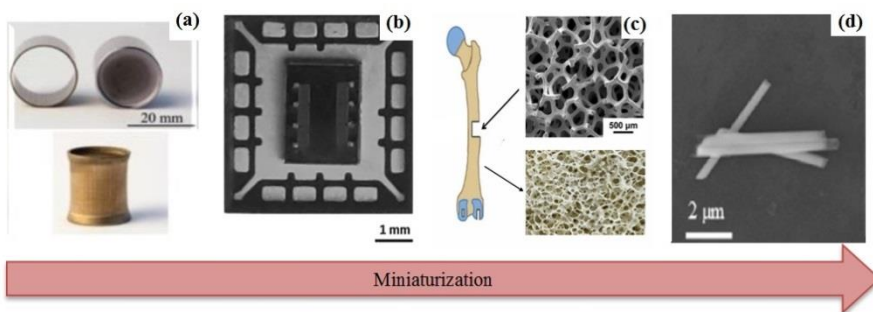
Fig. 1. *Illustration of various W containing materials and their products appeared in publications since 2016: plasma-facing W-Fe-Ni composite for fusion reactors prepared by vacuum diffusion bonding* [21] *(a); Ni-Fe-W core micro-transformer for high frequency applications obtained by using electroplating and photolithography techniques* [33] *(b); electrodeposited porous Fe/Fe-W scaffold for bone tissue engineering* [41] *(c); and electrodeposited Fe-W magnetic nanowires* [14] *(d).*

1 pav. *Įvairios W turinčios medžiagos ir gaminiai iš jų, aprašyti nuo 2016 m.: su plazma kontaktuojantis W-Fe-Ni kompozitas lydymo reaktoriams, gautas vakuuminio difuzinio virinimo būdu* [21] *(a); Ni-Fe-W lydinio mikrotransformatoriaus šerdis aukšto dažnio įrenginiams, gauta elektrochemiškai nusodinant fotolitografiniame šablone* [33]*; elektrochemiškai nusodintas poringas Fe/Fe-W rėmelis kaulų audinių inžinerijai* [41] *(c); elektrochemiškai suformuotos Fe-W nanovielos* [14] *(d).*

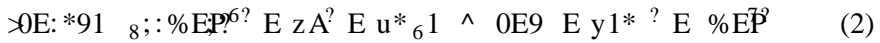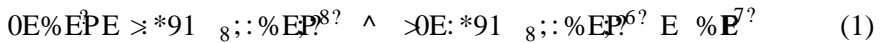## 1.2 Induced co-deposition

In previous section it was mentioned that electrodeposition of W with iron-group elements (Ni, Co, Fe) was coined as induced co-deposition, since W cannot be reduced alone from aqueous solution, but only with iron group elements. In fact, certain other elements such as Mo, P and Ge exhibit similar electrochemical behavior. Therefore, in many cases, proposed mechanism for W (or Mo) alloy can be generalized to other co-depositing iron group metals and vice versa. It must be pointed out, that the published mechanisms are derived from the experimental observations, but none of them can be claimed as undisputed. Moreover, the reports of different authors are sometimes inconsistent to each other, due to different experimental conditions (bath composition, concentration of bath constituents, high – low current density/overvoltage, hydrodynamic conditions, etc.).

One of the earliest theoretical works on induced codeposition of W with iron, cobalt and nickel performed by Holt and Vaaller suggests the catalytic reduction of WO_4^{2-} ion by iron group metal in zero valence state, which is reduced first [42]. Thus, electrodeposition leads to the formation of laminar structured coating with thin alternating layers of W and iron group metal. This model has lacked popularity, because non-laminated W alloys can be readily deposited, as well as inactive metals (Mn, Cu, Sn) could also catalyze the W deposition.

Not surprisingly that many attempts to establish the role of the hydrogen on induced co-deposition of W have been made, because in aqueous baths hydrogen evolution occurs as a side reaction resulting in a current efficiency less than 100 %. Nearly all of the proposed mechanisms consider tungsten oxide intermediate species absorbed on the cathode surface. Thus, Clark and Lietzke suggested that the deposition of a thin film of partly reduced tungstate on the cathode is followed by the catalytic reduction of this film by hydrogen in the presence of freshly deposited Fe, Co and Ni [43]. This suggestion has been expanded by Fukushima et al., who studied induced co-deposition of binary and ternary Mo alloys, assuming that the iron group metal can adsorb the hydrogen onto its surface and thus induce the reduction of molybdenum (or tungsten) oxide intermediate [44]. These concepts were developed from the observation that generally the current efficiency of deposition tends to be lower as the content of co-deposited Mo (W) is increasing [45]. The absorption and polarographic study on complex formation in citrate Co-W plating bath performed by Clark and Lietzke predicted the existence of the following types of complex species: (i) metal-

citrate, (ii) tungstate-citrate and (iii) metal-tungstate complexes [43], although their composition was not established.

The concept of iron group metal-tungstate complex compound as a precursor for alloys electrodeposition has been recovered by Younes, Eliaz and Gileadi [24,46,47]. Their research on Ni-W induced co-deposition from citrate-ammonia electrolyte lead to a hypothesis that the precursor for the deposition of alloy is a ternary complex of the type $[(Ni)(HWO_4)(Cit)]^{2-}$, which is formed in the reaction between Ni- citrate complex and W-citrate complex and discharged according to equation (1) and (2), respectively [46]:

$$0E\%EPE \succcurlyeq *91 \;_8;:\%EP?^{8?} \ \wedge \ \succ 0E: *91 \;_8;:\%EP?^{6?} \ E \ \%E?^{7?} \tag{1}$$

$$\succ 0E: *91 \;_8;:\%EP?^{6?} \ E \ zA^? \ E \ u*_61 \ \wedge \ 0E9 \ E \ y1*^? \ E \ \%EP?^{72} \tag{2}$$

Another point of view was described by Podlaha and Landolt suggesting that the precursor for deposition of Ni-Mo alloy is an adsorbed complex containing both metals [48].

$$/K1 \;_8^{6?} \ E \ 0E\%EPE \ t*_61 \ E \ tA^? \ \backslash \ \succ 0E\%EP/K1 \;_6 \, ?^2_{\textcircled{0}} \ E \ v1*^? \tag{3}$$

$$\succ 0E\%EP/K1 \;_6 \, ?^2_{\textcircled{0}} \ E \ t*_61 \ E \ vA^? \ \backslash \ /K:_{\textcircled{a}} \ E \ 0E\%EPE \ v1*^? \tag{4}$$

The model of Podlaha and Landolt gives the mathematical description of kinetic and transport regimes of molybdenum reduction reaction and provides a solid interpretation of experimental results obtained at different current densities, agitation speed and Ni:Mo ratio in the solution, as well as it considers the indirect influence of adsorbed hydrogen intermediates of the reaction rate. The model has been further adopted by Gomez et al. for the deposition of Mo alloy with Co [49] and reviewed in [5,9].
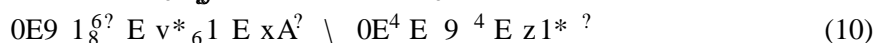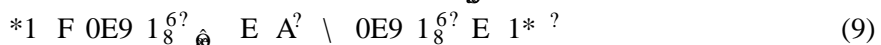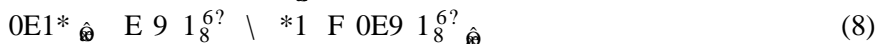
Nevertheless, the presence of mixed complex compounds in plating solution is rather difficult to detect and there are only few works succeeded to determine them. The experimental works of Weston et al. with UV spectroscopy implied that significant amount of cobalt in gluconate Co-W plating bath is indeed present in the form of a mixed $[Co\text{-}gluc\text{-}WO_4^{2-}]$ complex [26]. Also, the presence of a heteropolynuclear Co-W-citrate complex has been detected by gel chromatography in the work of Belevskii [50]. Noticeably, the electroactive species are often charged negatively. Nevertheless, cathodic reduction of anions is a well-known electrochemical process (e.g. reduction of metal-cyanic complexes, $Cr_2O_7^{2-}$, etc.), which can be explained by the mass transport of negatively charged species to the cathode due to the diffusion (driven by the chemical potential gradient) or/and convection force rather than due to electrolytic migration [51].

Several researches address the role of Fe, Co and Ni hydroxyl species in the formation of electroactive complex compound. The first model employing the electrodeposition of Ni-W alloy appeared in 1977 in the work

of Vasko [52]. The equations (5) and (6) represent the general scheme of the overall Ni-W alloy deposition process. Despite this mechanism has been lacked popularly for many decades, nowadays, some researches revive the interest in this model [53,54].

$$0E1* \ ^> E \ u*_6 1 \ E \ 91 \ ^{6?}_8 \ \wedge \ \succ*_{\tilde{a}} 0E_{\ddot{a}} 9 \ _{\mathring{a}} 1 \ _9 ?_{\hat{e}} \tag{5}$$

$$\succ*_{\tilde{a}} 0E_{\ddot{a}} 9 \ _{\mathring{a}} 1 \ _9 ?_{\hat{e}} \ E \ J \ A^? \ \wedge \ 0E9 \ E \ I \ 1 \ ^{6?} \ E \ J 1* \ ^? \tag{6}$$

The mechanism of W co-deposition with iron group metals involving the hydroxo-species as charge-transfer particles seems to be quite viable, because electrochemically active Fe, Co and Ni hydroxyl species MOH^{n+} can ensure a relatively high partial current density for metal deposition [55]. For instance, it is confirmed that the electrodeposition of cobalt occurs via the formation of $CoOH^+$ and $Co(OH)_2$ species [56,57]. In addition, the role of hydroxide species in the mechanism of alloys induced co-deposition is supported by the experimental observation that electrodeposited coatings can contain ~2 at.% of co-deposited non-metallic elements such as O and H. The following complex mechanism for Ni-W alloy deposition preceded through the stage of formation of heterometallic cluster compound with nickel-tungsten was suggested by Krasikov in order to explain the light elements co-deposition [54]:

$$0E1* \ ^> E \ A^? \ \backslash \ 0E1* \ _{\hat{\text{ê}}} \tag{7}$$

$$0E1* \ _{\hat{\text{ê}}} \ E \ 9 \ 1 \ ^{6?}_8 \ \backslash \ *1 \ F \ 0E9 \ 1 \ ^{6?}_8 \ _{\hat{\text{ê}}} \tag{8}$$

$$*1 \ F \ 0E9 \ 1 \ ^{6?}_8 \ _{\hat{\text{ê}}} \ E \ A^? \ \backslash \ 0E9 \ 1 \ ^{6?}_8 \ E \ 1* \ ^? \tag{9}$$

$$0E9 \ 1 \ ^{6?}_8 \ E \ v*_6 1 \ E \ xA^? \ \backslash \ 0E^4 \ E \ 9 \ ^4 \ E \ z1* \ ^? \tag{10}$$

Authors also mention that a fraction of nickel ions not interacting with tungstate ions can be reduced to metallic nickel in a parallel path. Similar concept of dual pathway mechanism was suggested by Obradovič based on UV spectrophotometry investigation of Ni-W alloy electrodeposition from citrate-ammonia electrolyte [58]. The mechanism assumes two parallel reactions taking place during electrodeposition: (*i*) iron group metal reduction from its complex compound, and (*ii*) reduction of the protonated W-citrate complex from heterometallic specie. The ratio between these two reactions generally determines the chemical composition of deposits obtained.

As the induced co-deposition phenomenon is still under research, various interpretations of the obtained experimental data exist. The possible mechanisms explaining this phenomenon were recently reviewed in [9,24] and extensively discussed in [25,26,46,57].

1.3 Bath chemistry

The understanding of the bath chemistry is an important step towards the rationalization of the fundamental phenomena involved. It helps to achieve a better control of the metallic growth process during electrodeposition, which is required for production of novel materials with desired characteristics. The typical electrolytic bath for M-W alloys electrodeposition consists from: iron group metal salt (usually sulfate or chloride), W source (WO_4^{2-} ions), complexing agent (typically an organic acid) and buffering agent, the most common one is ammonia. Complexing agents are added to the solution in order to approach the electrode potentials of two different metals to be electrodeposited and to avoid precipitation of sparingly soluble Fe-, Co- and Ni-tungstate and -hydroxides.

The formulation of electrolytic bath for Fe-W alloys deposition has several specific concerns as compared to Co and Ni-W alloys plating, which should be taken into consideration. Solutions based on Fe(II) tends to fast oxidation by dissolved oxygen, because the standard potential for oxygen reduction is more positive than in the case of Fe^{3+} reduction to Fe^{2+} (E_{O_2/H_2O} = 1.23 V and $E_{Fe^{3+}/Fe^{2+}}$ = 0.771 V) [59]. Complexing agents added to the bath can only inhibit this process, but not prevent it. Therefore, in order to prolong the lifetime of Fe(II)-electrolytes, some reducing agents are often added, such as iron powder, hydroxylamine, hydrazine, formic acid or L-ascorbic acid [60–62]. Nevertheless, those compounds can affect the bath chemistry and coatings properties in a rather unpredictable way.

The spontaneous reaction of Fe(II) oxidation to Fe(III) in the presence of dissolved oxygen occurs as follows:

$$4Fe^{2+} + O_2 + 2H_2O = 4Fe^{3+} + 4OH^- \qquad (11)$$
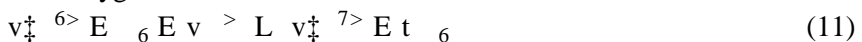
The calculated value of K_{eq} for this reaction is 9.8~10^{30}. This result means that practically all of the amount of Fe^{2+} eventually will oxidize to Fe^{3+}. However, the solubility product of iron(III) hydroxide is in order of 10^{-36} (and for iron(III) tungstate it is 10^{-13}), which implies that very small concentrations of Fe^{3+}, OH^- and WO_4^{2-} are required to form a precipitate and destabilize the plating solution.

There are only a few studies dealing with electrodeposition of Fe-W alloys from Fe(III)-based electrolytes [14–17]. The stability of Fe(III) plating baths is governed by competing reactions of Fe^{3+} ion hydrolysis and complexing in aqueous solutions. The development of Fe(III)-based electrolytes could be a good alternative for Fe(II)-based solutions, but the selection of an appropriate complexing agent able to prevent the formation of sparingly soluble iron hydroxides and ensure the thermodynamic bath

stability in the presence of tungstate ions over the pH range should be realized in a wise manner.

One of the most studied complexing agents is citric acid, which has been used for electrodeposition of Fe-W [16,17,28], Co-W [27,34], Ni-W [29,47], Ni-Fe-W [31] alloys, etc. The protonation of citric acid is well-studied and has been reported by several authors [16,46]. It has been shown, that in the pH range of 7-8 the acid is completely dissociated giving the $HCit^{3-}$ ion, which is assumed to be the main ligand in all the complexes [46]. An addition of complexing agent significantly shifts the equilibria due to the formation of metal complexes compounds with ligands and concomitant redistribution of various metal poly- and hydroxo-species which are formed in aqueous solution [9,63]. The complexation of tungstate with citrate ions is reported elsewhere [63]. However, the distribution of W species in the presence of induced metals has been provided only for a few systems, that is, the Co-W [27], Ni-W [46], and Ag-W [25].

Other complexing agents, such as gluconate [26,64,65], glycolate [66], nitrilotriacetate [14], tartrate [67] and pyrophosphate [68] have been also used for W alloys electrodeposition, but they are studied in a significantly smaller extent as compared to citrate based electrolytes.

Ammonia (and ammonium salts) is frequently used in bath formulation in order to increase the solubility of metal complexes compounds and provide a buffer capacity. The maximum buffer capacity of ammonia in citrate solutions has a maximum at pH 7-9 [69,70]. This is also one of the reasons why most of citrate-ammonia electrolytes operate at this pH range (in addition to formation of $HCit^{3-}$ ions). However, commonly the electrodeposition of W alloys is carried out at elevated temperatures (60-80 °C) and during long-term operation a significant amount of ammonia can be easily evaporated, thus changing the alloy deposition rate and pH. Several attempts to develop ammonia-free electrolytes for W alloys deposition were reported [17,71,72]. Interestingly, deposition of Ni-W from ammonia-free plating bath, resulted in an increased W content in the alloy [72]; however, there are no similar data reported for Fe- and Co-W alloys. Boric and phosphoric acids, are often used as buffering agents in ammonia-free solutions [27,35,73–75]. Furthermore, various organic additives, such as brighteners, leveling agent, grain refiners, stress relievers (saccharin, Rokafenol, butindiol, glycerol, etc.) [32,76–81] can be also used in bath formulation in order to achieve a desired performance of the electrolyte.

The estimation of species distribution is of particular importance for the evaluation of the bath stability and other processes occurring during electroplating. It gives the possibility to get further insight onto the

22

deposition mechanism and correlate the theoretical data with the experimental ones. For instance, the increase in W content in Co-W alloy at pH >5 was correlated with the rapid rise in concentration of a W-citrate complex, $(WO_4)(HCit)H^{4-}$ [27]. In addition, the species distribution can help to understand the origin of the compositional variation within the coating thickness and increase (or decrease) in cathodic current efficiency during electrodeposition [66]. Nevertheless, the straightforward and accurate prediction of alloys composition as a function of pH and other bath constituents is limited, because the electrolyte may contain also compounds with enhanced molecular mass [50], heterometallic species, and other species those stability constants are not know and, therefore, cannot be considered in calculation.

1.4 Properties of W alloys with iron group metals and their composites

Electrodeposition technique is an extremely powerful tool in materials design. While the chemical composition and structure are the key factors determining the properties of material, electroplating gives the possibility to produce alloys with specific composition, nano- or amorphous internal ordering and specific texture and, therefore, different characteristics.

The data on mechanical properties of electrodeposited binary and ternary W alloys with iron group metals were summarized in [9]. Different compositions and coatings obtained under different conditions were compiled. Generally, the mechanical properties (hardness and strength) improve as the W content is increased due to reduction of the crystallite size, as it is predicted by the Hall–Petch relation, that is, the strength is increasing as the inverse square root of the grain size:

$$H \quad \rule{2cm}{0.5cm} \quad \frac{k_y}{\sqrt{D}} \qquad (12)$$

where H is a hardness, σ_y is a material strength, σ_0 is a material constant for resistance of the lattice to dislocation motion, k_y is a strengthening coefficient (unique to each material) and D is the grain size.

The smaller grains increase the number of grain boundaries, which are able to stop the dislocation motion and thus the hardness increases. In addition, solid solution strengthening and nanostructurization processes can be involved. Nevertheless, it has been shown that for W contents higher than 10 at.% in Ni-W [81] and 25 at.% in Co-W alloys [27], the crystallite size reduces below a critical value and the Hall–Petch breakdown occurs, which

23

is about 10 nm and 5 nm for Ni- and Co-W alloys, respectively. This critical grain size value sometimes can be correlated to the transitional state between nanocrystalline and amorphous/amorphous-like structure. The amorphous structure promotes branching of the shear bands and thus the hardness decreases. Remarkably, the hardness of Fe-W alloy with 30 at.% of W can reach values as high as 13 GPa (at 2 mN), which is higher than that reported for Co- and Ni-W alloys and even comparable to the hardness of electrolytic chromium [82]. The measured hardness of Fe-, Co- and Ni-W alloys can vary significantly dependently on the alloys composition (W content) and applied experimental conditions. Considering the tests carried out at the same conditions on M-W alloys with similar W content, the highest hardness has been reported for Fe-W coatings, followed by Co-W and Ni-W in a descending order.

Nevertheless, amorphous materials are often brittle [83] due to high internal stress originated from the hydrogen evolution during M-W alloys electrodeposition. Thermal treatment can reduce imbedded stress of the coatings and further improve their mechanical properties. Most of the studies concerning the effect of heat treatment on hardness of electrodeposited W alloys have been performed on Ni-W [84–87] and Ni-Fe-W systems [32,83]. Only a few studies have assessed the thermal stability and phase transformations occurring upon annealing of Fe-W [28,71,88] and Co-W alloys [13,89]. When subjected to thermal treatment electrodeposited nanocrystalline and amorphous alloys recrystallize with the formation of more coarse grains and new phases (intermetallic phases, oxides, carbides, etc.). Typically amorphous-like W alloys (W-rich alloys) have enhanced thermal stability perhaps due to a thermodynamic phenomenon, where grain boundary energy is reduced upon solute segregation to the intercrystalline regions [90]. In fact, amorphous Fe-W alloys are characterized with outstanding thermal stability keeping the partially amorphous structure up to 600 °C [71]. At elevated temperatures above 800°C the recrystallization occurs with the formation of α-Fe, Fe_2W and $FeWO_4$ phases [71]. The formation of intermetallic phases at elevated temperatures such as Ni_4W, NiW and Co_3W is expected from binary phase diagrams and was also observed after annealing treatment of electrodeposited Ni-W and Co-W alloys, respectively [13,85]. However, the origin of precipitated oxide (and carbide) phases during annealing is still under debate. Some authors report on the crucial role of co-deposited impurities (mainly O and C) and demonstrate that impurity particles can alter grain growth and influence the microstructure development during the thermal treatment [87,91]. Others

suggest that oxygen impurity originates from some residual air in argon atmosphere, where annealing tests were performed [13].

Many researches address the importance of mechanical characteristics of coatings for their tribological properties giving the relationships between hardness (or plasticity) and wear [81,92,93]. The general idea is that the materials with higher ratio between hardness and elastic modulus, so-called elastic strain to failure, will better resist the permanent plastic defamation, hence, minimize wear resulted from the plastic deformation [93]. The studies performed on Ni-W coatings, which typically undergo sliding wear, have shown that, indeed, elastic-plastic behavior is the controlling factor [81,94]. In addition, it was demonstrated that Co-W layers have better resistance to high loads under friction conditions due to the formation of stable hexagonal close-packed (hcp) structure, which impedes the plastic flow [95]. Nonetheless, the tribological behavior of Fe-W alloys is primary determined by chemical stability of Fe and not only by mechanical characteristics. At dry friction conditions Fe-W alloys undergo severe tribooxidation [82]. Formed iron oxides act as abrasive third body particles, which increase the asperity contact between two sliding solids, thus resulting in a high coefficient of friction and larger wear volume.

The map provided in [9] assesses the wear rate of different W alloys in similar tribo-systems. According to that, the Co-W alloys undergo the lowest wear, as compared to Co-W-P, Fe-W, TiN and electrolytic Cr. Similar data were reported in [26] (despite different test configuration was used), suggesting that Co-W alloys are one of the best candidates to replace hard chromium coatings. Nevertheless, it is worth notice, that the comparison of tribological properties based on the published data is quite complicated because of the different electrodeposition and testing conditions used, that is, the load, amplitude, speed, displacement, relative humidity, temperature, etc. Moreover, a common unit to express the degree of wear is lucking. Hence, the wear is often expressed in terms of specific wear rate (mm^3/Nm), wear loss (μg, kg/Nm, etc.), wear depth (μm) or dissipated energy ($\mu m^3/J$). Some of the wear characteristics of M-W alloys and their composites are provided in Table 1.

Table 1. *Wear resistance of different tungsten alloys and composite coatings under dry friction conditions.*
OHW Įvairių Fe-W lydinių bei Fe-W/Al$_2$O$_3$ kompozitų atsparumas nusidėvėjimui sausos trinties sąlygomis.

Coating, reference	Electrodeposition conditions	Wear test conditions	Wear
Co-W [75]	DC, citrate-borate bath, 58 °C, 10 mA/cm^2, pH 6.7, copper substrate	ball-on-flat, corundum counterbody, 10 Hz, 10 000 cycles, 100 µm amplitude, 2 N	$4.3 \cdot 10^3$ µm^3/J
Ni-P-W [102]	DC, citrate bath, 70 °C, pH 8-9, aluminum substrate	ball-on-disk, M50 steel counterbody, 0.1 m/s, 28 min, 1 N	$2.4 \cdot 10^{-5}$ mm^3/Nm
Ni-W [79]	DC, Citrate-ammonia bath, 50 °C, 40 mA/cm^2, steel substrate	pin-on-disk, 1100 m sliding distance, 0.3 m/s, Steel St52 counterbody, 20 N	$7 \cdot 10^{-6}$ mm^3/Nm
Fe-W-P [80]	DC, citrate bath, 70 °C, pH 8, 30 mA/cm^2 , 316L steel substrate	ball-on-disk, alumina ball, 0.1 m/s, 90 min, 5 N	$1.7 \cdot 10^{-7}$ µm^3
Ni-Fe-W [81]	DC, Citrate-ammonia bath, 50 °C, 40 mA/cm^2, steel substrate	pin-on-disk, low carbon steel pin, 0.5 m/s, 5N	$5 \cdot 10^{-10}$ kg/Nm
Fe-W [103]	DC, citrate bath, 70 °C, 10 mA/cm^2, pH 6.7, St3 steel substrate	ball-on-flat, corundum counterbody, 5 Hz, 50 000 cycles, 200 µm amplitude, 20 N	4.5 µm
Ni-W/Al$_2$O$_3$ [104]	DC, citrate bath, pH 8, 60 °C, 70 mA/cm^2, US 35 kHz, 40 g/L of Al$_2$O$_3$, steel substrate	ball-on-disk, alumina ball, 60 rpm, 20 000 cycles, 5 mm diameter of the wear track, 1N	$2.2 \cdot 10^{-6}$ mm^3/Nm
Ni/Al$_2$O$_3$ [105]	PC (20 ms ON/ 80 ms OFF, dc 20%), Watts bath, 30mA/cm^2, 20 g/L of Al$_2$O$_3$, steel substrate	ball-on-disk, steel counterbody, 1 m/s, 45 N, water lubricated	$3 \cdot 10^{-7}$ mm^3/Nm
Ni-W-P/SiC [106]	DC, citrate bath, pH 6.5, 55 °C, 40 mA/cm^2, 3 g/L of rod-shape SiC, 150 rpm	rotary disk, 70 rpm, 30 min, 5.9 N	180 mg
Ni-Fe/Al$_2$O$_3$ [99]	DC, citrate bath, pH 3, 31 °C, 40 mA/cm^2, cast Fe substrate	rotary disk, NC6 steel ball, 23 MPa	$240 \cdot 10^{-5}$ g of NC6 steel ball

Fabrication of composite materials is one of the common approaches, which enable to combine alloys properties with significantly different physical or chemical properties of second phase particles that produce a material with unique characteristics different from the individual components. Many studies have been concerned the electrodeposition of Ni and Ni-W matrix composites with oxide and carbide particles (Al_2O_3, SiC, TiO_2), because of their high hardness, oxidation and thermal resistance that may improve the strength and corrosion resistance of the resulting composite coatings [96–100]. It must be point out that the presence of particles by themselves cannot ensure the desired performance of the coating. Often, the incorporation of particles causes porosity, bad adhesion and weak interface bonding with the matrix. All these effects can eventually reduce the overall performance of the surface, particularly, corrosion resistance [99]. Therefore, the appropriate design of the composite system is essential.

At optimized conditions, the hardness of the composite coatings increases due to the grain refining and dispersion strengthening effects provided by particles [100]. In addition, even naturally soft WS_2 particles (~3 GPa) incorporated in Ni matrix resulted in an increased hardness of the coating due to pronounced texturing effect [101]. Also, micro- and nano- second phase particles typically improve the wear resistance of composites, as they can provide self-lubricating effect, serve as spacers between two bodies in contact and increase the elasticity of the coating [100,101,105,107]. However, the corrosion behavior of the composites is rather more complicated. Well-dispersed Ni-W composites with Al_2O_3 particles have shown good corrosion resistance in sulfides and chlorides medium due to the partial blocking of corrosion pits by inert alumina particles [108]. Nonetheless, the presence of alumina particles in Ni-Fe/Al_2O_3 had a detrimental effect on corrosion resistance of the composite coating, because the increase of co-deposited Al_2O_3 lead to an increase in Fe content in Ni-Fe matrix and as a consequence corrosion preceded through the selective dissolution of iron-rich areas [99].

W alloys and composites with iron group metals possess tunable magnetic properties and are of great interest for a variety of magnetic applications. Among investigated films are: binary Co-W [27] and Fe-W alloys [14,109], ternary Co-Ni-W [73] and Ni-Fe-W [31,33,110] alloys and also Ni/W and Fe/W composite coatings [111]. Both hard and soft magnetic properties have been reported for Co-W deposits depending on the W content [27]. Otherwise, these M-W alloys are generally characterized by low coercive field, that is, the soft or semi-soft magnetic properties (H_c<200 Oe) within all W concentration range and are suitable for read/write heads in

hard disc, sensors and microelectromechanical systems. The common feature is that the saturation magnetization tends to decrease monotonically, as the amount of W increases, due to the gradual dilution of non-magnetic tungsten atoms. It must be pointed out that the magnetic properties of W alloys (coercivity, saturation magnetization, anisotropy easy axes direction, remanent-to-saturation ratio, etc.) are strongly dependent on the microstructure of electrodeposited films, and not only on the W content [9].

1.5 Summation

It is important to achieve a deep understanding of the phenomena involved in electroplating of W alloys with iron group metals. The deposition conditions applied (current density, current mode), bath formulation (concentration of metal species, complexing agents, additives, pH), and experimental set-up (agitation, heating, position of the electrodes, etc.) have direct influence on the composition, structure and properties of resulted coatings. Fe-, Co- and Ni-W alloys have many similarities, but also several specific features can be distinguished. Ni-W coatings possess outstanding corrosion resistance, electric and magnetic properties, what makes them appealing for the fabrication of micro-electronic devices. Co-W alloys have high potential to be applied for the fabrication of interconnects and protective coatings alternative to hard chromium, due to their attractive mechanical properties and remarkable resistance to wear and elevated temperatures. In contrast, Fe-W system is not such well-studied and the comprehensive investigation on interrelationship between electrodeposition conditions, composition, structure and properties is lucking. Currently, the main attention toward fabrication of these alloys is targeted to the production of magnetic devices, due to excellent soft magnetic properties of Fe. In addition, electrodeposition of Fe-based composites remains poorly explored, as compared to other M-W matrix composites.

2. EXPERIMENTAL METHODS

Different techniques were used to obtain and characterize Fe-W alloys and composite coatings. The specific bath composition, electrodeposition conditions, and procedures for mechanical, magnetic, wear and corrosion properties measurement are described in detail in appended articles for each specific case. The general research methodology is shown in Fig. 2.
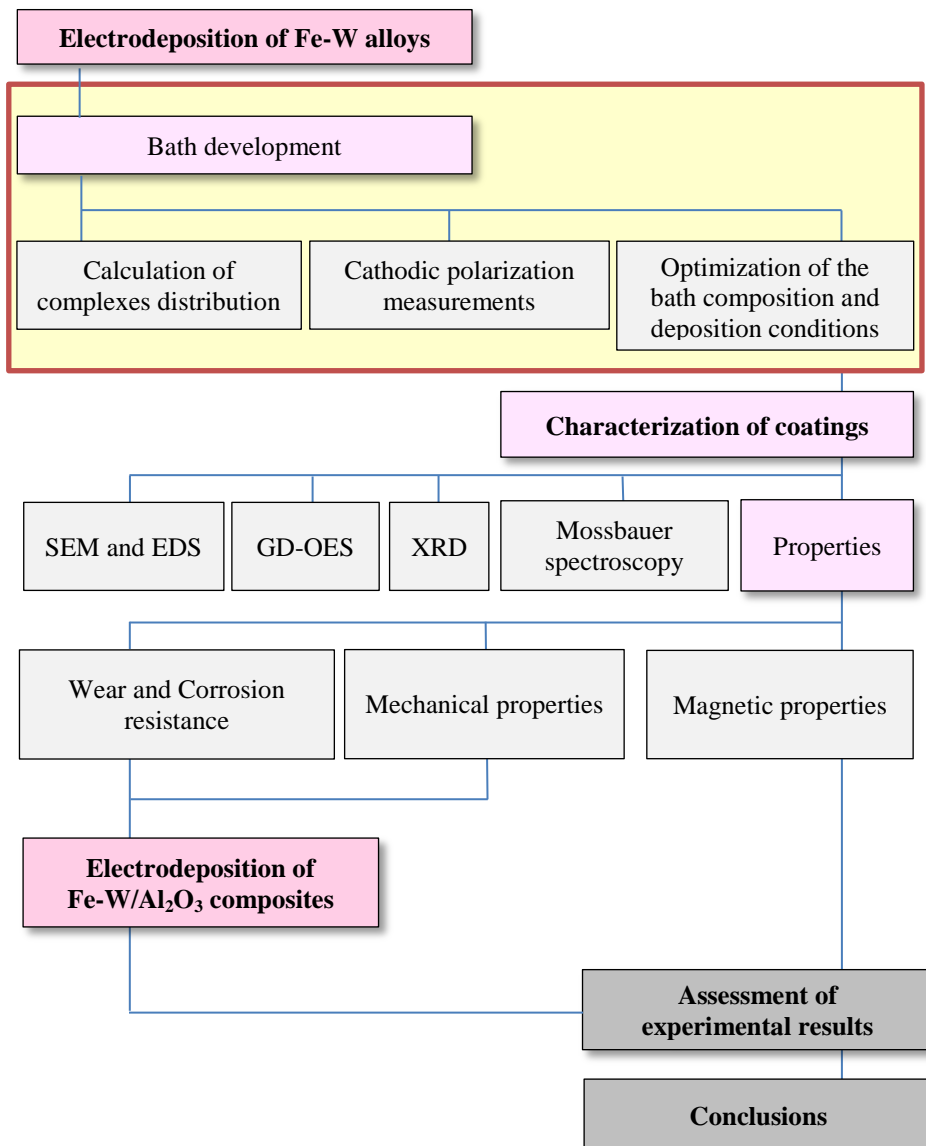
Fig. 2. The research methodology for investigation of Fe-W alloys and composite coatings.
2 pav. Fe-W lydinių bei kompozitų tyrimų metodologija.

2.1 Calculation of complexes distribution

Simulation of complexes distribution is an approach to understand the complex bath chemistry of electrolyte and unveil the factors controlling the performance of the plating solution. The distribution of metal species in electrolyte is a function of other species in the bath and also is a function of pH. This function can be calculated by solving an equation set, which includes the following relations and quantities: (i) the equilibrium constants for all compounds added to or formed in the solutions, using values of equilibrium constants (β); (ii) the mass balance equations for all forms in the equilibrium mixture (13), and (iii) the charge balance equation, where "Cat" and "An" denote cation and anion, respectively (14).

$$> ?_{\hat{e}} \quad L \quad \tilde{A} >_{\dot{U}}^{\acute{a}>} \, ? \, ? \tag{13}$$

$$\tilde{A} J_{\dot{U}}\% = {}^{\acute{p}}_{U} ? \, L \quad \tilde{A} J_{\dot{U}}\# \quad {}^{\acute{a}?}_{U} \, ? \tag{14}$$

For this purpose, a complete system of equations related to all equilibria in the solutions was solved using adopted Maple6 (Waterloo Maple Software and University of Waterloo). The Table 2 lists the equilibrium constants used in these calculations.

This methodology was applied to calculate the complexes distribution in a new glycolate-citrate electrolyte and estimate the thermodynamic stability of Fe-based solutions. More specific details on calculation are given in Paper 1 and Paper 2.

2.2 Electrodeposition of coatings

Electrodeposition of Fe-W and Fe-W/Al$_2$O$_3$ coatings was performed in a typical three-electrode cell, where Cu plate was used as working electrode, Ag/AgCl/KCl$_{sat}$ as reference electrode and platinized titanium mesh was used as a counter electrode. All the potentials given in this work are measured against reference electrode. Prior to electrodeposition, the substrates were degreased in acetone and ethanol, and activated in 2 M sulfuric acid for 1 minute in an ultrasonic bath, followed by Ni-seed layer electrodeposition at 30 mA/cm^2 for 1 min from chloride bath operated at 65 °C in order to improve adhesion. The electrolyte volume was kept at 250 mL. Polarization measurements have been performed in order to estimate the deposition conditions for Fe-W alloys. The curves were recorded at different temperatures at 5 mV/s scan rate using AUTOLAB system (GPES software), and later were corrected for ohmic drop that was determined using FRA 4.9 software. All solutions were open to air.

Table 2. *Reactions and their equilibrium constants, β, expressed as logβ used for calculations.*

OHₒₒWHO¡Pusiausvyrinės reakcijos ir skaičiavimuose panaudotos jų pusiausvyros konstantos, Ε, išreikštos kaip logɓ.

Equilibrium reaction	logβ
Citric acid [112] ***and Glycolic acid*** [113]	
← ⁸? E > ∧ ← ⁷? 7	11.8
←⁸? E t > ∧ 6← ⁶?	17.52
← ⁸? E u > ∧ 7← ?	21.89
← ⁸? E v > ∧ 8←	24.83
Ž ? E > ∧ 6Ž	3.83
Fe(III) hydrolysis [114]	
‡⁷> E 6 ∧ ‡ ⁶> E >	-2.19
‡⁷> E t 6 ∧ ‡ : ;6> E t >	-5.76
‡⁷> E u 6 ∧ ‡ : ;7 E u >	-14.30
‡⁷> E v 6 ∧ ‡ : ;8 E v >	-21.71
t ‡⁷> E t 6 ∧ ‡6: ;6⁸> E t >	-2.92
W(VI) hydrolysis [115]	
y > E x 86? ∧ u 6 E :65 9?	53.98
sv > E st 86? ∧ y 6 E 56 85 54?	110.03
sz > E st 86? ∧ { 6 E 56 7 :?	132.51
86? E > ∧ 8?	4.6
8? E > ∧ 6 8	3.6
Fe(III)- and W(VI) with glycolic acid [116,117]	
‡ ⁷> E Ž ? ∧ Ž 6>	2.90
‡ ⁷> E Ž ? ∧ Ž > E >	1.59
‡ ⁷> E tŽ ? ∧ ‡ :Ž ;Ž E >	4.00
‡ ⁷> E uŽ ? ∧ ‡ :Ž ;6Ž ? E >	5.50
86? E t Ž ? E t > ∧ 6Ž 6? E t 6	15.7
Fe(III)-citric acid [118,119]	
‡ ⁷> E ← ⁷? ∧ ‡	24.84
‡ ⁷> E t← ⁸? ∧ ‡ :← ;6 9?	32.73
‡ ⁷> E t← ⁸? E > ∧ ‡ :← ;6 8?	38.74
‡ ⁷> E t← ⁸? E t > ∧ ‡ 6:← ;6 7?	43.53
t‡ ⁷> E t← ⁸? ∧ ‡ 6:← ;6 6?	48.0
‡ ⁷> E t← ⁷? E ? ∧ ‡ :← ;6 ;?8?	10.46
‡ ⁷> E ← ⁸? ∧ ‡ ?	11.40
W(VI)-citric acid [63]	
86? E ← ⁷? E > ∧ 8;:← ; ?8?	10.21
86? E ←⁷? E t > ∧ 8;:← ; 6 7?	17.03
86? E ← ⁷? E u > ∧ 8;:← ; 7 6?	21.67
86? E ← ⁷? E v > ∧ 8;:← ; 8?	22.82
t 86? E t ← ⁷? E v > ∧ 8;6:← ;6 8 7?	34.89
t 86? E t ← ⁷? E w > ∧ 8;6:← ;6 9 9?	39.3
86? E t ← ⁷? E x > ∧ 8;:← ;6 :? 6?	34.51
t 86? E ← ⁷? E v > ∧ 8;6:← ; 8 7?	31.7

31

In order to obtain Fe-W composites, the base Fe(III) glycolate-citrate electrolyte was used: 1 M glycolic acid, 0.3 M citric acid, 0.1 M $Fe_2(SO_4)_3$ and 0.3 M Na_2WO_4. Before adding the particles, the bath pH was adjusted to 7.0 with NaOH at room temperature. Sub-microsized alumina particles (purchased from Alfa Aesar) with the concentration of 25 g L^{-1}, 50 g L^{-1} and 100 g L^{-1} were added to the base electrolyte and the suspensions were intensively stirred at 300 rpm for 24 hours prior to first electrodeposition in order to hydrate the particles. Before starting the electroplating, the electrolytes were placed in an ultrasonic bath for 10 min to prevent agglomeration. The electrodeposition set-up was similar to that used for Fe-W alloys electrodeposition.

2.3 Characterization of coatings

Scanning Electron Microscopy (SEM) is one of the most commonly used imaging techniques to obtain the high–resolution images of a solid sample surface in micro- and nanometer scale. SEM analysis was used for characterization of Fe-W alloys and Fe-W/Al_2O_3 composite coatings in Papers 1-5.

Confocal microscopy is an optical imaging technique, which allows to obtain micrographs with increasing contrast and optical resolution as compared to classical light microscopy, what is achieved by means of using a spatial pinhole to block out-of-focus light in image formation. The 3D images of Fe-W surfaces were obtained by Leica DCM confocal system as described in Paper 2.

Energy-dispersive X-ray Spectroscopy (EDS) is an analytical technique commonly used for qualitative and quantitative determination of elemental composition of a sample. Nevertheless, EDS analysis has several limitations with respect to quantification of light elements and low concentrations due to two main issues: (i) elements with $Z < 11$ emit low energy X-rays which are subject to strong absorption by the specimen; and (ii) the yield of fluorescence increases with the atomic number and de-excitation of light elements occurs mainly by the emission of Auger electrons. The specific experimental details on EDS analysis are provided in Papers 1-5.

Glow Discharge Optical Emission Spectroscopy (GD-OES) has been recognized as a powerful tool for reliable in-depth elemental analysis of solids. The principle of GD-OES is the analysis of the light emitted by excited atoms after ejection from a sample by bombardment with Ar^+ created in a glow discharge. The spectroscope operates over the wave length ranging from 110 nm to 800 nm. Thus, GD-OES can be used for accurate quantification of light elements such as hydrogen, oxygen, carbon and

sodium. This method has been employed for in-depth elemental analysis of Fe-W layers as described in Paper 3.

Inductively Coupled Plasma Optical Emission Spectrometry (ICP-OES) is an analytical technique, which gives the elemental composition of a sample. The spectrometer analyses the solution, where the material has been previously dissolved. In this study ICP-OES technique was used to obtain a composition of the calibration samples for GD-OES analysis and also for normalization of magnetic hysteresis loops by mass of the material (Paper 2 and 3).

X-ray Diffraction analysis (XRD) is a structural analysis technique. It provides information on crystal structure, phase, preferred crystal orientation (texture), and other structural parameters, such as average grain size, crystallinity, strain, and crystal defects. However, the application of XRD analysis for investigation of the phase composition in amorphous/amorphous-like materials is limited. The characterization of various as-deposited and annealed Fe-W coatings by XRD has been performed in Papers 1-4.

Mössbauer spectroscopy is a versatile technique that can give very precise information about the chemical, structural and magnetic properties of material. The most commonly studied isotope which has a probability to absorb the photon is ^{57}Fe, what makes Mössbauer spectroscopy analysis appealing for the investigation of nanocrystalline and amorphous Fe-W alloys, as it was discussed in Paper 2.

Vibrating Sample Magnetometry (VSM) is a method to estimate magnetic properties of a material. The sample is mechanically vibrated within a uniform magnetic field, and the change in the magnetic field of the sample induces an electrical field in the sensing coils that is proportional to the magnetization of the sample. The software converts the signal change to values and gives the graphical relationship between the saturation magnetization and the magnetic field strength, known as hysteresis loops. The specific experimental conditions are provided in Paper 2.

Nanoindentation is one of the most common and versatile technique used for investigation of mechanical behavior of the materials at very small length scales, such as hardness, elastic modulus, plasticity, strain, stress, etc. During the nanoindentation the sample is loaded by an indenter (usually made of diamond) in a control mode. While indenting, the dependence of the load applied on the penetration depth of the tip is recorded by the software. Using obtained load-displacement curves and known geometry of the indentation tip, one can express a variety of mechanical characteristic of material, based,

33

for example, on the Oliver-Phar method [120]. Fe-W coatings have been subjected to nanoindentation tests as described in Papers 2 and 4.

Wear tests were used to estimate the resistance of the surface to wear in a specific environment under well-defined conditions. In this study, ball-on-flat configuration was employed for the evaluation of the tribological behavior of electrodeposited Fe-W alloys under dry and lubricating conditions, and ball-on-disc configuration test was used for the investigation of Fe-W/Al_2O_3 composite coatings under dry friction. All the tribological tests were performed in ambient air at 20 ± 2 °C and 48-55% relative humidity and corundum ball with 6 mm diameter was the counter body. The experimental details on the investigation of tribological behavior of Fe-W alloys are given in Paper 5. The evaluation of wear resistance of Fe-W/Al_2O_3 composite coatings was carried out under dry friction conditions by applying 2 N load for 500 m with a rotation speed of 4 cm s^{-1} (rotation diameter 3 mm). The specific wear rate was calculated according to the equation (15):

$$K = \frac{A \cdot l}{L \cdot D} \qquad (15)$$

where K is the specific wear rate (mm^3/N m), A is the cross-section area of wear track (mm^2), l is the length of the wear track (mm), L is the applied load and D is the sliding distance.

Electrochemical Impedance Spectroscopy (EIS) is an electrochemical method, which is widely applied to study the kinetics of corrosion or deposition of metals and alloys. The method is based on the sinusoidal potential perturbation at different frequencies and registration of the electrode response to these perturbations. The interpretation of EIS data is traditionally relied on fitting the experimental data to the equivalent electrical circuit elements. The elements are then attributed to physical processes in the system (e.g. double layer capacitance, charge transfer resistance, etc.). In this study, the corrosion measurements were conducted in 0.1 M NaCl medium by applying the sinusoidal voltage with 5 mV amplitude in the frequency range of 10 kHz - 0.01 Hz, and the fitting of EIS data has been performed using Z-View software.

Potentiodynamic polarization is the characterization of a metal or alloy by its current-potential relationship, which can be used to determine various corrosion characteristics of metallic specimens in aqueous environments such as tendency to passivation, corrosion current density, corrosion rate, etc. The measurements were conducted in 0.1 M NaCl medium in the potential range from -1 to 1 V at a sweep rate of 1 mV/s.

2.4 Summation

Different physical, chemical and electrochemical methods and theoretical approaches have been used for bath development and characterization of Fe-W alloys, which allowed obtaining a clear picture of the overall coating performance and map the composition-properties interrelation.

3. RESULTS AND DISCUSSIONS

The results presented in five attached articles are shortly described in this section emphasizing the most important findings of the research, while the detailed discussions are provided in appended articles. Whenever is need, some additional data not included in the publication are provided. In addition, the list of investigated properties of the obtained Fe-W based materials and general conclusions are presented.

3.1 Development of Fe(III)-based glycolate-citrate bath

As was discussed in *chapter 1.3*, Fe(II) compounds are thermodynamically unstable in the open to air solutions and oxidize fast to Fe(III). Therefore, efforts were devoted to the development of thermodynamically stable solution for Fe alloys electrodeposition based on Fe(III) compounds. However, the applicability of Fe(III)-based solutions is limited due to the formation of sparingly soluble Fe(III) hydroxide. Indeed, the solubility product of $Fe(OH)_3$ is in order of 10^{-36}, that means the stability of the bath is governed by the concentration of "free" Fe^{3+} ions. Therefore, the development of stable Fe(III)-based plating bath consists in the selection of suitable complexing agent able to reduce the concentration of Fe^{3+} below the maximum thermodynamic concentration $[Fe^{3+}]_{sat}$, which can be calculated from the solubility product of iron hydroxide according to equation (16):

$$\left[Fe^{3+}\right]_{sat} = \frac{L_{Fe(OH)_3}}{K_{H_2O}^2}\left[H^+\right]^3 \tag{16}$$

where L is the solubility product of hydroxide and - K_W is ionic product of water.

Previous research on Ni-W electrodeposition [66] suggested that glycolic acid (H_2Gly) can be a better candidate for the plating bath formulation, as compared to citrate electrolyte because it increases the current efficiency and the W content in the alloy.

Our study on Fe-W electrodeposition from Fe(III)-based electrolytes containing glycolic acid as a complexing agent shows that in the solutions containing just one complexing agent, that is glycolate, the concentration of "free" iron ions is approaching the thermodynamic concentration calculated from the equation (16), $[Fe^{3+}] \approx [Fe^{3+}]_{sat}$. Therefore, these electrolytes are in the thermodynamically metastable state and can be stable only for a short period, due to kinetic peculiarities of hydrolysis in the aqueous solutions. However, an addition of citric acid to the glycolate solution increases the stability of the bath for the whole pH range due to the formation of Fe(III) and W(VI) complexes compounds with glycolate and citrate anions, and

lowering the concentration of "free" Fe^{3+} ions (more details are given in Paper 1). The suggested glycolate-citrate bath was studied by simulation of complexes distribution in order to unveil the factors controlling the bath performance.
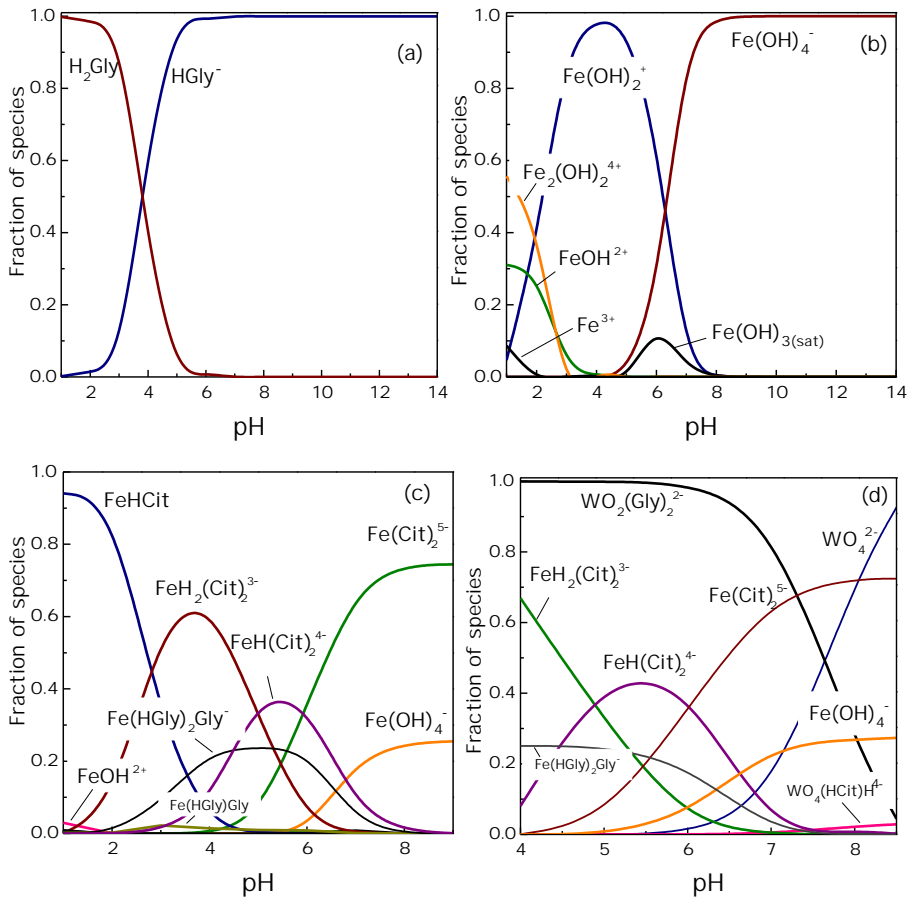
Fig. 3. Calculated complexes distribution: for glycolic acid solution at the following total concentrations of constituents $[H_2Gly]_{tot}=1.0M$ (a); iron species in water solution $[Fe(III)]_{tot}=0.2M$ (b); iron species in glycolate-citrate solution, $[Fe(III)]_{tot}=0.2M$, $[H_2Gly]_{tot}=1.0M$, $[H_4Cit]_{tot}=0.3M$ (c); and Fe and W species in glycolate-citrate solution $[Fe(III)]_{tot}=0.2M$, $[W(VI)]_{tot}=0.3M$, $[H_2Gly]_{tot}=1.0M$, $[H_4Cit]_{tot}=0.3M$ (d).

3 pav. Apskaičiuotas kompleksų pasiskirstymas glikolio rūgšties tirpaluose esant šioms bendroms pradinių medžiagų koncentracijoms: $[H_2Gly]_{tot}=1.0M$ (a); Fe(III) junginiai vandeniniame tirpale $[Fe(III)]_{tot}=0,2M$ (b); Fe(III) junginiai glikoliatiniame-citratiniame tirpale: $[Fe(III)]_{tot}=0,2$ M, $[H_2Gly]_{tot}=1.0M$, $[H_4Cit]_{tot}=0,3M$ (c); Fe(III) ir W(VI) junginiai glikoliatiniame-citratiniame tirpale: $[Fe(III)]_{tot}=0,2M$, $[W(VI)]_{tot}=0,3M$, $[H_2Gly]_{tot}=1.0M$, $[H_4Cit]_{tot} = 0,3M$ (d).

Citric acid is one of the most extensively studied complexing agents for W alloys electrodeposition and the distribution of citrate species was previously evaluated in [16,46]. In contrast, the use of glycolic acid as a complexing agent for alloys deposition was not broadly explored yet. The Fig. 3a shows the distribution of mono-protonated glycolic acid species. As it is seen, the glycolic acid is 50 % deprotonated at pH ~ 4, and completely protonated at pH > 6.

Many studies report the importance of metal hydroxyl species in the mechanism of iron-group metals and alloys electrochemical formation. Therefore, the distribution of Fe^{3+} species in aqueous solution was studied prior to the formulation of a final equation set. According to the Fig. 3b, the $Fe(OH)_2^+$ specie predominates at pH range from 2 to 7, while above pH 7 the predominant specie is $Fe(OH)_4^-$. The addition of complexing agents (glycolic and citric acids) shifts the equilibria in solution toward the formation of complexes compounds. In fact, different Fe(III)-citrate complexes dominate over the pH range: FeHCit at pH 1-3, $FeH_2Cit_2^{3-}$ at pH 3-5, $FeH(Cit)_2^{4-}$ at pH 5-6 and $FeCit_2^{5-}$ specie dominates at pH above 7 (Fig. 3c). The maximum fraction of complex compound of Fe(III) with glycolic acid is observed at pH 4-7; approximately 20% of all iron ions are in $Fe(HGly)_2Gly$ complex.

Fig. 3d shows the calculated distribution of Fe and W species in a new glycolate-citrate electrolyte, which was used in this research for electrodeposition of Fe-W alloys. An addition of tungstate WO_4^{2-} ions modifies the distribution of iron complexes due to the concomitant formation of W(VI) and Fe(III) complexes with citric and glycolic acid. Remarkably, 99 % of tungsten in solution is present in the form of glycolate complex up to pH 7. The reduction of $WO_2(Gly)_2^{2-}$ concentration at pH > 7 is accompanied with an increase in concentration of "free" WO_4^{2-} ions. Citric acid bonds only ~ 5 % of tungsten ions at this pH. In contrast, the major part of iron is complexed by citrate ligands within the whole pH range, suggesting that namely the formation of Fe-citrate complexes stabilizes the glycolate-citrate electrolyte. Noticeably, almost 25 % of iron is present in form of hydroxo-complex $Fe(OH)_4^-$ at pH > 7. The formation of W-glycolate complex over the W-citrate is expected to have a significant influence on the electrodeposition process of Fe-W alloys, similarly to Ni-W electrodeposition [66].

Indeed, the distribution of Fe(III) and W(VI) complexes compounds significantly influence the deposition rate of Fe, W, as well as the rate of side reaction (mainly hydrogen evolution), hence resulting in a variation of W content in alloy with pH. The calculated partial currents of Fe, W deposition and side reaction as a function of pH reveal the correlation

between the fraction of predominant specie in the bath, W content in alloy and deposition current efficiency. The Fig. 4 illustrates the variation of the W content and alloy deposition current efficiency as a function of pH (the graphical dependences of partial currents are published in Paper 2). The results show, that an increase of W content in alloy is accompanied with the increase in current efficiency, which can reach up to 60-70 % when deposition is carried out at pH nearly 7, at 65 °C.
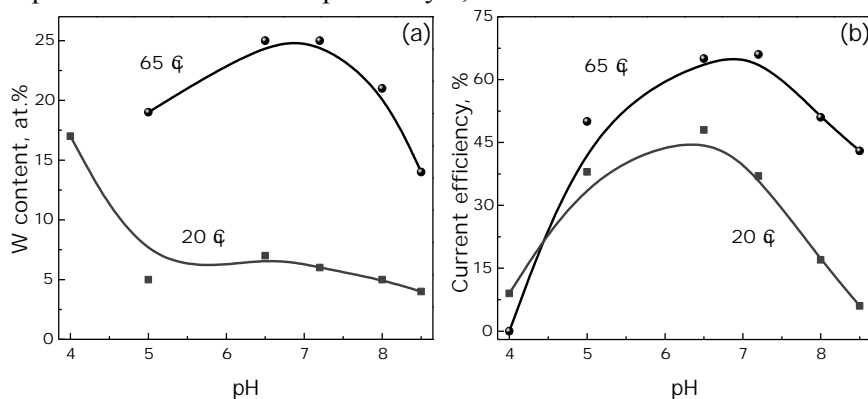
Fig. 4. *Influence of pH on: W content in the alloy (a); current efficiency at the cathodic current density of -15 mA cm^{-2}(b). Electrodeposition bath contained 1.0 M glycolic acid, 0.3 M citric acid, 0.1 M Fe$_2$(SO$_4$)$_3$ and 0.3 M Na$_2$WO$_4$. Electrodeposition temperature is indicated next to the corresponding curve.*
4 pav. *pH įtaka: W kiekiui lydinyje (a); srovinei išeigai esant katodinės srovės tankiui 15 mA cm^{-2}(b). Elektrolito sudėtis: 1,0M glikolio rūgštis, 0,3M citrinų rūgštis, 0,1M Fe$_2$(SO$_4$)$_3$, 0,3M Na$_2$WO$_4$. Elektrolito temperatūra nurodyta šalia kreivių.*

Remarkably, the CE of Fe-W alloys electrodeposited from glycolate-citrate bath is considerably higher than for other Fe-W alloys deposited from Fe(II)- or Fe(III)-based electrolytes achieved by using an insoluble anode [82,121]. As depicted in Fig. 5, W-glycolate complex is a molecule with small volume which can move faster to the cathode and thus benefit the electricity transportation and discharge easier as compared to complex W-citrate molecules:
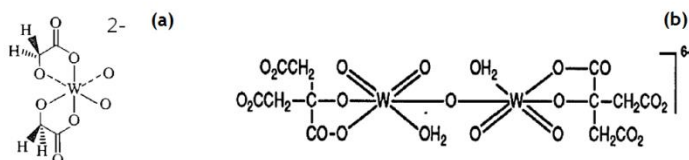
Fig. 5. *The structure of W(VI) complexes: glycolate complex [117] (a); one of the W(VI)-citrate complexes [63] (b) .*
5 pav. *W(VI) kompleksų struktūros: glikoliatinio komplekso [117] (a); viena iš W(VI) citratinių kompleksų [63] (b).*

39

At higher pH the current efficiency drops significantly, as well as the W content in alloy (Fig. 4b). This correlates well with the calculated complexes distribution. The decrease in concentration of predominant specie $WO_2Gly_2^{2-}$ and significant increase in the concentration of WO_4^{2-} ions at pH>7. Furthermore, the electrodeposition of Fe-rich alloys from weakly alkaline glycolate-citrate solution can be correlated with increase in concentration of $FeCit_2^{5-}$ and hydroxo-complex $Fe(OH)_4^-$ (Fig. 3d); both can form a parallel path for Fe(III) discharge and thus result in an increased Fe content in the alloy.

It is worth notice, that Fe-W alloys containing > 16 at.% of W can be produced only at elevated temperatures. Therefore, the alloys deposited at 65 °C and having > 16 at.% of W are considered in this study as W-rich, while Fe-W alloys deposited at room temperature and having < 10 at.% of W are considered W-low (or Fe-rich). Accordingly, 10-15 at.% of W is considered as a moderate W content.

3.2 Composition and structure of electrodeposited Fe-W alloys

Electrodeposited Fe-W alloys are typically gray in appearance. Fig. 6 shows the representative SEM images of the surface morphology of Fe-W deposits with different W contents.

It can be seen, that the surface morphology is strongly influenced by W content in the alloys. The surface of Fe-W coatings with up to 10 at.% of W is porous and shows a micro-globular structure with high inter-granular distances between globules resembling a cauliflower structure. The cross-section analysis of W-low samples depicts the presence of internal cracks, which appear most probably due to abundant hydrogen evolution when depositing at room temperature. Further increase in W content leads to a disappearance of pores and substantial surface refining. The cross-section area of W-rich samples appears to be cracks-free (cross-sectional images are shown in Paper 3). As shown by confocal microscopy analysis, the average roughness of the electrodeposited samples decreases linearly from ~ 62 nm to ~ 13 nm as the W content in the alloys increases from 6 to 25 at.%, and thus Fe-W alloys with 15-25 at.% of W generally exhibit a mirror-like appearance. It is worth notice that all the coatings were well-adhered to the substrate.
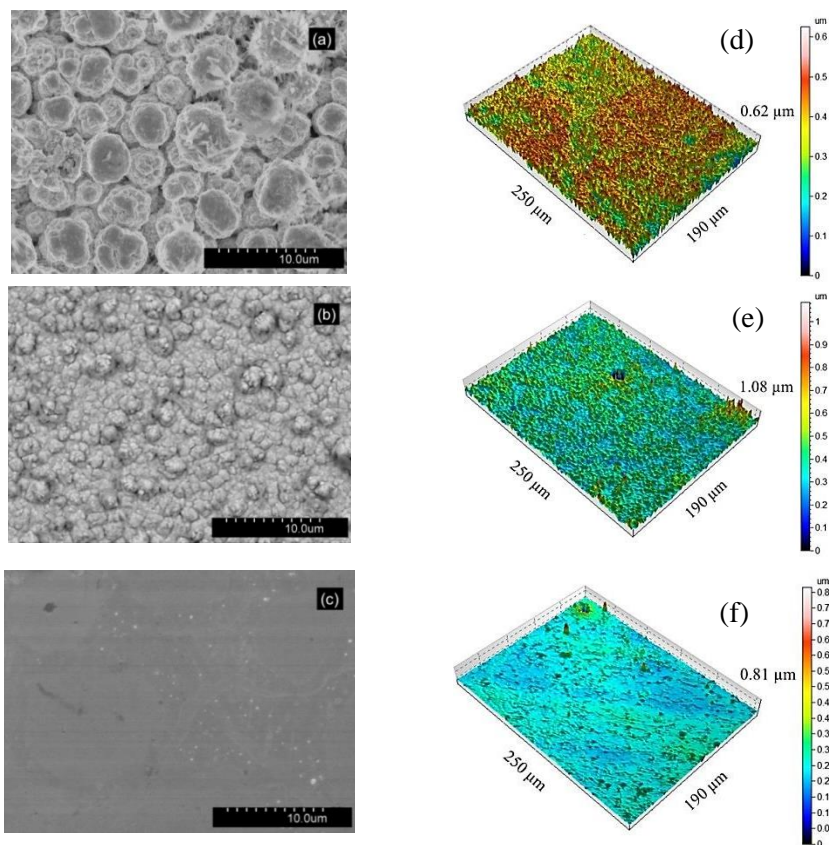
Fig. 6. *SEM images of the surface of Fe-W alloys with different W content: 6 at.% (a); 12 at.% (b); 25 at.% (c); and their corresponding confocal microscopy images (d-f).*
6 pav. *Fe-W lydinių, turinčių skirtingą W kiekį, SEM atvaizdai: 6 at.% (a); 12 at.% (b); 25 at.% (c); jų atitinkami atvaizdai, gauti konfokaliniu mikroskopu (d-f).*

The presence of high amount of oxygen and carbon was detected by EDS analysis on the Fe-W alloys surface. Previous studies on electrodeposited Co-W and Ni-W alloys also addressed the question whether the tungsten alloys contain significant amounts of co-deposited oxygen or it is mainly present in the top surface layer [13,122]. In order to investigate the distribution of non-metallic elements within the thickness of Fe-W layers, the samples with different W content were subjected to GD-OES analysis.

41
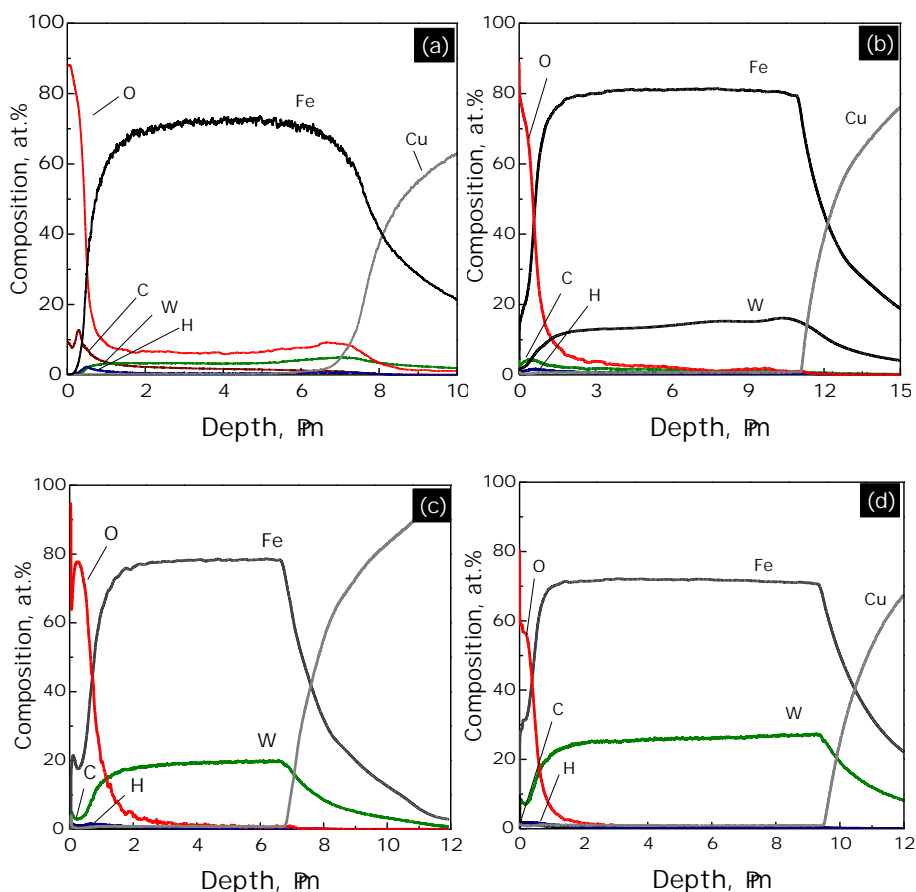
Fig. 7: *Compositional depth profiles obtained by GD-OES on Fe-W samples with different composition: 4 at.% of W, pH 6.5, 20 °C (a); 16 at.% of W, pH 5, 65 °C (b); 20 at.% of W, pH 8, 65 °C (c); and 25 at.% of W, pH 6.5, 65 °C (d).*
***7 pav.** Fe-W lydinių, turinčių skirtingą W kiekį, sudėties profiliai, nustatyti GD-OES metodu: W 4 at.%, pH 6.5, 20 °C (a); W 16 at.%, pH 5, 65 °C (b); W 20 at.%, pH 8, 65 °C (c); W 25 at.%, pH 6.5, 65 °C (d).*

Indeed, the characteristic compositional depth profiles reveal the presence of a strongly oxidized top surface layer of ~1-2 μm thickness, while only traces of O and C were observed in the bulk of the coatings (Fig. 7). The surface layer consists mainly of O and Fe and contains relatively high amounts of C and H as compared to the concentration deeper down in the material. In fact, the formation of strongly bonded O-rich chemisorbed layer on the top of W containing alloy is expected because the O activation energy for desorption from the surface is high, 269-480 kJ/mol [13]. The presence of carbon and hydrogen contaminations on the surface of electrodeposited coatings can be explained by absorption of some citrate/glycolate species

42

from the plating electrolyte after electroplating. In addition, Fig. 7 depicts the constant ratio between the contents of Fe and W in deposit inside the layers, demonstrating a homogeneous growth of the alloy during electrodeposition independently of deposition temperature and plating pH.

Generally, the structure of electrodeposited W alloys transforms from nanocrystalline to amorphous-like as the W content increases [9,123]. Representative XRD patterns of electrodeposited Fe-W alloys with various W contents are shown in Fig. 8. It is observed, that the corresponding values of $2\Theta_{hkl}$ characteristic peaks for pure iron shift towards lower angles as the W content increases. At the same time, the peaks become broader and intensity reduces, thus only one broad peak appears at $\sim 43\,°$, when the tungsten content reaches its maximum in the alloy, that is, the 25at.%. The broadening of the XRD peaks is commonly attributed to the reduction of crystallite size according to Scherrer equation:

$$B(2\Theta)T\ \frac{K\ \tilde{}\ C}{L\ \cos\tilde{}}$$
(17)

where B is the peak width, K is a Scherrer constant which varies from 0.62 to 2.08 (for cubic crystals commonly taken as 0.94), λ is a wavelength of X-rays, L is the crystallite size and Θ is a peak position.

The calculated values of the Fe-W crystallite size are given in Table 3. Despite the calculated crystallite size of Fe-W alloys with maximum tungsten content is less than 10 nm, it is generally considered that the structure of the tungsten alloys obtained by electrodeposition is not perfectly amorphous and must be referred to as "amorphous-like" [122].

Table 3. *Estimated crystallite size, lattice constant (α) and interplanar distance (d) obtained for Fe and Fe-W deposits plated from the glycolate-citrate bath.*
OHⱭHO¡Fe ir Fe-W lydinių, gautų iš glikoliatinio-citratinio tirpalo, apskaičiuoti kristalitų dydžiai, gardelės konstantos (a) ir tarpplokštuminiai atstumai (d).

W content (at.%)	(110) peak position 2Θ (degrees)	Estimated crystallite size (nm)	α_0 (Å)	d_{110} (Å)
0	44.53	37.3	2.8788	2.0346
4	43.84	34.1	2.9219	2.0661
6	43.52	31.5	2.9423	2.0795
12	43.46	18.0	2.9462	2.0832
17	43.18	15.8	2.9643	2.0951
21	42.62	10.1	3.0014	2.1213
25	42.64	7.5	3.0001	2.1214
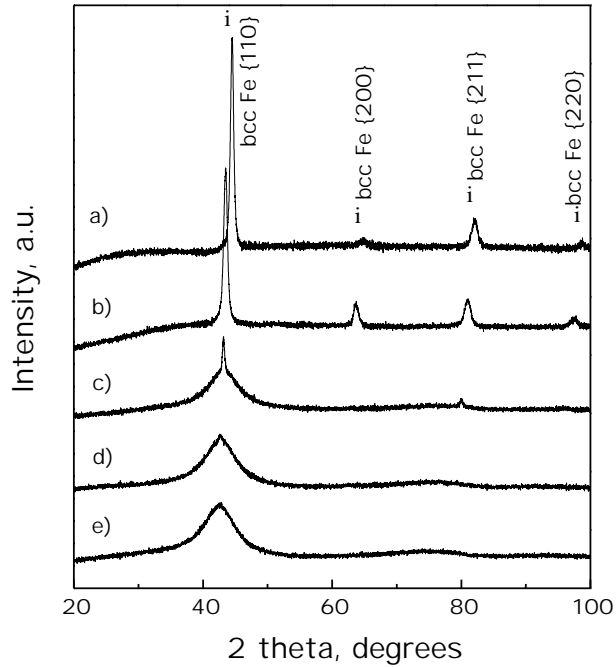
Fig. 8. *X-ray diffraction patterns recorded for Fe (a) and Fe–W electrodeposits having various W content: 6 at.% (b), 17 at.% (c), 21 at.% (d), and 25 at.% of W (e). Peaks were identified based on ASTM Cards 06-0696 (Fe).*
***8 pav.** Fe (a) bei Fe-W lydinių, turinčių skirtingą W kiekį, rentgeno spindulių difrakcijos spektrai: 6 at.% (b); 17 at.% (c); 21 at.% (d); 25 at.% (e). Smailės identifikuotos pagal kortelę ASTM Cards 06-0696 (Fe).*

The shift in corresponding $2\Theta_{hkl}$ values can be explained according to Bragg's law, which states that the values of Θ_{hkl} depend on the lattice parameter, α_0, and average closest distance, d_{hkl}, between atoms in the lattice in a following way:

$$\sin^2 \Theta_{hkl} = \frac{\lambda^2}{4\,\alpha_0^2}(h^2 + k^2 + l^2) \tag{18}$$

and for bcc crystals:

$$d_{hkl} = \frac{\alpha_0}{\sqrt{h^2 + k^2 + l^2}} \tag{19}$$

where λ - the wavelength of X-rays (in Å), Θ_{hkl} - the Bragg angle for (hkl) plane (in radians), hkl – Miller indexes.

The α and d_{110} values calculated from the strongest peak position are shown in Table 3. An increase in lattice parameter and interplanar distance is proportional to the atomic fraction of W and it is most likely due to the

44

partial replacement of some Fe atoms by bigger W atoms in the lattice and formation of tungsten solid solution in iron. Formation of solid solution is rather typical for electrodeposited alloys and for Fe-W it is supported by the fact that Fe and W have homotypic lattices differing by not more than 15 % [3] ($\alpha_{bcc,Fe}$=2.8665 Å, α_{bccW}=3.1652 Å [124]).
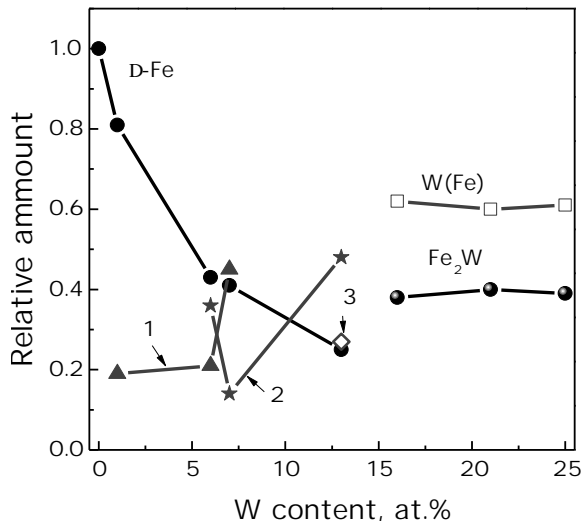
Fig. 9. Relative amount of phases identified by Mössbauer spectroscopy. 1, 2 and 3 correspond to the compounds where 1, 2 or 3 Fe atoms are replaced by W, respectively.
9 pav. Santykiniai fazių kiekiai identifikuoti iš Mosbauerio spektroskopijos duomenų. 1, 2 ir 3 atitinka junginius, kuriuose 1, 2 arba 3 Fe atomai pakeisti W atomais.

In order to validate this hypothesis the Mössbauer spectroscopy analysis was performed on electrodeposited Fe and Fe-W samples with increasing W content. Indeed, it is found that with the increase in W content, the relative amount of α-Fe phase decreases, while the amount of Fe(W) solid solution increases, that is, the observed sub-spectra having smaller hyperfine fields correspond to some iron atoms being replaced by W atoms in α-Fe lattice. Based on hyperfine parameters there are up to 3 iron atoms replaced by W atoms (1, 2 and 3 in Fig. 9). All spectra of W-rich samples (16–25 at.%) have almost the same shape, which can be ascribed to the Fe_2W intermetallic compound and Fe solid solution in W. The detailed discussion on Mössbauer spectroscopy analysis and its utility for evaluation of amorphous-like Fe-W alloys is provided in Paper 2.

Electrodeposited Fe-W alloys undergo phase transformation when subjected to elevated temperatures. Annealing tests coupled with XRD

45

analysis show that Fe-W alloys with maximum W content (25 at.%) exhibit outstanding thermal stability retaining a fully amorphous-like structure up to 400 °C. The recrystallization starts at 600 °C, however, a partially amorphous structure is kept even after annealing at 800 °C. In fact, the amount of nanocrystalline phase consisted of α-Fe, Fe_2W and Fe_6W_6C was estimated to be around 24 %. Moreover, the presence of light elements, O and C detected in composition of as-deposited coatings by EDS and GD-OES analyses, lead to precipitation of Fe_3W_3C and Fe_6W_6C phases in W-rich alloys after annealing at 800 °C, and to precipitation of $FeWO_4$ phase in nanocrystalline W-low coatings annealed at 600 °C. The thorough discussion on the annealing treatment effects is given in Paper 3 and 4.

### 3.3 Mechanical and magnetic properties of Fe-W alloys

Mechanical and magnetic properties of Fe-W alloys were evaluated as a function of their composition and internal structure in order to unveil the perspectives on their sustainable application. The values of hardness and elastic modulus (reduced Young's modulus) extracted from the load-displacement curves using the method of Oliver and Pharr are presented in Fig. 10. The increase of tungsten leads to an increase in both hardness and elastic modulus. Hardness increases from 4.1 GPa for the alloy with 6 at.% W to 10.4 GPa for the alloy with 25 at.%. of W. Accordingly, the elastic modulus increases from 83 to 216 GPa. Among various strengthening mechanisms observed on nanocrystalline materials, the increase in hardness of electrodeposited Fe-W alloys is most likely due to the reduction of the grain size. Indeed, a linear dependence of the hardness as a function of the crystallite is obtained, as typical for Hall-Petch plots (Fig. 11[*]). Small crystallites create a large number of the gain boundaries able to impede the dislocation motion. Consequently, the plastic deformation is mainly governed by the lattice dislocation within individual grains, resulting in a higher strength. Moreover, the formation of stable intermetallic phase Fe_2W (as proven by Mössbauer spectroscopy) can contribute to the increased hardness for the samples having >16 at.% of W.

A comparison of mechanical properties of obtained electrodeposited Fe-W coatings with previously published data on W alloys with iron group metals revealed that alloys having similar W content exhibit higher hardness than Co- and Ni-W alloys and even the hardness is comparable to that of

---

[*]Corrigendum to "Mapping of mechanical and magnetic properties of Fe-W alloys electrodeposited from Fe(III)-based glycolate-citrate bath", Mater. Des. 139 (2018) 429–438

electrodeposited chromium (under similar measurement conditions). In addition, the hardness of Fe-W alloy having 25 at.% of W electrodeposited from glycolate-citrate electrolyte agrees with the data obtained for the same alloy composition produced from citrate-ammonia electrolyte. Thus, the new electrolyte can be considered as more advantageous for electrodeposition of hard Fe-W coatings in light of its environmental sustainability (Paper 2).
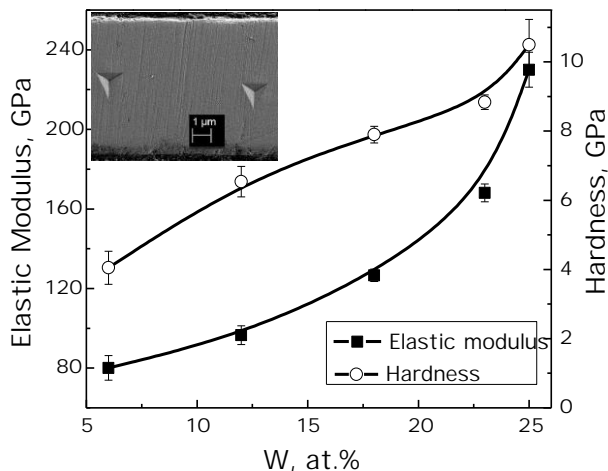
Fig. 10. *Hardness and elastic modulus of Fe-W alloys plotted as a function of the W content, at applied load of 20 mN. The SEM image of indented area of Fe-W alloy with 23 at.% of W after corresponding test is shown in insert.*
10 pav. *Fe-W lydinių kietumo bei elastinio modulio priklausomybės nuo W kiekio lydinyje esant 20 mN apkrovai. Įklijoje – Fe-23 at.% W lydinio indentavimo vieta po testavimo.*
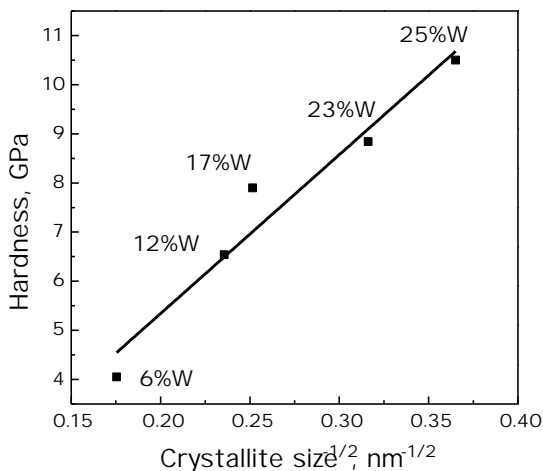
Fig. 11. *Hall-Petch plot for Fe-W alloys (hardness vs. square-root of the crystallite size).*
**11 pav.** *Fe-W lydinių Hall-Petch grafikas (kietumas nuo kvadratinės šaknies iš kristalito dydžio priklausomybė).*

47

Remarkably, that the mechanical properties of electrodeposited Fe-W alloys were enhanced through the controlled heat treatment. In fact, the hardness of Fe-W alloy with 25 at.% of W increased up to ~16 GPa after annealing at 600 °C due to the precipitation of fine α-Fe crystallites. At higher annealing temperatures, that is, the 800 °C, the hardness was reduced due to formation of coarse grains. The detailed discussion of the effect of annealing treatment on mechanical properties of Fe-W alloys is given in Paper 4.

Magnetic measurements were performed on as-deposited Fe-W alloys covering the overall composition range in order to assess the nature of these coatings (hard, semi-hard or soft) and the eventual changes in saturation magnetization. As expected, the gradual increase in W content in Fe-W alloys leads to a reduction of the saturation magnetization as due to the non-magnetic properties of W (Fig. 12). Nevertheless, alloys produced at room temperature exhibit much sharper reduction in saturation magnetization at around 12 at.% of W, while deposits produced at 65 °C and having 16 at.% of W still maintain relatively high magnetization. This can be attributed to the structural differences among the coatings obtained at different temperatures. In fact, at room temperature the formation of amorphous-like structure is achieved at 12-14 at.% of W. Meanwhile Fe-W alloys with 16-18 at.% of W deposited at higher temperature probably contain some Fe(W) crystals embedded in amorphous-like matrix, as some of the nanocrystalline peaks appear on the top of amorphous shoulder in corresponding XRD patterns (see Fig. 8c). Moreover, the high value of the saturation magnetization obtained for the nanocrystalline materials is due to the contribution of α-Fe phase, whereas the reduced values for amorphous-like coatings are due to the phase transformation to intermetallic Fe_2W and W(Fe).

While the saturation magnetization is an intrinsic property and depends on the composition of alloy, the coercivity depends on many parameters such as microstructure, grain size and shape, texture and internal stress. The coercivity values of the investigated Fe-W alloys are in the range from 20 to 90 Oe when applying the magnetic field in-plane, and from 10 to 190 Oe for the perpendicular-to-plane direction. Thus, a semi-soft magnetic character is obtained for all the samples (Paper 2).
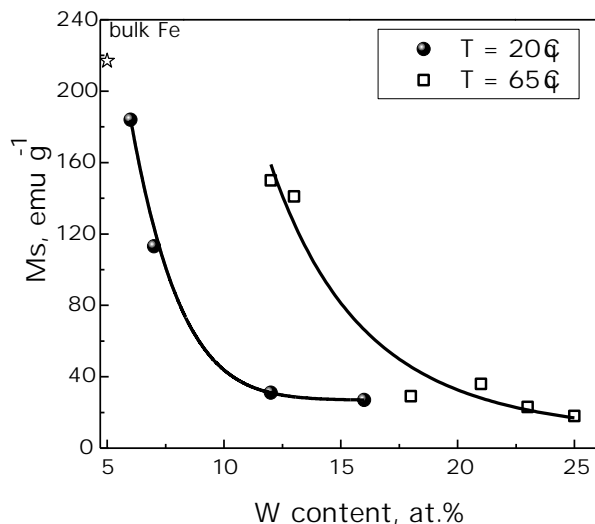
Fig. 12. *Dependence of the saturation magnetization (M$_S$) of Fe-W coatings as a function of their composition. The deposition temperature is indicated in the legend of graph. The saturation magnetization of bulk iron is taken from* [125].
**12 pav.** *Fe-W lydinių dangų magnetinio įsotinimo (M$_S$) priklausomybė nuo jų sudėties. Elektronusodinimo temperatūra pažymėta legendoje. Tūrinės Fe magnetinio įsotinimo vertė paimta iš* [125].

3.4 Corrosion and wear of Fe-W alloys

Corrosion behavior of electrodeposited Fe and Fe-W coatings having various W contents was investigated using voltammetry and electrochemical impedance spectroscopy techniques in 0.1 M NaCl solution at room temperature. Noticeably, cathodic and anodic branches of recorded voltammograms are asymmetric, probably due to the peculiarities of cathodic hydrogen evolution and active anodic metal dissolution (Fig. 13). Therefore, the polarization curves were evaluated in terms of corrosion potential E_{corr} and corrosion current density j_{corr} calculated using Tafel fit and Allen-Hickling equation (Table 4).

With increasing in W content in alloy the surface shows lower corrosion current density (j_{corr}), but the less noble corrosion potential (E_{corr}). Usually, the lowering of corrosion potential indicates the higher tendency of the electrode to be dissolved in an electrolyte. Nevertheless, the different hydrogen overvoltage on Fe-W surface with different W content may vary without a direct correlation with the corrosion rate. Moreover, accumulation of corrosion products on surface could cause the lower values of E_{corr}, thus a clear indication of corrosion resistance can be obtained by j_{corr}. The lowest corrosion current density of $6.4 \cdot 10^{-6}$ A/cm^2 is obtained for the sample with

49

the highest W content, 25 at.%. Thus, these coatings show potentially better corrosion resistance in tested medium.
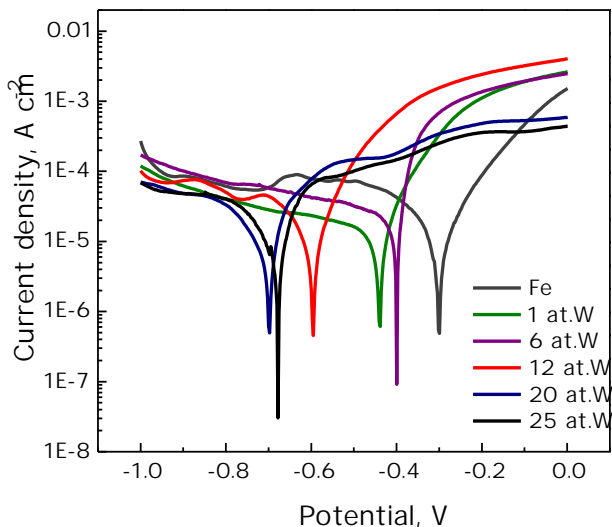
**Fig. 13.** *Potentiodynamic polarization curves for the investigated Fe-W coatings obtained in 0.1 M NaCl at 20 °C.*
13 pav. *Tirtų Fe-W lydinių potenciodinaminės kreivės 0,1M NaCl tirpale; 20 °C.*

Table. 4. *Extracted corrosion parameters from E vs. j plots shown in Figure 13 and corresponding EIS data.*
OHΨHO¡Apskaičiuoti Fe ir Fe-W lydinių korozijos parametrai iš E-j kreivių (13 pav.) ir atitinkamų EIS duomenų.

Coating	E_{corr}, V	j_{corr}, A/cm^2	R_{corr}, ˜cm^2
Fe	-0.302	$1.5 \cdot 10^{-5}$	60.03
Fe-1 W	-0.441	$1.2 \cdot 10^{-5}$	55.44
Fe-7 W	-0.399	$1.3 \cdot 10^{-5}$	39.64
Fe-10 W	-0.597	$1.0 \cdot 10^{-5}$	63.19
Fe-20 W	-0.680	$1.2 \cdot 10^{-5}$	164.35
Fe-25 W	-0.700	$6.4 \cdot 10^{-6}$	278.90

The corrosion process of Fe-W coatings was investigated by EIS. The representative Nyquist plots for Fe-W alloys with 7 at.% and 25 at.% of W are shown in Fig. 14.
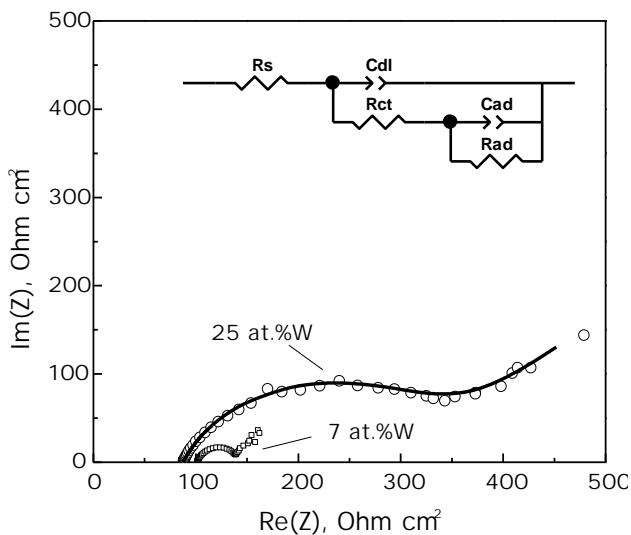
Fig. 14. *Nyquist plots for Fe-7at.%W and Fe-25at.%W alloys coatings in 0.1M NaCl solution at OCP. In insert the equivalent circuit used for data fitting is shown. R_s is a solution resistance (uncompensated resistance), R_{ct} is a charge transfer resistance having meaning of corrosion resistance; C_{dl} is a constant phase element having meaning of double layer capacitance; R_{ad} and C_{ad} are resistance and capacitance, respectively, which simulate the charge transfer on adsorbed intermediates.*

14 pav. *Fe-7at.%W bei Fe-25at.%W lydinių Nyquist diagramos gautos 0,1M NaCl esant atviros grandinės potencialui. Įklijoje pavaizduota elektrinė ekvivalentinė schema, panaudota duomenų apdorojimui. R_s – tirpalo varža (nekompensuojama varža), R_{ct} – krūvio pernašos varža, turinti korozijos varžos fizikinę prasmę, C_{dl} – dvigubojo elektrinio sluoksnio talpa, R_{ad} ir C_{ad} – atitinkamai varža ir talpa, modeliuojanti krūvio pernašą į adsorbuotą tarpinį junginį.*

The used equivalent circuit for fitting of EIS data supposes the complicated mechanism of alloy corrosion, which perhaps involves intermediate stages with the adsorption of Fe and W oxygen containing compounds. The equivalent circuit used to simulate the EIS consisted of R_s - solution resistance (uncompensated resistance); R_{ct} - charge transfer resistance; C_{dl} - a constant phase element having meaning of double layer capacitance of the electrolyte at alloy surface; R_{ad} and Ca_d are adsorption-related resistance and capacitance of intermediates, respectively. Accordingly, circuit $R_{ct}C_{dl}$ describes the Faraday process, that is, the resistance and capacities of the layer against electrochemical reaction, and $R_{ad}C_{ad}$ represents intermediate stage involving the process of blocking the coating's surface by adsorbed species. It is supposed that during corrosion

51

process W preferentially migrates toward the surface and forms oxides, which could block the surface and hinder the propagation of corrosion [28,29,126]. Moreover, the analysis of Fe-W corrosion products performed in [41] supposed the formation of $Fe_2(WO_4)_3$ and Fe_2O_3 compounds in the neutral media, and the following step reactions were proposed:

$$(A^{6>} E\ t\ 1*\ ^? \ \backslash\ (A1\ ®*\ _6 1 \tag{20}$$
$$(A^{6>} E\ 91\ _8^{6?} \ \backslash\ (A91\ _8 \tag{21}$$
$$(A1\ E\ u(A91\ _8 E\ 1_6 \backslash\ (A_6 1_7\ E\ (A_6:91\ _8;_7 \tag{22}$$

Similarly, $Ni(OH)_2$, NiO and WO_3 were found as corrosion products of Ni-W alloy in chloride medium [127], and the formation of cobalt and tungsten oxides as corrosion products of Co-W alloys has been suggested in [126].

Generally, the higher the charge transfer resistance (R_{ct}), the greater corrosion resistance of the system. The extracted values of R_{ct} for Fe and Fe-W coatings are provided in Table 4 having meaning of corrosion resistance (R_{corr}). Increasing in W content in alloy initially decreases the corrosion resistance and then after a particular composition the corrosion resistance starts to increase. In the present study, several factors influencing the corrosion behavior of Fe-W alloys can be distinguished: surface roughness and crystallite size. Indeed, Fe-W alloys with up to 10 at.% of W have a rough surface and internal cracks (Fig. 6, Papers 2 and 3), which increase the area of the Fe-W surface for the action of corrosive medium, thus reducing the corrosion resistance. Furthermore, the increase of corrosion resistance with gradual increase in W content can be associated with the significant surface refining and compaction, as well as with the transition from nanocrystalline to amorphous-like structure. Remarkably, the R_{corr} obtained for Fe-W coatings is comparable with that of other Fe-containing deposits: Ni-Fe-W alloy tested in similar corrosion medium (207.0 : ˜cm^2) [29], Ni-Fe/Al_2O_3 composite in sodium sulfate (~250 : ˜cm^2) [99], and Fe-W alloy electrodeposited from citrate bath and tested in sulfate-chloride medium (380.7 : ˜cm^2) [128]; while the corrosion resistance of Co-W and Ni-W alloys in neutral mediums is much higher: 1000 : ˜cm^2 and 6770 : ˜cm^2, respectively [29,126]. That could imply on detrimental and prevalent effect of Fe dissolution on corrosion properties of the coatings.

The lowest corrosion current and the highest corrosion resistance were obtained for the sample with highest W content, 25 at.% of W; therefore, this alloy composition was used for further evaluation of Fe-W wear resistance.

Frequently the wear resistance of coatings correlates with their structural and mechanical characteristics such as grain size, texture, hardness,

plasticity and etc. [81,92,93,95]. The general idea is that the materials with smaller grain size should better resist to plastic deformation; hence, the wear should be minimized. However, despite the fact that among all W alloy coatings W-rich Fe-W deposits possess the highest hardness and the grain size is below 10 nm, one of the specific tribological features of these coatings is rather high wear rate, which exceeds the wear rate of Co-W, Ni-W and electrolytic chromium coatings tested under similar conditions [82].

The tribological behavior of electrodeposited amorphous-like Fe-W coatings (25 at.% of W) was investigated under dry and lubricating conditions using ball-on-flat configuration by applying 1, 2 and 5 N load. It is observed that at dry friction conditions the coefficient of friction (COF) increases sharply at first 50-100 cycles independently of the applied load, then reaches the maximum and remains constant (Fig. 15). The mean of COF decreases with the increase in applied load. However, the depth profile analysis of Fe-W worn surface indicates the wear propagation at higher loads (Fig. 16). The profiles of Fe-W worn surface after dry friction are rather sharp, denoting the abrasive type of wear. Indeed, SEM and EDS analyses reveal the groove-like morphology of worn surface, but also the presence of well-adhered particles and increased oxygen content inside the wear track. According to EDS data, the oxygen content in debris particles, which tend to accumulate in piles at the edge of the track, can attain 50 at.% after dry friction, which corresponds to the atomic fraction of oxygen in mixed Fe_3O_4 oxide (Fig. 17). Therefore, slightly increased oxygen content inside the wear tack can be attributed to the presence of some iron oxide particles adhered to the worn surface after the test.
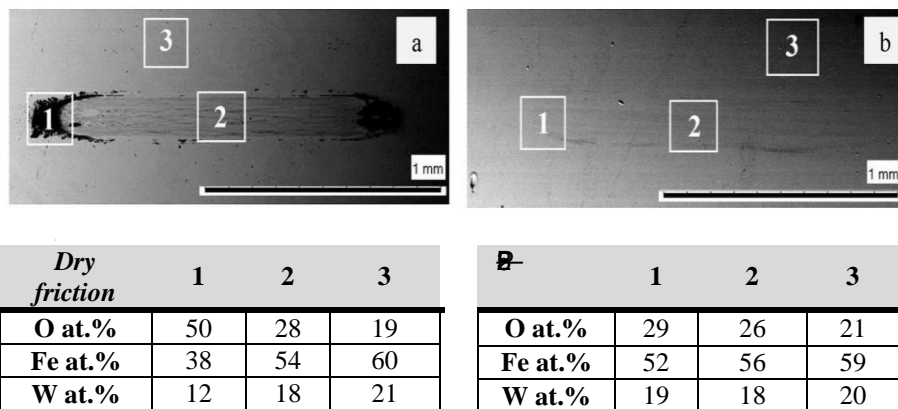
These observations imply that Fe-W undergo severe tribooxidation during fretting tests. The tribooxidation phenomenon can be explained as follows: when two surfaces slide together, the friction work is turned into thermal energy, which tends to maximize the potential energy at the interface. Since the maximized thermal energy is naturally an unstable state, the oxidation itself is a form of intrinsic response of material to recover the system equilibrium under friction conditions [129]. Thus, formed iron oxides act as third body particles, which form deep grove-like surface when sliding against corundum counter body increasing the asperity contact and resulting in high values of COF and wear depth.
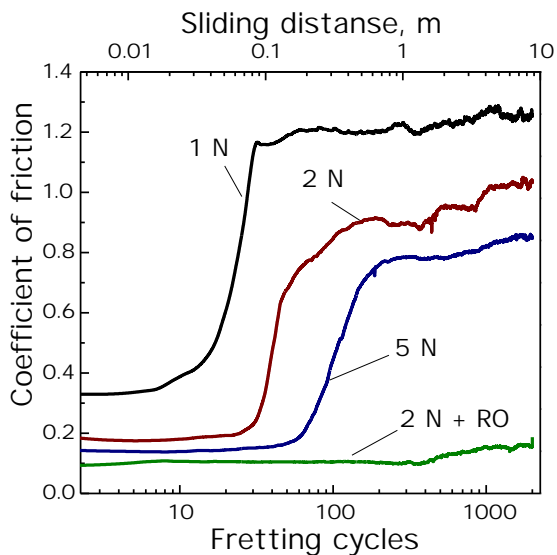
Fig. 15. *Evolution of the coefficient of friction of Fe-25at.%W alloy during dry friction at 1 N, 2N and 5 N load and in the presence of rapeseed oil film (RO).*
15 pav. *Fe-25at.%W lydinio trinties koeficiento kitimas sausos trinties sąlygomis esant 1N, 2N bei 3N apkrovoms, o taip pat ir esant rapsų aliejaus (RO) plėvelei.*
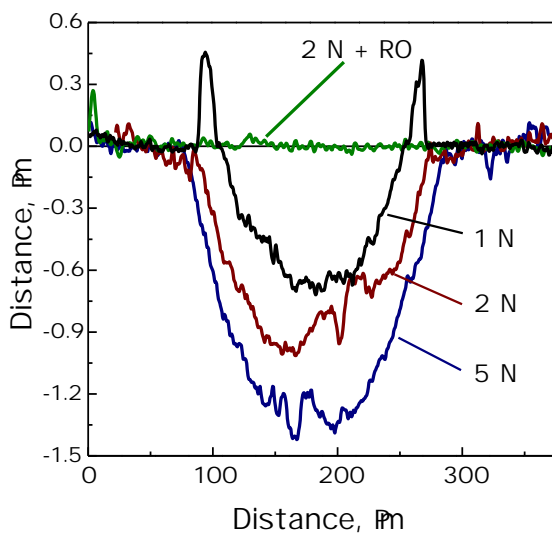

Fig. 16. *Depth profiles of Fe-25at.%W alloy worn surface after dry friction at 1 N, 2 N and 5 N loads and in the presence of rapeseed oil (RO) film.*
16 pav. *Fe-25at.%W lydinio esant sausai trinčiai arba rapsų aliejaus (RO) plėvelei naudojant 1N, 2N bei 5N apkrovas nusidėvėjimo paviršiaus gylio profiliai.*

Dry friction	1	2	3
O at.%	50	28	19
Fe at.%	38	54	60
W at.%	12	18	21

~~b~~	1	2	3
O at.%	29	26	21
Fe at.%	52	56	59
W at.%	19	18	20

Fig. 17. *SEM images and EDS analysis of wear tracks on Fe-25at.%W alloy after fretting test at 2 N: dry friction (a); in the presence of 1 µm rapeseed oil (b); 1, 2 and 3 denote corresponding EDS analyzed zones.*
17 pav. *Fe-25at.%W lydinio po trinties testų esant 2N apkrovai SEM atvaizdai ir EDS analizės duomenys: sausa trintis (a); esant 1 µm storio rapsų aliejaus plėvelei (b); skaičiais 1, 2 ir 3 pažymėtos vietos, kuriose atlikta EDS analizė.*
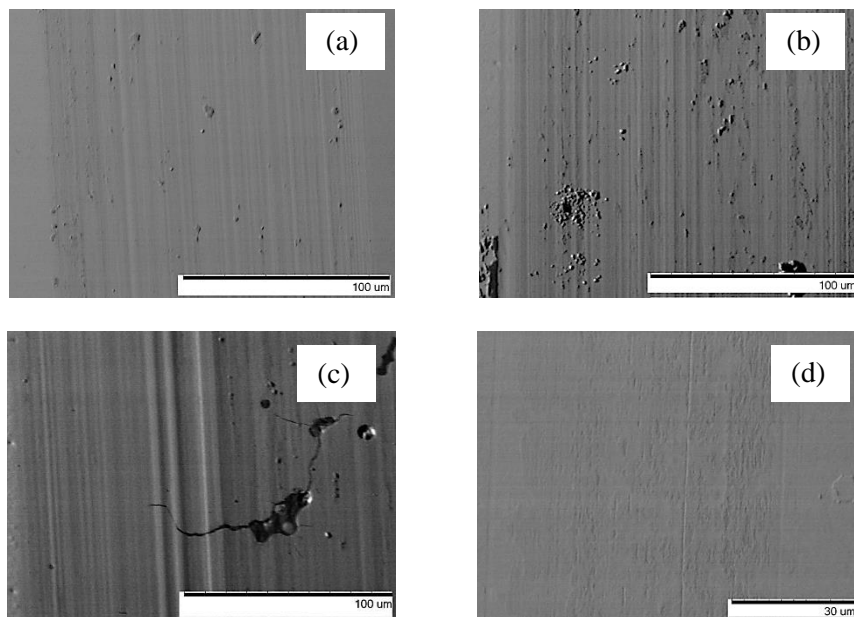
Fig. 18. *SEM images of wear tracks on Fe-25at.%W alloy under dry friction conditions at 1 N (a); 2 N (b); 5 N (c); and at 2 N load under lubricating conditions (d).*
18 pav. *Fe-25at.%W lydinio nusidėvėjimo takelio, susidariusio esant sausai trinčiai arba tepimo sąlygomis bei įvairiai apkrovai, SEM atvaizdai: 1N (a); 2N (b); 5N (c); 2N ir esant tepimui (d).*

55

The decrease in COF with the applied load (Fig. 15) could be linked to the different behavior of iron oxides: at 1 N the particles must be agglomerated on the surface causing high COF, and at higher loads they could partially embed into the coatings thus leading to the decrease in COF, but propagation of the cracks (Fig. 18a-c). Moreover, the presence of adhered iron oxide particles indicates the abrasive-adhesive wear mechanism of Fe-W surface.

Considering the tribooxidation as a driving factor of the wear propagation, the lubrication conditions were applied. In this study, rapeseed oil was used as a lubricant in order to increase the environment sustainability of the process. Indeed, rapeseed oil film of approximately 1 μm of thickness reduces COF by approximately five times as compared to dry friction conditions (Fig. 15). In addition, the roughness of the wear track after friction with lubricant is at the range of initial surface roughness, about few hundred nanometers. Moreover, no oxide particles were observed after sliding tests neither inside the wear track, nor at the counter-body (Fig. 18c). Hence, it can be suggested that at lubricating conditions the wear mechanism of Fe-W alloys changes from abrasive-adhesive to abrasive, where debris generated during the test act as "in-situ" polishing agent.

The minimal thickness of oil film when COF starts to decrease is 0.2 μm, but the lubricant layer could not resist more than 50 cycles and therefore, 0.5 μm should be applied in order to retain the experiment for 2.000 cycles. Moreover, the optimal thickness of rapeseed oil film that provides the lowest COF is 1 μm. That could be due to the better adherence of such film to the metallic surface of Fe–W coating (Paper 5).

3.5 Electrodeposited Fe-W/Al$_2$O$_3$ composite coatings

The tribological performance of Fe-W coatings can be significantly improved under lubricating conditions, as it was discussed previously. However, in order to extend the lifetime of the coating, the liquid lubricant must be injected regularly, what is not always reasonable in practice. Therefore, Fe-W/Al$_2$O$_3$ composite coatings were electrodeposited in order to improve the wear resistance of Fe-W alloys under dry friction conditions and possibly increase their corrosion resistance. Hence, sub-microsized alumina particles with various concentrations (25 g/L, 50 g/L and 100 g/L) were suspended in the base glycolate-citrate electrolyte. Fe-W alloys and Fe-W/Al$_2$O$_3$ composites were electrodeposited at the same conditions in order to track the changes caused by particles inclusion.

56
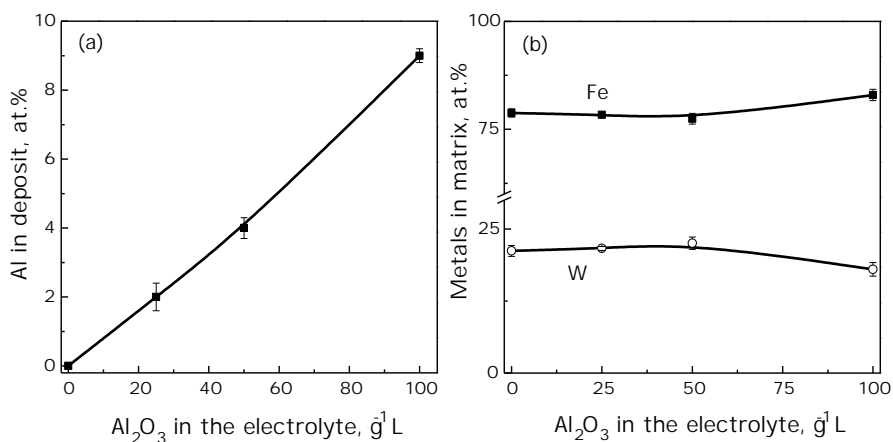
Fig. 19. *Effect of Al$_2$O$_3$ particles concentration in the electrolyte on their concentration in the deposit (a); and on the composition of Fe-W matrix (b). The coatings were obtained at 200 rpm, 40 mA cm^{-2}, 65 °C.*
19 pav. *Al$_2$O$_3$ dalelių koncentracijos elektrolite įtaka jų koncentracijai dangoje (a); ir Fe-W matricos sudėčiai (b). Dangos gautos esant 40 mA cm^{-2}, 65 ℃, 200 rpm.*

An increase in particles concentration in the electrolyte up to 100 g/L results in an increase of alumina content in the composite (Fig. 19a). At the same time, the incorporation of alumina particles does not influence essentially on the cathodic polarization, (E_{dep} -1.30 ± 0.05 mV), thus the composition of Fe-W matrix remains unaffected by particles inclusion and the W content attains 20 at.% independently on Al$_2$O$_3$ concentration (Fig. 19b). The slightly reduced W content in the matrix of the composite coating produced from solution with the highest particles concentration could be caused by the partial blocking of the electrode surface by non-conductive alumina particles, which results in an increased current density for alloy deposition.

The presence of incorporated alumina particles was confirmed by EDS point analysis on the top surface and cross-section of the coatings, and thus the black spots evidenced from the Fig. 20 are attributed to the Al$_2$O$_3$. The surface of the coatings is uniform, free of cracks and rather smooth. However, the addition of alumina particles increases the roughness gradually from ~80 nm up to 300 nm (Fig. 20a-d). The panels e-g in Fig. 20 illustrate the corresponding cross-sectional images of studied samples. For the pure Fe-W matrix some cracks appear near the substrate, perhaps, due to the high internal stress in electrodeposited coating.
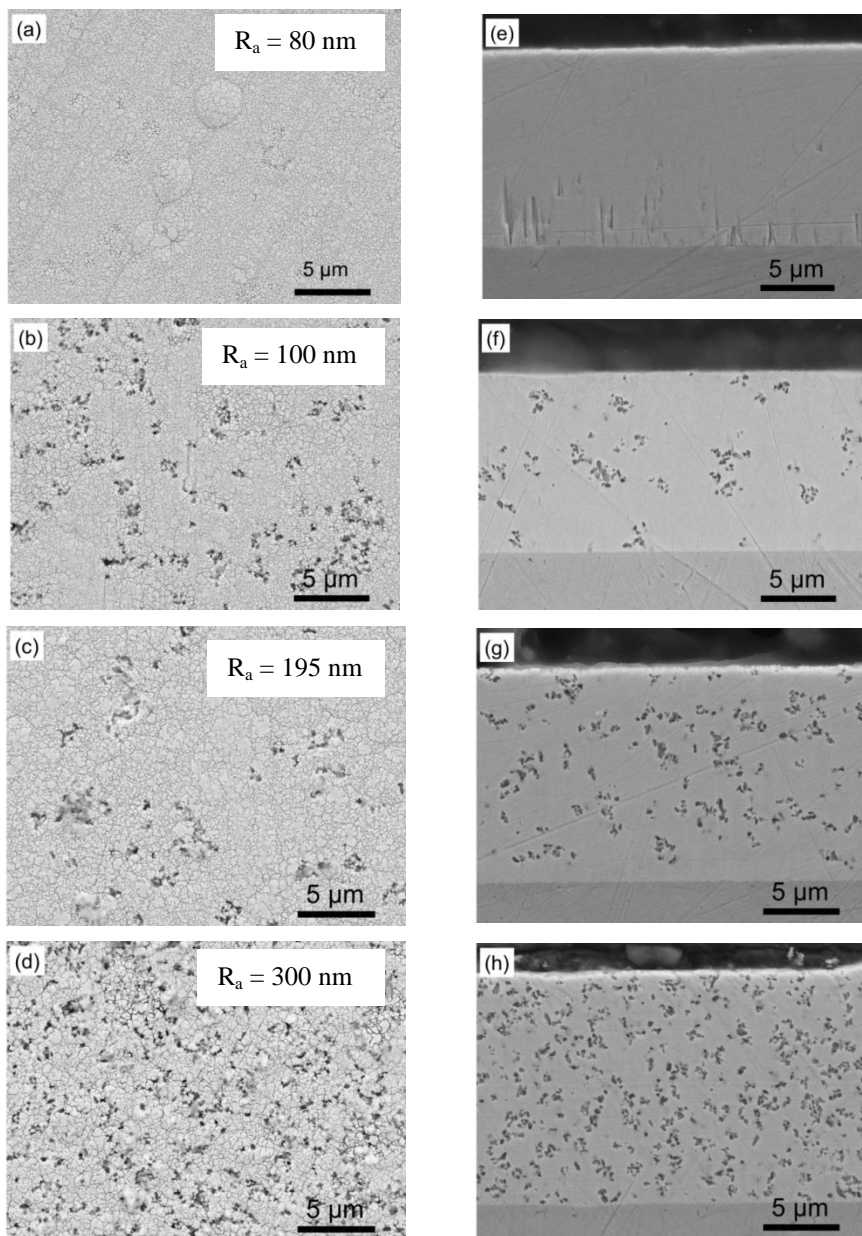
Fig. 20. *SEM images of the distribution of Al$_2$O$_3$ particles on the surface (a-d) and in the cross-section (e-h) of composite coatings obtained with various concentration of alumina in electrolyte: 0 g/L (a,e); 25 g/L (b,f); 50 g/L (c,g); and 100 g/L (d,h). Average surface roughness is indicated on the SEM image of corresponding surface. Electrodeposition conditions are the same as indicated in Fig. 19.*

20 pav. *Al$_2$O$_3$ dalelių pasiskirstymo kompozituose SEM atvaizdai: paviršiuje (a-d); skerspjūvyje (e-h). Dangos nusodintos esant įvairioms Al$_2$O$_3$ dalelių koncentracijoms: 0 g/l (a,e); 25 g/l (b,f); 50 g/l (c,g); 100 g/l (d,h).*

58

The investigation of tribological behavior of electrodeposited Fe-W and Fe-W/Al$_2$O$_3$ composite coatings was carried out under dry friction conditions using ball-on-disk configuration sliding tests where the measurement conditions were the same for all the tested tribo-pairs: normal load of 2 N, 500 m unidirectional sliding and 0.04 m/s rotation speed. The variation of the coefficient of friction recorded during the tests as a function of sliding distance is shown in Fig. 21. The COF of Fe-W alloys and composite coatings with low particles concentration is high, ~ 0.8-0.9, and the lowest COF, ~0.6, is obtained for the Fe-W/Al$_2$O$_3$ coating with the highest particles concentration.
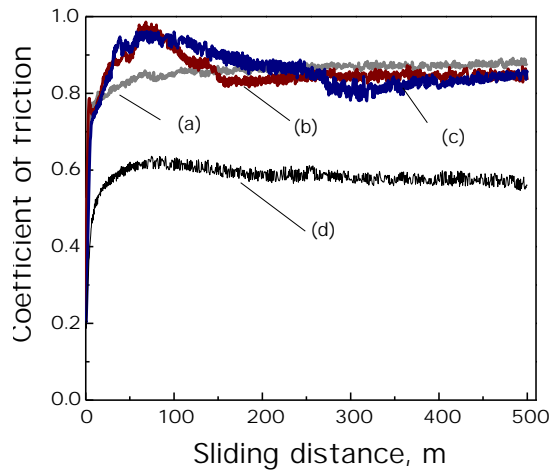

Fig. 21. *Evolution of the coefficient of friction under dry friction conditions of Fe-W (a) and Fe-W/Al$_2$O$_3$ composite coatings obtained with different concentration of alumina in the electrolyte: 25 g/L (b); 50 g/L (c); and 100 g/L (d). Tests were carried out at 2 N load, 4 cm/s, at 20 °C and 55 % relative humidity.*
***21 pav.** Trinties koeficiento kitimas sausos trinties sąlygomis: Fe-W lydinio (a); Fe-W/Al$_2$O$_3$ kompozitų, nusodintų iš elektrolitų, turinčių įvairias Al$_2$O$_3$ dalelių koncentracijas: 25 g/l (b); 50 g/l (c); 100 g/l (d). Testavimo sąlygos: 2N apkrova, 4 cm/s greitis, 20 ℃ ir 55 santykinė drėgmė.*

Besides the COF, the specific wear rate of Fe-W alloy and Fe-W/Al$_2$O$_3$ composite coatings was calculated according to the equation (15) and the results are shown in Fig. 22. It was found that the addition of Al$_2$O$_3$ particles reduces the specific wear rate: the lowest wear rate (1.8·10^{-7} mm^3/N m) is obtained for the sample with the highest particles concentration, which is an order of magnitude lower than that for pure Fe-W alloy matrix under similar tested conditions. The micro-sized Al$_2$O$_3$ particles significantly reduce the contact area of exposed Fe-W matrix and serve as spacers preventing

59

asperity contact between the sliding surfaces, thus lowering the tribooxidation and reducing the wear during friction.
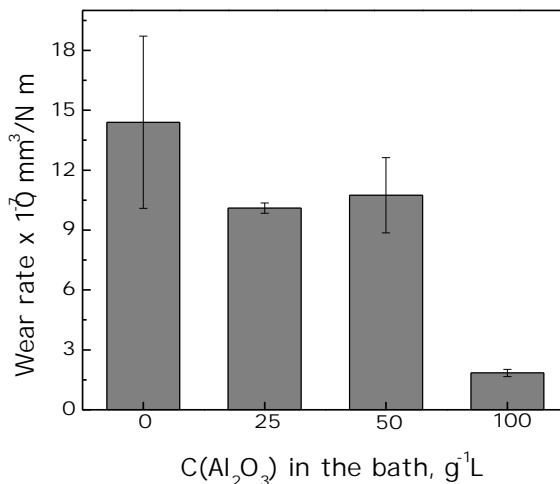
Fig. 22. Specific wear rate of Fe-W alloys and Fe-W/Al2O3 composite coatings under dry friction conditions as indicated in Fig. 21.

22 pav. *Fe-W lydinio ir Fe-W/Al₂O₃ kompozitų savitasis nusidėvėjimo greitis sausos trinties sąlygomis, kurios nurodytos 21 pav. aprašyme.*
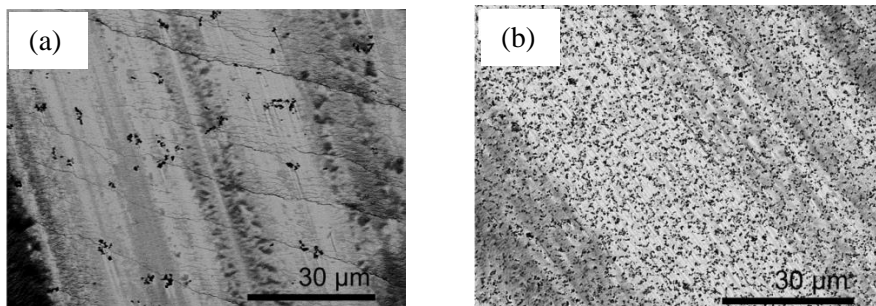

Fig. 23. *SEM images of the worn surface of the Fe-W/Al₂O₃ coatings deposited from the bath containing 25 g/L of alumina (a) and 100 g/l (b), after 500 m sliding under conditions indicated in Fig. 21.*

23 pav. *Fe-W/Al₂O₃ kompozito po 500 m trynimo (sąlygos nurodytos 21 pav. aprašyme) nusidėvėjimo paviršiaus SEM atvaizdai. Kompozitas nusodintas iš elektrolito, turinčio 25 g/l Al₂O₃ dalelių (a) ir 100 g/l Al₂O₃ dalelių.*

The cracks depicted on the worn surface of Fe-W/Al$_2$O$_3$ coatings having small particles concentration (Fig. 23a) could be attributed to their excessive brittleness; although, there are no cracks noticed inside the wear track of the composite coating with the highest particles concentration (Fig. 23b).

Corrosion resistance of Fe-W/Al$_2$O$_3$ composite coatings was investigated by EIS in 0.1 M NaCl medium at room temperature. The obtained Nyquist

60

plots are presented in Fig. 24 and the extracted values of R_{ct}, C_{dl}, C_{ad} and R_s are given in Table 5.
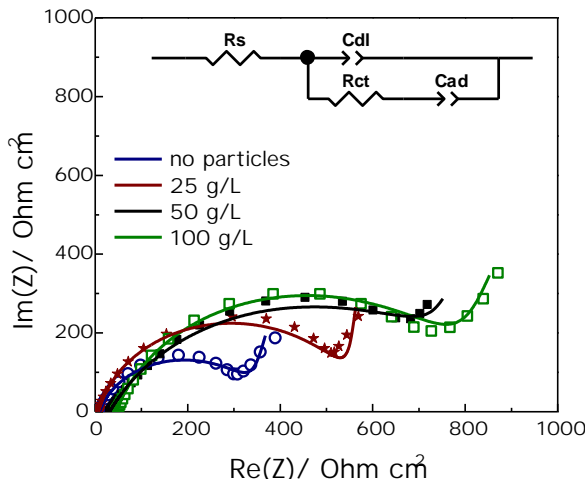

Fig. 24. *Nyquist plot for Fe-W and Fe-W/Al$_2$O$_3$ coatings electrodeposited under similar conditions and examined in 0.1 M NaCl solution at OCP. In insert is the equivalent circuit used for data fitting. The meanings of elements are provided in Fig. 14.*
24 pav. *Fe-W lydinio bei Fe-W/Al$_2$O$_3$ kompozito Nyquist diagramos gautos 0,1M NaCl esant atviros grandinės potencialui. Įklijoje pavaizduota elektrinė ekvivalentinė schema, panaudota duomenų apdorojimui. Diskretinių elementų fizikinės prasmės pateiktos 14 pav. aprašyme.*

Table 5. *Equivalent circuit parameters determined by fitting the impedance spectra of electrodeposited Fe-W and Fe-W/Al$_2$O$_3$ coatings in 0.1 M NaCl medium. "n" - is the exponent in the equation for the constant phase element.*
OHQWHO 5*ekvivalentinės elektrinės schemos parametrai apskaičiuoti iš Fe-W lydinių bei Fe-W/Al$_2$O$_3$ kompozitų elektrocheminio impedanso spektrų, gautų 0,1M NaCl tirpale. „n" – laipsnio rodiklis pastovios fazės elemento lygtyje.*

Coating	R_{ct}, Ω cm^2	C_{dl}, F/ cm^2	n (C_{dl})	C_{ad}, F/ cm^2	$n(C_{ad})$	R_s, Ω cm^2
Fe-W	355.2	$1.54\cdot10^{-3}$	0.80	$6.36\cdot10^{-2}$	0.89	8.8
Fe-W/2%Al$_2$O$_3$	569.1	$8.61\cdot10^{-4}$	0.85	$5.66\cdot10^{-2}$	0.95	6.9
Fe-W/6%Al$_2$O$_3$	843.8	$1.55\cdot10^{-3}$	0.71	$6.92\cdot10^{-2}$	0.98	31.2
Fe-W/9%Al$_2$O$_3$	795.1	$8.18\cdot10^{-4}$	0.81	$3.32\cdot10^{-2}$	0.85	45.6
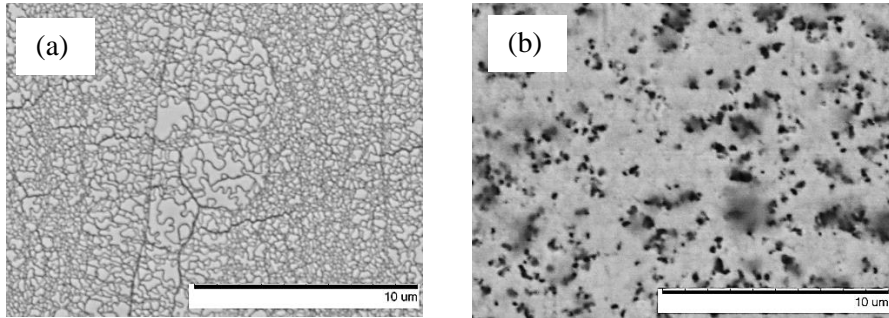
Fig. 25. *SEM images of Fe-W (a) and Fe-W/9%Al₂O₃ (b) surface after corrosion test in 0.1 M NaCl at room temperature.*
25 pav. *Fe-W (a) ir Fe-W/9 Al₂O₃ (b) paviršiaus SEM atvaizdai po korozijos testo 0,1M NaCl tirpale; temperatūra 20 C.*

It is seen from Fig. 24, with increase in particles concentration the radius of medium frequency capacitive loops also increases indicating the increase in corrosion resistance. The values of R_{ct} having meaning of corrosion resistance were obtained by fitting the EIS spectra with the equivalent circuit shown in insert Fig. 24. Thus, according to Table 5, the highest corrosion resistance is obtained for the composite coatings produced from the baths with 50 and 100 g/L of particles (6 and 9 at.% of co-deposited Al₂O₃ particles).

The surface of investigated Fe-W and Fe-W/Al₂O₃ coatings after corrosion test is cracked and the cracks propagation is along the grain boundaries as it can be observed in Fig. 25. The corrosion medium can penetrate faster through the cracks, and thus dissolution of Fe-W matrix is accelerated. As the content of co-deposited alumina particles increases, the number of cracks reduces. Therefore, it could be suggested that the well-dispersed alumina particles hinder the propagation of corrosion cracks, thus resulting in slightly increased corrosion resistance of the coatings as shown by EIS. Nevertheless, the increase in R_{corr} for the composites is not sufficiently high to claim the enhanced corrosion resistance of these novel materials, which still remains an order of magnitude lower than for similar Co- and Ni-W alloys and ceramic composites [29,97,126].

3.6 Summation

Fe-W alloys with various W contents from a few at.% to 25 at.% of W and Fe-W/Al₂O₃ composite coatings were electrodeposited from a newly developed glycolate-citrate bath based on Fe(III) salt. The thermodynamic stability of the plating bath was estimated by simulation of complexes distribution and the species distribution plots were provided in order to
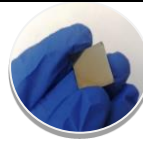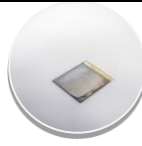
obtain a better understanding of the way how the bath composition and solution pH affect the W content, current efficiency and partial currents in the bath. The structural, mechanical, magnetic properties and thermal, wear and corrosion resistance of Fe-W layers were investigated as a function of W content in alloy. Moreover, novel Fe-W/Al_2O_3 composite coatings were electrodeposited from the same glycolate-citrate electrolyte with the addition of alumina particles in order to improve the performance of the coatings. The resulting functional properties of obtained coatings are determined by interrelation between several factors, such as elemental and phase composition, surface morphology and crystallite size. High W content promotes the smoothening of the surface, reduction of the crystallite size and phase transformation from solid solution to intermetallic phase leading to an increase in hardness and reduction of the saturation magnetization. Nevertheless, the wear and corrosion resistance of Fe-W deposits remain rather poor as compared to electrodeposited Co-W and Ni-W alloys. The co-deposition of submicrosized alumina particles helps to reduce the tribooxidation of Fe-W coatings; however, the corrosion resistance is not affected significantly and the increase in corrosion resistance observed by EIS measurements is rather due to the blocking of Fe-W surface by chemically resistant alumina particles, but not due to the impeding of Fe-W corrosion by itself.

The summary of investigated characteristics of electrodeposited Fe-W alloy and Fe-W/Al_2O_3 composite coatings is provided in Table 6, which can be used as a map for materials selection when aiming for a certain properties of interest.

Table 6. *Mapping of the properties of Fe-W based materials electrodeposited from glycolate-citrate Fe(III)-based electrolyte.*

ΗℚΗℚ Medžiagų Fe-W pagrindu, elektrochemiškai nusodintų iš glikoliatinio-citratinio elektrolito Fe(III) pagrindu, savybės.

Fe-W alloys			Fe-W/Al$_2$O$_3$ composites
Composition			
W < 10 at.%	11 at.% < W < 16 at.%	W > 17 at.%	2-9 at.% of Al$_2$O$_3$, ~ 20 at.% of W in matrix
Morphology			
Rough, porous, reassembling cauliflower structure	Compact, smooth surface with R_a < 100 nm;	Compact, mirror-like smooth surface, R_a ~ 10 nm	R_a up to 300 nm
Structure and phase composition			
Nanocrystalline structure d ~ 300 nm; α-Fe phase in mixture with Fe(W) solid solution	Tunable structure depending on electrodeposition conditions, mainly Fe(W) solid solution with small amount of α-Fe phase	Amorphous-like structure consisting of Fe$_2$W intermetallic phase and W(Fe) solid solution	Amorphous-like structure
Mechanical characteristics: Hardness and Young's modulus			
4-7 GPa 120-140 GPa	7-8 GPa 140-180 GPa	9-10 GPa 180-250 GPa	9-14 GPa 70-100 GPa
Thermal stability			
-	Up to 400 °C	Up to 600 °C	-
Corrosion properties (neutral medium)			
j_{corr}=1.3ˑ10^{-5} A/cm^2, R_{corr}~60 Ω·cm^2;	j_{corr}=9.97 ·10^{-6} A/cm^2, R_{corr} ~160 Ω·cm^2;	j_{corr} = 6.43 ·10^{-6} A/cm^2, R_{corr} ~300 Ω·cm^2;	R_{corr} up to 800 Ω·cm^2
Wear resistance			
-	-	Specific wear rate 1.5·10^{-6} mm^3/N m; Lubricating conditions: COF is 5 times lower with 1 μm rapeseed oil	Specific wear rate at dry friction: 1.8·10^{-7} mm^3/N m;
Magnetic properties			
Semi-soft magnetic; 100-190 emu/g;	Semi-soft magnetic; 30-150 emu/g	Semi-soft magnetic; 20-40 emu/g	-

CONCLUSIONS

1) Fe-W alloys and Fe-W/Al_2O_3 composite coatings were electrodeposited from the newly developed environmentally friendly glycolate-citrate electrolyte based on Fe(III)-salt. The electrodeposition current efficiency of approximately 70 % was achieved, which can be attributed to the formation of Fe(III) and W(VI) glycolate complex species.

2) The designed control over the composition and structure by variation of electrochemical conditions of the intrinsic properties of Fe-W alloys and Fe-W/Al_2O_3 composite coatings was achieved. In particular, the increase in W content from a few at.% to 25 at.% led to a structural transition from nanocrystalline coatings (α-Fe phase + Fe(W) solid solution) to amorphous-like alloys (Fe_2W intermetallic phase + W(Fe) solid solution).

3) Tailored extrinsic properties of the Fe-W based materials were thoroughly investigated:

- nanocrystalline Fe-W alloys have a combination of high saturation magnetization (100-190 emu/g) and relatively high hardness (up to 8 GPa), which is suitable for the fabrication of various microelectromechanical systems.

- amorphous-like Fe-W alloys and Fe-W/Al_2O_3 composite coatings with enhanced hardness (10-16 GPa) and outstanding thermal stability (up to 600 °C) are promising candidates for high-temperature applications.

4) One of the major drawbacks of Fe-W alloys is the high wear rate caused by tribooxidation ($1.5 \cdot 10^{-6}$ mm^3/N m,) which can be overcome under lubricating conditions (1 μm of rapeseed oil decreases the coefficient of friction by five times). Deposited (Fe-24at.%W + 9at.%Al_2O_3) composite can be considered an appropriate coating (specific wear rate at dry friction $1.8 \cdot 10^{-7}$ mm^3/N m) for cases wherein lubrication is not compatible.

5) Both Fe-W alloys and Fe-W/Al_2O_3 composite coatings were characterized by low corrosion resistance (≤ 850 Ω cm^2), thus limiting their application for corrosion protection. By contrast, the low corrosion resistance of Fe-W alloys in combination with low saturation magnetization and high hardness is suitable for the fabrication of biodegradable metallic implants.

FUTURE OUTLOOK

The results presented in this study reveal that the functional properties of Fe-W alloys can be easily controlled by changing the electrodeposition condition, thus making these coatings appealing alternative environmentally-friendly material for multiscale technologies, including fabrication of MEMS, protective coatings and even biomedicine application. However, a number of important aspects need to be studied in the future considering the implementation of Fe-W alloys for a real-world application.

Among the main perspectives is further optimization of the Fe(III)-glycolate-citrate bath, study on the effect of organic additives and stress relievers, which seems to be necessary for the up-scaling of the Fe-W electrodeposition process. Also, the newly developed bath may be considered for studies on electrodeposition of other Fe-based alloys alternatively to conventional Fe(II)-based ones.

Moreover, annealing treatment of Fe-W/Al_2O_3 composite coatings is of particular interest. The phase transformations of both metallic matrix and ceramic particles at elevated temperature may result a new material with advanced mechanical characteristics, such as extremely high hardness, ductility and toughness.

SANTRAUKA

Įvadas

   Susidomėjimas volframo lydiniais su geležies grupės metalais (Fe, Co, Ni) pastoviai auga dėl patrauklių funkcinių savybių: mechaninių, magnetinių, atsparumo korozijai bei terminio stabilumo. Labiausiai ištirti Ni ir Co lydiniai su volframu, tuo tarpu Fe-W lydiniai ištirti mažiau. Tačiau pastaruoju metu Ni ir Co naudojimas lydiniuose yra ribojamas dėl keliamų aplinkosaugos ir sveikatos problemų: ES Co(II) druskos laikomos kancerogeninėmis, o nikelis sukelia alergiją. Todėl pastaruoju metu didelis dėmesys skiriamas lydinių geležies pagrindu elektronusodinimui kaip alternatyva Co- arba Ni-lydiniams.

   Nežiūrint to, kad Fe-W lydinių elektronusodinimas tiriamas nuo ~1940 metų bei jų patrauklių savybių patvirtinimo daugeliu autorių, šie lydiniai yra paplitę mažai dėl to, kad elektrolitinių vonių sudėties užtikrinimas yra komplikuotas. Dažniausiai Fe-W lydinių elektronusodinimas buvo tiriamas iš elektrolitinių vonių Fe^{+2} druskų pagrindu, nes šių druskų tirpumas yra didesnis. Tačiau dėl greitos Fe^{+2} oksidacijos iki Fe^{+3} krenta duomenų atsikartojamumas bei atsiranda geležies hidroksidų nuosėdos, todėl sumažėja elektrolitinės vonios eksploatacijos laikas. Todėl komplikuotas vonios sudėties palaikymas didina darbuotojų darbo laiką, cheminių medžiagų sąnaudas bei sąlygoja dažną elektrolininės vonios utilizavimą. Be to, Fe-W lydiniai gaunami esant didesnei poliarizacijai nei Co-W arba Ni-W, todėl sumažėja lydinio srovinė išeiga ir pailgėja reikiamo storio dangos elektronusodinimo laikas. Be to, tokiuose elektrolituose dažnai naudojamas amoniakas, kad padidėtų metalų kompleksų tirpumas bei elektrolito buferinė talpa. Tačiau elektronusodinant aukštesnėse temparatūrose (60-80 qC) didelė amoniako dalis išgaruoja iš tirpalo, todėl pasikeičia elektrolito pH, lydinio nusodinimo greitis bei sudėtis. Vėliau elektrolitą utilizuojant amoniakas gali užteršti orą, dirvožemį bei vandenį.

   Todėl yra poreikis vystyti bei optimizuoti aplinkai draugišką elektrolitą pažangiems lydiniams elektronusodinti. Taip pat svarbu geriau valdyti metalų elektronusodinimo procesus bei suprasti fundamentalius šių lydinių elektronusodinimo dėsningumus. Tokiu būdu aplinkai draugiškas Fe-W lydinių elektronusodinimo tyrimas yra tarpdisciplininis iššūkis ir užpildo tarpą tarp medžiagotyros bei tvaraus vystymosi.

Disertacijos tikslas yra elektrochemiškai nusodinti iš aplinkai draugiško glikoliatinio-citratinio elektrolito bei apibūdinti gaunamus nanokristalinius bei amorfinio tipo Fe-W lydinius bei naują Fe-W/Al$_2$O$_3$ kompozitus.

Pagrindiniai uždaviniai yra šie:

1) sukurti naują elektrolitą nusodinti Fe-W lydinius bei Fe-W/ Al$_2$O$_3$ kompozitus, atitinkantį aplinkai draugiškumo kriterijų, t.y. vengiant naudoti pavojingas chemines medžiagas, naudojant termodinamiškai stabilius Fe^{+3} junginius vietoje Fe^{+2} junginių bei padidinti lydinio srovinę išeigą.

2) patikimai kontroliuoti gaunamų Fe-W lydinių bei Fe-W/Al$_2$O$_3$ kompozitų sudėtį bei struktūrą keičiant elektrocheminius nusodinimo parametrus (pH, srovės tankį, temperatūrą, maišymo intensyvumą bei elektrolito sudėtį) ir gaunant nanokristalines bei amorfinio tipo struktūras;

3) nustatyti sąryšius tarp vidinių parametrų (sudėties, struktūros, kristalitų dydžio, fazinės sudėties, magnetinio įsotinimo) ir išorinių (kietumo, nusidėvėjimo, korozijos bei terminio stabilumo), kad būtų nustatytos elektronusodintų Fe-W lydinių ir Fe-W/Al$_2$O$_3$ kompozitų pritaikymo perspektyvos.

Eksperimentų metodika

Bendra tyrimų metodologija pavaizduota 2 pav. (29 psl.).

Elektrolitų joninės sudėties apskaičiavimas. Elektrolitų joninės sudėtys apskaičiuotos naudojantis Waterloo Maple 6 programa sprendžiant lygčių sistemą, kurią sudaro: (a) visų į elektrolitą įdėtų ir susidariusių junginių jonizacijos arba disociacijos konstantos (E); (b) visų medžiagų masių balanso lygtys; (c) krūvio balanso lygtys.

Fe-W lydinių ir Fe-W/Al$_2$O$_3$ kompozitų elektronusodinimas. Elektronusodinimas buvo atliekamas įprastoje 3-elektrodų celėje; darbinis elektrodas – varis arba nerūdijantis plienas, pagalbinis – platinuoto titano tinklelis, lyginamasis – sotus Ag/AgCl/KCl elektrodas. Pagrindinio elektrolito sudėtis buvo tokia:

0,1M glikolio rūgštis,

0,3M citrinos rūgštis

0,1M Fe$_2$(SO$_4$)$_3$

0 ÷ 0,5 M Na$_2$WO$_4$;

Elektrolito pH buvo keičiamas nuo 4,0 iki 8,5 pridedant NaOH arba H$_2$SO$_4$; katodinės srovės tankis nuo 5 and 50 mA/cm^2.

68

Kompozitų dangos buvo gaunamos į minėtą elektrolitą pridedant 5 g/l, 50 g/l arba 100 g/l submikroninių Al_2O_3 dalelių.

Elektronusodinimas atliktas 65 °C temperatūroje, naudojant 40 mA/cm^2 srovės tankį ir 200 rpm apsisukimų greitį.

Paviršiaus morfologija, sudėtis ir struktūra. Paviršiaus morfologija buvo tiriama skenuojančiais elektroniniais mikroskopais, o elementinė sudėtis buvo nustatyta EDX detektoriumi, prijungtu prie SEM. Sudėties kitimo profiliai nustatyti rusenančio išlydžio optinės emisijos spektroskopijos (GD-OES) metodu. Gautų dangų struktūra buvo tiriama naudojant rentgeno spindulių difrakciją (XRD), o volframo įtaka fazių virsmams buvo tiriama Mössbauer spektroskopijos metodu.

Mechaninės savybės. Fe-W lydinių mechaninės savybės buvo tiriamos nanoidentavimo metodu esant 20 mN apkrovai. Identavimas buvo atliekamas gauto lydinio dangos skersinio pjūvio vietose. Kietumo ir elastinio modulio vertės buvo apskaičiuojamos Oliver ir Pharr metodu, o visi pateikti rezultatai yra statistiškai apdoroti.

Magnetinės savybės. Fe-W lydinių magnetinės savybės buvo nustatomos kambario temperatūroje naudojant vibruojančio pavyzdžio magnetometrą MicroSense (LOT-Quantum Design). Histerezės kilpos gautos lygriagrečiai ir statmenai pavyzdžiui naudojant maksimalų lauko stiprį ±20 kOe.

Tribologinės savybės. Gautų elektrocheminių Fe-W dangų tribologinės savybės buvo įvertinamos testuojant „rutulys ant plokštumos" metodu, kai danga buvo sausa arba esant reikiamo storio alyvos plėvelei – rapso aliejaus kontroliuojamo storio plėvelė (0,2÷5,0 μm), uždedama prieš testą. Visuose eksperimentuose naudotas 6 mm skersmens korundo rutuliukas. Fe-W lydiniai buvo tiriami esant 1N, 2N ir 5N apkrovai; atliekami 2000 ciklų (visas slydimo atstumas 4 m) esant 2 Hz dažniui ir 1 mm poslinkiui.

Fe-W/Al_2O_3 dangos buvo tiriamos „rutulys ant disko" metodu esant 2N apkrovai ir 4 cm s^{-1} sukimosi greičiui (sukimosi skersmuo 3 mm).

Visi tribologiniai testai atlikti esant 20 ± 2 °C temperatūrai ir 48-55 % santykinei drėgmei.

Korozinės savybės. Gautų dangų korozinės savybės 0,1M NaCl tirpale buvo tiriamos elektrocheminio impedanso spektroskopijos (EIS) metodu: amplitudė 5 mV, dažnis nuo 10 kHz iki 0,01 Hz. EIS parametrai apskaičiuoti naudojantis programa ZView.

Rezultatai ir jų aptarimas

Glikoliatinio-citratinio elektrolito Fe(III) kompleksų pagrindu kūrimas

Fe-W lydinio elektronusodinimo elektrolito joninės sudėties matematinis modeliavimas parodė, kad jeigu elektrolite yra tik vienas ligandas – glikoliatas, „laisvų" Fe^{3+} jonų koncentracija pasiekia arba net ir viršija galimą termodinaminę koncentraciją, apskaičiuojamą iš $Fe(OH)_3$ tirpumo sandaugos, t.y. $[Fe^{3+}] \approx [Fe^{3+}]_{sat}$, t.y. toks elektrolitas yra metastabilios būsenos ir gali egzistuoti palyginus trumpą laiką, kurį sąlygoja kompleksų hidrolizės iki hidroksidų kinetika. Tuo tarpu, įvedant antrąjį ligandą – citratą – elektrolito stabilumas padidėja (sumažėja „laisvų" Fe^{3+} jonų koncentracija) visame tiriamame pH intervale (žr. 3 pav., 37 psl.). Šiuo atveju Fe(III) ir WO_4^{2-} jonai sudaro kompleksus su skirtingais ligandais: beveik visa Fe(III) yra surišta citratiniame komplekse visame pH intervale, o iki 99 % W(VI) yra arba glikoliatinio komplekso $WO_2(Gly)_2^{2-}$ formoje (pH<7), arba „laisvų" WO_4^{2-} jonų formoje (95% „laisvų" jonų ir 5 % citratiniame komplekse esant pH>7). Reikia pažymėti, kad esant pH>7, beveik 25 % Fe(III) yra hidrokso komplekso $Fe(OH)_4^-$ formoje.

Fe(III) ir W(VI) kompleksų pasiskirstymo ypatybės turi didelę įtaką Fe, W bei vandenilio skyrimosi greičiams esant įvairiems pH (žr. 4 pav., 39 psl.). Volframo kiekio augimas lydinyje yra lydimas srovinės išeigos padidėjimo, kuris siekia 60-70   , kai lydinys nusodinamas esant pH ~7 ir 65 °C temperatūroje. Gautos šios Fe-W lydinio srovinės išeigos vertės glikoliatiniame-citratiniame elektrolite yra žymiai didesnės nei gautos elektrolituose Fe(II) arba Fe(III) pagrindu naudojant netirpius anodus [82,121]. Tai gali būti siejama su tuo, kad kompleksas W(VI)-glikoliatas yra molekulė, kuri užima daug mažesnį tūrį nei kompleksas W(VI)-citratas (žr. 5 pav., 39 psl.), todėl krūvio pernaša į glikoliatinį volframo kompleksą gali vykti lengviau nei į citratinį.

Esant pH>7 srovinė išeiga ir W kiekis lydinyje žymiai sumažėja. Tai koreliuoja su apskaičiuotu kompleksų pasiskirstymu (3d pav., 37 psl.), t.y. sumažėja dominuojančio komplekso $WO_2Gly_2^{2-}$ koncentracija ir padidėja WO_4^{2-} jonų koncentracija. Be to, padidėja $FeCit_2^{5-}$ ir $Fe(OH)_4^-$ kompleksų koncentracijos, kurie gali dalyvauti lygiagrečioje Fe(III) jonų išsikrovimo reakcijoje, taip padidinant Fe kiekį lydinyje.

Elektronusodintų Fe-W lydinių sudėtis ir struktūra

Gautų Fe-W lydinių paviršiaus morfologija labai priklauso nuo W kiekio lydinyje (6 pav., 41 psl.). Kai W kiekis lydinyje yra mažesnis nei 10 at.%, lydinys yra poringas, susiformuoja mikro-globulės, tarp kurių atstumai yra santykinai dideli, paviršius pasižymi „kalafioro" morfologija. Didėjant W kiekiui lydiniuose poringumas išnyksta ir paviršius tampa žymiai lygesnis: vidutinis šiurkštumas tiesiškai mažėja nuo ~ 62 nm iki ~ 13 nm, kai W kiekis lydinyje padidėja nuo 6 iki 25 at.%, t.y. Fe-W lydiniai, kuriuose yra 15-25 at.% W pasižymi veidrodiniu blizgesiu.

Tiriant lydinius EDS metodu gaunamas didelis kiekis deguonies Fe-W lydinių paviršiuje. Detaliau nemetalų pasiskirstymas Fe-W lydiniuose buvo tiriamas GD-OES metodu. Buvo gauta, kad iš tiesų, viršutiniuose Fe-W lydinio sluoksniuose (iki ~1-2 µm gylio) yra daug oksidų ir mažai volframo, tuo tarpu tik deguonies ir anglies pėdsakai randami gilesniuose sluoksniuose (žr. 7 pav., 42 psl.). Iš jo matyti, kad gilesniuose sluoksniuose Fe ir W santykis yra vienodas. Anglies ir vandenilio priemaišų atsiradimas lydiniuose siejamas su citratą/glikoliatą turinčių dalelių adsorbcija ir jų „apauginimu" Fe ir W.

Būdingi elektrochemiškai nusodintos Fe ir Fe-W lydinių rentgeno spindulių difrakcijos spektrai pateikti 8 pav. (44 psl.). Atitinkamos būdingų Fe smailių $2\Theta_{hkl}$ padėtis slenkasi į mažesnių kampų pusę, kai W kiekis lydinyje didėja. Tai galima sieti su tam tikro kiekio Fe atomų gardelėje pakeitimu didesniais W atomais ir kieto volframo tirpalo geležyje susidarymu. Tuo pat metu smailė tampa platesnė ir jos intensyvumas mažėja, kol atsiranda viena plati smailė esant ~ 43°, kai volframo kiekis pasiekia 25 at.%. Toks smailės išplatėjimas siejamas su kristalitų mažėjimu ir perėjimu iš nanokristalinės struktūros į „amorfinio" tipo struktūrą.

Fe-W lydinių fazinės sudėties pokyčiai buvo tiriami Mosbauerio spektroskopijos metodu. Gauta, kad didėjant volframo kiekiui lydinyje mažėja a -Fe fazės kiekis, ir didėja Fe(W) kieto tirpalo kiekis, t.y. vyksta Fe atomų pakeitimas W atomais a -Fe gardelėje. Iš gautų spektrų nustatyta, kad gardelėje volframo atomais gali būti pakeičiama iki 3 Fe atomų (žr. 9 pav., 45 psl.). Kai volframo kiekis lydinyje yra didesnis (16–25 at.%), spektrų forma yra beveik tokia pati, ir tai priskiriama intermetalido Fe_2W susidarymui bei tikėtina, tam tikro kiekio geležies kieto tirpalo volframe susidarymui.

Fe-W lydinių mechaninės ir magnetinės savybės

Mechaninės ir magnetinės Fe-W lydinių savybės pateikiamos kaip lydinio sudėties ir struktūros funkcija. Kietumo ir elastinio modulio vertės, kurios pateiktos 10 pav. (47 psl.) apskaičiuotos iš apkrovos-slinkties kreivių Oliver-Pharr metodu. Gauta, kad didėjant volframo kiekiui lydinyje padidėja ir kietumas, ir elastinis modulis; kietumas padidėja nuo 4 GPa iki 10 GPa, o elastinis modulis nuo 80 iki 216 GPa, kai volframo kiekis padidėja nuo 4 at. % iki 25 at. . Elektronusodintų Fe-W lydinių atveju kietumo padidėjimą galima susieti su kristalitų dydžio mažėjimu (11 pav., 47 psl.): maži kristalitai sukūria daug tarpkristalitinių briaunų, kurios stabdo dislokacijų judėjimą. Taigi, plastines deformacijas apsprendžia gardelės dislokacijos kristalito viduje, todėl atsparumas padidėja (Hall-Petch mechanizmas). Be to, intermetalo Fe_2W fazė taip pat padidina Fe-W lydinių, turinčių >16 at.% W, kietumą. Reikia pažymėti, kad Fe-W lydinių, turinčių didesnį volframo kiekį, kietumas yra didesnis nei Co-W ir Ni-W, ir yra palyginamas su elektrolitiniu chromu, kurio naudojimas ribojamas.

Fe-W lydinių mechanines savybes galima pagerinti juos kaitinant. Pvz., Fe-W lydinį (25 at.% W) pakaitinus 600 °C, kietumas padidėja iki ~16 GPa, nes į atskirą fazę iškrenta α-Fe kristalitai.

Siekiant nustatyti Fe-W lydinių feromagnetiko tipą (kietasis, pusiau minkštas arba minkštasis) ir magnetinio įsotinimo pokyčius buvo tiriami lydiniai, kuriuose volframo kiekis svyravo plačiose ribose. Kaip ir tikėtasi, didėjant volframo kiekiui lydinyje magnetinis įsotinimas mažėja, nes volframas yra nemagnetikas (žr. 12 pav., 49 psl.). Lydinių, nusodintų kambario temperatūroje, žymiai staigesniu magnetinio įsotinimo sumažėjimu esant jau 12 at. W, tuo tarpų lydiniai elektronusodinti esant 65°C temperatūrai ir turintys 16 at.% W vis dar išlaiko pakankamai aukštą įmagnetinimą. Tai matyt susiję su lydinių, nusodintų skirtingose temperatūrose, struktūros skirtumais. Lydinių, nusodintų esant 20 C struktūra yra metastabili ir netvarkinga , kai W kiekiai yra mažesni, tuo tarpu 65°C temperatūroje Fe-W lydinių pakankamai aukštas elektrokristalizacijos greitis, ir formuojasi stabili kristalinė struktūra (žr. 8 pav., 44 psl.).

Tirtų Fe-W lydinių koercityvumas yra 20-90 Oe ribose, kai magnetinis laukas yra lygiagretus tiriamajam pavyzdžiui, ir 10-190 Oe ribose, t.y. Fe-W lydiniai yra pusiau minkšti magnetikai.

Fe-W lydinių korozija ir nusidėvėjimas

Fe ir įvairių Fe-W lydinių korozija buvo tiriama voltameprometriniu ir elektrocheminio inmpedanso spektroskopijos (EIS) metodu 0,1M NaCl

tirpale kambario temperatūroje. Gauti duomenys pateikti atitinkamai 13 ir 14 pav. (50, 51 psl.). Iš poliarizacinių kreivių buvo nustatomas korozijos potencialas, E_{corr}, ir korozijos srovės tankis, j_{corr}, naudojantis Tafelio ir Allen-Hickling metodais. Gauti duomenys pateikti 4 lentelėje (50 psl.).

Kaip matyti, didėjant W kiekiui lydinyje j_{corr} mažėja, nežiūrint to, kad E_{corr} neigiamėja. Kadangi metalams koroduojant vienu metu vienodais greičiais vyksta du procesai (metalų oksidacija ir vandenilio redukcija), ir jų kinetikos dėsningumus lemia skirtingi faktoriai, tiesioginės koreliacijos tarp j_{corr} ir E_{corr} gali ir nebūti. Mažiausia korozijos srove ($6.4 \cdot 10^{-6}$ A/cm^2) pasižymi lydinys, turintis 25 at.% W.

Tiriant elektrodinius procesus EIS metodu galima spręsti apie procesų kinetiką ir mechanizmą. Du būdingieji Fe-W lydinių (W kiekis 7 at.% ir 25 at.%) korozijos EIS spektrai pateikti 14 pav. Šiuos spektrus atitinka gana komplikuota elektrinė ekvivalentinė schema (14 pav.), kuri modeliuoja dviejų stadijų krūvio pernašą esant tarpiniam adsorbuotam junginiui ir diskretinių elementų elektrocheminiai atitikmenys yra tokie: R_s – tirpalo varža (iš esmės tai nekompensuojama varža), R_{ct} – krūvio pernašos varža, kuri atitinka korozijos varžą (R_{corr}); C_{dl} – pastovios fazės elementas, kuris modeliuoja dvigubąjį elektros sluoksnį; R_d ir C_d modeliuoja krūvio pernašą į adsorbuotą tarpinį junginį. Tarpiniais adsorbuotais junginiais gali būti deguonį turintys Fe ir W junginiai.

Bendru atveju, kuo didesnė korozijos varžą, tuo didesnis metalo atsparumas korozijai. Fe ir Fe-W lydinių korozijos varžos pateiktos 4 lentelėje (50 psl.). Kaip matyti iš pateiktų duomenų, kai W kiekis lydinyje yra mažas (<10 at.%), korozijos varža mažėja palyginus su gryna Fe, nors korozijos srovės šiek tiek mažėja. Tai rodo, kad tokios sudėties lydinių korozija labai jautri korozijos potencialo pokyčiams (pvz., oksidatorių buvimui korozijos terpėje). Iš tiesų, Fe-W lydinių su mažu volframo kiekiu paviršius yra šiurkštus ir viduje yra įtrūkimų, ir visa tai didina paviršiaus plotą, kontaktuojantį su korozijos terpe. Kai lydiniuose volframo yra daugiau, danga tampa kompaktiška, kristalitai susmulkėja. Tai matyt ir sąlygoja, kad didžiausiu atsparumu korozijai (mažiausia korozijos srovė ir didžiausia korozijos varža) pasižymi amorfinio tipo Fe-W lydiniai, t.y. turintys 25 at.   W.

Elektronusodintų Fe-W lydinių, turinčių amorfinio tipo struktūrą, tribologinės savybės buvo tiriamos sausos trinties ir esant tepimo alyvos plėvelėms naudojant 1N, 2N ir 5N apkrovas. Nustatyta, kad nepriklausomai nuo taikytos apkrovos, trinties koeficientas didėja pirmųjų 50-100 ciklų metu, po to jis išlieka pastovus (15 pav., 54 psl.). Trinties koeficientas

mažėja didėjant apkrovai, tačiau prasiskverbimo profilis gilėja (16 pav., 54 psl.).

Fe-W lydinių nusidėvėjimo sausos trinties sąlygomis profilis yra gana aštrus, būdingas abrazyviniam nusidėvėjimui. SEM ir EDS duomenys rodo griovelių tipo morfologiją, o taip pat yra prilipusių dalelių. Be to, nusidėvėjimo griovelyje užfiksuotas padidintas deguonies kiekis (17 pav., 55 psl.). Iš EDS duomenų seka, kad deguonies kiekis nuolaužų dalelėse, kurios kaupiasi treko kraštuose sausos trinties sąlygomis, siekia 50 at.%, o tai reiškia, kad šios dalelės sudarytos iš Fe_3O_4. Tokiu būdu, duomenys rodo, kad sausos trinties sąlygomis vyksta triboaksidavimo reakcija: kai du paviršiai trinasi vienas į kitą, trinties darbas generuoja šiluminę energiją, kurios maksimali vertė yra kūnų sąlyčio riboje. Tokia būsena yra termodinamiškai nestabili, ir oksidacijos reakcija yra savaiminis sistemos atsakas atstatant termodinaminę pusiausvyrą sausos trinties sąlygomis [128]. Tokiu būdu susidaręs geležies oksidas veikia kaip trečiojo kūno dalelės, kurios ir suformuoja gilų griovelį, padidina kontakto plotą ir sąlygoja didelį trinties koeficientą ir gilų nusidėvėjimo profilį. Trinties koeficiento sumažėjimą didėjant apkrovai (žr. 15 pav.) galima paaiškinti skirtinga geležies oksido dalelių elgsena: esant palyginus mažai 1N apkrovai oksido dalelės aglomeruojasi paviršiuje, todėl trinties koeficientas yra didelis, tuo tarpu esant didesnėms apkrovoms oksido dalelės „įmušamos" į dangą, todėl trinties koeficientas sumažėja, bet atsiranda įtrūkimų (18 a-c pav., 55 psl.). Be to, įsiterpusios oksido dalelės sąlygoja abrazyvinį-adhezinį Fe-W lydinių nusidėvėjimo mechanizmą.

Triboaksidacijos vaidmenį nusidėvėjime mažina tepimas. Šiame darbe rapsų aliejus, kaip aplinkai draugiška medžiaga, buvo naudojamas tepimui. Rapsų aliejaus 1 Pm storio sluoksnis trinties koeficientą sumažina maždaug 5 kartus lyginant su sausa trintimi (15 pav., 54 psl.). Be to, nusidėvėjimo griovelio šiurkštumas yra artimas pradinio paviršiaus šiurkštumui, t.y. kelių šimtų nanometrų eilės. Be to, oksidų neaptikta nei nusidėvėjimo griovelyje, nei ant korundo rutuliuko (18 pav., 55 psl.). Tokiu būdu esant tepimui Fe-W lydinių nusidėvėjimo mechanizmas yra abrazyvinis, ir nuolaužos susidariusios trynimo metu veikia kaip poliravimo agentas *in situ*.

Elektronusodintos Fe-W/Al₂O₃ kompozicinės dangos

Fe-W dangų tribologinė elgsena pagerėja tepimo sąlygomis. Tačiau, kad dangos tarnavimo laikas pailgėtų, tepti būtina reguliariai, o tai ne visada priimtina. Todėl buvo testuojamos elektrochemiškai nusodintos Fe-W/Al₂O₃

kompozicinės dangos, kurių atsparumas nusidėvėjimui sausos trinties sąlygomis ir galimai korozijai, būtų didesnis nei Fe-W lydinių.

Kompozicinės Fe-W/Al$_2$O$_3$ dangos buvo nusodinamos iš pagrindinio glikoliatinio-citratinio elektrolito jame suspenduojant submikroninio dydžio Al$_2$O$_3$ daleles (25 g/l, 50 g/l ir 100 g/l). Dangų nusodinimo sąlygos buvo tokios pat, kaip ir Fe-W lydinių nusodinimo atvejais: 40 mA cm^{-2}, 65 °C, 200 rpm.

Didinant Al$_2$O$_3$ dalelių koncentraciją didėja Al$_2$O$_3$ dalelių koncentracija dangoje, kuri pasiekia maksimalią 9 at.% vertę (19a pav., 57 psl.). Įsiterpiant Al$_2$O$_3$ dalelėms neturi žymios įtakos katodinei poliarizacijai (E_{dep}= -1.30 ± 0.05 mV), t.y. Fe-W matricos susidarymui dalelių įsiterpimas įtakos nedaro, ir W kiekis pasiekia 20 at. nepriklausomai nuo Al$_2$O$_3$ koncentracijos elektrolite (19b pav., 57 psl.).

Kaip matyti iš 20 pav. (58 psl.) pateiktų dangų skerspjūvio atvaizdų, dalelių pasiskirstymas yra vienodas, ir dangose nėra įtrūkimų.

Fe-W lydinių ir Fe-W/Al$_2$O$_3$ kompozitų dangų tribologinė elgsena buvo lyginama atlikus „rutuliuko ant disko" testus esant vienodoms sąlygoms: apkrova statmena kryptimi 2N, slydimo atstumas abiem kryptimis 500 m ir 0,04 m/s sukimosi greitis.

Apskaičiuotieji savitieji nusidėvėjimo greičiai pateikti 22 pav. (60 psl.). Gauta, kad Al$_2$O$_3$ dalelių įterpimas sumažina savitąjį nusidėvėjimo greitį iki 1.8·10^{-7} mm^3/N m, kai aliuminio oksido dalelių koncentracija elektrolite yra maksimali, ir ši nusidėvėjimo vertė yra maždaug 10 kartų mažesnė nei Fe-W lydinio. Įsiterpusios Al$_2$O$_3$ mikrodalelės žymiai sumažina Fe-W matricos kontakto plotą, o tuo pat metu ir tribooksidaciją, sumažėja nuolaužų kontaktas tarp dviejų besitrinančių kūnų, ir taip sumažėja nusidėvėjimas trinties metu. Buvo gauta žemiausia trinties koeficiento vertė ~0,6, kai ir Fe-W/Al$_2$O$_3$ kompozitas buvo nusodinamas esant didžiausiai dalelių koncentracijai elektrolite 100 g/l (žr. 21 pav., 59 psl.).

Fe-W/Al$_2$O$_3$ kompozitų atsparumas korozijai buvo tiriamas EIS metodu 0,1M NaCl tirpale kambario temperatūroje. Gautos Nyquist diagramos pateiktos 24 pav. (61 psl.), o apskaičiuotos diskretinių elementų R_{ct}, C_{dl}, C_d ir R_s vertės pateiktos 5 lentelėje (61 psl.). Gauta, kad didžiausios korozijos varžos R_{ct} vertės gautos kompozitų, nusodintų iš elektrolitų su didžiausia Al$_2$O$_3$ dalelių koncentracija, ir turinčių 6 at. % ir 9 at. Al$_2$O$_3$ koncentracija, atveju. Kaip matyti iš 25 pav. (62 psl.), po korozijos testo Fe-W ir Fe-W/Al$_2$O$_3$ kompozitų, turinčių 2 at.% Al$_2$O$_3$, paviršiuje atsiranda įtrūkimų palei kristalitų briaunas, ir korozijos terpė gali greičiau prasiskverbti į dangą ir padidinti Fe-W matricos korozijos greitį. Kai Al$_2$O$_3$ dalelių kiekis dangoje

padidėja, sumažėja įtrūkimų, sumažėja kontakto su korozija plotas ir korozijos varža padidėja nuo ~350 to ~ 850 Ω cm^2. Tačiau tokios korozijos varžos vertės yra mažesnės nei panašių Co- ir Ni-W kompozitų [29,97,125].

Išvados

1) Fe-W lydinių ir Fe-W/Al$_2$O$_3$ kompozicinių dangų dangos elektrochemiškai nusodintos iš naujo aplinkai draugiško glikoliatinio-citratinio elektrolito Fe(III) pagrindu, kuris yra termodinamiškai stabilus. Jame gauta iki 70   srovinė išeiga, ir tokia aukšta jos vertė gali būti siejama su Fe(III) ir W(VI) ypatingu glikoliatinių ir citratinių kompleksų pasiskirstymu elektrolite.

2) Keičiant elektrochemines dangų nusodinimo sąlygas galima keisti Fe-W lydinių bei Fe-W/Al$_2$O$_3$ kompozitų dangų sudėtį ir struktūrą. Būtent, W kiekį dangoje galima keisti nuo kelių at. % iki 25 at.   , ir tuo pat metu dangų struktūra pakinta nuo nanokristalinių (a -Fe fazė ir W kieto tirpalo Fe mišinys) iki amorfinio tipo (Fe$_2$W intermetalido ir Fe kieto tirpalo W mišinys).

3) Kruopščiai ištirtos Fe-W pagrindu gautų dangų savybės:

   - nanokristaliniai Fe-W lydiniai ir pasižymi aukštu magnetiniu įsotinimu (100-190 emu/g) ir santykinai aukštu kietumu (iki 8 GPa), ir jie tinka įvairių mikroelektromechaninių sistemų gamybai;
   - amorfinio tipo Fe-W lydiniai bei Fe-W/Al$_2$O$_3$ kompozitai pasižymi dideliu kietumu (10-16 GPa) bei dideliu terminiu atsparumu (iki 600 °C), todėl tinka gaminiams, veikiantiems aukštose temperatūrose.

4) Vienas iš didžiausių Fe-W lydinių trūkumų yra didelis nusidėvėjimas sausos trinties sąlygomis dėl vykstančios tribokorozijos (1,5·10^{-6} mm^3/N m). Tačiau tepimo sąlygomis nusidėvėjimas ir trinties koeficientas mažėja: 1 mm storio rapsų aliejaus sluoksnis trinties koeficientą sumažina 5 kartus). Nusodinto kompozito (Fe-24at.%W + 9at.%Al$_2$O$_3$) nusidėvėjimo greitis sausos trinties sąlygomis yra žymiai mažesnis (1.8·10^{-7} mm^3/N m), ir rekomenduojamas naudoti įrenginiuose, kuriuose reguliarus tepimas yra nepageidaujamas.

5) Ir Fe-W lydiniai, ir Fe-W/Al$_2$O$_3$ kompozitai pasižymi santykinai nedideliu atsparumu korozijai (korozijos varža ($\leq$ 850 Ω cm^2), todėl jų panaudojimas apsaugai nuo korozijos yra ribotas. Tačiau mažai atsparūs korozijai Fe-W lydiniai, pasižymintys mažu magnetiniu įsotinimu, gali būti naudojami bioskaidžių implantų gamybai.

REFERENCES

[1] M. Schlesinger (ed.), M. Paunocic (ed.), Modern Electroplating, 5th edition, 2010. doi:10.1149/1.2425993

[2] C. Larson, Global comparisons of metal finishing sectors: Part 2, some technology and operational variations, Trans. IMF. 90 (2012) 232–236. doi:10.1179/0020296712Z.00000000054

[3] Y.D. Gamburg, G. Zangari, Theory and Practice of Metal Electrodeposition, 2011. doi:10.1017/CBO9781107415324.004

[4] G. Zangari, Electrodeposition of Alloys and Compounds in the Era of Microelectronics and Energy Conversion Technology, Coatings. 5 (2015) 195–218. doi:10.3390/coatings5020195

[5] G.V. Constantinos, R.E. White, Modern aspects of electroctrochemistry N42, 2008. doi:10.1007/978-0-387-49489-0

[6] W. Schwarzacher, Electrodeposition: A Technology for the Future, Electrochem. Soc. Interface. 15 (2006) 32–35.

[7] G. Zangari, Electrodeposition for Energy Conversion: Electrochemistry over Matter, ECS Interface. 20 (2011) 31–32. doi:10.1149/2.F03112if

[8] A. Baysal, N. Ozbek, S. Akman, Determination of Trace Metals in Waste Water and Their Removal Processes, Waste Water - Treat. Technol. Recent Anal. Dev. (2013) 145–171. doi:http://dx.doi.org/10.5772/52025

[9] N. Tsyntsaru, H. Cesiulis, M. Donten, J. Sort, E. Pellicer, E.J. Podlaha-Murphy, Modern trends in tungsten alloys electrodeposition with iron group metals, 2012. doi:10.3103/S1068375512060038

[10] Z. Mahidashti, M. Aliofkhazraei, N. Lotfi, Review of Nickel-Based Electrodeposited Tribo-Coatings, Trans. Indian Inst. Met. 71 (2018) 257–295. doi:10.1007/s12666-017-1175-x

[11] D.R. Askeland, P.P. Fulay, W.J. Write, The science and engeneering of materials, 2010

[12] M.X. Donten, H. Cesiulis, Z. Stojek, Electrodeposition and properties of Ni-W, Fe-W and Fe-Ni-W amorphous alloys. A comparative study, Electrochim. Acta 45 (2000) 3389–3396. doi:10.1016/S0013-4686(00)00437-0

[13] N. Tsyntsaru, H. Cesiulis, A. Budreika, X. Ye, R. Juskenas, J.P. Celis, The effect of electrodeposition conditions and post-annealing on nanostructure of Co-W coatings, Surf. Coatings Technol. 206 (2012) 4262–4269. doi:10.1016/j.surfcoat.2012.04.036

[14] E.P. Barbano, I.A. Carlos, E. Vallés, Electrochemical synthesis of Fe-W and Fe-W-P magnetic amorphous films and Fe-W nanowires, Surf. Coatings Technol. 324 (2017) 80–84. doi:10.1016/j.surfcoat.2017.05.071

[15] I.Y. Yermolenko, M.V. Ved, N.D. Sakhnenko, Y.I. Sachanova, Composition, Morphology, and Topography of Galvanic Coatings Fe-Co-W and Fe-Co-Mo, Nanoscale Res. Lett. 12 (2017) 352. doi:10.1186/s11671-017-2128-3

[16] G. Yar-Mukhamedova, M. Ved, N. Sakhnenko, A. Karakurkchi, I. Yermolenko, Iron binary and ternary coatings with molybdenum and tungsten, Appl. Surf. Sci. 383 (2016) 346–352. doi:10.1016/j.apsusc.2016.04.046

[17] Y.D. Gamburg, E.N. Zakharov, The effect of hydrogen on amorphization of

iron-tungsten alloys produced by electrochemical synthesis, Russ. J. Electrochem. 44 (2008) 736–739. doi:10.1134/S1023193508060141.

[18] G. Samsonov, Handbook of the Physicochemical Properties of the Elements, 1968. doi:10.1007/978-1-4684-6066-7_7

[19] E. Lassner, W.-D. Schubert, Tungsten Properties, Chemistry, Technology of the Element, Alloys, and Chemical Compounds, 2012

[20] A. Bose, R. Sadangi, R.M. German, A Review on Alloying in Tungsten Heavy Alloys, Suppl. Proc. (2012) 453–465. doi:10.1002/9781118356074.ch59

[21] C.H. Henager, W. Setyawan, T.J. Roosendaal, N.R. Overman, B.A. Borlaug, E.L. Stevens, K.B. Wagner, R.J. Kurtz, G.R. Odette, B.N. Nguyen, K.H. Cunningham, Ductile-phase toughened tungsten for plasma-facing materials in fusion reactors, Int. J. Powder Metall. 53 (2017) 53–69

[22] B. Gludovatz, S. Wurster, T. Weingartner, A. Hoffmann, R. Pippan, Influence of impurities on the fracture behaviour of tungsten, Philos. Mag. 91 (2011) 3006–3020. doi:10.1080/14786435.2011.558861

[23] A. Brenner, P. Burkhead, E. Seegmiller, Electrodeposition of tungsten alloys containing iron, nickel, and cobalt, J. Res. Natl. Bur. Stand. 39 (1947) 351. doi:10.6028/jres.039.023

[24] N. Eliaz, E. Gileadi, Induced Codeposition of Alloys of Tungsten, Molybdenum and Rhenium with Transition Metals, Mod. Asp. Electrochem. (2008) 191–301. doi:10.1007/978-0-387-49489-0_4

[25] A. Kola, X. Geng, E.J. Podlaha, Ag-W electrodeposits with high W content from thiourea-citrate electrolytes, J. Electroanal. Chem. 761 (2016) 125–130. doi:10.1016/j.jelechem.2015.12.002

[26] D.P. Weston, S.J. Harris, P.H. Shipway, N.J. Weston, G.N. Yap, Establishing relationships between bath chemistry, electrodeposition and microstructure of Co-W alloy coatings produced from a gluconate bath, Electrochim. Acta. 55 (2010) 5695–5708. doi:10.1016/j.electacta.2010.05.005

[27] N. Tsyntsaru, H. Cesiulis, E. Pellicer, J.P. Celis, J. Sort, Structural, magnetic, and mechanical properties of electrodeposited cobalt-tungsten alloys: Intrinsic and extrinsic interdependencies, Electrochim. Acta. 104 (2013) 94–103. doi:10.1016/j.electacta.2013.04.022

[28] S. Wang, C. Zeng, Y. Ling, J. Wang, G. Xu, Phase transformations and electrochemical characterizations of electrodeposited amorphous Fe–W coatings, Surf. Coatings Technol. 286 (2016) 36–41. doi:10.1016/j.surfcoat.2015.12.011

[29] K.R. Sriraman, S. Ganesh Sundara Raman, S.K. Seshadri, Corrosion behaviour of electrodeposited nanocrystalline Ni-W and Ni-Fe-W alloys, Mater. Sci. Eng. A. 460–461 (2007) 39–45. doi:10.1016/j.msea.2007.02.055

[30] H.R. Lashgari, D. Chu, S. Xie, H. Sun, M. Ferry, S. Li, Composition dependence of the microstructure and soft magnetic properties of Fe-based amorphous/nanocrystalline alloys: A review study, J. Non. Cryst. Solids. 391 (2014) 61–82. doi:10.1016/j.jnoncrysol.2014.03.010

[31] M. Spasojević, L. Ribić-Zelenović, A. Maričić, P. Spasojević, Structure and magnetic properties of electrodeposited $Ni_{87.3}Fe_{11.3}W_{1.4}$ alloy, Powder Technol. 254 (2014) 439–447. doi:10.1016/j.powtec.2014.01.017

[32] S.-J. Mun, M. Kim, T.-H. Yim, J.-H. Lee, T. Kang, Mechanical and Structural Characteristics of Electrodeposited Ni–Fe–W Alloy after Heat-

Treatment, J. Electrochem. Soc. 157 (2010) D177–D180. doi:10.1149/1.3292282

[33] B.M. Mundotiya, D. Dinulovic, L. Rissing, M.C. Wurz, Fabrication and characterization of a Ni-Fe-W core microtransformer for high-Frequency power applications, Sensors Actuators, A Phys. 267 (2017) 42–47. doi:10.1016/j.sna.2017.09.032

[34] A. Bodaghi, J. Hosseini, Corrosion resistance and electrocatalytic properties of Co–W alloy coatings, Surf. Eng. 28 (2012) 632–635. doi:10.1179/1743294412Y.0000000024

[35] C.N. Tharamani, P. Beera, V. Jayaram, N.S. Begum, S.M. Mayanna, Studies on electrodeposition of Fe-W alloys for fuel cell applications, Appl. Surf. Sci. 253 (2006) 2031–2037. doi:10.1016/j.apsusc.2006.03.077

[36] Z. Matilda, D. Jakub, S. Ján, D. Edmund, Ni-W Alloys for Hydrogen Evolution, 844 (2016) 167–171. doi:10.4028/www.scientific.net/MSF.844.167

[37] L. Elias, P. Cao, A.C. Hegde, Magnetoelectrodeposition of Ni–W alloy coatings for enhanced hydrogen evolution reaction, RSC Adv. 6 (2016) 111358–111365. doi:10.1039/C6RA23944G

[38] J. Cheng, Y.F. Zheng, In vitro study on newly designed biodegradable Fe-X composites (X = W, CNT) prepared by spark plasma sintering, J. Biomed. Mater. Res. - Part B Appl. Biomater. 101 (2013) 485–497. doi:10.1002/jbm.b.32783

[39] C.A. Emond, V.B. Vergara, E.D. Lombardini, S.R. Mog, J.F. Kalinich, Induction of rhabdomyosarcoma by embedded military-grade Tungsten/Nickel/Cobalt Not by Tungsten/Nickel/Iron in the B6C3F1 mouse, Int. J. Toxicol. 34 (2015) 44–54. doi:10.1177/1091581814565038

[40] B.E. Schuster, L.E. Roszell, L.E. Murr, D.A. Ramirez, J.D. Demaree, B.R. Klotz, A.B. Rosencrance, W.E. Dennis, W. Bao, E.J. Perkins, J.F. Dillman, D.I. Bannon, In vivo corrosion, tumor outcome, and microarray gene expression for two types of muscle-implanted tungsten alloys, Toxicol. Appl. Pharmacol. 265 (2012) 128–138. doi:10.1016/j.taap.2012.08.025

[41] J. He, F.L. He, D.W. Li, Y.L. Liu, D.C. Yin, A novel porous Fe/Fe-W alloy scaffold with a double-layer structured skeleton: Preparation, in vitro degradability and biocompatibility, Colloids Surfaces B Biointerfaces. 142 (2016) 325–333. doi:10.1016/j.colsurfb.2016.03.002

[42] M.L. Holt, L.E. Vaaler, Electrolytic Reduction of Aqueous Tungstate Solutions, (1948)

[43] W.E. Clark, M.H. Lietzke, The Mechanism of the Tungsten Alloy Plating Procesd, J. Electrochem. Soc. (1952) 245–249. doi:10.1149/1.2779712

[44] H. Fukushima, T. Akiyama, S. Akagi, K. Higashi, Role of Iron-Group Metals in the Induced Codeposition of Molybdenum From Aqueous Solution, Nippon Kinzoku Gakkaishi/Journal Japan Inst. Met. 42 (1978) 980–985. doi:10.2320/jinstmet1952.42.10_980

[45] D.W. Ernst, R.F. Amlie, M.L. Holt, Electrodeposition of Molydenum Alloys from Aqueous Solutions, J. Electrochem. Soc. 102 (1955) 461. doi:10.1149/1.2430124

[46] O. Younes, E. Gileadi, Electroplating of Ni/W Alloys, J. Electrochem. Soc. 149 (2002) C100. doi:10.1149/1.1433750

[47] O. Younes-Metzler, L. Zhu, E. Gileadi, The anomalous codeposition of tungsten in the presence of nickel, Electrochim. Acta. 48 (2003) 2551–2562.

doi:10.1016/S0013-4686(03)00297-4

[48] E.J. Podlaha, D. Landolt, Induced Codeposition: III. Molybdenum Alloys with Nickel, Cobalt and Iron, J. Electrochem. Soc. 144 (1997) 1672–1680.

[49] E. Gómez, E. Pellicer, E. Vallés, Electrodeposited cobalt molybdenum magnetic materials, J. Electroanal. Chem. 517 (2001) 109–116

[50] S.S. Belevskii, S.P. Yushchenko, A.I. Dikusar, Anomalous electrodeposition of Co-W coatings from a citrate electrolyte due to the formation of multinuclear heterometallic complexes in the solution, Surf. Eng. Appl. Electrochem. 48 (2012) 97–98. doi:10.3103/S1068375512010036

[51] C. Wagner, The Cathodic Reduction of Anions and the Anodic Oxidation of Cations, J. Electrochem. Soc. 101 (1954) 181–184. doi:10.1149/1.2781227.

[52] A. Brenner, Electrodeposition of Alloys: Principle and Practice, Electrodepos. Alloy. I (1963). doi:10.1016/B978-1-4831-9807-1.50001-5

[53] R. Juškenas, I. Valsiunas, V. Pakštas, A. Selskis, V. Jasulaitiene, V. Karpavičiene, V. Kapočius, XRD, XPS and AFM studies of the unknown phase formed on the surface during electrodeposition of Ni-W alloy, Appl. Surf. Sci. 253 (2006) 1435–1442. doi:10.1016/j.apsusc.2006.02.018

[54] V.L. Krasikov, A.V. Krasikov, Mechanism for Induced Codeposition of Alloys and Some Single Refractory Metals, Bull. Saint Petersbg. State Inst. Technol. 37 (2016) 8–14. doi:10.15217/issn1998984-9.2016.37.8

[55] M. Zamani, A. Amadeh, S.M. Lari Baghal, Effect of Co content on electrodeposition mechanism and mechanical properties of electrodeposited Ni-Co alloy, Trans. Nonferrous Met. Soc. China (English Ed. 26 (2016) 484–491. doi:10.1016/S1003-6326(16)64136-5

[56] J.T. Matsushima, F. Trivinho-Strixino, E.C. Pereira, Investigation of cobalt deposition using the electrochemical quartz crystal microbalance, Electrochim. Acta. 51 (2006) 1960–1966. doi:10.1016/j.electacta.2005.07.003

[57] H. Cesiulis, A. Budreika, Electroreduction of Ni (II) and Co (II) from Pyrophosphate Solutions, Materials Science (Medžiagotyra) 16 (2010) 52-56.

[58] M.D. Obradović, R.M. Stevanović, A.R. Despić, Electrochemical deposition of Ni-W alloys from ammonia-citrate electrolyte, J. Electroanal. Chem. 552 (2003) 185–196. doi:10.1016/S0022-0728(03)00151-7

[59] B. Morgan, O. Lahav, The effect of pH on the kinetics of spontaneous Fe(II) oxidation by O2 in aqueous solution - basic principles and a simple heuristic description, Chemosphere. 68 (2007) 2080–2084. doi:10.1016/j.chemosphere.2007.02.015

[60] R. Rennuka, S. Ramamurthy, Electroplating of Iron-Phosphorous Alloy Part I-Influence of Reducing Agents on the Stability of the Plating Bath, Bull. Electrochem. 13 (1997) 456–460

[61] Z. Ghaferi, S. Sharafi, M.E. Bahrololoom, Effect of current density and bath composition on crystalline structure and magnetic properties of electrodeposited FeCoW alloy, Appl. Surf. Sci. 355 (2015) 766–773. doi:10.1016/j.apsusc.2015.07.083

[62] V. Torabinejad, M. Aliofkhazraei, S. Assareh, M.H. Allahyarzadeh, A.S. Rouhaghdam, Electrodeposition of Ni-Fe alloys, composites, and nano coatings–A review, J. Alloys Compd. 691 (2017) 841–859. doi:10.1016/j.jallcom.2016.08.329

[63] J.J. Cruywagen, L. Krüger, E.A. Rohwer, Complexation of tungsten(VI)

with citrate, J. Chem. Soc. Dalt. Trans. (1991) 1727–1731. doi:10.1039/DT9910001727

[64] D. Weston, S. Harris, H. Capel, N. Ahmed, P. Shipway, J. Yellup, Nanostructured Co-W coatings produced by electrodeposition to replace hard Cr on aerospace components, Trans. Inst. Met. Finish. 88 (2010) 47–56. doi:10.1179/174591909X12596810686490

[65] S.A. Silkin, A.V. Gotelyak, N.I. Tsyntsaru, A.I. Dikusar, Size effect of microhardness of nanocrystalline Co-W coatings produced from citrate and gluconate solutions, Surf. Eng. Appl. Electrochem. 51 (2015) 228–234. doi:10.3103/S106837551503014X

[66] L.M. Chang, Z.T. Wang, S.Y. Shi, W. Liu, Study on microstructure and properties of electrodeposited Ni-W alloy coating with glycolic acid system, J. Alloys Compd. 509 (2011) 1501–1504. doi:10.1016/j.jallcom.2010.10.136

[67] M. Svensson, U. Wahlström, G. Holmbom, Compositionally modulated cobalt-tungsten alloys deposited from a single ammoniacal electrolyte, Surf. Coatings Technol. 105 (1998) 218–223. doi:10.1016/S0257-8972(98)00458-7

[68] M. Donten, H. Cesiulis, Z. Stojek, Electrodeposition of amorphous/nanocrystalline and polycrystalline Ni-Mo alloys from pyrophosphate baths, Electrochim. Acta. 50 (2005) 1405–1412. doi:10.1016/j.electacta.2004.08.028

[69] H. Cesiulis, E. Podlaha-Murphy, Electrolyte considerations of electrodeposited Ni-W alloys for microdevice fabrication, Mater. Sci. 9 (2003) 5–9. doi: 10.1016/j.jelechem.2015.12.002

[70] V. Vasauskas, J. Padgurskas, R. Rukuiža, H. Cesiulis, J.P. Celis, D. Milčius, I. Prosyčevas, Cracking behavior of electrodeposited nanocrystalline tungsten-cobalt and tungsten-iron coatings, Mechanika 72 (2008) 21–27.

[71] N. Tsyntsaru, J. Bobanova, X. Ye, H. Cesiulis, A. Dikusar, I. Prosycevas, J.P. Celis, Iron-tungsten alloys electrodeposited under direct current from citrate-ammonia plating baths, Surf. Coatings Technol. 203 (2009) 3136–3141. doi:10.1016/j.surfcoat.2009.03.041

[72] O. Younes, L. Zhu, Y. Rosenberg, Y. Shacham-Diamand, E. Gileadi, Electroplating of amorphous thin films of tungsten/nickel alloys, Langmuir. 17 (2001) 8270–8275. doi:10.1021/la010660x

[73] A.M.P. Sakita, E.C. Passamani, H. Kumar, D.R. Cornejo, C.S. Fugivara, R.D. Noce, A.V. Benedetti, Influence of current density on crystalline structure and magnetic properties of electrodeposited Co-rich CoNiW alloys, Mater. Chem. Phys. 141 (2013) 576–581. doi:10.1016/j.matchemphys.2013.05.066

[74] Y.L. Chiu, N. Baluc, R. Schaublin, Nanostructured tungsten-iron alloy prepared by electrodeposition, Int. J. Mod. Phys. B. 20 (2006) 4195–4200.

[75] N. Tsyntsaru, A. Dikusar, H. Cesiulis, J.P. Celis, Z. Bobanova, S. Sidel'Nikova, S. Belevskii, Y. Yapontseva, O. Bersirova, V. Kublanovskii, Tribological and corrosive characteristics of electrochemical coatings based on cobalt and iron superalloys, Powder Metall. Met. Ceram. 48 (2009) 419–428. doi:10.1007/s11106-009-9150-7

[76] S. Khorsand, K. Raeissi, F. Ashrafizadeh, M.A. Arenas, Relationship between the structure and water repellency of nickel-cobalt alloy coatings prepared by electrodeposition process, Surf. Coatings Technol. 276 (2015) 296–304. doi:10.1016/j.surfcoat.2015.07.010

[77]   H. Cesiulis, Z. Stojek, Electrodeposition and properties of Ni W , Fe W and Fe Ni W amorphous alloys. A comparative study, Electrochim. Acta. 45 (2000) 3389–3396. doi:10.1016/S0013-4686(00)00437-0

[78]   L. Elias, A. Chitharanjan Hegde, Electrodeposition of laminar coatings of Ni-W alloy and their corrosion behaviour, Surf. Coatings Technol. 283 (2015) 61–69. doi:10.1016/j.surfcoat.2015.10.025

[79]   J. Auerswald, H.-J. Fecht, Nanocrystalline Ni–W for Wear-Resistant Coatings and Electroforming, J. Electrochem. Soc. 157 (2010) D199. doi:10.1149/1.3291984

[80]   F. Zouch, Z. Antar, A. Bahri, K. Elleuch, M. Ürgen, Tribological Study of Fe–W–P Electrodeposited Coating on 316 L Stainless Steel, J. Tribol. 140 (2017) 011301. doi:10.1115/1.4036628.

[81]   K.R. Sriraman, S.G. Sundara Raman, S.K. Seshadri, Synthesis and evaluation of hardness and sliding wear resistance of electrodeposited nanocrystalline Ni-W alloys, Mater. Sci. Eng. A. 418 (2006) 303–311. doi:10.1016/j.msea.2005.11.046

[82]   Z.I. Bobanova, A.I. Dikusar, H. Cesiulis, J.-P. Celis, N.I. Tsyntsaru, I. Prosycevas, Micromechanical and tribological properties of nanocrystalline coatings of iron-tungsten alloys electrodeposited from citrate-ammonia solutions, Russ. J. Electrochem. 45 (2009) 895–901. doi:10.1134/S1023193509080096

[83]   F. He, J. Yang, T. Lei, C. Gu, Structure and properties of electrodeposited Fe-Ni-W alloys with different levels of tungsten content: A comparative study, Appl. Surf. Sci. 253 (2007) 7591–7598. doi:10.1016/j.apsusc.2007.03.068

[84]   N. Imaz, J.A. Díez, E. Pellicer, J. Sort, H. Grande, E. García-Lecina, Thermal treatment effect on the mechanical, tribological and corrosion properties of Ni–W alloy obtained by direct and pulse plating electrodeposition, Trans. Inst. Met. Finish. 95 (2017) 31–38. doi:10.1080/00202967.2017.1260885

[85]   S. Hayata, S. Oue, H. Nakano, T. Takahash, Effect of Annealing on the Structure and Hardness of Electrodeposited Ni-W Alloys, ISIJ Int. 5 (2015) 1083–1090. doi:10.2355/isijinternational.55.1083

[86]   M.H. Allahyarzadeh, M. Aliofkhazraei, A.R. Rezvanian, V. Torabinejad, A.R. Sabour Rouhaghdam, Ni-W electrodeposited coatings: Characterization, properties and applications, Surf. Coatings Technol. 307 (2016) 978–1010. doi:10.1016/j.surfcoat.2016.09.052

[87]   C.J. Marvel, D. Yin, P.R. Cantwell, M.P. Harmer, The influence of oxygen contamination on the thermal stability and hardness of nanocrystalline Ni-W alloys, Mater. Sci. Eng. A. 664 (2016) 49–57. doi:10.1016/j.msea.2016.03.129

[88]   M.C. Chou, C.F. Chu, S.T. Wu, Phase transformations of electroplated amorphous iron-tungsten-carbon film, Mater. Chem. Phys. 78 (2003) 59–66. doi:10.1016/S0254-0584(02)00217-1

[89]   N. Tsyntsaru, G. Kaziukaitis, C. Yang, H. Cesiulis, H.G.G. Philipsen, M. Lelis, J.P. Celis, Co-W nanocrystalline electrodeposits as barrier for interconnects, J. Solid State Electrochem. 18 (2014) 3057–3064. doi:10.1007/s10008-014-2488-x

[90]   A.J. Detor, M.K. Miller, C.A. Schuh, Solute distribution in nanocrystalline Ni–W alloys examined through atom probe tomography, Philos. Mag. 86

(2006) 4459–4475. doi:10.1080/14786430600726749

[91] C.J. Marvel, P.R. Cantwell, M.P. Harmer, The critical influence of carbon on the thermal stability of nanocrystalline Ni-W alloys, Scr. Mater. 96 (2015) 45–48. doi:10.1016/j.scriptamat.2014.10.022

[92] D.H. Jeong, U. Erb, K.T. Aust, G. Palumbo, The relationship between hardness and abrasive wear resistance of electrodeposited nanocrystalline Ni-P coatings, Scr. Mater. 48 (2003) 1067–1072. doi:10.1016/S1359-6462(02)00633-4

[93] A. Leyland, A. Matthews, On the significance of the H/E ratio in wear control: A nanocomposite coating approach to optimised tribological behaviour, Wear 246 (2000) 1–11. doi:10.1016/S0043-1648(00)00488-9

[94] T.J. Rupert, C.A. Schuh, Sliding wear of nanocrystalline Ni-W: Structural evolution and the apparent breakdown of Archard scaling, Acta Mater. 58 (2010) 4137–4148. doi:10.1016/j.actamat.2010.04.005

[95] E. Vernickaite, H. Cesiulis, N. Tsyntsaru, Evaluation of corrosion and tribological behavior oe electrodeposited tungsten alloys, Proc. Int. Conf. BALTTRIB'2017. doi: 10.15544/balttrib.2017.36

[96] M. Hashemi, S. Mirdamadi, H.R. Rezaie, Effect of SiC nanoparticles on microstructure and wear behavior of Cu-Ni-W nanocrystalline coating, Electrochim. Acta. 138 (2014) 224–231. doi:10.1016/j.electacta.2014.06.084

[97] M.G. Hosseini, M. Abdolmaleki, J. Ghahremani, Investigation of corrosion resistance of electrodeposited Ni–W/SiC composite coatings, Corros. Eng. Sci. Technol. 49 (2014) 247–253. doi:10.1179/1743278213Y.0000000120

[98] S. Yari, C. Dehghanian, Deposition and characterization of nanocrystalline and amorphous Ni-W coatings with embedded alumina nanoparticles, Ceram. Int. 39 (2013) 7759–7766. doi:10.1016/j.ceramint.2013.03.033

[99] R. Starosta, A. Zielinski, Effect of chemical composition on corrosion and wear behaviour of the composite Ni-Fe-Al$_2$O$_3$ coatings, J. Mater. Process. Technol. 157–158 (2004) 434–441. doi:10.1016/j.jmatprotec.2004.09.068

[100] N.P. Wasekar, S.M. Latha, M. Ramakrishna, D.S. Rao, G. Sundararajan, Pulsed electrodeposition and mechanical properties of Ni-W/SiC nano-composite coatings, Mater. Des. 112 (2016) 140–150. doi:10.1016/j.matdes.2016.09.070

[101] E. García-Lecina, I. García-Urrutia, J.A. Díez, J. Fornell, E. Pellicer, J. Sort, Codeposition of inorganic fullerene-like WS$_2$ nanoparticles in an electrodeposited nickel matrix under the influence of ultrasonic agitation, Electrochim. Acta. 114 (2013) 859–867. doi:10.1016/j.electacta.2013.04.088

[102] A. Akyol, H. Algul, M. Uysal, H. Akbulut, A. Alp, A Novel Approach for Wear and Corrosion Resistance in the Electroless Ni-P-W alloy with CNFs Co-Depositions, Appl. Surf. Sci. (2018). doi:10.1016/j.apsusc.2018.05.152

[103] N.I. Tsyntsaru, Z.I. Bobanova, D.M. Kroitoru, V.F. Cheban, G.I. Poshtaru, A.I. Dikusar, Effect of a Multilayer Structure and Lubrication on the Tribological Properties of Coatings of Fe-W Alloys, Surf. Eng. Appl. Electrochem. 46 (2010) 538–546. doi:10.3103/S1068375510060025

[104] E. Beltowska-Lehman, P. Indyka, A. Bigos, M. Kot, L. Tarkowski, Electrodeposition of nanocrystalline Ni-W coatings strengthened by ultrafine alumina particles, Surf. Coatings Technol. 211 (2012) 62–66. doi:10.1016/j.surfcoat.2011.10.021

[105] R.S. Bajwa, Z. Khan, V. Bakolas, W. Braun, Water-lubricated Ni-based composite (Ni-Al$_2$O$_3$, Ni-SiC and Ni-ZrO$_2$) thin film coatings for industrial

applications, Acta Metall. Sin. English Lett. 29 (2016) 8–16. doi:10.1007/s40195-015-0354-1

[106]   A.A. Aal, S.M. El-Sheikh, Y.M.Z. Ahmed, Electrodeposited composite coating of Ni-W-P with nano-sized rod- and spherical-shaped SiC particles, Mater. Res. Bull. 44 (2009) 151–159. doi:10.1016/j.materresbull.2008.03.008

[107]   L. Shi, C. Sun, P. Gao, F. Zhou, W. Liu, Mechanical properties and wear and corrosion resistance of electrodeposited Ni-Co/SiC nanocomposite coating, Appl. Surf. Sci. 252 (2006) 3591–3599. doi:10.1016/j.apsusc.2005.05.035

[108]   M. Allahyarzadeh, M. Aliofkhazraei, A.S. Rouhaghdam, V. Torabinejad, Electrodeposition of multilayer Ni–W and Ni–W–alumina nanocomposite coatings, Surf. Eng. 33 (2017) 327–336. doi:10.1080/02670844.2016.1277640

[109]   Q.Q. Ren, J.L. Fan, Y. Han, H.R. Gong, Structural, thermodynamic, mechanical, and magnetic properties of FeW system, J. Appl. Phys. 116 (2014) 0–9. doi:10.1063/1.4894396

[110]   P. Esther, C. Kennady, Structural and magnetic properties of electrodeposited Ni-Fe-W thin films, J. Non-Oxide Glas. 1 (2009) 301–309.

[111]   H. Chiriac, A.E. Moga, C. Gherasim, N. Lupu, Synthesis and Characterization of Fe-W and Ni-W Composite Coatings, 11 (2008) 123–132.

[112]   A. Survila, Z. Mockus, S. Kanapeckaite, Kinetics of Sn and Co codeposition in citrate solutions, Electrochim. Acta. 46 (2000) 571–577. doi:10.1016/S0013-4686(00)00633-2

[113]   E. Bulemela, L. Trevani, P.R. Tremaine, Ionization constants of aqueous glycolic acid at temperatures up to 250°C using hydrothermal pH indicators and UV-visible spectroscopy, J. Solution Chem. 34 (2005) 769–788. doi:10.1007/s10953-005-5113-x

[114]   A. Stefánsson, Iron (III) hydrolysis and solubility at 25 °C, Environ. Sci. Technol. 41 (2007) 6117–6123. doi:10.1021/es070174h

[115]   J. Aveston, Hydrolysis of Tungsten(VI): Ultracentrifugation, Acidity Measurements, and Raman Spectra of Polytungstates, Inorg. Chem. 3 (1964) 981–986. doi:10.1021/ic50017a012

[116]   R. Portanova, L.H.J. Lajunen, M. Tolazzi, J. Piispanen, Critical evaluation of stability constants for a-hydroxycarboxilic acid complexes with protons and metal ions ans the accompaying enthalpy changes. Part II. Aliphatic 2-hydroxycarboxylic acids, IUPAC Tech. Rep. 75 (2003) 495–540.

[117]   M.M. Caldeira, M.L. Ramos, V.M.S. Gil, Complexes of W(VI) and Mo(VI) with glycolic, lactic, chloro- and phenyl-lactic, mandelic, and glyceric acids studied by 1H and 13C nuclear magnetic resonance spectroscopy, Can. J. Chem. 65 (1987) 827–832. doi:10.1139/v87-140

[118]   C.F. Timberlake, Iron-Malate and Iron-Citrate Comfilexes, J. Chem. Soc. (1964) 5078–5085.

[119]   A.M.N. Silva, X. Kong, M.C. Parkin, R. Cammack, R.C. Hider, Iron(III) citrate speciation in aqueous solution, Dalt. Trans. (2009) 8616. doi:10.1039/b910970f

[120]   W.C. Oliver, G.M. Pharr, Measurement of hardness and elastic modulus by instrumented indentation: Advances in understanding and refinements to methodology, J. Mater. Res. 19 (2004) 3–20. doi:10.1557/jmr.2004.19.1.3

[121] Y.D. Gamburg, E.N. Zakharov, G.E. Goryunov, Electrodeposition, Structure, and Properties of Iron – Tungsten Alloys, Russ. J. Electrochem. 37 (2001) 670–673

[122] M. Donten, Bulk and surface composition, amorphous structure, and thermocrystallization of electrodeposited alloys of tungsten with iron, nickel, and cobalt, J. Solid State Electrochem. 3 (1999) 87–96. doi:10.1007/s100080050133

[123] R. Juškenas, I. Valsiunas, V. Pakštas, R. Giraitis, On the state of W in electrodeposited Ni-W alloys, Electrochim. Acta. 54 (2009) 2616–2620. doi:10.1016/j.electacta.2008.10.060

[124] V.A. Lubarda, On the effective lattice parameter of binary alloys, Mech. Mater. 35 (2003) 53–68. doi:10.1016/S0167-6636(02)00196-5

[125] B.D. Cullity, C.D. Graham, Introduction to Magnetic Materials (2nd Edition), 2009. doi:10.1016/S1369-7021(09)70091-4

[126] E. Vernickaite, N. Tsyntsaru, H. Cesiulis, Electrodeposition and corrosion behaviour of nanostructured cobalt–tungsten alloys coatings, Trans. Inst. Met. Finish. 94 (2016) 313–321. doi:10.1080/00202967.2016.1220071

[127] M. Wang, Z. Wang, Z. Guo, Electrodeposited free-crack NiW films under super gravity filed: Structure and excellent corrosion property, Mater. Chem. Phys. 148 (2014) 245–252. doi:10.1016/j.matchemphys.2014.07.041

[128] E. Vernickaite, Z.Z. Antar, A. Nicolenco, R. Kreivaitis, N. Tsyntsaru, H. Cesiulis, Tribological and Corrosion Properties of Iron-Based Alloys, Proc. 8th Int. Sci. Conf. "BALTTRIB 2015". doi:10.15544/balttrib.2015.29

[129] H.A. Abdel-Aal, On the interdependence between kinetics of friction-released thermal energy and the transition in wear mechanisms during sliding of metallic pairs, Wear 254 (2003) 884–900. doi:10.1016/S0043-1648(03)00243-6

ACKNOWLEDGEMENTS

CURRICULUM VITAE

Personal information
Name: Aliona
Surname: Nicolenco
Date of birth: 29 June 1992
Place of birth: Colibaş, Republic of Moldova
E-mail: aliona.nicolenco@chgf.vu.lt
Mob. No: +370 64553258

Affiliation
Department of Physical Chemistry, Faculty of Chemistry and Geoscience, Vilnius University, Naugarduko str. 24, LT 03225, Vilnius, Lithuania
E-mail: info@chgf.vu.lt
Tel. nr. +370 (5) 219 3105

PREVIOUS SCIENTIFIC/PROFESSIONAL ACTIVITIES:

10.2015– 12.2018	PhD student at Vilnius University, Lithuania**.** Supervisors: Prof. H. Cesiulus, Dr. N. Tsyntsaru. *Electrodeposition of Fe-W alloys from environmentally-friendly bath and their characterization*
01.2014– 01.2016	Junior scientific researcher at Laboratory of Electrophysical and Electrochemical Treatment of Materials Boris Lazarenko, Institute of Applied Physics of the Academy of Sciences of Moldova.
09.2013- 06.2015	Master of Exact Science in Coordination Chemistry, Moldova State University. Supervisor: V. Tsapkov. *The metal complexes of cobalt, nickel and copper with 1,3-diphenilpirazol-4-carbaldehyde thiosemicarbazone*
09.2009- 06.2013	Bachelor of Exact Science in Chemistry, Moldova State University. Supervisor: Dr. O. Sharaevskaia. *Study of the complexation process of Bi^{3+} cation with sodium salt of 4-pheniltiosemicarbazone-1,2-naftaquinone-4-sulfonic acid in presence of some ions*

TRAININGS:

Scientific

26- 30.03.2018	3rd e-MINDS Training School "Electrochemical processing methodologies and corrosion protection for device and systems miniaturization", Siofiok, Hungary
7-12.01.2018	SELECTA Winter school "Gateway to industry: Introducing materials to market. Practical aspects", Cambridge, UK.
3-8.09.2017	SELECTA Summer school "Gateway to Academics: Materials modelling for target applications", Ioannina, Greece.

2-6.04.2017	2nd e-MINDS Training School "Electrochemical processing methodologies and corrosion protection for device and systems miniaturization", Schwäbisch Gmünd, Germany.
5-9.12.2016	4th SELECTA Workshop "Bridging innovation and entrepreneurship with sustainable materials development", Goteborg, Sweden.
29-31.08.2016	3rd SELECTA Workshop "Micro and nano-electrodeposition for MEMS/NEMS and micro/nano-robotic platforms. Overview of lithography methods. Impact to society", Wiener Neustadt, Austria
06-10.03.2016	2nd SELECTA Workshop „Training on research methodologies, characterization techniques and reporting scientific results", Dresden, Germany.
03-07.11.2015	1st SELECTA Workshop „Fundamentals of electrodeposition of metallic alloys: state-of-the-art at European and International levels´ Vrnjacka Banja, Serbia

Trainings in soft skills

04.09.2017	Competively Grant Writing, Ioannina, Greece. Trainer: Ms. Lotte Jaspers, Yellow Research, Amsterdam.
31.08.2016	How to write scientific papers, Wiener Neustadt, Austria. Trainer: Prof. Lindsay Greer, editor of Philosophical Magazine, UCAM.
09.03.2016	Effective oral presentations, Dresden, Germany. Trainer: Mr. Jean Luc Doumont, Principiae, Belgium.
07.11.2015	Internationalization of research, bridging scientific research environment between Eastern and Western Europe, Vrnjacka Banja, Serbia. Trainer: Prof. Dr. Miroslav Trajanovic – Serbia EURAXESS network, Researchers in Motion, pan-European initiative, Serbia.

INTERNATIONAL CONFERENCES:

27-29.06.2018	32nd International Conference on Surface Modification Technologies, San Sebastian, Spain. *Effect of alumina sub-microparticles on the mechanical, tribological and corrosion properties of electrodeposited Fe-W composite coatings (oral presentation).*
16-18.04.2018	6th World Congress on Nanotechnology and Material Science, Valencia, Spain. *Functional electrodeposited Fe-W alloys for target application (oral presentation).*
16-17.11.2017	International Conference BALTTRIB'2017, Kaunas, Lithuania. *Wear resistance of electrodeposited Fe-W alloys under dry and lubricating conditions (oral presentation).*
6-9.06.2017	XII ECHEMS Meeting "Electrochemistry in… ingenious molecules, surfaces and devices", Milano Marittima, Italy.

	Interdependences between the composition and structure of Fe-W coatings electrodeposited from glycolate-citrate plating bath (poster presentation).
14-17.03.2017	60th International Conferenced for Students of Physics and Natural Sciences (Open Readings), Vilnius, Lithuania. *Electrodeposited Fe-W alloys as a material for MEMS fabrication (poster presentation).*
19-22.09.2016	The 2016 E-MRS Fall Meeting, Warsaw, Poland. *Electrodeposition of Fe-W alloys from glycolate-citrate plating bath: in-depth characterization by GD-OES (poster presentation).*
12-16.09.2016	The 8th International Conference on Materials Science and Condensed Matter Physics, Chisinau, Moldova. *Magnetic and mechanical properties of electrodeposited Fe-W alloys (oral presentation).*

INTERNSHIPS

20.1-20.2.2018	CIDETEC research institute, San Sebastian, Spain. Advisor: Dr. N. Imaz, Dr. E. García-Lecina *Development and characterization of Fe-W/Al_2O_3 composite coatings*
15.07-15.08.2016	Leibniz Institute for Solid State and Materials Research, Dresden, Germany. Advisor: Dr. Margitta Uhlemann *Magneto-electrodeposition of metallic films and their characterization by GD-OES*
6.06-6.07.2016	Autonomous University of Barcelona, Bellatera, Spain. Advisor: Prof. Jordi Sort *Evaluation of mechanical and magnetic properties of Fe-W alloys with various W content and possible changes induced by nanoindentation*

AWARDS

30.03.2018	"Best Student presentation" at 3rd e-MINDS training school, COST Action e-MINDS (MP1407). *Functional electrodeposited Fe-W: design, characterization and properties.*
21.02 2018	"Best Video Award" by COST Action e-MINDS (MP1407). *Functional electrodeposited Fe-W alloys for environmentally sustainable applications.*

Paper 1

Fe (III)-based ammonia-free bath for electrodeposition of Fe-W alloys

A. Nicolenco, N. Tsyntsaru, H. Cesiulis

Journal of The Electrochemical Society 164, 2017, D590-D597

Reprinted with permission from *Journal of The Electrochemical Society*

Fe (III)-Based Ammonia-Free Bath for Electrodeposition of Fe-W Alloys

A. Nicolenco,[a] N. Tsyntsaru,[a,b,z] and H. Cesiulis[a]

[a]*Department of Physical Chemistry, Vilnius University, Vilnius LT-03225, Lithuania*
[b]*Institute of Applied Physics of ASM, Chisinau, MD – 2028, Moldova*

Electrodeposited Fe-W alloys are the subject of extensive studies to be applied in versatile engineering applications, and many solutions based on Fe(II) complexes are described for their deposition. However, in aqueous solutions containing dissolved oxygen, Fe(II) compounds are unstable thermodynamically and tend to oxidize to Fe(III) state that decreases the sustainability of the baths. The aim of the present study was to develop an environment-friendly and thermodynamically stable Fe(III)-based electrolyte for electrodeposition of Fe-W alloys with tunable composition. It was found that: (i) concurrent use of two complexing agents as citric and glycolic acids stabilizes Fe(III)-based bath in neutral and weak alkaline medium (no precipitates are formed); (ii) the current efficiency of the process can reach up to 60–70%, which has never been reported before for Fe-W alloys electrodeposition; (iii) nanocrystalline Fe-W coatings containing 11–24 at.% of W can be obtained from Fe(III)-based glycolate-citrate bath at temperature range 20–65°C. The increase in tungsten content in the alloy resulted in decreased grain size up to < 5 nm; (iv) smooth, free of cracks and having deposition rates up to 0.18 μm/cm[1] alloys are successfully electrodeposited at elevated temperatures from elaborated glycolate-citrate electrolyte.

The rapid development of modern technologies in the chemical engineering requires obtaining of new materials with tunable composition, microstructure, and properties. Electrodeposited tungsten alloys with Fe, Co and Ni attracted much attention as alternative for electrolytic chromium replacement[1,2] produced from the bath based on highly toxic Cr(VI). Recently, the increased interest is particularly focused on the electrodeposition of Fe-W alloys including for such emerging applications as production of lithium ion batteries,[3] recording media,[4] catalyst[5] and fuel cells.[6]

Nevertheless, that the electrodeposition of Fe-W alloys is actively studied since 1940 s,[7] the development and optimization of new electrolytes are still highly demanded. Thus, citrate baths were extensively investigated[8–11] for Fe-W alloys electrodeposition. Also, ammonia was usually added to the electrolytes for alloys deposition as it increases the solubility of metal's complexes and influences on the species distribution,[12,13] and has a significant effect on W co-deposition and bath stability. Such citrate-ammonia electrolytes enable to produce rather smooth and silvery to gray in appearance Fe-W coatings,[4,14] but the performance of those electrolytes is significantly affected by competing reactions of hydrolysis and complexing.[10] Thus, in order to deposit reach in tungsten (up to 30–35 at.%) Fe-W alloys from citrate-ammonia baths the optimum values of pH 7.0–8.5 should be used.[15] Nevertheless, in order to reduce the environmental impact of electrochemical bath containing ammonia salts, attempts to find ammonia-free baths were explored.[1,16–19] An example of successful elaboration of ammonia-free baths was demonstrated for Ni alloys electrodeposition,[20,21] where electrolytes based on glycolic acid were used, but there are no similar data reported for Fe-W alloys deposition.

At this point it is worth to note, that the chemical stability is an important characteristic of electroplating baths especially for ones used for iron alloys electrodeposition[22,23] that complicates bath maintenance. The standard potential for oxygen reduction is more positive than for Fe^{3+} reduction to Fe^{2+}, hence the spontaneous reaction in the presence of dissolved oxygen occurs:

$$4Fe^{2+} + O_2 + 4H^+ = 4Fe^{3+} + 2H_2O \qquad [1]$$
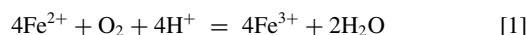
The value of K_{eq} for this reaction can be estimated based on the tabulated data of standard reduction potentials and using the well-known relationship between standard cell potential (ΔE^0) and equilibrium constant (K_{eq}):

$$\Delta E^0 = \frac{RT}{nF} ln K_{eq} \qquad [2]$$

It was found that K_{eq} is big as 1.3·10.[31] This result means that practically total amount of Fe^{2+} eventually will oxidize to Fe^{3+} irrespectively on the complexation of iron ions. Thus, electrolytes based on Fe(II) salts are unstable thermodynamically and the solution content is governed by the Fe(II) oxidation kinetics. It was shown[24,25] that mentioned above citrates and ammonia inhibit the kinetics of Fe(II) oxidation to Fe(III), but cannot prevent it. Some attempts were made to prolong bath life by adding reducing agents,[26–28] but those compounds can affect the bath maintenance and coatings properties.

In this view, it should be reasonable to use electrolytes based on Fe(III) salts to avoid oxidation of Fe(II) species. Nevertheless, study on the electrodeposition of Fe-W alloys from Fe(III) solutions is rather limited. The reason is that the current efficiency and tungsten content are significantly lower for alloys obtained from Fe(III) in comparison to Fe(II) studied electrolytes.[12,14,25,29] Howbeit, it is worth to mention, that the straight comparison of Fe(II) and Fe(III)-based solutions operating at the same conditions remains poorly explored. Therefore, the aim of this study is to explore the new sustainable electrolytic bath based on Fe(III) salt as an alternative to conventional Fe(II) –based bath, and to compare the main characteristics of the Fe-W alloys deposition process occurring in the Fe(III)- and Fe(II)-based solutions.

Experimental

Fe-W alloys were electrodeposited from citrate and glycolate-citrate baths containing Fe(II) or Fe(III) sulfate as a source of iron. The composition of the baths and their lab codes are presented in Table I, and chemicals used have been of analytical grade (A.R.). All solutions were prepared by regular dissolving of components. However, the equilibrium of species during preparation of citrate Fe(III)-based solution was setting within longer period of time. The initial C3 solution was brown, but it changes the color to green after a few hours of electrodeposition. So, in order to obtain reproducible results from this bath, electrodeposition has been carried out after 500 C/cm^{2} passed through the solution. The influence of electrolyte run on the electrodeposition of Fe-W,[18] zinc and nickel,[30] chromium[31] were also detected and it is important parameter to be taken into account.

[z]E-mail: ashra_nt@yahoo.com

Table I. Electrolytes composition used for Fe-W alloys deposition and their lab codes (C2, C3, GC2, GC3).

Components	Composition of electrolytes, mol/L			
	Cit-Fe(II) C2	Cit-Fe(III) C3	Glyco-Cit-Fe(II) GC2	Glyco-Cit-Fe(III) GC3
$Na_2WO_4 \cdot 2H_2O$	0.40	0.40	0.40	0.40
$FeSO_4 \cdot 7H_2O$	0.20	-	0.20	-
$Fe_2(SO_4)_3 \cdot H_2O$	-	0.10	-	0.10
$C_6H_8O_7 \cdot H_2O$ (citric acid)	0.20	0.20	0.30	0.30
$Na_3C_6H_5O_7 \cdot 2H_2O$ (tri-sodium citrate)	0.45	0.45	-	-
$C_2H_4O_3$ (glycolic acid)	-	-	1.00	1.00

Adjustment of pH was made by adding NaOH or H_2SO_4. Electrodeposition of thin films was performed in a typical three-electrode cell. The pure copper sheet with 4.5 cm² area was used as a working electrode. Platinized titanium was used as a counter electrode, and saturated Ag/AgCl was used as reference electrode. All values of electrode potentials are presented against this reference electrode. Prior electrodeposition, the samples were polished, degreased and activated in 2 M sulphuric acid for 1 minute. In order to improve adhesion to the substrate a thin Ni seed-layer was deposited at a cathodic current density of 20 mA/cm² for 1 minute from 1 M nickel chloride solution in 2.2 M hydrochloric acid. Polarization curves were recorded at 20°C and 65°C, and 5 mV/s scan rate using AUTOLAB system (GPES software), and later were corrected for ohmic drop that was determined using FRA 4.9 software.

The current efficiency (CE) of the alloys and resulted thickness of the coatings were determined based on Faraday's law, as was described elsewhere.[32] The thickness of electrodeposited Fe-W coatings was ~5 μm. The thickness of several samples was measured on cross-section in order to confirm the values calculated based on CE. Partial current densities for the corresponding metal were calculated based on the composition and mass of the coating according to following equation:

$$j_M = \frac{n_M \omega_M F}{\mu_M t} \qquad [3]$$

here j_M is the partial current density for the corresponding metal "M" (in A/cm²); n_M is the number of electrons involved in the charge transfer reaction, ω_M is the weight of metal "M" (g/cm²), F is Faraday constant, μ_M is the atomic mass of metal "M" (g/mol), t is the electrodeposition time (s).

The stability of solutions was estimated based on the calculation of species distribution in the electrolyte, taking into account more than 40 simultaneously occurring equilibrium reactions. For this purpose, a system of equations was solved using adopted Maple6 (Waterloo Maple Software and University of Waterloo). The set of equations was based on: (i) the equilibrium constants for all compounds added to or formed in the solutions: acids deprotonation,[33,34] iron hydrolysis,[35,36] polymerization of tungstate,[37] glycolate complexes with Fe and W[38–41] and metal complexes with citrate;[42–45] (ii) the mass balance equations $[J]_{tot} = \sum [J_i^{n+/-}]$ for all forms in the equilibrium mixture; (iii) the charge balance $\sum n_i [Cat_i^{n+}] = \sum n_i [An_i^{n-}]$, where "$Cat$" and "$An$" denote cation and anion, respectively. In our study, glycolic and citric acids are considered as mono- and four protonated, respectively.

The composition and microstructure of the deposited alloys were identified by scanning electron microscope (SEM) using Hitachi TM3000 instrument. The chemical composition of the alloys was determined with the energy dispersive X-ray spectroscopy (EDS) analysis tool attached to the SEM. The crystallographic structure and phase composition of the obtained coatings was studied by means of Rigaku MiniFlex II diffractometer with Cu Kα radiation (λ = 1.54183 Å) operated at 30 kV and 30 mA. The mean crystallite size was estimated based on the peak width and position using Scherrer's equation.

Results and Discussion

***Thermodynamics of Fe(III)-based electrolytes for Fe-W alloys electrodeposition.*—**The development of stable Fe(III)-based plating bath consists in the selection of suitable complexing agents able to prevent formation of sparingly soluble iron hydroxides. In this work we focused on glycolic acid, which might be considered as an alternative complexing agent to conventional baths for Fe-W alloys deposition. In order to evaluate the influence of glycolic acid on the bath stability the thermodynamic calculations were performed considering the influence of the solution content on the concentration of "free" Fe^{3+} ions.

The maximum concentration of Fe^{3+} ions in the electrolyte is limited by the solubility product of $Fe(OH)_3$. In each complex system, the concentration of particular component depends on the whole composition of the solution. Therefore, it is essential to take into account the ionic strength of solution. Using the second approximation of Debye–Hückel theory and considering the ionic strength of investigated electrolytes I ≈ 2 M, the solubility product of freshly formed $Fe(OH)_3$ was estimated as $L_{Fe(OH)_3}^{I=2M} = 7.4 \cdot 10^{-36}$.

The distribution of species as a function of pH was calculated, and for some ions, it is presented in Figure 1. On the Figures 1a, 1b the line marked as $[Fe^{3+}]_{sat}$ is a maximum thermodynamic concentration of Fe^{3+} ions in the solution, and it was calculated as a function of pH based on $Fe(OH)_3$ solubility product using following expression:

$$[Fe^{3+}]_{sat} = \frac{L_{Fe(OH)_3}}{K_{H_2O}^3} \cdot [H^+]^3 \qquad [4]$$

here K_{H_2O} is the ionization constant of water.

Evidently, the electrolyte is stable and no precipitates are noticed if $[Fe^{3+}]<[Fe^{3+}]_{sat}$, i.e. the electrolyte is considered as thermodynamically stable below the line $[Fe^{3+}]_{sat}$.

As it is shown in Figure 1a, Fe(III)-based glycolate solutions are stable in the acidic media only, while citrate solutions without adding of Na_2WO_4 are stable in the wide range of pH. However, considering the electrodeposition of Fe-W alloys with relatively high amount of tungsten, the electrodeposition should be carried out from neutral or weak alkaline solutions.[2,11,15] In the presence of Na_2WO_4 formation of complexes with WO_4^{2-} occurs as well, and ligands are redistributed between Fe(III) and tungstate, therefore the concentration of "free" Fe^{3+} ions increases and thus the stability of solutions decreases sufficiently (Figure 1b).

In citrate solutions at pH<6 complex $(WO_4)_2(HCit)H_4^{3-}$ predominates, while at pH above 6 the concentration of W-citrate complexes decreases and WO_4^{2-} dominates (Figure 1c). Hence, at pH above 6 the Fe-citrate complexes are formed and the concentration of free Fe^{3+} ions decreases respectively.

Glycolic acid is the weaker complexing agent for Fe^{3+} than citrate. Despite the concentration of glycolic acid several times exceeded the concentration of metals, the stability line of glycolate bath is situated closer to $[Fe^{3+}]_{sat}$. Therefore, in the pure glycolate solutions $[Fe^{3+}] \approx [Fe^{3+}]_{sat}$ and these electrolytes can be stable only for a while, due to kinetic peculiarities of hydrolysis in the complex solutions, i.e. glycolate solutions are in the thermodynamically metastable state.
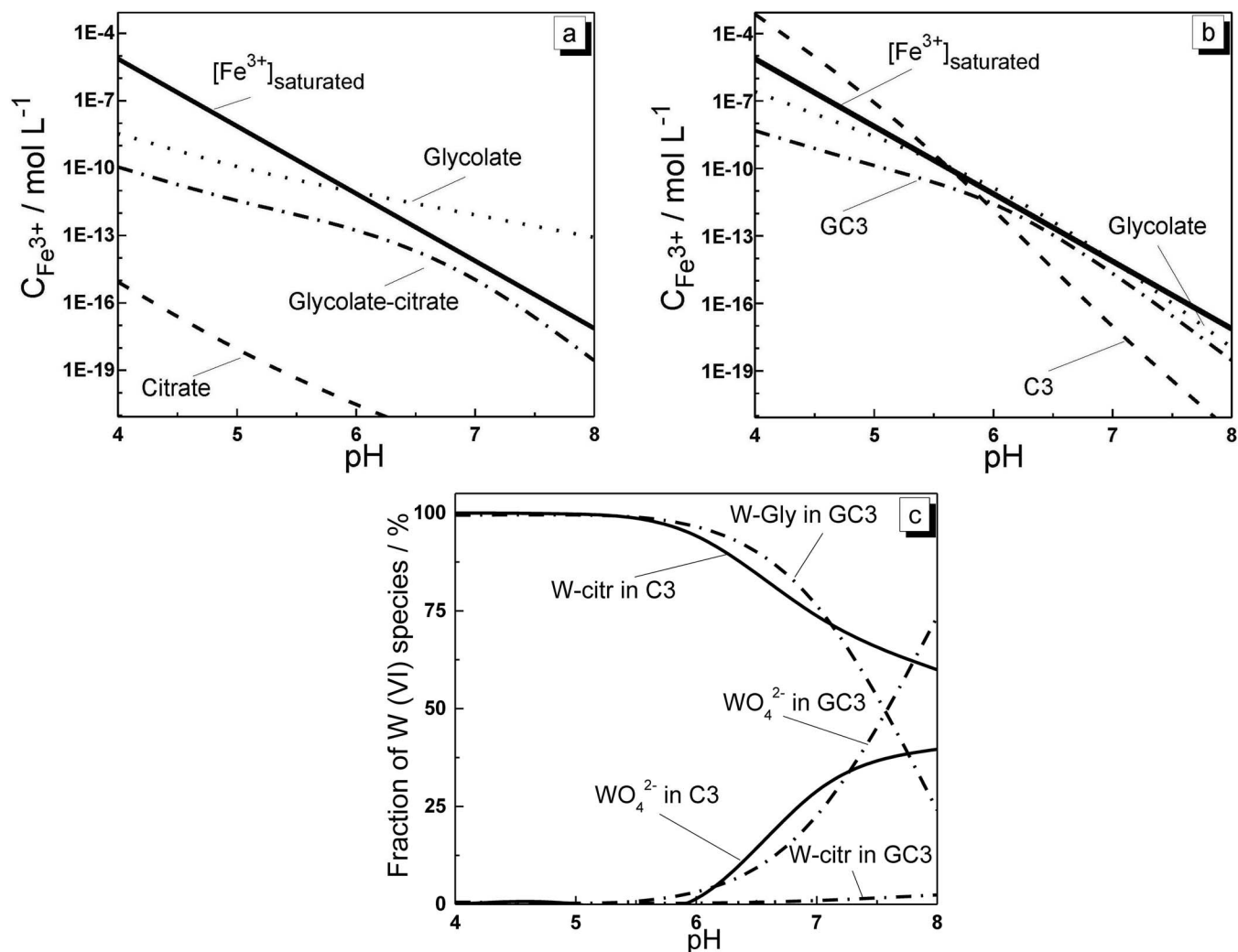
Figure 1. Calculated concentrations of some species as a function of pH in the Fe(III)-based solutions: (a) Fe^{3+} without sodium tungstate; (b) Fe^{3+} with sodium tungstate; (c) fractions of W(VI) species: free WO_4^{2-} and complexes with citrates and glycolates; "W-Cit" means the sum $[(WO_4)(HCit)H^{4-}]+[(WO_4)_2(HCit)H_4^{3-}]$ and "W-Gly" means $[WO_2Gly_2^{2-}]$. The types of electrolytes are market next to the corresponding curve. Compositions of electrolytes are given in Table I.

It was assumed, that addition of citric acid to glycolate bath should stabilize electrolyte due to formation of Fe(III) and W(VI) complexes with citrate and glycolate ones. Tungsten forms stronger complexes with glycolate ($WO_2Gly_2^{2-}$) than with citrate, and in the glycolate-citrate solutions tungsten complexes dominate over the citrate, while Fe(III) ions are mainly in the citrate complexes (see Figures 1b and 1c), that indeed stabilizes glycolate-citrate solution. The formation of W-glycolate complex over the W-citrate is expected to have a significant influence on the electrodeposition process, resulting in easier deposition of metallic ions on the cathode from the complex with smaller molecular volume.

For electrodeposition of the alloys we used pH 6.5–6.7, considering the electrodeposition of Fe-W alloys with high tungsten content. At this pH the concentration of W(VI)-glycolate complexes in GC3 bath and W(VI)-citrate complexes in C3 bath begins to decrease and concentration of "free" WO_4^{2-} increases, therefore less amount of free Fe^{3+} ions are present in the solution, leading to the higher stability. It is also worth to notice, that thermodynamic calculations certainly represent a good approach to understanding the bath stability, however they do not consider kinetic of the process.

Cathodic polarization study.—Complex formation of Fe(II), Fe(III) and W(VI) with citrate and glycolate results in sufficient shifts

of Nernst equilibrium potentials in the investigated solutions especially for Fe(III) reduction to iron (see Table II). Polarization curves were recorded in order to estimate the electrodeposition conditions for Fe-W alloys (Figure 2). Also, cathodic polarization curves were obtained for pure Fe deposition in order to specify the role of W(VI) in electrodeposition of Fe-W alloy. Electrodeposition of pure iron was carried out from electrolytes contained the same components as listed in Table I, but without sodium tungstate. The plateau on the polarization curves in the range of potentials −0.7 to −1.1 V is observed for Fe deposition, while for Fe-W it was observed in the narrower potential range. Potentiostatic depositions corresponding to potential range −0.7 V ÷ −0.9 V have been carried out for 30 minutes from investigated electrolytes. It was determined that metals do not deposit in the corresponding potential ranges. The similar plateau obtained for Fe-W electrodeposition is described by Gamburg.[18] It might be attributed to the water decomposition, reduction of dissolved oxygen and partial reducing of iron compounds.

As it is seen from Figure 2, the decreasing in polarization is observed after adding sodium tungstate into solution, while pure iron deposition occurs at relatively higher polarizations from all investigated solutions. The sufficient increase of cathodic current density for Fe-W alloy is noticed at potentials more negative than −0.9 V (the ohmic drop was taken into account) attesting the start of deposition.

Table II. Standard reduction potentials, E^0, and Nernst equilibrium potentials, E_N, in the investigated solutions at pH 6.7 for reduction of ferric/ferrous and tungstate ions (vs. NHE). Values of the equilibrium concentration of "free" Fe^{3+}, Fe^{2+} and WO_4^{2-} ions were taken from Fig. 1. Compositions of solutions and their lab codes are shown in Table I.

		E_N, V			
Electrochemical reaction	E^0, V	C2	C3	GC2	GC3
$Fe^{3+} + 3e^- = Fe$	−0.036		−0.294		−0.266
$Fe^{2+} + 2e^- = Fe$	−0.440	−0.596		−0.553	
$WO_4^{2-} + 4H_2O + 6e^- = W + 8OH^-$	−1.050	−0.508	−0.482	−0.494	−0.493
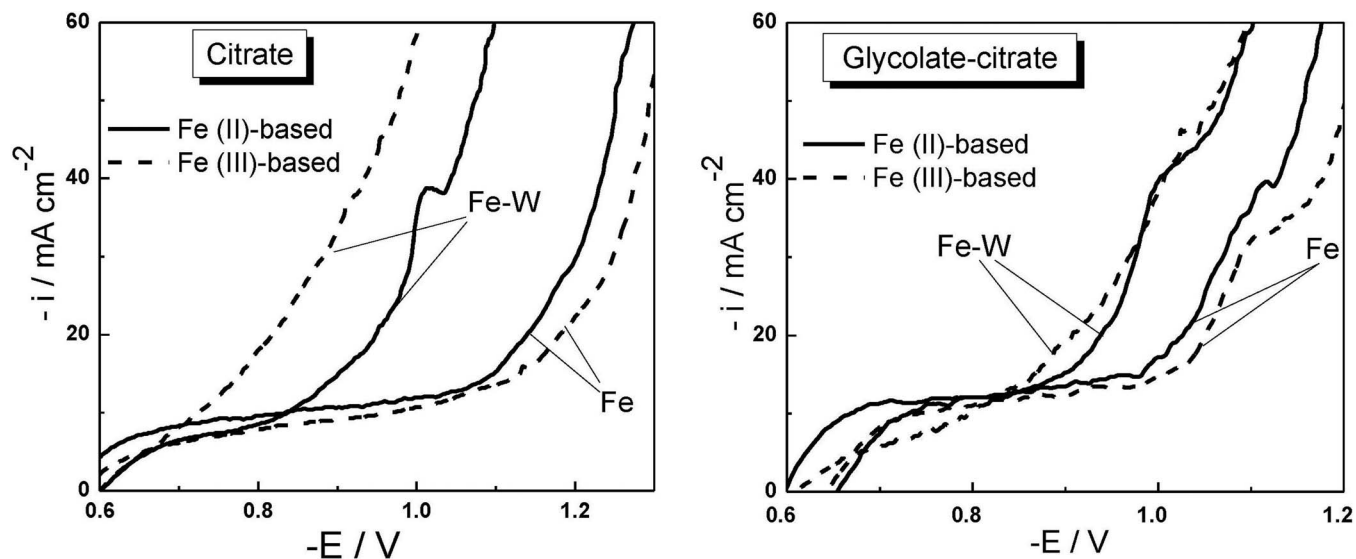
Figure 2. Cathodic polarization curves for Fe and Fe-W alloy deposition from citrate and glycolate-citrate electrolytes obtained at 65°C.

The given current increases with the temperature growth, which in its turn influence on the potential shift to the smaller polarizations.

The partial current densities obtained for Fe and Fe-W deposition were calculated and are shown in Table III. It is seen that at 20°C the co-deposition of tungsten with iron results in higher partial current densities of Fe and decreased partial current of the side reaction, as compared to pure Fe deposition. Whereas at 65°C the partial current for W increases, but partial current densities for Fe and side reaction are decreased. Moreover, the general trend is observed that above the total current density 20 mA/cm² the partial current density of the side reaction (which is mainly the hydrogen evolution) significantly increases, influencing on the current efficiency and morphology of the obtained coatings, which will be discussed below.

Composition, morphology and structure of Fe-W coatings.—In order to determine the optimum conditions for Fe-W electrodeposition, the temperature was varied between 20°C and 65°C and the cathodic current density from 5 to 50 mA/cm², while the concentration of electrolyte components and pH were kept constant. The poor adhesion of Fe-W coatings on copper substrate was observed,
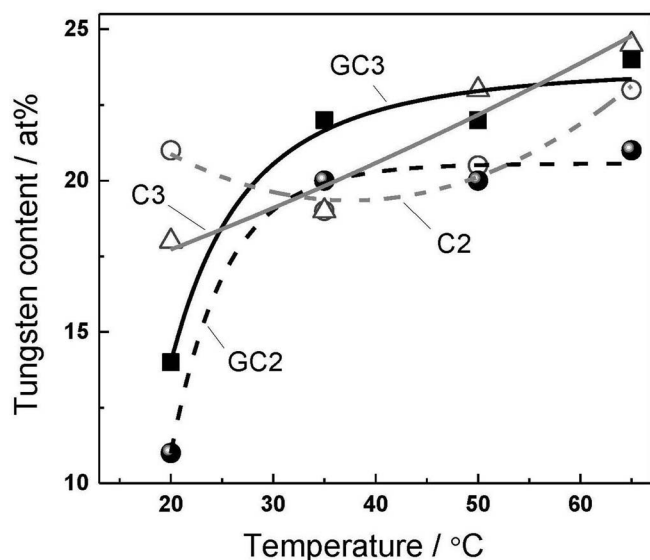
apparently due to the difference between crystallographic structures of these materials.[46] The adhesion was improved essentially by the electrodeposition of nickel seed-layer prior the deposition of alloys.

The tungsten content in Fe-W alloys obtained from the glycolate-citrate baths depends on the temperature, whereas for alloys obtained from the citrate baths it is less dependent (Figure 3). Markedly, Fe-W coatings electrodeposited at room temperature from glycolate-citrate based solutions have lower tungsten content than obtained from citrate solutions. Probably, it is due to slightly lower concentration of "free" WO_4^{2-} ions in the GC3 bath than in C3 electrolyte (Figure 1c), that result in lower partial current density for tungsten codeposition from GC3 solution at room temperature.

EDS analysis data show that electrodeposited Fe-W coatings contain a significant percentage of oxygen, which is higher than that for other tungsten alloys with iron group metals.[9] However, the oxygen content does not correlate with current density, temperature or alloy composition. This fact attests that obtained oxygen content is linked probably only with oxidation of surface by water or air. The results obtained in Ref. 9 on oxygen content in tungsten alloys with Co, Ni and Fe confirm that only thin surface layer contains high amount of

Table III. Partial current densities for metals (Fe and W) and side reaction obtained in the GC3 electrolyte without and with sodium tungstate.
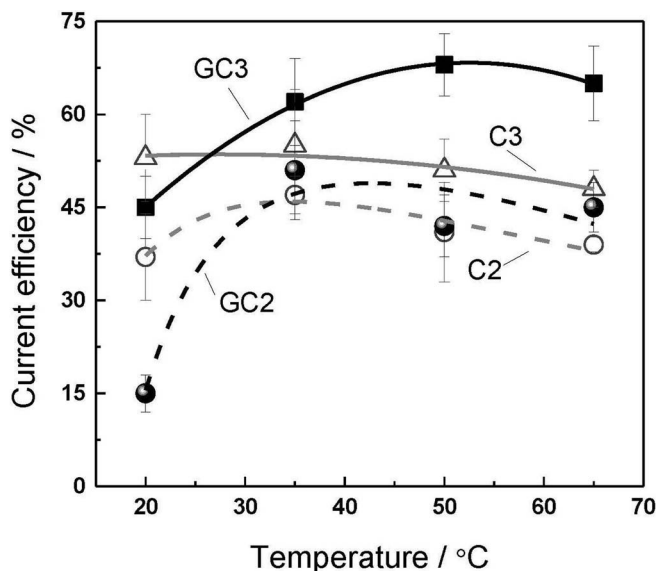
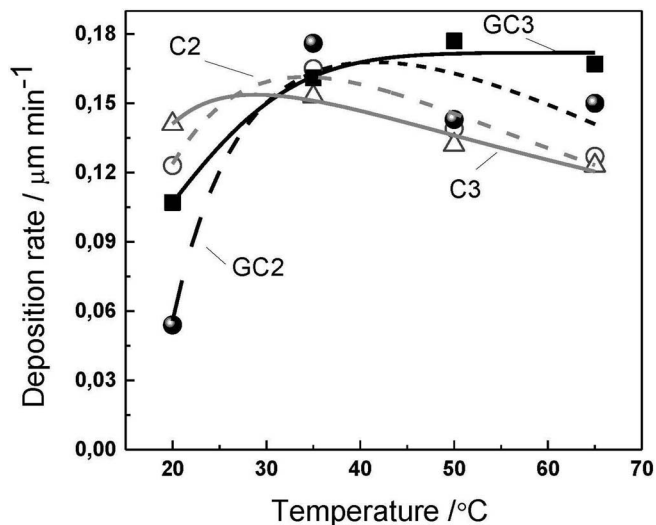|		Fe			Fe-W			
		-$j_{partial}$, mA/cm²			-$j_{partial}$, mA/cm²			
T°C	-j, mA/cm² total	Fe	Side reaction	E, V	Fe	W	Side reaction	E, V
20	15	2	13	−1.25	7	2	6	−1.20
	40	5	35	−1.41	9	3	28	−1.35
65	15	8	7	−1.17	7	4	4	−1.07
	40	14	26	−1.26	17	12	11	−1.19

Figure 3. Temperature influence on tungsten content in the Fe-W alloys electrodeposited from the investigated solutions at cathodic current density 20 mA/cm². Lab codes and composition of solutions are indicated in Table I.

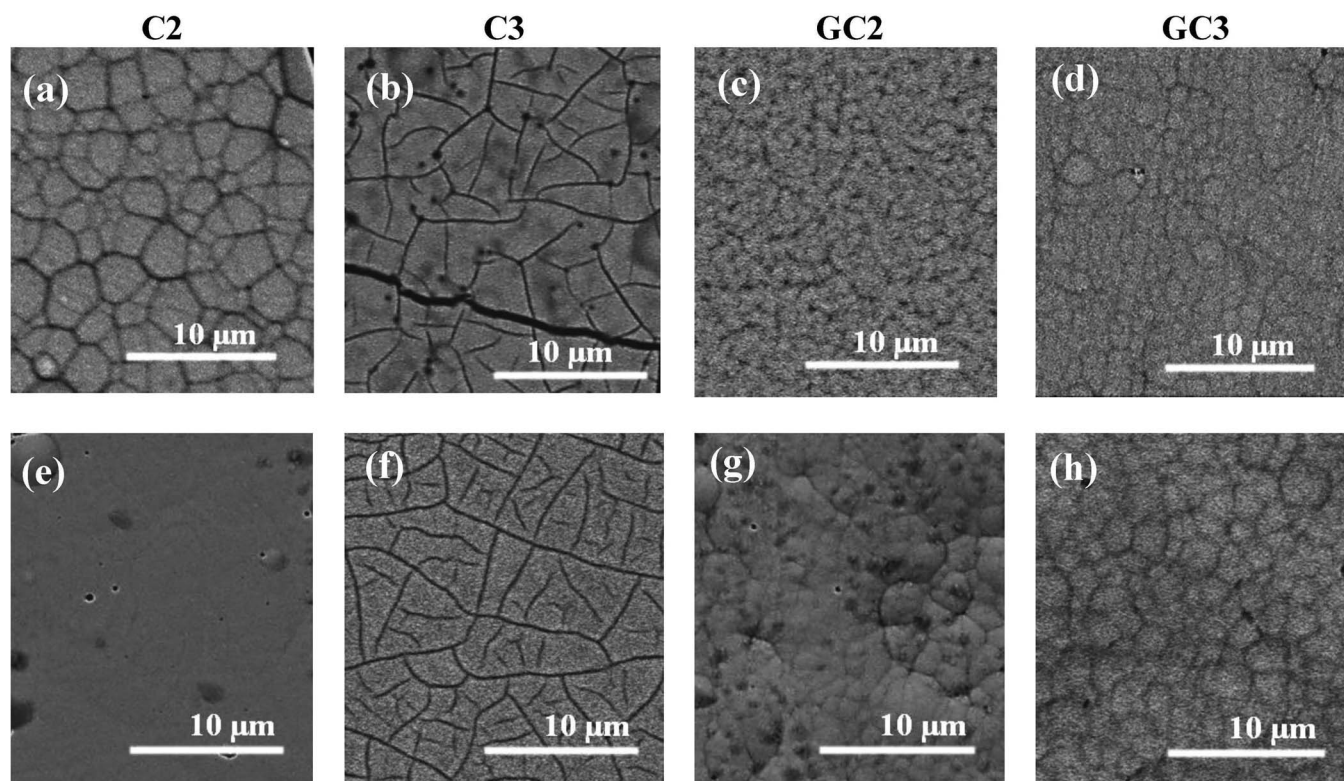**Figure 5.** Temperature influence on Fe-W coatings deposition rates from studied solutions at cathodic current density 20 mA/cm². Lab codes and composition of solutions are indicated in Table I.

oxygen, whereas practically no oxygen was determined in the deeper layers of coatings.

The values of CE attained at various temperatures (20–65°C) for the different Fe-W solutions are presented in Figure 4. CE obtained for Fe(II)-based solutions are lower than that for Fe(III)-based solutions especially for GC2 (∼15%) and it is even lower than that for citrate C2 bath. It is worth to notice, that the CE calculation for Fe(II)-based electrolytes is rather questionable, because of the lack of the control of iron ions oxidation. Therefore, we used only Fe(II)-based freshly prepared baths. It is expected, that with accumulation of Fe^{3+} ions in electroplating bath the CE can increase by ∼10%.[12] In fact, the usage of Fe(III)-based solutions warrants the constant composition of solution because eliminates the chemical oxidation of Fe(II) compounds by dissolved oxygen and oxometalates.[19] The highest values of current efficiency were attained in the all investigated solutions

at cathodic current density of 20 mA/cm². As it is seen, the nature of solution is a key-factor governing CE, whereas variations of CE with temperature is rather weak and CE changes in the range of about ±10% for each solution if temperature exceeds 30°C. The lowest values of CE were obtained for Fe(II)-based solutions. The presence of glycolic acid contributed to the significant increase of CE up to 60–70% for Fe-W alloys deposition from GC3 electrolyte in comparison with other electrolytes. Such high CE has been not noticed for Fe-W alloys deposition earlier. This result seems very appealing, since the value of CE for Fe alloys deposition usually does not exceed 40% and 20% in Fe(II)- and Fe(III)-based electrolytes respectively.[14,18] On the other hand, increased values of CE for Fe(III)-based solutions are defined also by lower weigh of electrochemical equivalent for Fe in comparison with Fe(II)-based solutions. Therefore, it is not adequate to compare CE values obtained from solutions where particular metal is present in the different oxidation states. In the given case, a comparison of deposition rates should be more appropriate in order to assess the efficacy of electroplating baths. These data are presented in Figure 5. As it is seen, the alloy deposition rates for GC3 bath is high enough especially at elevated temperatures, whereas for other solutions this parameter is ranged from 0.12 to 0.15 µm/cm¹.

Another important characteristic of electrodeposited alloys is the surface morphology. The SEM images of Fe-W coatings deposited at different temperatures from investigated electrolytes are presented in Figure 6. The surface of electrodeposited coatings is smooth (roughness of the coatings was ca. 100–150 nm dependently on W content) and typically contains micro-spheres. The temperature has effect on the surface morphology: increase in the temperature up to 65°C results in obtaining of smoother coatings from C2 and GC2 solutions, while it does not influence essentially on the morphology of coatings electrodeposited from the GC3 solution. Also, high internal stress which can appear due to the hydrogen evolution leads to the cracks propagation for coatings deposited at room temperature and relatively high current densities. Remarkably, the alloys obtained from Fe(III)-based glycolate-citrate electrolyte are more compact and with less stress even electrodeposited at room temperature.

Thus, influence of the current density on morphology of Fe-W alloys deposited from GC3 electrolyte is shown in Figure 7. Fe-W alloys deposited at 5 mA/cm² have holes resulted from hydrogen evolution on the whole surface. With increase in the current density the nucleation rate increases and crystallite refinement takes place, thus the surface becomes smoother. However, at cathodic current densities higher than 30 mA/cm², the surface becomes cracked due to the progressive increase in hydrogen evolution.


Figure 4. Temperature influence on current efficiency for Fe-W electrodeposition in the investigated solutions at cathodic current density 20 mA/cm². Lab codes and composition of solutions are indicated in Table I.

Figure 6. SEM images of Fe-W alloys obtained at -20 mA/cm^2 from different electrolytes at 20°C (a, b, c, d) and 65°C (e, f, g, h).

The alloys investigation by X-ray diffraction reveals that the shape of XRD patterns for Fe-W alloys obtained at the same temperature depends on the content of tungsten regardless of the solution type used for electrodeposition. The typical XRD patterns of Fe-W alloys electrodeposited at 20°C are presented in Figure 8. In general, the broadening of XRD peaks with increase in W content in the alloy is obtained, as it was observed for the electrodeposited W- and Mo- containing alloys with iron group metals.[9,10,47] In order to understand Fe-W coatings structure, pure Fe also was electrodeposited from similar bath composition to GC3, but without tungstate. It can be seen, that a well-defined polycrystalline structure of body-centered Fe is obtained for pure electrodeposited Fe. The shift of four peaks, characteristic to pure iron to the lower 2 theta angles in the case of alloy having 11 at.% of W can be observed. Indeed, calculations using Vegard's equation[48] show the increase in average closest distance between two adjacent atoms, which is probably caused by the substitution of Fe atoms by the bigger W atoms in the lattice. It might be supported by the fact that solubility limit of W in bcc Fe is ~14 at.%.[49] Hence, the formation of solid solution of W in Fe is expected at W content up to this value. When content of tungsten equal or exceeds 14 at.%, only one broad peak appears which is typical for "amorphous-like" structure, that is associated with decrease in crystallite size from 30 to ~5 nm. This amount of W in the alloy can be considered as determining for tran-

sition from the nanocrystalline to amorphous-like structure of Fe-W coatings at room temperature. Moreover, this transition at rather low tungsten content is characteristic for tungsten alloy deposits obtained at room temperature due to specific nucleation process.[50]

Conclusions

Fe-W alloys have been successfully electrodeposited from newly developed Fe(III)-based electrolyte contained both citric and glycolic acid as complexing agents and the main characteristics of the deposition process were compared to the ones obtained using Fe(II) baths. The simulation of electrolytes stability shows that the investigated Fe(III)-based glycolate-citrate electrolyte is thermodynamically stable in the neutral and weakly alkaline solutions due to peculiarities of Fe(III) and W(VI) complexes distribution in the concurrent presence of citrate and glycolate ions. In these solutions W(VI) forms dominantly complexes with glycolate ions, whereas Fe(III) with citrates. The current efficiency of the electrodeposition process occurring in Fe(III) glycolate-citrate bath reaches up to 60–70%, which is much higher than that obtained in the citrate baths or any other previously reported iron-based electrolytes. Compact and smooth coatings with high W content are obtained at elevated temperatures and low current densities, since at these conditions the partial current of side reaction
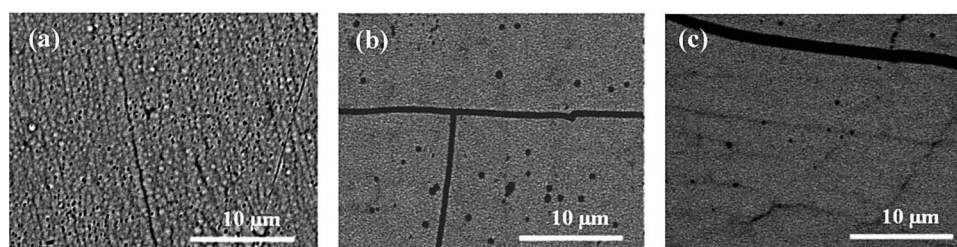
Figure 7. SEM images of Fe-W alloys obtained from GC3 electrolyte at 20°C at the following current densities: (a) 5 mA/cm^2; (b) 30 mA/cm^2; (c) 40 mA/cm^2.
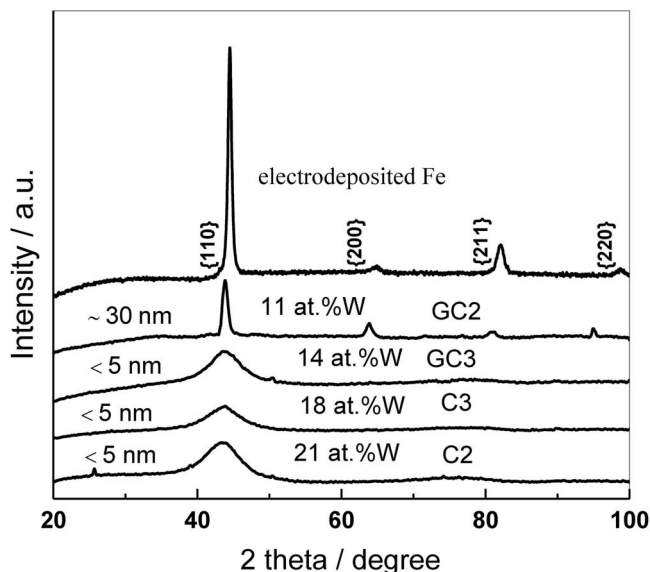
Figure 8. Representative XRD patterns of Fe-W alloys deposited from different electrolytes at 20°C and −20 mA/cm^2. The peaks were identified based on 06–0696 (Fe) ASTM Cards. Estimated values of crystallite size are shown next to the corresponding pattern.

is small. The increased content of tungsten in Fe-W alloys results in the decrease in values of crystallite size from 30 to ∼5 nm.

Thus, elaborated environmentally friendly electrolyte has high importance due to the possibility to obtain good quality Fe-W coatings from Fe(III)-based solution with tunable W content, high current efficiency and deposition rate; also it may be considered for electrodeposition of other Fe based alloys.

References

1. S. Wang, C. Zeng, Y. Ling, J. Wang, and G. Xu, *Surf. Coat. Technol.*, **286**, 36 (2016).
2. N. Tsyntsaru, A. Dikusar, H. Cesiulis, J. P. Celis, Z. Bobanova, S. Sidel'nikova, S. Belevskii, Y. Yaponttseva, O. Bersirova, and V. Kublanovskii, *Powder Metall. Met C+*, **48**, 419 (2009).
3. S. Changwei, Ye Mengchao, Z. Linxing, H. Jianping, Li Junmin, and G. Junming, *Surf. Rev. Lett.*, **23**, 1550100 (2015).
4. N. Thangaraj, K. Tamilarasan, and D. Sasikumar, *Indian J. Pure Appl. Phys.*, **52**, 395 (2014).
5. M. V. Ved, T. O. Nenastina, V. V. Shtefan, T. M. Bairachna, and M. D. Sakhnenko, *Mater. Sci.*, **44**, 840 (2008).
6. C. Tharamani, P. Beera, V. Jayaram, N. Begum, and S. Mayanna, *Appl. Surf. Sci.*, **253**, 2031 (2006).
7. L. Holt and R. Black, *J. Electrochem. Soc.*, **82**(1), 205 (1942).
8. G. Croopnik, (1985).
9. M. Donten, *J. Solid State Electrochem.*, **3**, 87 (1999).
10. N. Tsyntsaru, H. Cesiulis, M. Donten, J. Sort, E. Pellicer, and E. J. Podlaha-Murphy, *Surf. Eng. Appl. Electrochem.*, **48**, 491 (2012).
11. M. Donten, Z. Stojek, and H. Cesiulis, *Electrochim. Acta*, **45**, 3389 (2000).
12. M. Lietzke and M. Holt, *J. Electrochem. Soc.*, **94**, 252 (1948).
13. N. Eliaz and E. Gileadi, in *Modern Aspects of Electrochemistry*, Vol. **42**, C. Vayenas, Editor, p. 191, Springer, New York (2008).
14. Zh. Bobanova, A. Dikusar, H. Cesiulis, J. -P. Celis, I. Tsyntsaru, and I. Prosycevas, *Russ. J. Electrochem.*, **45**, 895 (2009).
15. V. Vasauskas, J. Padgurskas, R. Rukuiza, H. Cesiulis, J. -P. Celis, D. Milcius, and I. Prosycevas, *Mekhanika*, **21**, 1392 (2008).
16. O. Younes, L. Zhu, Y. Rosenberg, Y. Shacham-Diamand, and E. Gileadi, *Langmuir*, **17**, 8270 (2001).
17. N. Tsyntsaru, Zh. Bobanova, D. Kroitoru, V. Cheban, G. Poshtaru, and A. Dikusar, *Surf. Eng. Appl. Electrochem.*, **46**, 538 (2010).
18. Y. Gamburg, E. Zakharov, and G. Goryunov, *Russ. J. Electrochem.*, **37**, 670 (2001).
19. G. Yar-Mukhamedova, M. Ved, N. Sakhnenko, A. Karakurkchi, and I. Yermolenko, *Appl. Surf. Sci.*, **383**, 346 (2016).
20. L. Chang, Z. Wang, S. Shi, and W. Liu, *J. Alloys Compd.*, **509**, 1501 (2011).
21. A. Afshar, A. Dolati, and M Ghorbani, *Mater. Chem. Phys.*, **77**, 352 (2002).
22. J. Weiss, *Ber. Bunsenges. Phys. Chem.*, **73**(2), 131 (1969).
23. B. Morgan and O. Lahav, *Chemosphere*, **68**, 2080 (2007).
24. G. Krishnamurti and P. Huang, *Clays Clay Miner.*, **39**, 28 (1991).
25. M. Izaki, in *Modern Electroplating*, 5th. ed., M. Schlesinger and M. Paunovic, Editors, John Wiley & Sons, New Jersey (2010).
26. R. Renuka and S. Ramamurthy, *Bull. Electrochem.*, **13**(12), 456 (1997).
27. V. C. Kieling, *Surf. Coat. Technol.*, **96**(2-3), 135 (1997).
28. D. Park, B. Yoo, S. Kelcher, and N. Myung, *Electrochim. Acta*, **51**, 2523 (2006).
29. S. Yao and M. Kowaka, *J. Metal Finish. Soc. Japan.*, **39**(11), 736 (1988).
30. Y. Gamburg and G. Zangari, *Theory and practice of metal electrodeposition*, Springer, New York Dordrecht Heidelberg London (2011).
31. N. Mandich and D. Snyder, in *Modern Electroplating*, 5th. ed., M. Schlesinger and M. Paunovic, Editors, John Wiley & Sons, New Jersey (2010).
32. P. Padhakrishnamurty, *Bull. Electrochem.*, **15**(7–8), 252 (1999).
33. L. Sillen and A. Martel, *Stability constants of metal–ion complexes*, Vol. **2**, Chemical Society, London (1971).
34. E. Bulemela, L. Trevani, and P. Tremaine, *J. Solution Chem.*, **34**, 769 (2005).
35. A. Stefansson, *Environ. Sci. Technol.*, **41**, 6117 (2007).
36. R. Lemire, U. Berner, C. Musikas, D. A. Palmer, P. Taylor, and O. Tochiyama, *in Chemical thermodynamics of iron*, Vol **13a**, J. Perrone, Editor, Elsevier, Amsterdam (2013).
37. J. Aveston, *Inorg. Chem.*, **3**, 981 (1964).
38. A. Martell and R. Smith, *Critical stability constants*, Vol **3**, 495 p., Plenum Press, New York (1977).
39. R. Portanova, *Pure Appl. Chem.*, **75**, 495 (2003).
40. S. Muthu Priya and S. Shailaja, *OSR J. Appl. Chem.*, **8**, 1 (2015).
41. M. Aldeir, M. Ramos, and V. Gil, *Canadian J. Chem.*, **64**, 827 (1987).
42. C. Timberlake, *J. Chem. Soc.*, **0**, 5078 (1964).
43. M. Andre, N. Silva, X. Kong, M. Parkin, R. Cammack, and R. Hider, *Dalton Trans.*, **40**, 8616 (2009).
44. I. Gautier-Luneau, C. Merle, D. Phanon, C. Lebrun, F. Biaso, G. Serratrice, and J. L. Pierre, *Chem.–Eur. J.*, **11**, 2207 (2005).
45. J. Cruywagen, L. Krüger, and E. Rohwer, *J. Chem. Soc. Dalton Trans.*, **7**, 1727 (1991).
46. M. Donten, T. Gromulski, and Z. Stojek, *J. Alloys Compd.*, **279**, 272 (1998).
47. M. Lu and C. Chien, *J. Appl. Phys.*, **67**, 5787 (1990).
48. N. Tsyntsaru, H. Cesiulis, E. Pellicer, J. -P. Celis, and J. Sort, *Electrochim. Acta*, **104**, 94 (2013).
49. E. Lassner and W. Schubert, *Tungsten: Properties, Chemistry, Technology of the Element Alloys and Chemical Compounds*, 434 p., Kluwer Academic / Plenum Publishers, New York (1999).
50. E. Vernickaite, N. Tsyntsaru, and H. Cesiulis, *Trans. IMF*, **94**, 313 (2016).

Paper 2

Mapping of mechanical and magnetic properties of Fe-W alloys electrodeposited from Fe(III)-based glycolate-citrate bath

A. Nicolenco, N. Tsyntsaru, J. Fornell, E. Pellicer, J. Reklaitis,
D. Baltrunas, H. Cesiulis, J. Sort

Mapping of magnetic and mechanical properties of Fe-W alloys electrodeposited from Fe(III)-based glycolate-citrate bath

Aliona Nicolenco [a], Natalia Tsyntsaru [a,b,*], Jordina Fornell [c], Eva Pellicer [c], Jonas Reklaitis [d], Dalis Baltrunas [d], Henrikas Cesiulis [a,**], Jordi Sort [c,e]

[a] Vilnius University, Physical Chemistry Department, Naugarduko str. 24, Vilnius LT-03225, Lithuania
[b] Institute of Applied Physics of ASM, Academiei str. 5, Chisinau MD-2028, Republic of Moldova
[c] Departament de Física, Facultat de Ciències, Universitat Autònoma de Barcelona, Bellaterra E-08193, Spain
[d] Center for Physical Sciences and Technology, Savanorių av. 231, Vilnius LT-02300, Lithuania
[e] Institució Catalana de Recerca i Estudis Avançats (ICREA), Pg. Lluís Companys 23, Barcelona E-08010, Spain

HIGHLIGHTS

- Fe-W coatings having 6-25 at.%W are designed by fine control of deposition parameters in a glycolate-citrate Fe(III)-bath.
- Fe-W alloy's structure ranges from a mixture of α-Fe and Fe(W) to W(Fe) and Fe_2W above 15 at.% of W.
- The hardness of Fe-W alloy with 25 at.%W reached ~10 GPa, which is comparable to that of electrodeposited Cr.
- Hardening phenomenon could be related to the formation of Fe_2W intermetallic phase, along with grain size refinement.
- The increase in W at.% leads to reduction of saturation magnetization due to amorphization and phase transition processes.
- Fe-W coatings with 10-13 at.% of W produced at 65°C show an optimum combination of mechanical and magnetic properties.

GRAPHICAL ABSTRACT
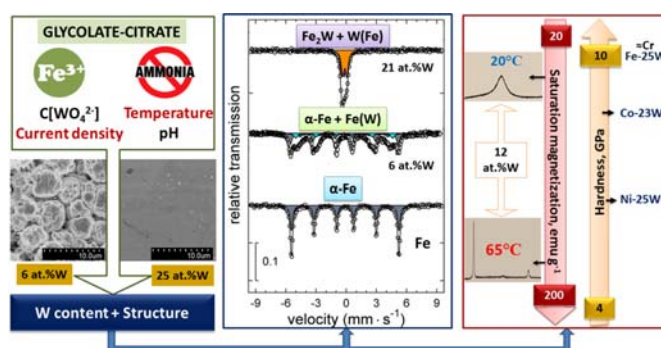
ARTICLE INFO

ABSTRACT

Electrodeposition of Fe-W coatings has been carried out from an environmentally friendly Fe(III)-based glycolate-citrate bath. Samples with tungsten content from 6 to 25 at.% were electrodeposited in a controlled way by changing electrodeposition parameters: current density, pH, and temperature. X-ray diffraction analysis showed that the structure of Fe-W coatings transforms from nanocrystalline to amorphous-like as the W content increases and the crystallite size reduces below 10 nm. However, the peculiarities of the structural transitions are linked not only with the W content. Deposition temperature plays a crucial role, due to the different activation energy of crystallization. Following the direct Hall–Petch relation, a maximum hardness of ~10 GPa was found for the alloy with the highest W content, making it comparable to that of electrolytic chromium. The Fe_2W intermetallic compound forms at higher W concentration as proven by Mössbauer spectroscopy, and contributes to

* Correspondence to: N. Tsyntsaru, Vilnius University, Physical Chemistry Department, Naugarduko str. 24, Vilnius LT-03225, Lithuania.
** Corresponding author.
E-mail addresses: tintaru@phys.asm.md (N. Tsyntsaru), henrikas.cesiulis@chf.vu.lt (H. Cesiulis).

the increased hardness of these alloys. The alloys retain a soft magnetic character within a wide compositional range, although increasing the W content leads to a reduction of the saturation magnetization. Fe-12 at.% W coatings show an optimum combination of mechanical and magnetic properties, thus making these newly developed coatings appealing environmentally-friendly alternative materials for multi-scale technologies.

1. Introduction

Electrodeposition of binary W alloys with iron group metals (Fe, Co, Ni) has recently attracted much attention since the addition of tungsten typically enhances the corrosion and wear resistance, hardness, and thermal resistance of the iron group metal [1–4]. These alloys have been recognized as promising protective coatings for hard chromium replacement. Furthermore, W alloys with iron group metals show interesting magnetic properties, such as high magnetic moment, low coercivity and tunable magnetic anisotropy [5,6]. In this context, the electrodeposition of Fe-W alloys could be targeted for the fabrication of magnetic micro-/nanoelectromechanical systems (MEMS/NEMS) where the combination of tunable magnetic properties and high hardness is needed [7,8]. Nonetheless, so far, electrochemical studies have mostly concentrated on Ni- and Co-W alloys, while the literature dealing with the design of electrodeposited Fe-W coatings for target applications is rather scarce. This is probably due to the difficulties to manage Fe-containing plating baths and their low current efficiency. However, recently, the use of both Ni and Co is discouraged because of environmental issues and, therefore, there is growing interest in developing new procedures to electrodeposit Fe-based alloys as alternatives to Co and Ni ones.

The functional properties of electroplated coatings are strongly influenced by the electrochemical parameters, particularly the current density, electrolyte pH and deposition temperature. These parameters have a direct influence on the composition and structure of the coatings [9]. Indeed, in Co-W and Ni-W alloys, it has been shown that the saturation magnetization is inversely proportional to the tungsten content. This is due to the inclusion of non-magnetic W atoms into the iron-group metal lattice and also the pronounced reduction in the crystallite size (eventually, amorphization) that occurs for high W content in the alloys [8,9]. While the saturation magnetization is an intrinsic parameter and essentially depends only on the composition of the alloy, the coercivity is much more dependent on the microstructure (crystallite size, texture, internal stress, etc.). Nonetheless, in most cases the coercivity of W-containing coatings does not exceed 200 Oe, thus soft magnetic properties are generally observed [10].

Data on the mechanical properties of electrodeposited binary and ternary W alloys with iron group metals were summarized in [9]. Different compositions and coatings obtained under different conditions were compiled. Generally, the mechanical properties improve as the W content is increased, which brings about an increase in hardness and strength as it is predicted by the Hall–Petch relation, while keeping relatively high ductility. However, it has been shown that for W contents higher than 10 at.% in Ni-W [1] and 25 at.% in Co-W alloys [8], the crystallite size reduces below a critical value and the Hall–Petch breakdown occurs. Remarkably, the hardness of Fe-W alloy with 30 at.% of W can reach values as high as 13 GPa (at 2 mN), which is higher than that reported for Co- and Ni-W alloys and even comparable to the hardness of electrolytic chromium [11]. To the best of our knowledge, a detailed investigation on the electrochemical synthesis and physical properties of Fe-W alloys in a wide compositional range is lacking.

According to [11], a maximum value of 30 at.% of W in Fe-W alloys can be achieved by increasing the deposition temperature and applied current density. Nevertheless, as the applied current density reaches higher absolute values, the inclusion of carbon and oxygen impurities

becomes unavoidable [12]. The incorporation of these non-metallic elements adversely affects the quality of the coatings and causes a reduction of both the hardness and the ferromagnetic response [13,14]. In addition, the current efficiency of the process decreases when increasing the current density (or when lowering the temperature) due to the large amount of hydrogen evolved on the cathode during the deposition [15]. Generally, even in optimized Fe-containing baths, the current efficiency does not exceed 50%. This is mostly because of the fast oxidation and precipitation of hydroxides in the case of Fe(II) bath, and low complexes stability in the case of Fe(III)-based electrolytes [16,17]. In our previous research a new environmentally-friendly glycolate-citrate electrolyte was used for Fe-W alloys deposition [18]. The lifetime of the bath was significantly increased due to replacement of Fe(II) by Fe(III) precursor and the current efficiency of the process was increased up to 60%–70%, what makes the glycolate-citrate bath preferable for industrial design. The thermodynamic stability of this bath in neutral and weakly alkaline solutions is governed by the peculiarities of Fe^{3+} and WO_4^{2-} complexes distribution with citrate and glycolate ions, and affords reproducible results.

The aim of the present study is to establish interdependences between deposition conditions, chemical composition and structure of the deposits. Furthermore, the magnetic and mechanical properties are assessed with the aim of providing a map of "composition-properties" interrelationships for "W-low" and "W-rich" Fe-W coatings.

2. Experimental

2.1. Synthesis of Fe-W coatings

A series of Fe-W alloys were prepared by electrodeposition from an aqueous solution with the following composition: 1 M glycolic acid, 0.3 M citric acid, 0.1 M $(Fe)_2(SO_4)_3$ and $0 \div 0.5$ M Na_2WO_4. The effect of the sodium tungstate concentration was investigated at pH 6.5 and 65 °C, and cathodic current densities of 15 and 40 mA cm^{-2}. The influence of pH on tungsten content, current efficiency and partial currents was evaluated in the range from 4.0 till 8.5. Bath pH was adjusted with either NaOH or H_2SO_4. The electrodeposition was performed in a typical three-electrode cell under stagnant conditions. The bath volume was kept at 250 mL. Flat Si chips with an evaporated Cu seed-layer (with an average roughness, R_a, ~6 nm) were used as working electrodes. The working area was 2.25 cm^2. Platinized titanium mesh was used as a counter electrode and saturated Ag/AgCl/KCl$_{sat}$ electrode was used as a reference electrode. Prior to electrodeposition, the substrates were degreased in acetone and ethanol, and activated in 2 M sulfuric acid for 1 min in an ultrasonic bath. The deposition current efficiency (CE) and partial current densities were calculated as described elsewhere [18]. Table 1 lists the different Fe-W samples prepared and the type of characterization performed on each one.

2.2. Compositional and structural characterization

The morphology of the deposited alloys was studied by scanning electron microscopy (SEM) using high resolution Hitachi SU-70 instrument. Their chemical composition was determined with an energy dispersive X-ray spectroscopy (EDX) analysis tool attached to the SEM. Surface roughness was measured by Confocal Microscopy (Leica DCM 3D system). The crystallographic structure and phase composition of

Table 1
Experimental design.

W content, at.%	Deposition conditions				Characterization methods			
	T °C	C(WO$_4^{2-}$), mol L^{-1}	i, mA cm^{-2}	pH	XRD	Mössbauer spectroscopy	Magnetic measurements	Mechanical tests
0	65	0	15	6.5	✓	✓		
1		0.01			✓			
6	20	0.20			✓	✓	✓	✓
7		0.30				✓	✓	
12		0.40					✓	
	65	0.10				✓	✓	✓
17	20	0.40			✓		✓	
	65	0.30		5.0	✓	✓	✓	✓
21			40		✓	✓	✓	
23			15	8.0			✓	✓
25			15	6.5	✓	✓	✓	✓

the coatings were studied by means of X-ray diffraction (XRD) using a Rigaku MiniFlex II diffractometer with Cu Kα radiation (λ = 1.54183 Å) operated at 30 kV and 30 mA. The mean crystallite size was estimated from the XRD data using the Debye-Scherrer equation. Phase composition was evaluated using Mössbauer spectroscopy. The relative amount of phases was normalized by weight of Fe-W deposit. Mössbauer spectra were recorded using a constant acceleration spectrometer in the transmission geometry. The ^{57}Co source in Rh matrix with an activity of 10 mCi was held at room temperature. The velocity scale was calibrated using the magnetic sextet of a high-purity iron foil absorber as a standard. The experimental spectra were fitted by the least-squares method using the WinNormos package in IgorPro 5.05A environment. All isomer shifts reported in this work refer to the ^{57}Co(Rh) source at room temperature.

2.3. Assessment of the mechanical and magnetic properties

Nanoindentation was used to determine the hardness and the elastic modulus of the electrodeposited Fe-W coatings. Indentations were done on the cross-section of ~10 μm thick coatings. To prepare the samples for nanoindentation, a cut perpendicular to the surface of the Fe-W layers was embedded in resin mold, grinded with SiC abrasive paper up to P2500 and polished with 1 μm diamond suspension as a final step. The indentations were performed on a Nanoindenter XP from MTS equipped with a Berkovich pyramidal-shaped diamond tip under load-control mode. The nanoindentation function consisted of a loading segment of 30 s, followed by a load holding segment of 10 s and an unloading segment of 30 s. The maximum applied load was set to 20 mN. The load was selected so that the lateral size of the indentation impressions remained much smaller than the film thickness (to avoid influence from the resin). Indentations were performed in the middle of the cross-section area. The thermal drift during nanoindentation was kept below 0.1 nm s^{-1} in all cases. The elastic modulus and hardness were derived from the initial part of the unloading–displacement curve by applying the method of Oliver and Pharr [19]. Fifteen indentations were performed on each sample and average values of elastic modulus and hardness are reported. The magnetic properties of the Fe-W alloys were studied at room temperature using a Vibrating Sample Magnetometer from MicroSense (LOT-Quantum Design). Hysteresis loops were recorded along the in-plane and the perpendicular-to-plane directions with a maximum applied field of ± 20 kOe. For proper normalization of the hysteresis loops, the coatings were subsequently microwave-digested with concentrated HNO$_3$ and HF. The resulting solutions were analyzed by inductively coupled plasma optical emission spectrometry (ICP-OES) in a Perkin-Elmer spectrometer Optima 4300DV.

3. Results and discussion

3.1. The influence of tungstate concentration and pH on Fe-W alloy electrodeposits

In order to map the "composition-properties" interrelationships, Fe-W alloys with a tungsten content varying in a wide range were deposited. The composition of the alloys was changed by varying the concentration of sodium tungstate in the bath from 0 to 0.50 M while the concentration of Fe^{3+} ions was kept constant. The simulation of species distribution (performed similarly as reported in [18]) shows that the investigated Fe(III)-based glycolate-citrate electrolyte is thermodynamically stable in neutral and weakly alkaline solutions due to the peculiarities of Fe(III) and W(VI) complexes distribution in the concurrent presence of citrate and glycolate ions. In these solutions, W(VI) predominantly forms complexes with glycolate ions, whereas Fe(III) forms complexes with citrates. Fig. 1 shows the dependence of "free" glycolate ions as a function of the sodium tungstate amount added to the solution, demonstrating that tungstate forms complexes with glycolate at the expenses of the decrease of concentration of "free" glycolate-ions, whereas the concentration of Fe(III) complexes with glycolate remains constant (in the investigated solution ~0.05 mol L^{-1}).
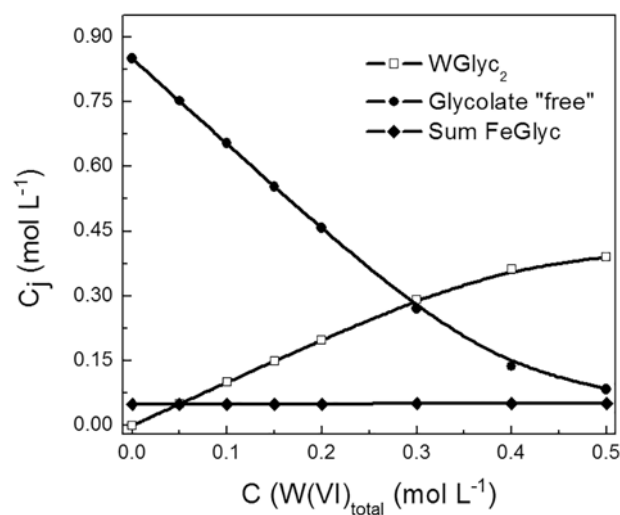
Fig. 1. Dependence of the concentration of "free" glycolate ions ("free" glycolate), WO$_2$(HGly)$_2^{2-}$ (WGlyc$_2$) and the sum of concentrations of Fe(III) complexes with glycolate (Sum FeGlyc) on the total concentration of W(VI) present in the solution. pH 6.5; composition of solution 1 M glycolic acid, 0.3 M citric acid, 0.1 M (Fe)$_2$(SO$_4$)$_3$ and 0 ÷ 0.5 M Na$_2$WO$_4$.

It was reported earlier that the maximum amount of W co-depositing with iron group metal is restricted to an upper limit [9,17, 20–22], which for Fe-W alloy is ~35 at.% [12]. Indeed, Fig. 2 shows that an increase of tungstate concentration from 0.01 to 0.30–0.40 M results in a significant increase of the W content in the electrodeposits from a few at.% to a maximum amount of 25–27 at.%, while further increase in the concentration of Na_2WO_4 does not cause any increase of the tungsten content in the alloy. This stays in line with a modelling approach proposed by Podlaha and Landolt [23], which explained the induced co-deposition of Mo and W with iron group metal through a catalytic reaction, where the precursor was an intermediate mixed complex compound of both metals adsorbed on the electrode surface and subsequently reduced. When the W content in the deposit reaches its upper limit, the absorbed layer becomes saturated, and this corresponds to the certain concentration of tungstate in the solution (Fig. 2).

For a given tungstate concentration in the solution, the tungsten content in as-plated Fe-W alloys slightly depends on the applied current density: an increase of the current density leads to a reduction of the W content in deposits for tungstate concentrations ranging from 0.01 M to 0.30 M (Fig. 2). Generally, the elemental composition of an electrodeposited alloy depends on the ratio of the partial current densities of the alloy's constituents. However, this value is influenced by a number of factors such as the chemistry of the solution, total current density or applied potential, temperature, hydrodynamics and interdependencies of the rate of one metal electrodeposition to another, among others.

In our case, the main three electrochemical reactions occurring are the deposition of iron, the deposition of tungsten and the hydrogen evolution (side reaction). As it is shown in Fig. 3, the increase in tungstate concentration does not lead to a linear increase in the partial current for tungsten at a constant total current. Conversely, this has an effect on the partial currents of iron and hydrogen. In other words, the rates of all three electrochemical reactions are dependent on each other in a complex way. An estimation of the partial currents for Fe-W deposition shows that an increase in the partial current of W deposition is accompanied by a decrease of that of the side reaction for concentrations of tungstate up to 0.30 M (Fig. 3). Moreover, at 15 mA cm^{-2} the partial current ascribed to tungsten reduction is higher than at 40 mA cm^{-2} up to 0.1 M tungstate in solution. This explains why the W content is lower in coatings deposited at higher current densities from diluted solutions (Fig. 2).

In addition, alloys deposited from solutions with low tungstate concentration and having <10 at.% of W were poorly adhered to the substrate, powder-like and brittle. Therefore, the bath containing 0.30 M
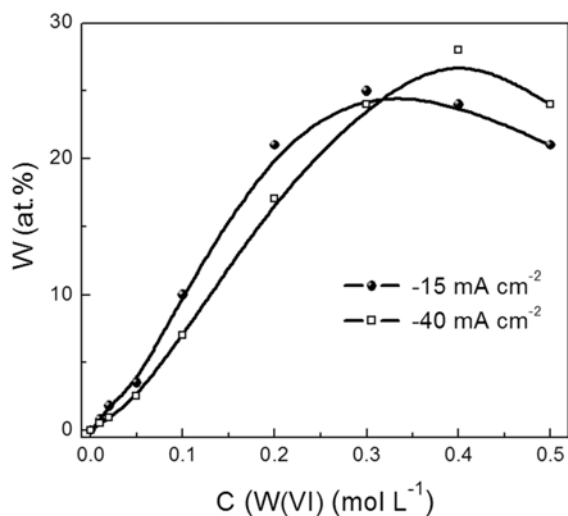

Fig. 2. Dependence of tungsten content in the deposits on sodium tungstate concentration in the bath at 65 °C and pH 6.5.
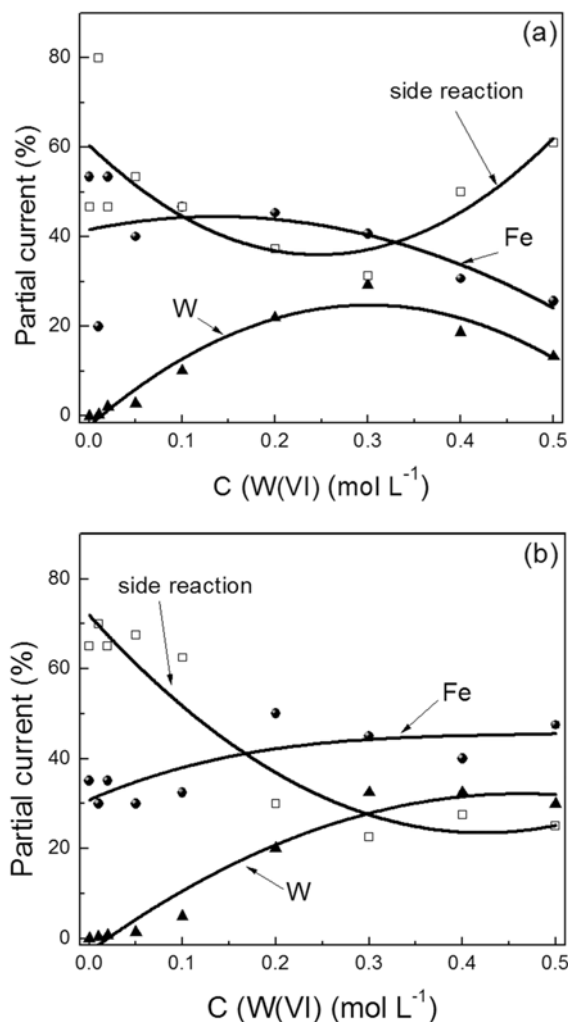

Fig. 3. Distribution of partial currents in glycolate-citrate electrolyte (1 M glycolic acid, 0.3 M citric acid, 0.1 M (Fe)$_2$(SO$_4$)$_3$) at different concentrations of sodium tungstate in the bath, at cathodic current density of: 15 mA cm^{-2} (a), and 40 mA cm^{-2} (b).

of Na_2WO_4 was selected for further investigations in order to obtain compact Fe-W alloys and to evaluate the resulting coating properties.

The composition of W-containing electrodeposited alloys is also very sensitive to the solution pH [24–27]. Since the distributions of Fe(III) and W(VI) complexes with citrates and glycolate depends on pH [18], this has an influence on the deposition rates for Fe and W as well as for hydrogen evolution, hence resulting in a variation of the W content on pH, as shown in Fig. 4. Namely, at room temperature, the composition of the coatings remains almost constant irrespectively of pH in the range of 5.0–8.5 (Fig. 4a). In addition, the current efficiency is relatively low, achieving the maximum current efficiency (CE ~ 47%) at pH 6.5 (Fig. 4b). However, at pH > 7 the partial current of W deposition decreases along with a simultaneous decrease in partial current for Fe and a significant increase in partial current of the side reaction (Fig. 4c). This correlates with the complexes distributions [18], i.e., the decrease in concentration of predominant species $WO_2Gly_2^{2-}$ and the significant increase in the concentration of WO_4^{2-} ions and the $(WO_4)(HCit)H^{4-}$ complex with increase in pH. The maximum W content and the maximum current efficiency correspond to the maximum concentration of $WO_2Gly_2^{2-}$ complex.

At higher temperature (65 °C), the W content varies from 17 to 25 at.%, achieving the maximum at pH ~7 (Fig. 4a). Thus, Fe-rich samples can be produced only at room temperature, while the deposition of W-rich Fe-W alloys requires higher temperatures. An increase of the W content in the alloy is accompanied by an increase in CE, as it is
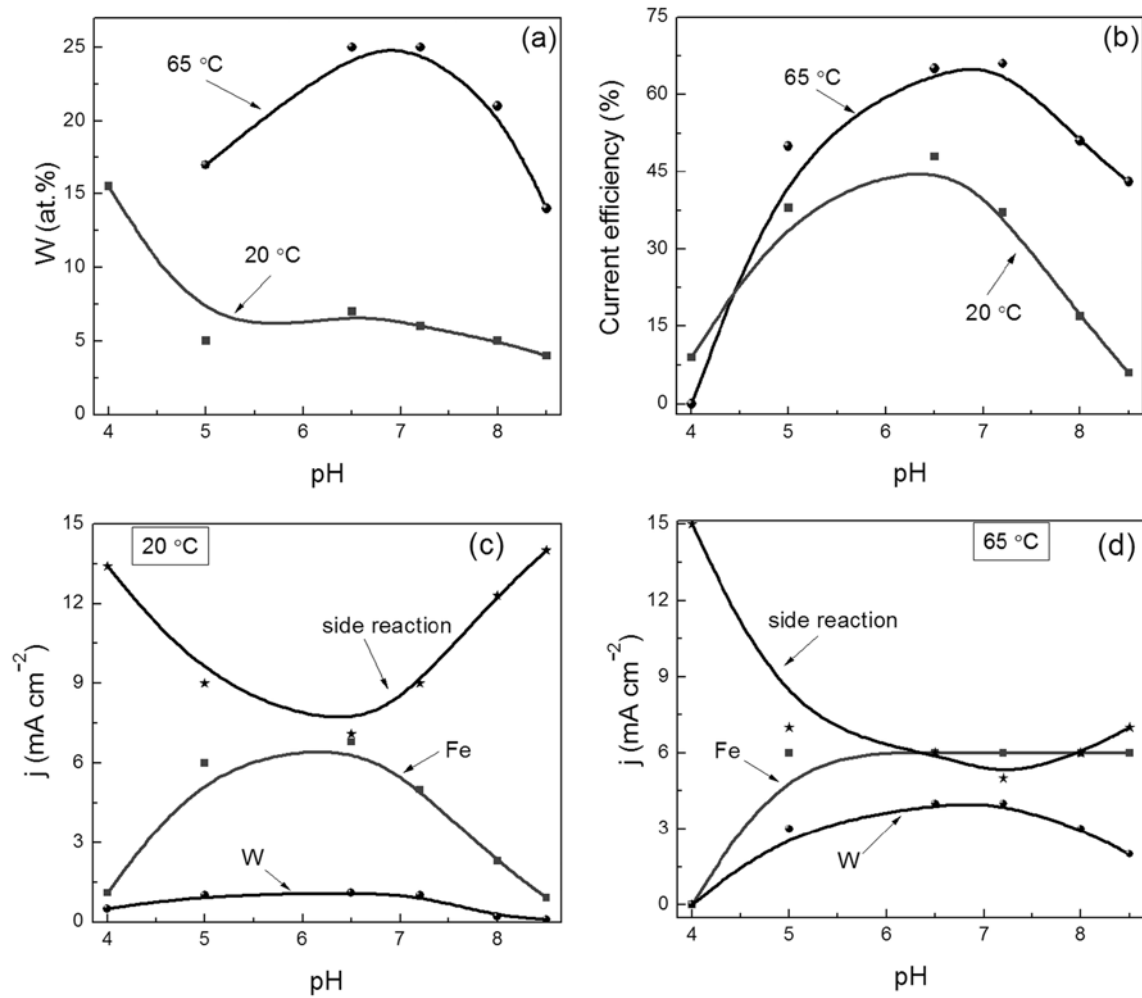
Fig. 4. Influence of pH on: W content in the alloy (a); current efficiency at cathodic current density of −15 mA cm^{-2} (b); partial current densities at 20 °C (c); partial current densities at 65 °C (d). Electrodeposition bath contained 1 M glycolic acid, 0.3 M citric acid, 0.1 M (Fe)$_2$(SO$_4$)$_3$ and 0.3 M Na$_2$WO$_4$.

expected from Podlaha-Landolt co-deposition model [23], and it can reach 60–70% (Fig. 4b). It is worth noticing that the CE of Fe-W alloys electrodeposited from glycolate-citrate bath is considerably higher than for other Fe(II) or Fe(III) based electrolytes described elsewhere [11,17,28]. Remarkably, at 65 °C and pH 4, deposition of Fe-W alloy is precluded, whereas at room temperature Fe-W alloys with 16 at.% of W can be obtained. It can be seen from Fig. 4d that the alloy deposition is accompanied by an intensive hydrogen evolution at pH 4 and 65 °C, thereby hindering the growth of the alloy.

3.2. Surface morphology and structural properties of Fe-W alloy electrodeposits

Fig. 5 shows representative SEM images of Fe-W alloys with different W contents. The surface of the alloys with up to 10 at.% of W is typically porous and shows a micro-globular structure with high intergranular distances. Further increase in the W content leads to a remarkable disappearance of pores and substantial surface refining. The average roughness of the electrodeposited samples decreases linearly from ~62 nm to ~13 nm as the W content in the alloys increases from 6 to 25 at.%, and thus Fe-W alloys with 15–25 at.% of W generally exhibit a mirror-like appearance.

Based on the results shown in Section 3.1, Fe-rich samples with W content from 6 to 17 at.% were deposited at 20 °C, while W-rich samples with W content from 12 to 25 at.% of W were obtained at 65 °C. Thus, alloys containing 12–17 at.% of W could be deposited at both

temperatures (Table 1). Eventual structural changes caused by increasing W content and the influence of deposition temperature for coatings in the range of 12–17 at.% W were studied.

Selected XRD patterns for Fe-W alloys and for Fe electrodeposited from a similar W-free electrolyte are shown in Fig. 6. The crystallographic structure of the films transforms from nanocrystalline to amorphous-like when the W content increases. The broadening of the diffraction peaks is attributed to grain size refinement, which typically occurs at higher W concentrations [29,30]. Remarkably, the threshold for the formation of the amorphous-like structured Fe-W alloys depends on the deposition temperature, similar to the case of Co-W obtained from citrate-borate electrolyte [31]. In our previous work, we found that at room temperature an amorphous-like structure for Fe-W alloy was achieved at W concentrations above 12–14 at.% [18]. Hence, an alloy with 17 at.% of W obtained at 20 °C is amorphous-like (Fig. 6c). Meanwhile, the appearance of two nanocrystalline peaks on the XRD pattern for the Fe-W alloy with 17 at.% of W deposited at 65 °C (Fig. 6d) probably indicates the presence of some Fe(W) crystals embedded in an amorphous matrix.

The difference in structure for alloys obtained at 20 °C and 65 °C and having the same composition probably is caused by different mobility of deposited Fe and W atoms. Indeed, the activation energy of crystallization of Fe-W alloy is high, i.e. one hundred and thirteen kilocalorie mol^{-1} (472 kJ/mol) [27]. Such value implies a big difference in the crystallization rate: by applying the Arrhenius equation it is found that the rate of crystallization at 20 °C is 6 · 10^9 times lower

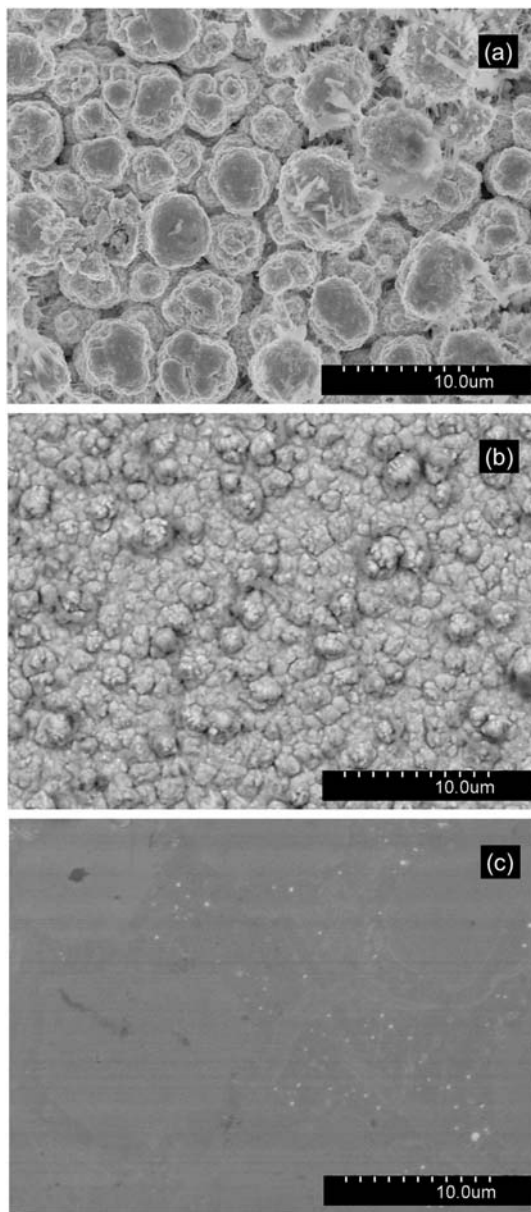Fig. 5. SEM images of Fe-W alloys with a W content of 6 at.% (a), 12 at.% (b) and 25 at.% (c).
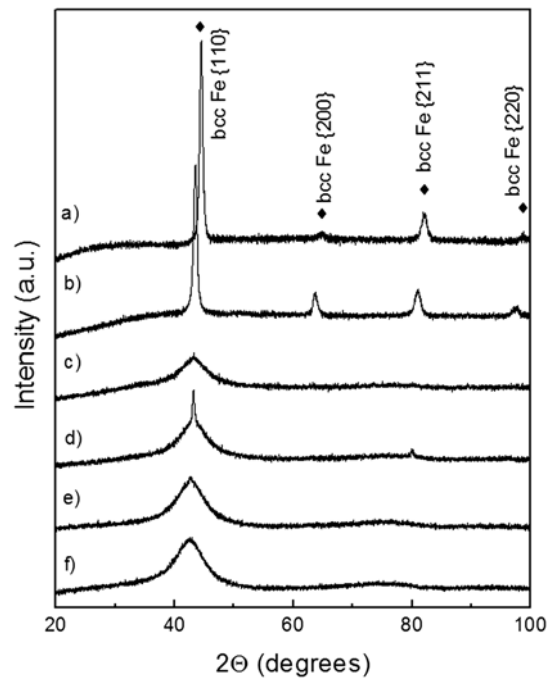

Fig. 6. XRD patterns recorded on Fe (a) and Fe-W coatings with different W content: 6 at.% obtained at 20 °C (b), 17 at.% at 20 °C (c), 17 at.% at 65 °C (d), 21 at.% at 65 °C (e), and 25 at.% of W at 65 °C (f). Peaks were identified based on the ASTM Card 06-0696 (Fe).

than at 65 °C. Therefore, atoms deposited at lower temperature tend to stay in place forming metastable disordered or amorphous-like structure, having many boundaries between chaotically placed crystallites of 4–5 nm in size. Meanwhile, at 65 °C the rate of crystallization is high, and during electrodeposition the thermodynamically stable crystalline structure of Fe-W alloys is formed.

As it is seen from Fig. 6, the corresponding values of $2\theta_{hkl}$ characteristic for pure iron are shifted towards lower angles as the W content increased. This is most likely due to the partial replacement of some Fe atoms by bigger W atoms in the lattice as typically observed in solutions. In order to obtain a better understanding of the structural changes caused by the addition of W to pure Fe, the samples (Table 1) were also analyzed by Mössbauer spectroscopy. Each spectrum was described using a set of subspectra, each subspectrum corresponding to a different environment of the iron atoms (Fig. 7). Based on the area of the Mössbauer spectra the amount of phases was estimated (Fig. 8).

For alloys containing W below 14 at.% the obtained spectra are typical to ferromagnetic compounds. The main contribution to these spectra (in this range of contents of W) is the α-Fe phase (hyperfine

parameters: $\delta = -0.109$ mm/s, $\Delta \approx 0.0$ mm/s and $B_{hf} = 33.1$ T). With the increase of the W content, the relative amount of this pure α-Fe phase decreases, while the relative amount of the Fe-W solid solution increases, i.e. the observed subspectra having smaller hyperfine fields correspond to some iron atoms being replaced with W atoms in the α-Fe lattice. It was shown in [32,33] that the hyperfine field decreases on average by 4.1 T when replacing single iron atoms with tungsten atoms in NN (nearest neighbor) shells. The hyperfine field decreases by 2.6 T by replacing Fe by W in the next-nearest neighbor (NNN) (nearest-nearest neighbor) shells. Configuration (m,n) in Table 2 denotes m atoms of Fe in NN shell and n atoms in NNN shell being replaced by W atoms. Based on hyperfine parameters (Table 2) there are up to 3 iron atoms replaced by W atoms (1, 2 and 3 on the Fig. 8). The formation of solid solution is rather typical for electrodeposited alloys and for Fe-W it is supported by the fact that Fe and W have homotypic lattices differing by not >15% in cell parameters [34] ($\alpha_{bccFe} = 2.8665$ Å, $\alpha_{bccW} = 3.1652$ Å [35]).

At higher W concentrations, the spectra change from ferromagnetic to paramagnetic kind. All spectra of W-rich samples (15–25 at.%) have almost the same shape, which can be described with two doublets. Based on hyperfine parameters, one is clearly ascribed to the Fe_2W intermetallic compound [36,37] and the second one can be referred to as Fe solid solution in W [36]. According to the phase diagram, the solubility limit of W in bcc Fe is ~14.3 at.%. This correlates well with the two separated subspectra characteristic for Fe-W alloys having at.% of W above 16–17%.

3.3. Magnetic properties of the Fe-W electrodeposited alloys

Magnetic measurements were performed on Fe-W alloys covering the overall range of compositions (Table 1), in order to assess the nature of these coatings (hard, semi-hard or soft magnetic) and the eventual changes in saturation magnetization. As expected, the addition of small amounts of tungsten to iron leads to a reduction of the saturation magnetization since W is a non-magnetic element (Fig. 9). Interestingly, the saturation magnetization, M_s, decrease also depends on the electrodeposition temperature: alloys containing 6–16 at.% W deposited at
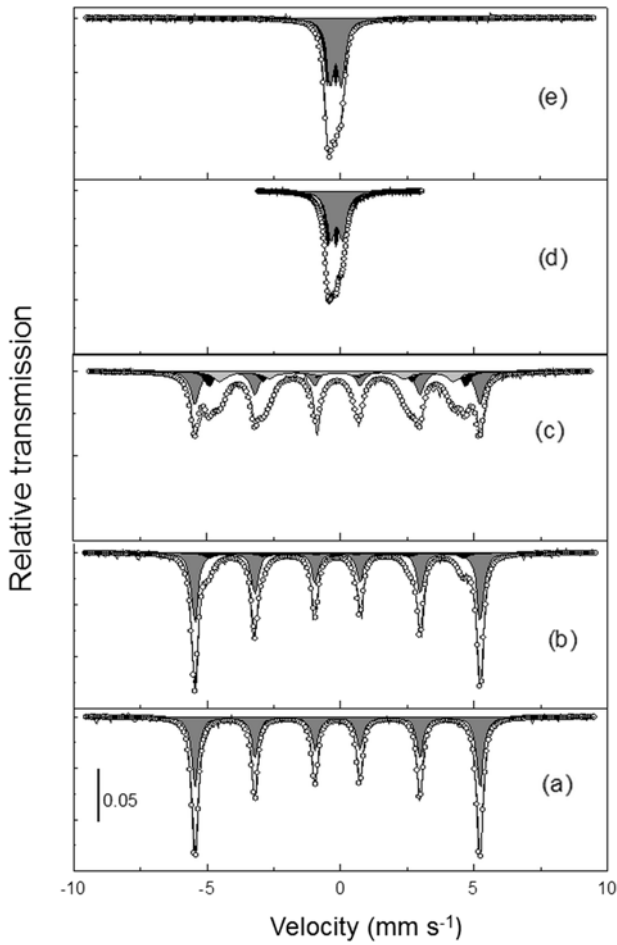
Fig. 7. Mössbauer spectra of Fe(a) and Fe-W coatings with different W content: 1 at.% (b), 6 at.% (c), 17 at.% (d), 21 at.% (e). Deposition conditions are given in Table 1.

Table 2
Fitted values of hyperfine parameters of different Fe-W alloys (W – tungsten concentration in at.%; δ – isomer shift; Δ – quadrupole splitting, Bhf – hyperfine field; k – relative amount of component; (m,n) – atomic configuration). Deposition conditions are given in Table 1.

W (at.%)	δ (mm/s)	Δ (mm/s)	Bhf (T)	k	(m,n)	Remarks
0	−0.109	0.0	33.1	1.00		α-Fe
1	−0.109	0.0	33.2	0.84		α-Fe
	−0.165	0.0	29.4	0.16	(1,0)	
6	−0.109	0.0	33.1	0.42		α-Fe
	−0.105	0.0	29.8	0.22	(1,0)	
	−0.128	0.0	27.1	0.35	(1,1)	
12	−0.109	0.0	33.0	0.25		α-Fe
	−0.115	0.0	28.5	0.51	(1,1)	
	−0.163	0.0	24.2	0.24	(2,0)	
17	−0.31	0.31	0.0	0.36		Fe_2W
	−0.13	0.43	0.0	0.64		W(Fe)
21	−0.34	0.33	0.0	0.42		Fe_2W
	−0.17	0.42	0.0	0.58		W(Fe)
25	−0.33	0.34	0.0	0.41		Fe_2W
	−0.17	0.42	0.0	0.59		W(Fe)

structure at relatively high contents of W, while the ones deposited at lower temperature become amorphous-like when the amount of W exceeds 12 at.%. Thus, a significant fraction of α-Fe remains when electrodepositing at 65 °C, and, consequently, M_s is larger. Conversely, at 20 °C, for a W concentration around 12–16 at.% the films become almost amorphous and therefore M_s significantly decreases. Amorphous-like Fe-W alloys show a weak ferromagnetic signal (40–20 emu g^{-1}) which is probably related to the formation of both W(Fe) and Fe_2W phases as it is proved by Mössbauer spectroscopy in the corresponding W concentration range (Fig. 8). Theoretical calculations provided in [38] show that the Fe_2W intermetallic alloy indeed possesses a ferromagnetic character (M = 0.57 μ_B). Therefore, it can be assumed that the decrease in M_s for Fe-W alloys with high W content is caused by the phase transition from the ferromagnetic Fe(W) bcc solid solution (for high Fe contents) to a mixture of both non-ferromagnetic W(Fe) and weakly ferromagnetic Fe_2W phases (for high W contents). A similar behaviour was noticed for amorphous Co-W alloys [8], where non-ferromagnetic character was achieved only beyond 30 at.% of W.

The coercivity values of the investigated Fe-W alloys are in the range from 20 to 90 Oe when applying the magnetic field in-plane, and from 10 to 190 Oe for the perpendicular-to-plane direction. Thus, a semi-soft magnetic character is obtained for all the samples. The change in the shape of the hysteresis loops when measured in-plane and perpendicular-to-plane configurations reveals that the Fe-W alloys with low W contents exhibit in-plane magnetic effective anisotropy

room temperature exhibit a rapid decrease of M_s with the increase in the amount of W, whereas alloys deposited at 65 °C and containing ~12 at.% W maintain relatively high M_s values. Such essential difference in M_s values can be attributed to the structural differences among the coatings obtained at different temperatures. As it was shown in Section 3.2, the alloys electrodeposited at 65 °C keep the crystalline
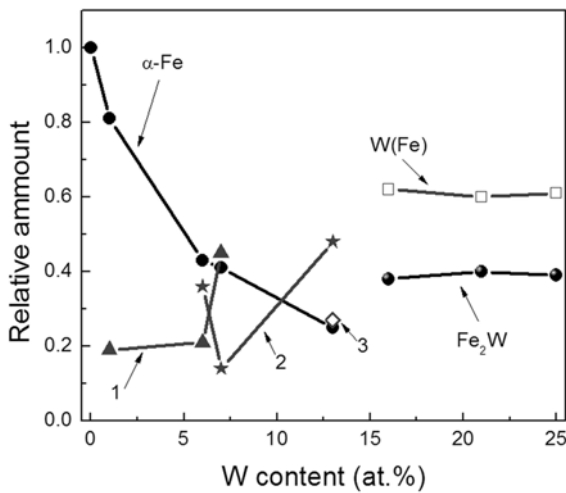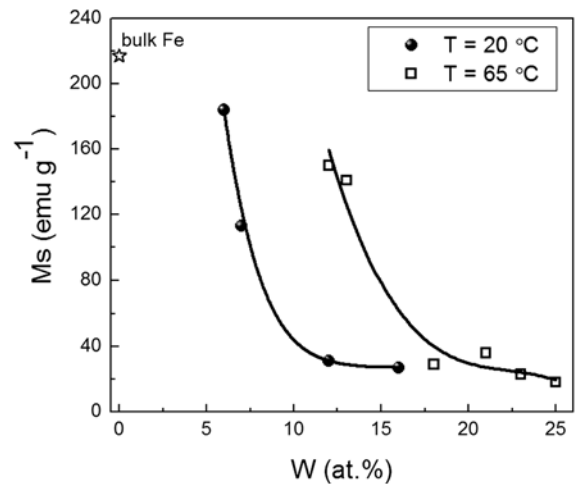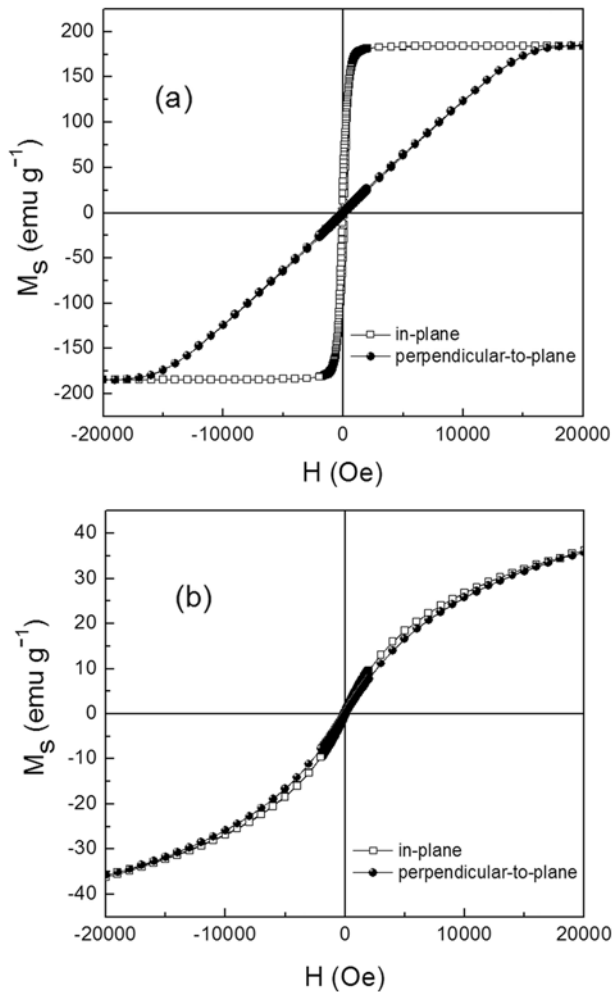

Fig. 8. Relative amount of phases identified by Mössbauer spectroscopy. 1, 2 curves and point 3 correspond to the compounds where 1, 2 and 3 Fe atoms are replaced to W, respectively. Deposition conditions are given in Table 1.

Fig. 9. Dependence of the saturation magnetization (M_s) of Fe-W coatings as a function of their composition.

Fig. 12. Hall-Petch plot for Fe-W alloys showing the hardness as a function of the square-root of the crystallite size determined from XRD measurements.
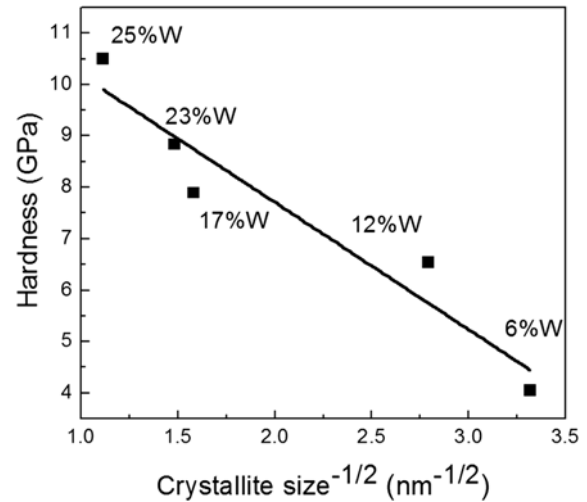

Fig. 10. Hysteresis loops of Fe-W coatings: nanocrystalline sample with 6 at.% of W (a), and amorphous sample with 21 at.% of W (b) recorded for an external magnetic field applied along in-plane and perpendicular-to-plane directions.

(Fig. 10a). Remarkably, the difference in shape between in-plane and perpendicular-to-plane loops disappears in the W-rich, amorphous-like films (Fig. 10b). This could be due to the reduction of M_s, which
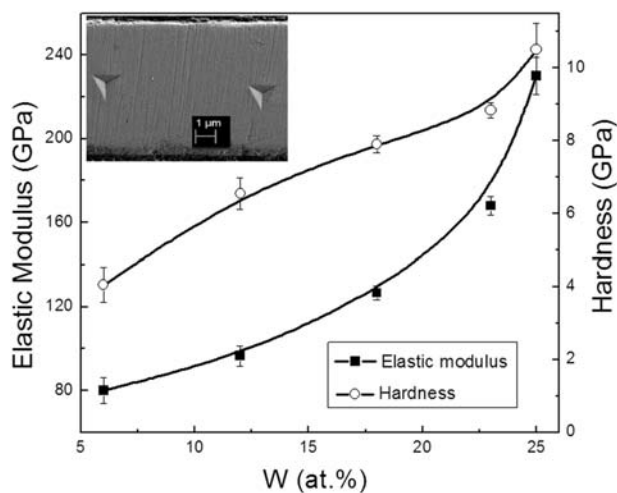
Fig. 11. Hardness and elastic modulus of Fe-W alloys plotted as a function of the W content, at applied load of 20 mN. A SEM image showing the indent imprints on the cross-section area of Fe-W alloy with 23 at.% of W is shown as an inset.

brings about a decrease of the demagnetizing field and a concomitant reduction of shape anisotropy effects.

3.4. Mechanical properties of the Fe-W electrodeposited alloys

Fe-W alloys deposited at 65 °C retain higher M_s values even at relatively high W content as compared to room temperature. Therefore, samples deposited at 65 °C with tungsten content 12–25 at.% were subjected to mechanical studies. An additional sample containing 6 at.% W obtained at 20 °C was also mechanically characterized in order to cover the whole range of alloy composition (Table 1).

The evaluation of mechanical properties of Fe-W electrodeposited alloys as a function of the tungsten content was carried out at the cross-section of the samples by nanoindentation. The values of hardness and elastic modulus (i.e., reduced Young's modulus) extracted from the load-displacement curves using the method of Oliver and Pharr [19] are presented in Fig. 11. The increase of tungsten leads to an increase in both hardness and elastic modulus. Hardness increases from 4.1 GPa for the alloy with 6 at.% W to 10.4 GPa for the alloy with a W content of 25 at.%. The substantial increase of hardness observed on these nanocrystalline alloys is due to the interplay of several factors: (i) grain boundary strengthening, as a result of the nanocrystalline nature of the as-deposited coatings, (ii) partial or total amorphization induced by W addition (the lack of long-range order precludes the occurrence of the conventional deformation mechanisms in crystalline materials, driven by dislocations, stacking faults, grain boundary sliding, etc.), (iii) solid solution strengthening, caused by the presence of small amounts of a mechanically hard alloying element, in this case W. Additionally, as it has been shown by Mössbauer spectroscopy, at higher W concentration the intermetallic Fe_2W phase is formed. This may also contribute to the observed hardening effect, particularly for the Fe-W alloys with W content larger than 17 at.%.

Previous works have shown that the grain boundary contribution in this type of alloys is much stronger than the solid solution strengthening effect caused by W [39]; consequently, plastic deformation is mainly governed by the lattice dislocations within individual grains, which tend to accumulate at grain boundaries. To corroborate this point, the hardness values are plotted in Fig. 12 as a function of $\langle D \rangle^{-1/2}$ (where D is the crystallite size). A linear relationship, typical for Hall-Petch plots, is obtained, hence confirming that grain boundaries play a crucial role in the mechanical properties of these electrodeposited films. The decrease in crystallite size essentially creates a higher volume of grain boundaries and thus impedes the dislocation motion in these
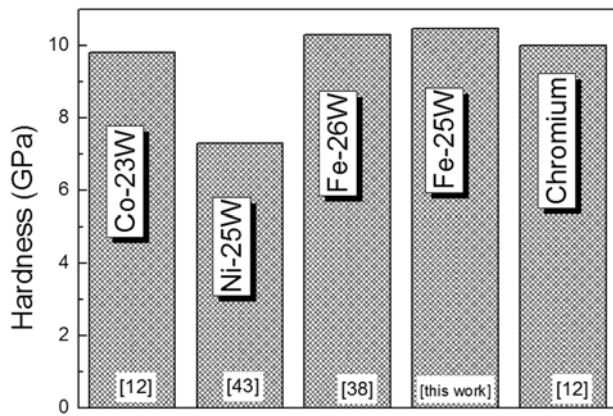
Fig. 13. Hardness of W alloys with iron group metals and of electrolytic chromium measured by nanoindentation at a maximum applied load of 20 mN. Corresponding references are indicated on the figure.

Fig. 14. Mapping of mechanical and magnetic properties of Fe-W alloys. All of the samples were electrodeposited at 65 °C, except the one with 6 at.% of W, which was obtained at 20 °C.

nanocrystalline materials, resulting in larger mechanical strength. The influence of crystallite size on the hardness is well-known, even for single electrodeposited metals [40]. However, in the case of binary systems, such as Fe-W, the decrease in crystallite size is induced by the increase in W content in the alloy. Therefore, it is not necessarily straightforward to distinguish between the various mechanisms involved in the alloy strengthening process.

Elastic modulus is of particular importance for both the design and fabrication of micro-electro-mechanical systems (MEMS) because it frequently plays an important role in the lifetime, reliability, and failure mechanisms of miniaturized devices. Materials with a higher elastic modulus can better maintain a linear (and reversible) relationship between the applied load and the induced deformation. The values of elastic modulus of Fe-W alloys (Fig. 11) measured using nanoindentation show an increase from 83 GPa to 216 GPa for alloys with 6 and 25 at.% of W, respectively. This value is close to that of pure bulk iron [41] and even comparable to steel or Si [42].

A comparison of the mechanical properties for the obtained coatings with previously published data on W alloys with iron group metals and electrolytic chromium is presented in Fig. 13. It is important to mention that the comparison of mechanical properties of different materials should be done carefully by taking into account the differences in starting conditions (e.g., surface polishing) and indentation parameters (i.e. applied load, loading rate, indenter geometry, etc.). Therefore, to compare the hardness values of this work with those in the literature, alloys with similar compositions and maximum applied loads have been selected. Summarizing, the alloy deposited from the investigated Fe(III)-glycolate-citrate bath has approximately the same hardness as the alloys deposited from conventional citrate-ammonia bath. At an applied load of 20 mN their hardness is ~10 GPa which is higher than that of W alloys co-deposited with Co or Ni and comparable to that of electrolytic chromium.

Fig. 14 shows a mapping of hardness and saturation magnetization for Fe-W alloys as a function of the W content, as discussed in the previous sections. It can be seen that a combination of enhanced mechanical strength and high saturation magnetization is achieved for alloys with 10–14 at.% of W deposited at 65 °C. At this concentration range Fe-W alloys are characterized by relatively high saturation magnetization, due to the contribution from magnetic α-Fe phase which is still present. Simultaneously, the solid solution strengthening caused by the increased W content causes an increase of hardness (for this amount of W, hardness is comparable to that of electrodeposited Ni-W alloy [43]). Therefore, Fe-W alloys having low W content could be targeted for the design of recording components because of their magnetic properties. Taking into account that Fe-W alloys are characterized by low coercive field within a wide range of composition, these materials could be of interest for the design and fabrication of MEMS such as pressure
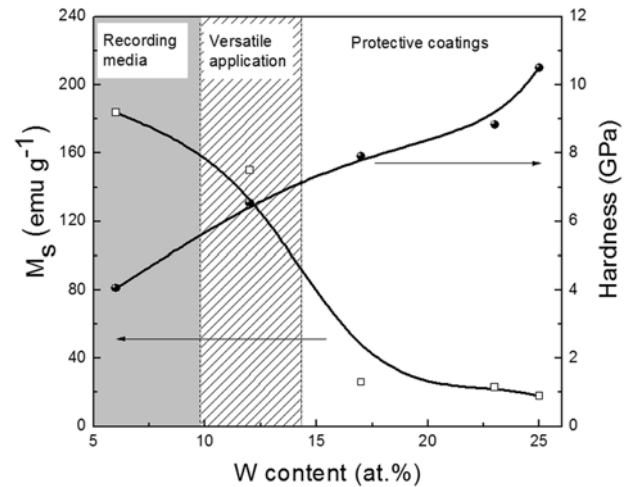
sensors, microgears, micromotors, microcoils or thermal actuators. Nonetheless, although alloys richer in W possess low magnetization, they show outstanding mechanical properties, close to those of electroplated Cr. Mechanically hard Fe-based materials with low M_s could be targeted for medicine applications, particularly for the design of a MRI-compatible heart implanted pacemaker, which nowadays are mainly based on Ni compounds, which could be allergenic [44].

4. Conclusions

Fe-W alloys with varying W content (from a few at.% to 25 at.%) were electrodeposited from Fe(III)-based glycolate-citrate electrolyte by fine tuning the following deposition parameters: concentration of tungstate, deposition temperature, current density and pH. On the basis of the observed interdependencies, the electroplating at higher temperature, lower current densities and pH close to neutral promotes the growth of fully dense coatings.

The incorporation of W atoms has a great impact on the mechanical and magnetic properties of the coatings. Thus, Fe-W alloy with 25 at.% of W exhibits a maximum hardness of 10.4 GPa, which is comparable to the hardness of electrolytic chromium. The hardening effect follows the direct Hall-Petch relation. Moreover, the formation of the Fe_2W intermetallic compound at high W concentration, as proved by Mössbauer spectroscopy, may contribute to the increased hardness of these alloys.

Magnetic measurements reveal that the alloys are magnetically soft (or semi-soft) within a wide range of compositions. The decrease in M_s for alloys with higher W content is due to the phase transformations caused by the addition of W to pure Fe, namely the transformation from α-Fe + Fe(W) phase to amorphous W(Fe) solid solution plus intermetallic Fe_2W. At room temperature, M_s tends to decrease from 184 emu g^{-1} for the alloy with 6 at.% of W to 18 emu g^{-1} for the alloy with a W content of 25 at.%. Fe-W alloys deposited at higher temperature (e.g., 65 °C) maintain relatively high M_s up to 12 at.% of W. This is attributed to the different crystallographic properties of the films when deposited at different temperatures. Therefore, the deposition temperature is an important parameter to consider in the fabrication of magnetic components with high hardness, since they are expected to have relatively high amount of W.

A mapping of mechanical and magnetic properties of Fe-W is shown in Fig. 14. Fe-W coatings with 10–14 at.% of W produced at 65 °C show an optimum combination of mechanical and magnetic properties, thus

making these newly developed coatings appealing sustainable and "green" multifunctional materials.

Acknowledgements

References

[1] K.R. Sriraman, S. Ganesh Sundara Raman, S.K. Seshadri, Synthesis and evaluation of hardness and sliding wear resistance of electrodeposited nanocrystalline Ni–W alloys, Mat. Sci. Eng. A-Struct. 418 (2006) 303–311, https://doi.org/10.1016/j.msea.2005.11.046.

[2] H. Alimadadi, M. Ahmadi, M. Aliofkhazraei, S.R. Younesi, Corrosion properties of electrodeposited nanocrystalline and amorphous patterned Ni–W alloy, Mater. Des. 30 (2009) 1356–1361, https://doi.org/10.1016/j.matdes.2008.06.036.

[3] G. Yar-Mukhamedova, M. Ved, N. Sakhnenko, A. Karakurkchi, I. Yermolenko, Iron binary and ternary coatings with molybdenum and tungsten, Appl. Surf. Sci. 383 (2016) 346–352, https://doi.org/10.1016/j.apsusc.2016.04.046.

[4] S. Wang, C. Zeng, Y. Ling, J. Wang, G. Xu, Phase transformations and electrochemical characterizations of electrodeposited amorphous Fe–W coatings, Surf. Coat. Technol. 286 (2016) 36–41, https://doi.org/10.1016/j.surfcoat.2015.12.011.

[5] N. Ćirović, P. Spasojević, L. Ribić-Zelenović, P. Mašković, A. Maričič, M. Spasojević, Synthesis, structure and properties of nickel–iron–tungsten alloy electrodeposits. Part II: effect of microstructure on hardness, electrical and magnetic properties, Sci. Sinter. 48 (2016) 1–16, https://doi.org/10.2298/SOS1601001C.

[6] E.P. Barbano, I.A. Carlos, E. Vallés, Electrochemical synthesis of Fe–W and Fe–W–P magnetic amorphous films and Fe–W nanowires, Surf. Coat. Technol. 324 (2017) 80–84, https://doi.org/10.1016/j.surfcoat.2017.05.071.

[7] E. Slavcheva, W. Mokwa, U. Schnakenberg, Electrodeposition and properties of NiW films for MEMS application, Electrochim. Acta 50 (2005) 5573–5580, https://doi.org/10.1016/j.electacta.2005.03.059.

[8] N. Tsyntsaru, H. Cesiulis, E. Pellicer, J.-P. Celis, J. Sort, Structural, magnetic, and mechanical properties of electrodeposited cobalt–tungsten alloys: intrinsic and extrinsic interdependencies, Electrochim. Acta 104 (2013) 94–103, https://doi.org/10.1016/j.electacta.2013.04.022.

[9] N. Tsyntsaru, H. Cesiulis, M. Donten, J. Sort, E. Pellicer, E.J. Podlaha-Murphy, Modern trends in tungsten alloys electrodeposition with iron group metals, Surf. Eng. Appl. Electrochem. 6 (2012) 491–520, https://doi.org/10.3103/S1068375512060038.

[10] Z. Ghaferia, S. Sharafia, M.E. Bahrololoom, Effect of current density and bath composition on crystalline structure and magnetic properties of electrodeposited FeCoW alloy, Appl. Surf. Sci. 355 (2015) 766–773, https://doi.org/10.1016/j.apsusc.2015.07.083.

[11] Zh. Bobanova, A. Dikusar, H. Cesiulis, J.P. Celis, I. Prosycevas, Micromechanical and tribological properties of nanocrystalline coatings of iron–tungsten alloys electrodeposited from citrate-ammonia solutions, Russ. J. Electrochem. 45 (2009) 895–901, https://doi.org/10.1134/S1023193509080096.

[12] N. Tsyntsaru, H. Cesiulis, H. Cesiulis, J.P. Celis, Zh. Bobanova, S. Sidel'nikova, S. Belevskii, Y. Yaponttseva, O. Bersirova, V. Kublanovskii, Tribological and corrosive characteristics of electrochemical coatings based on cobalt and iron superalloys, Powder Metall. Met. Ceram. 48 (2009) 419–428, https://doi.org/10.1007/s11106-009-9150-7.

[13] C.J. Marvel, D. Yin, P.R. Cantwell, M.P. Harmer, The influence of oxygen contamination on the thermal stability and hardness of nanocrystalline Ni–W alloys, Mater. Sci. Eng. A 664 (2016) 49–57, https://doi.org/10.1016/j.msea.2016.03.129.

[14] C.J. Marvel, P.R. Cantwell, M.P. Harmer, The critical influence of carbon on the thermal stability of nanocrystalline Ni–W alloys, Scr. Mater. 96 (2015) 45–48, https://doi.org/10.1016/j.scriptamat.2014.10.022.

[15] N. Thangaraj, K. Tamilarasa, D. Sasikumar, Effect of current density on electrodeposited ferrous tungsten thin films, Indian J. Pure Appl. Phys. 52 (2014) 395–398.

[16] V.V. Kuznetsov, K.E. Golyanin, T.V. Pshenichkina, Electrodeposition of iron–molybdenum alloy from ammonia–citrate electrolyte, Russ. J. Electrochem. 48 (2012) 1107–1112, https://doi.org/10.1134/S1023193512110109.

[17] A. Brenner, P.S. Burkhead, E. Seegmiller, Electrodeposition of W alloys containing iron, nickel and cobalt, J. Res. Natl. Bur. Stand. 39 (1947) 351–383.

[18] A. Nicolenco, N. Tsyntsaru, H. Cesiulis, Fe (III)-based ammonia-free bath for electrodeposition of Fe–W alloys, J. Electrochem. Soc. 164 (2017) D590–D596, https://doi.org/10.1149/2.1001709jes.

[19] W.C. Oliver, G.M. Pharr, Measurement of hardness and elastic modulus by instrumented indentation: advances in understanding and refinements to methodology, J. Mater. Res. 19 (2004) 3–20, https://doi.org/10.1557/jmr.2004.19.1.3.

[20] O. Younes-Metzler, L. Zhu, E. Gileadi, The anomalous codeposition of tungsten in the presence of nickel, Electrochim. Acta 48 (2003) 2551–2562, https://doi.org/10.1016/S0013-4686(03)00297-4.

[21] N. Eliaz, T.M. Sridhar, E. Gileadi, Synthesis and characterization of nickel tungsten alloys by electrodeposition, Electrochim. Acta 50 (2005) 2893–2904, https://doi.org/10.1016/j.electacta.2004.11.038.

[22] Z.A. Hamid, Development of electrodeposition of cobalt-tungsten alloys from acidic bath containing cationic surfactants, Mater. Lett. 57 (2003) 2558–2564, https://doi.org/10.1016/S0167-577X(02)01311-3.

[23] E.J. Podlaha, D. Landolt, Induced codeposition: III. Molybdenum alloys with nickel, cobalt and iron, J. Electrochem. Soc. 144 (1997) 1672–1680, https://doi.org/10.1149/1.1837658.

[24] Zh.I. Bobanova, V.I. Petrenko, G.F. Volodina, D.M. Kroitoru, A.I. Dikusar, The effect of the pH on the composition and properties of Co–W alloys manufactured from gluconate electrolyte, Surf. Eng. Appl. Electrochem. 51 (1) (2015) 25–37, https://doi.org/10.3103/S1068375515010020.

[25] E. Gileadi, N. Eliaz, The mechanism of induced codeposition of Ni–W alloys, ECS Trans. 2 (2007) 337–349, https://doi.org/10.1149/1.2408887.

[26] F. Su, C. Liu, P. Huang, Effect of complexing agents and pH on microstructure and tribological properties of Co–W coatings produced by double pulse electrodeposition, Appl. Surf. Sci. 258 (2012) 6550–6557, https://doi.org/10.1016/j.apsusc.2012.03.075.

[27] Y. Ruan, S. Yao, M. Kowaka, Amorphization of electrodeposited Fe–W alloy films and electrochemical behaviour, J. Non-Cryst. Solids 117 (1990) 752–755.

[28] Yu. Gamburg, E. Zakharov, G. Goryunov, Electrodeposition, structure, and properties of iron–tungsten alloys, Russ. J. Electrochem. 37 (2001) 670–673, https://doi.org/10.1023/A:1016752231015.

[29] M.H. Allahyarzadeh, M. Aliofkhazraei, A.R. Rezvanian, V. Torabinejad, A.R. Sabour Rouhaghdam, Ni–W electrodeposited coatings: characterization, properties and applications, Surf. Coat. Tech. 307 (2016) 978–1010, https://doi.org/10.1016/j.surfcoat.2016.09.052.

[30] R. Juskenas, I. Valsiunas, V. Pakstas, R. Giraitis, On the state of W in electrodeposited Ni–W alloys, Electrochim. Acta 54 (2009) 2616–2620, https://doi.org/10.1016/j.electacta.2008.10.060.

[31] E. Vernickaite, N. Tsyntsaru, H. Cesiulis, Electrodeposition and corrosion behaviour of nanostructured cobalt–tungsten alloys coatings, Trans. IMF 94 (2016) 313–321, https://doi.org/10.1080/00202967.2016.1220071.

[32] S.M. Dubiel, W. Zinn, Changes in the electronic structure of iron induced by substitutional impurity W atoms, Phys. Rev. B 30 (1984) 3783–3789, https://doi.org/10.1103/PhysRevB.30.3783.

[33] E. Jartych, J.K. Zuravicz, D. Oleszak, M. Pekala, Structure and magnetic properties of mechanosynthesized iron–tungsten alloys, J. Magn. Magn. Mater. 218 (2000) 247–255, https://doi.org/10.1016/S0304-8853(00)00394-2.

[34] Y. Gamburg, G. Zangari, Theory and Practice of Metal Electrodeposition, Springer, New York, 2011https://doi.org/10.1007/978-1-4419-9669-5.

[35] V.A. Lubarda, On the effective lattice parameter of binary alloys, Mech. Mater. 35 (2003) (2003) 53–68.

[36] D.M. Minić, Synthesis, characterization and stability of amorphous alloys, Sci. Sinter. 38 (2006) 83–92, https://doi.org/10.2298/SOS0601083M.

[37] A.P. Kuprin, I.G. Murzin, CEMS study of ion-beam mixing at a Fe/W interface, Nucl. Instr. Meth. Phys. Res. 76 (1993) 218–220, https://doi.org/10.1016/0168-583X(93)95186-9.

[38] Q.Q. Ren, J.L. Fan, Y. Han, H.R. Gong, Structural, thermodynamic, mechanical, and magnetic properties of FeW system, J. Appl. Phys. 116 (2004)https://doi.org/10.1063/1.4894396.

[39] C.A. Schuh, T.G. Nieh, H. Iwasaki, The effect of solid solution W additions on the mechanical properties of nanocrystalline Ni, Acta Mater. 51 (2003) 431–443, https://doi.org/10.1016/S1359-6454(02)00427-5.

[40] Z.C. Cordero, B.E. Knight, C.A. Schuh, Six decades of the Hall–Petch effect – a survey of grain-size strengthening studies on pure metals, Int. Mater. Rev. 61 (8) (2016) 495–512, https://doi.org/10.1080/09500608.2016.1191808.

[41] G.V. Samsonov, Handbook of the Physicochemical Properties of the Elements, 1968https://doi.org/10.1007/978-1-4684-6066-7.

[42] Tai-Ran Hsu, MEMS and Microsystems– Design, Manufacture, and Nanoscale Engineering, 2nd edition John Wiley & Sons, New Jersey, 2008.

[43] L. Sanghyeon, C. Minyoung, P. Subeen, J. Hyunsung, Y. Bongyoung, Mechanical properties of electrodeposited Ni–W thin films with alternate W-rich and W-poor multilayers, Electroch. Acta 153 (2015) 225–231, https://doi.org/10.1016/j.electacta.2014.11.190.

[44] S. Risquez, M. Woytasik, H. Cai, H. Philippe, F. Bayle, E. Lefeuvre, J. Moulin, Micromolding of Ni–P with reduced ferromagnetic properties for 3D MEMS, J. Electrochem. Soc. 164 (2017) B3096–B3100, https://doi.org/10.1149/2.0151705jes.

In-depth characterization of as-deposited and annealed Fe-W coatings electrodeposited from glycolate-citrate plating bath

A. Mulone, A. Nicolenco, V. Hoffmann, U. Klement, N. Tsyntsaru,

H. Cesiulis

In-depth characterization of as-deposited and annealed Fe-W coatings electrodeposited from glycolate-citrate plating bath

A. Mulone [a], A. Nicolenco [b], V. Hoffmann [c], U. Klement [a, **], N. Tsyntsaru [b, d], H. Cesiulis [b, *]

[a] *Chalmers University of Technology, Department of Industrial and Materials Science, Gothenburg, Sweden*
[b] *Vilnius University, Department of Physical Chemistry, Lithuania*
[c] *Leibniz Institute for Solid State and Materials Research Dresden, Dresden, Germany*
[d] *Institute of Applied Physics of ASM, Chisinau, Republic of Moldova*

ABSTRACT

Fe-W coatings with 4, 16 and 24 at.% of W were electrodeposited under galvanostatic conditions from a new environmental friendly Fe(III)-based glycolate-citrate bath. This work aims to find correlations between composition including the light elements, internal structure of the electrodeposited Fe-W alloys and functional properties of material. The obtained alloys were characterized by Glow Discharge Optical Emission Spectrometry (GD-OES), Scanning Electron Microscopy (SEM) with Energy Dispersive X-ray Spectroscopy (EDS), Transmission Electron Microscopy (TEM), and X-ray Diffraction (XRD). Compositional depth profiles of 10 μm thick coatings obtained by GD-OES show that the distribution of metals is uniform along the entire film thickness, while SEM imaging depicted the presence of cracks and O- and W-rich areas inside the Fe-W coating with 4 at.% W. In the samples with 16 and 24 at.% of W, oxygen and hydrogen are present mostly at the surface about 1 μm from the top while traces of carbon are distributed within the entire coatings. With increasing W content, the structure of the coatings changes from nanocrystalline to amorphous which was shown by XRD and TEM analysis. Also, the surface of coatings becomes smoother and brighter, that was explained based on the local adsorption of intermediates containing iron and tungsten species. Annealing experiments coupled with XRD analysis show that the thermal stability of Fe-W alloys increases when the W content increases, i.e. the coating with 24 at.% W retains the amorphous structure up to 600 °C, where a partially recrystallized structure was observed. Upon recrystallization of the amorphous samples the following crystalline phases are formed: α-Fe, Fe_2W, Fe_3W_3C, Fe_6W_6C, and $FeWO_4$. Hence, the Fe-W coatings with higher W content (>25 at.%) can be considered as suitable material for high temperature applications.

© 2017 Elsevier Ltd. All rights reserved.

1. Introduction

The interest in W alloys has continuously grown due to their advantageous properties. The addition of tungsten to iron group metals improves the properties of alloys such as hardness, corrosion resistance and thermal stability [1–4]. For these reasons W alloys with Fe, Co and Ni can represent an alternative to hard chromium coatings which are deposited using carcinogenic compounds (i.e. Cr^{6+}) [5]. In the past, electrochemical studies were concentrated mostly on Ni-W and Co-W alloys, while the

investigations on electrodeposited Fe-W coatings are rather scarce. As the use of Co and Ni is more and more discouraged because of environmental issues, the electrodeposition of Fe-based alloys has gained in importance.

However, electrodeposition of Fe-W alloys is usually associated with low current efficiency. It could be attributed to the fast oxidation of Fe^{2+} to Fe^{3+} (when Fe(II)-based electrolyte is used) and higher cathodic polarization of Fe-W alloys (above -1.00 V) as compared to Ni-W or Co-W ($-0.65 \div -1.00$ V), which results in a higher partial current density of side reaction [2,6]. Moreover, as was shown in Ref. [7], the electrolytes based on Fe(II) compounds are unstable thermodynamically and are governed by the Fe(II) oxidation kinetics. Most recent successful attempts to obtain Fe alloys with refractory metals from Fe(III) electrolytes were reported [8–10]. Nonetheless, the current efficiency of the deposition in

---

* Corresponding author.
** Corresponding author.
   E-mail addresses: uta.klement@chalmers.se (U. Klement), henrikas.cesiulis@chf. vu.lt (H. Cesiulis).

referred studies did not exceed 40% [9,11].

The appropriate electrodeposition conditions influence the composition and structure of electrodeposited alloys. Thus, the W content in electrodeposited alloys can vary within a wide range, depending on the deposition conditions, but usually it does not exceed 30–35 at.% [12]. Generally, the structure of W-containing alloys with iron group metals tends to transit from nanocrystalline to "amorphous-like" with increase in W content in the alloy [12]. Thus, Fe-W alloys can be deposited with an amorphous [13] or nanocrystalline structure [14]. This tunable structure represents a useful opportunity when aiming for certain properties of interest. As a matter of fact the nanocrystalline W alloys are characterized with higher saturation magnetization [15] while amorphous alloys usually exhibit higher hardness and corrosion resistance [16].

As a novel approach, an environmental friendly and thermo-dynamically stable glycolate-citrate bath was employed for Fe-W alloys, which allowed to produce Fe-W coatings with up to 60–70% of current efficiency from Fe(III)-based solution [7,17]. An increase of current efficiency in this electrolyte was associated with specific complexes distribution of Fe and W, and we were able to produce Fe-rich and W-rich Fe-W alloys with tunable mechanical and magnetic properties by fine control of the deposition conditions.

However, it was observed that the tungsten content is not the sole factor influencing the structure and properties of the electro-deposited alloy. During the electrodeposition, various non-metallic elements can be incorporated and alter grain growth and influence the microstructure development during the thermal treatment [18,19].

Former works on W alloys with iron group metals show that after a thermal treatment the microhardness and corrosion resistance of electrodeposits increases due to formation of stable intermetallic compounds (Fe_2W), which is usually observed at temperatures higher than 400 °C [6,20,21].

The effects of heat treatments on compositional and structural features of the deposited W alloys considering various tungsten contents and the co-deposited impurities have been studied most extensively for Ni-W alloys [18,19,22–27]. While scarce literature on Fe-W alloys electrodeposited from citrate-ammonia baths shows better thermal stability properties as compared to other W alloys with Ni and Co, retaining the nanocrystalline structure after annealing up to 700–800 °C [14].

The quantification of incorporated co-deposited non-metallic elements seems to be a crucial step towards characterization of functional materials. Typically, electrodeposition of metal alloys from aqueous solutions occurs along with abundant hydrogen evolution on the cathode. This leads to a local increase in pH at the electrode/solution interface and may cause the formation of insoluble hydroxides which become incorporated in the coating [28].

The precipitation of hydroxides at the electrode/solution interface with the layer growth is expected to have an impact on the physical and chemical properties of the obtained deposits [29]. Also, carbon is a common impurity in electrodeposited coatings. Its incorporation is often related to the organic additives used in the electrolytic bath [30]. Carbon presence within the alloy can lead to carbide phase precipitation during annealing with important implications both for the thermal stability and the mechanical properties of the coating [19]. The presence of oxygen as impurity and its effect on both thermal stability and mechanical properties has also been investigated for Ni-W alloy [18].

However, the quantitative determination of the full composition of electrodeposits often is a challenge. It is a well-known that EDS analysis has limitations with respect to quantification of light elements and low concentrations due to two main points: (i) elements with Z < 11 emit low energy X-rays which are subject to strong absorption by the specimen; and (ii) the yield of fluorescence increases with the atomic number and de-excitation of light elements occurs mainly by the emission of Auger electrons.

Therefore, meeting the existing demand for the quality control of functional materials, Glow Discharge Optical Emission Spectroscopy (GD-OES) can be applied for accurate composition analysis. Whereas the qualitative measurement of the light element depth distribution by GD-OES has been recognized as a powerful tool for reliable in-depth analysis, it is known that quantitative compositional depth profiling of light elements, especially of H and O, is very challenging [31]. No matrix-sensitive calibration material is available and matrix independent calibration make it uncertain. Therefore, in this study sintered calibration samples for O [32] and H [33] produced at IFW Dresden were used for multi-matrix calibration for the first time.

The aim of this paper is to study the interdependences between the composition and structure of Fe-W coatings by use a new analytical strategy and techniques including Scanning Electron Microscopy (SEM) with Energy Dispersive X-ray Spectroscopy (EDS), Transmission Electron Microscopy (TEM), GD-OES, and X-ray Diffraction (XRD) analysis. Furthermore, the annealing effects on the structure and morphology of the produced Fe-W alloys with different amounts of W are also studied. To the best of our knowledge, in depth characterization of electrodeposited Fe-W alloys and incorporation of light elements into deposits have not been performed before.

2. Experimental

2.1. Electrodeposition of Fe-W alloys

In our previous work [17] the influence of tungstate concentration and deposition parameters (current density, pH, temperature) on induced codeposition of W with Fe from recently developed glycolate-citrate Fe(III)-based electrolyte was studied. Fe-W samples with various W content from few at.% to 25 at.% can be deposited in a controlled way by changing electrodeposition parameters. At 65 °C the partial current for W deposition is higher than that for room temperature, which results in the increase of W content in the deposit at these conditions. Based on the published data [17], Fe-W coatings with 4, 16 and 24 at.% of W have been obtained from the electrolyte with following composition: 1 M glycolic acid, 0.3 M citric acid, 0.1 M $Fe_2(SO_4)_3$ and 0.3 M Na_2WO_4. The deposition conditions are given in Table 1. The bath pH was adjusted by addition of either NaOH or H_2SO_4. The cathodic current density of 15 mA cm^{-2} was applied as is the optimum for Fe-W alloys deposition from electrolyte used [17]. Electrodeposition of thin films was performed in a typical three-electrode cell. A pure copper sheet was used as the working electrode. Platinized titanium was used as a counter electrode, and saturated Ag/AgCl/KCl_{sat} was used as reference electrode and all potential values are presented in respect of this electrode. The deposition current efficiency was calculated based on the Faraday's law as described elsewhere [17].

Table 1
Operating conditions and EDS chemical composition of as-deposited Fe-W coatings.

Sample	T, °C	pH	j, mA cm^{-2}	CE, %	-E, V	Composition (at.%)				
						Fe	W	O	Fe	W
1	20	6.5	15	24	1.25	80	4	16	96	4
2	65	5.0	15	50	1.04	59	10	31	84	16
3	65	6.5	15	72	1.08	64	20	17	76	24

2.2. Coating characterization

Secondary electron imaging was used to acquire the images of the as-plated surfaces by using a Leo 1550 Gemini SEM with field emission gun and the cross-sectional images were acquired using back-scattered electrons. The chemical composition was measured both at the surface and on cross-sections of the samples using EDS and an accelerating voltage of 20 kV, the obtained results are shown in Table 1. TEM investigation was performed with a Zeiss EM 912 OMEGA microscope operating at an accelerating voltage of 120 kV.

The depth profiling analysis was carried out using a GDA750HR (Spectruma) with 2.5 mm source in DC mode. The discharge was operated in a high-purity Ar 5.0 atm and constant current (10 mA)/ constant voltage (700 V) control mode.

The calibration samples for GD-OES analysis were chosen in a way that a wide element concentration range was covered for further quantification. The sputtering rate factor of self-made calibration samples (ratio of the sputtering rate of the sample to the sputtering rate of Fe) was determined by density and crater volume measurements [34]. The wavelengths of the selected spectra emission lines were: 371 nm for Fe, 429 nm for W, 219 nm for Cu, 165 nm for C, 777 nm for O, and 121 nm for H. With help of sintered calibration samples with Cu, Mg and Al matrix for O produced at IFW Dresden [32] the matrix dependence of the emission yield of the O I 130.22 nm line was revealed [35]. The different emission yield of this line is caused by a strong line shift effect reported by Köster [36]. Therefore, Gonzalez-Gago et al. [35] proposed to use the oxygen triplet at 777 nm to overcome this problem. We have now confirmed the matrix independence of the line O I 777,194 nm for O in Cu, Mg and Al and a CDP of a 3.5 μm thick iron oxide layer with mainly Fe_3O_4 (28 wt.% O) revealed 33 wt.% O and the correct thickness. Systematic errors for the O value smaller than 30% are estimated. The emission yield of H was obtained with help of sintered calibration material with TiH_2 and ZrH_2 in Cu matrix [33]. It turned out [37] that these samples allow the reproducible quantification of less than 0.3 wt.% H in Cu matrix using the lines H I 121,567 nm, H I 486,135 nm and H I 656,279 nm.

Fig. 1 shows the calibration curves obtained for the elements Fe, W and O in constant voltage (700 V)/constant current (10 mA) mode. The calibration also included Na, S and N, although they were not observed in the EDS measurement. H, O and Na were calibrated with sintered calibration samples of IFW. Four Fe-W calibration samples were produced by melting and characterized by Inductively Coupled Plasma Optical Emission Spectroscopy (ICP-OES).

The crystallographic structure and phase composition of the obtained coatings were identified by means of a Rigaku MiniFlex II diffractometer with Cu Kα radiation (λ = 1.54183 Å) operated at 30 kV and 30 mA.

Vacuum annealing of the samples was performed in a controlled vacuum chamber (1×10^{-8} Pa) keeping the samples at 200 °C, 400 °C, 600 °C and 800 °C for 1 h. Samples were afterwards cooled down to room temperature inside the furnace.

3. Results and discussion

3.1. Characterization of as-plated Fe-W coatings: surface morphology, composition and crystallographic structure

SEM micrographs of the as-plated coatings with increasing W content are shown in Fig. 2a–c together with the cross-section of each sample after metallographic preparation (Fig. 2d–f).

By increasing the W content in the coatings the surface morphology is strongly influenced. The surface of the low W-
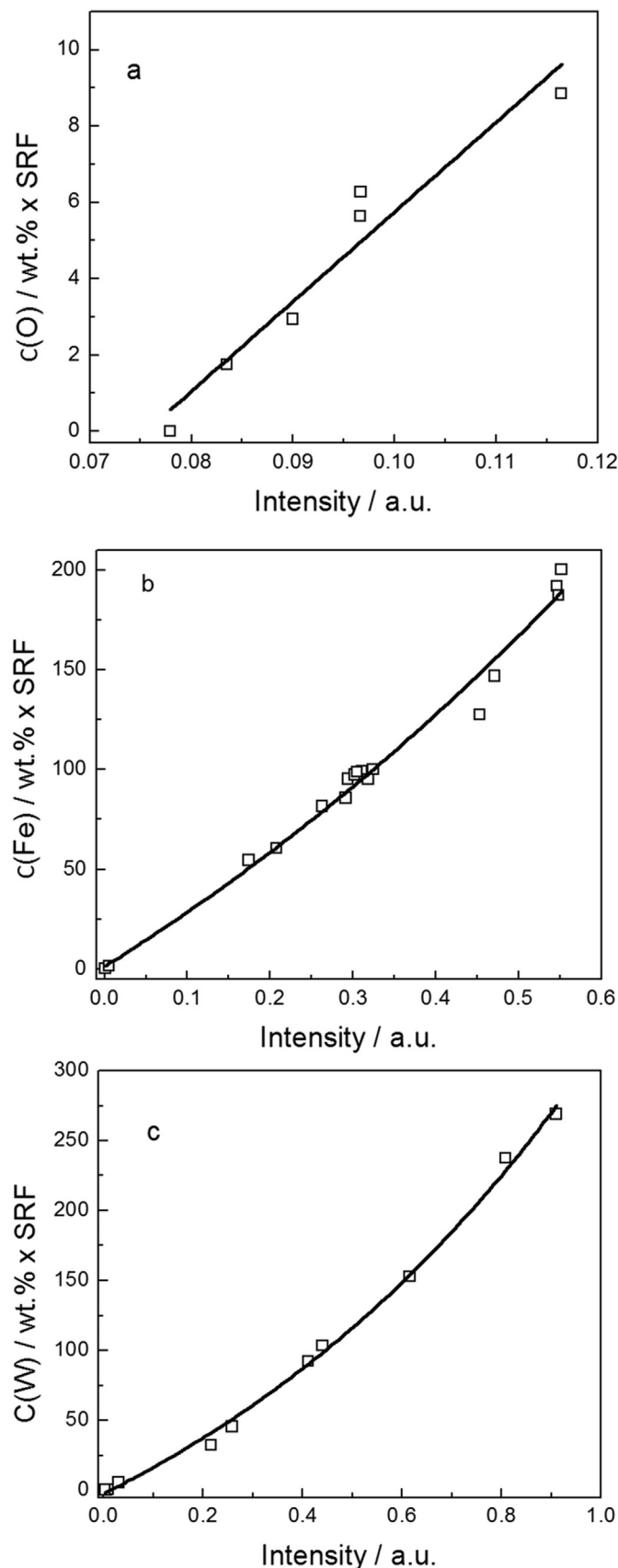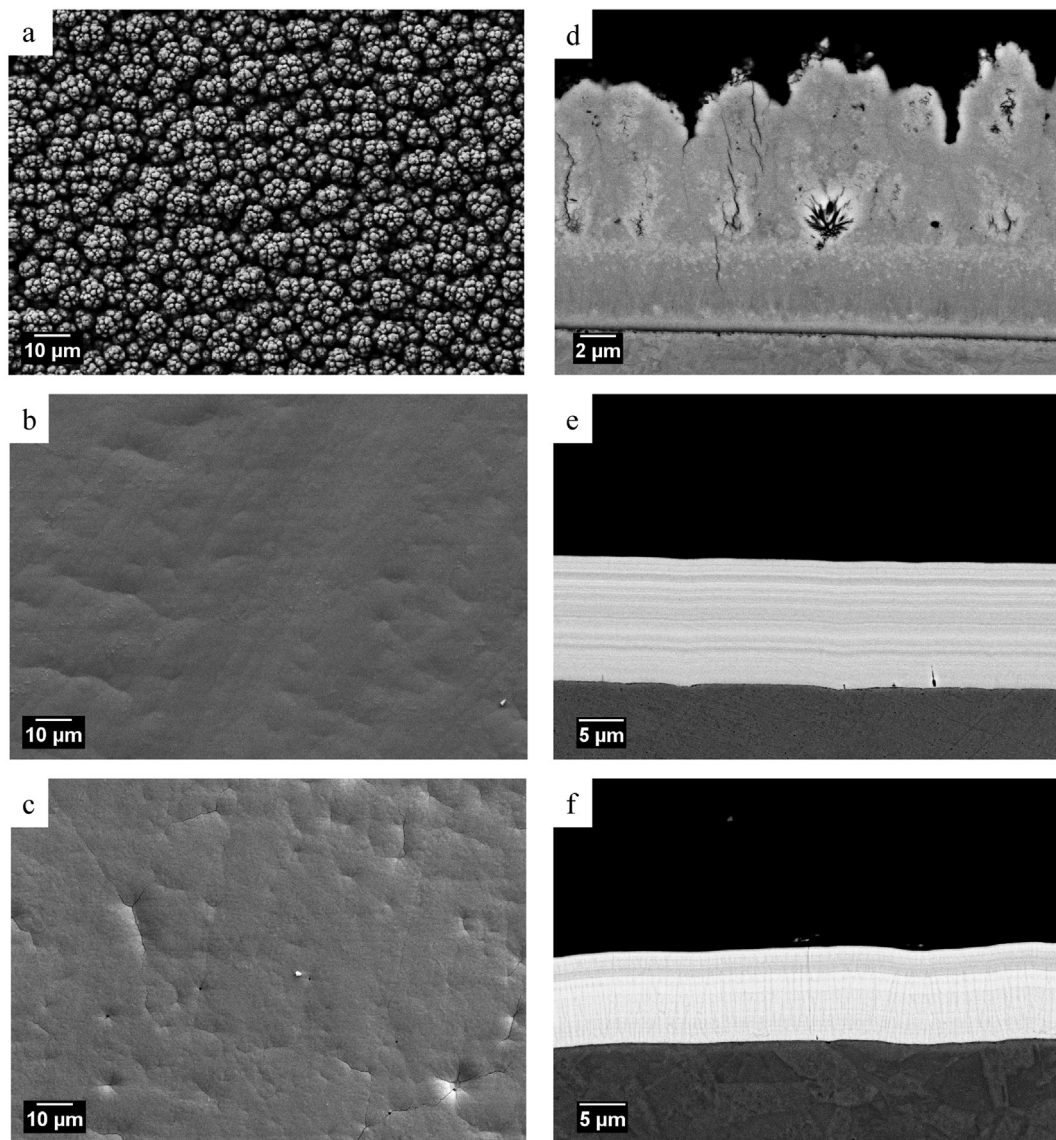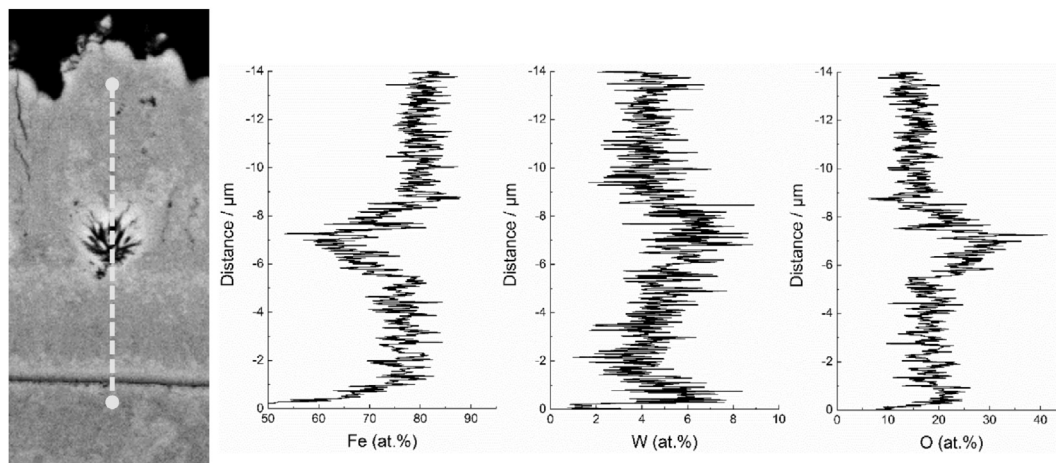

Fig. 1. GD-OES calibration curves for O 777 (a), Fe 371 (b) and W 429 (c). SRF- sputtering rate factor.

Fig. 2. Secondary electron images of the surface morphology of the 4 at.% W (a), 16 at.% W (b), and 24 at.% W samples (c); back-scattered electrons images of the cross-sections of the 4 at.% W (e), 16 at.% W (e), and 24 at.% W samples (f).

Fig. 3. EDS line scan along one of the nest of cracks observed on the cross-section of Fe-W coating with 4 at.% of W.

containing sample is characterized with a globular morphology resembling a cauliflower structure. The other two deposited samples show a smooth surface. Some superficial cracks observed for the W-rich samples can be inferred to the higher amount of W which leads to increased internal stresses in the coating and formation of microcracks [1,3].

Interestingly, the smoothening and leveling effect was achieved without using additives in the plating bath by fine control of the deposition parameters. Namely, it requires such values of overpotential that can ensure rather high crystallization and nucleation rate, but not too fast charge transfer [38]. In addition, the electrodeposition of W alloys with iron group metals occurs via formation of intermediate electroactive mixed complex which absorbed on the cathode surface at the first step and is subsequently reduced at the downstream steps [39,40]. Probably, adsorption of these complexes is localized on the blisters. The surface coverage by intermediates shall be partial and strong enough without possibility to migrate to the sites. Adsorbed intermediates are formed from the relatively big species, which preferentially are: at pH 5 - $WO_2Gly_2^{2-}$, $FeH_2(Cit)_2^{3-}$, $FeH(Cit)_2^{4-}$; at pH 6.5 - $WO_2Gly_2^{2-}$ and $FeH(Cit)_2^{4-}$ [7]. These adsorbed intermediate complexes act as leveling or brightening agents. In general case [38], during the electrodeposition of tungsten or molybdenum alloys with iron group metals the leveling and refining is accompanied by refinement of the deposits in regard to crystallite size with increase in refractory metal content in the alloys [12,25].

In Table 1, the chemical composition of the different samples measured by EDS on the sample surfaces is reported. Electrodeposited tungsten alloys normally contain some oxygen that is incorporated in form of oxides mainly in the top surface layer [13] but also within the coating, forming tungsten oxide streaks [18,41]. As it is seen from Table 1, there is no direct correlation between the W and O content in the alloy (as well as there is no clear influence of the deposition conditions). It is worth noticing that it is rather difficult to reproduce the data of the O content, while the tungsten content is constant when applying certain deposition conditions. Taking this into account, the composition of alloys is more correct to present as content of the metallic phase only (right column of Table 1). This assumption can be partially confirmed by the cross-section analysis of the three samples shown in Fig. 2d–f. In the cross-section of the low W containing sample (Fig. 2d) internal vertical cracks and nests of smaller cracks are seen. These nests appear predominantly at a certain distance from the substrate surface, probably due to the local increase in pH at the electrode/solution interface. The areas around these cracks appear brighter indicating a variation of chemical composition. The presence of these cracks seems also to influence the further growth of the film leading to a columnar-like growth. Fig. 3 shows the EDS line scan performed along one of the nests of cracks observed in Fig. 2d. The cracks appear to be in an O- and W-rich area and the brighter area around it is probably due to W segregation.

On the other hand, the cross-sections of the two samples with higher W content appear to be crack-free. Both cross-sections show the presence of contrast variations aligned horizontally with respect to the substrate. The contrast can be interpreted as a small local variation of the chemical composition along the thickness of the samples. However, a chemical variation is not revealed by the EDS line scan performed along both samples. Instead, a homogenous elemental distribution is observed, i.e. without any W- or O-enrichment as in the case of the Fe-W sample with 4 at.% W.

Furthermore, the oxygen quantity measured from the cross-section of the sample with 16 at.% W is strongly reduced with respect of the amount registered from the surface analysis, and in the case of the 24 at.% W sample oxygen is not even detected. These findings support the assumption of oxygen only being present at
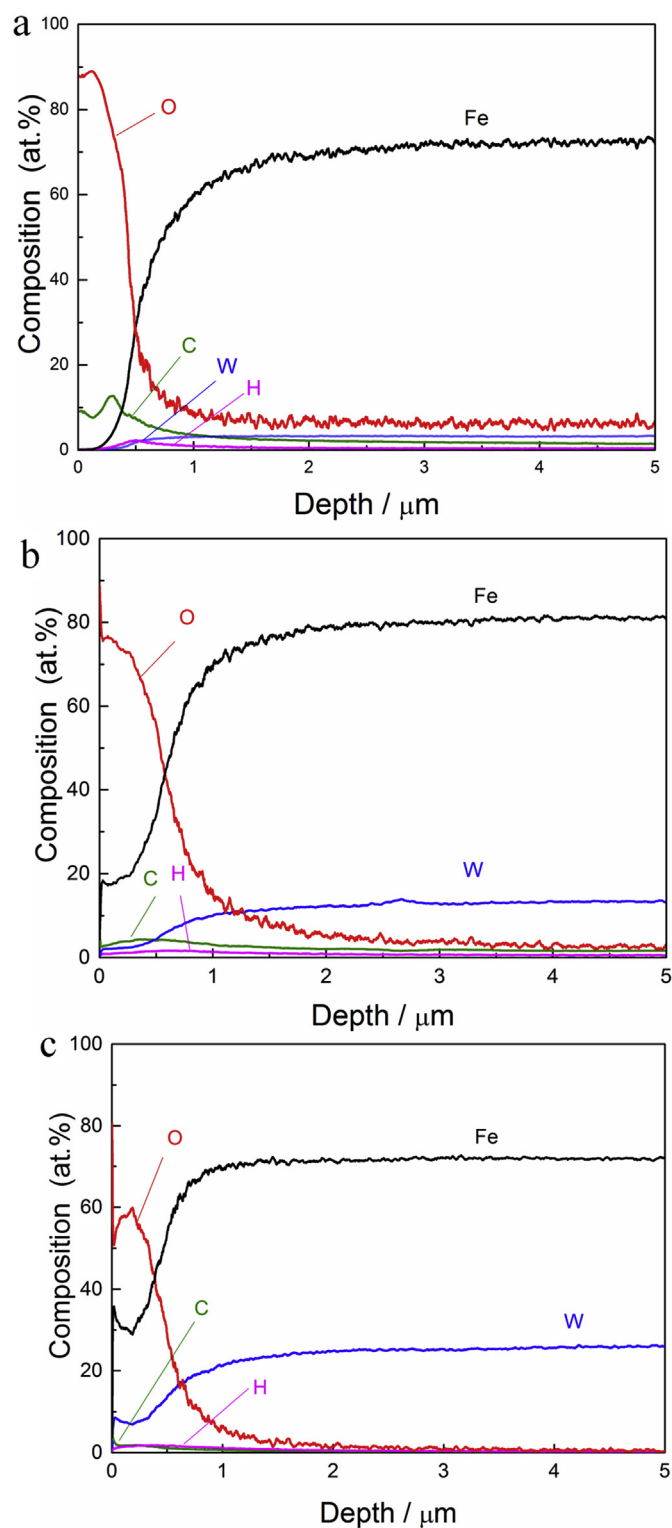

Fig. 4. Compositional depth profiles as obtained by GD-OES of Fe-W samples of different composition: 4 at.% of W (a), 16 at.% of W (b) and 25 at.% of W(c).

the surface in the case of the higher W content sample. Thus, increasing the W content in the coatings seems to stabilize the deposition of the Fe-W alloys and decreases the crack formation and oxygen incorporation during the alloy deposition.

The O content determined by EDS analyses is rather qualitative than quantitative and the results provide the composition not

deeper than approx. 1 μm from the analyzed surface. Yet, for understanding and thorough evaluation of functional properties of the Fe-W alloys, it is important to know their bulk composition. However, the quantitative determination of the full composition of electrodeposits including incorporated non-metallic elements such as O, H and C is a methodical challenge. Therefore, in this study, the experiments were carried out by means of GD-OES in order to get reliable compositional depth profiles (CDP) to determine if O is co-deposited with Fe and W or it is mainly present on the surface.

Representative examples of the CDPs obtained for the Fe-W samples under investigation are shown in Fig. 4. The Fe-W alloys of different composition are characterized by a strongly oxidized top surface layer of ~1–2 μm thickness. The surface layer consists mainly of O and Fe and contains relatively high amounts of C and H, as compared to the concentration deeper down in the material. Nevertheless, the distribution of both Fe and W inside the layers is constant, demonstrating a homogeneous growth of the alloy during electrodeposition independent of deposition temperature and plating pH. Small composition fluctuations are visible in the obtained GD-OES curves, which would resemble the composition variations aligned horizontally with respect to the substrate observed in the cross-section of the two samples with higher W content (Fig. 2 d–f). Studies on similar banded structures found on the cross-sections of electrodeposited Fe-alloys suggest that these structures are formed due to variation/incorporation of light impurities, i.e. oxygen and hydrogen, during the plating process [42]. However, it is hard to directly relate the fluctuations observed in the GD-OES curves to the banded structure observed by cross-sections imaging. As a matter of fact, the length-scale of such banded features (few hundreds of nm) is in the range of the depth resolutions limits of the performed GD-OES measurements. Even if in small amounts, the GD-OES results show that C is present in the bulk of the three deposited coatings. For the samples with 4 at.% W and 16 at.% W, the C content is varying between 1.5 and 2.5 at.% up to 5 μm below the surface, while for the sample with 24 at.% W, at the same distance from the sample surface the carbon is ranging from 0.2 to 0.4 at.%. The carbon co-deposition can be attributed to the inclusion of a reaction intermediate derived from organic acids. In the case of the electrolytic bath used in this study, the presence of carbon is due to the incorporation of some organic species while depositing the Fe-W coating from a solution containing organic ligands [43]. The measured profiles were also investigated for Na

and S content. However, no noticeable influence from these elements was observed in the quantification of the investigated samples. They have been observed by GD-OES but at concentrations lower than 0.2 at.%, which has not much influence on the layer properties and therefore these elements are not discussed.

A drastic decrease in the concentration of oxygen within first few microns was observed. Therefore, the nature of the top surface layer seems to be the spontaneous chemical oxidation due to the contact of alloy's surface with corrosive medium (electrolyte, water, air). Also, it is supposed that some H and C atoms remain adsorbed on the electrode surface and thus can be rather considered as impurities. However, some recent investigations have shown that certain minor contamination elements can interact strongly with the alloy and alter grain growth and microstructure development during annealing [3,19].

In Fig. 4a, the quantitative depth profile of the Fe-W sample deposited at room temperature is shown. In this case, O is not only present on the surface, but also homogeneously distributed in the interior of the layer. With about 7 at.%, the oxygen content in the alloy deposited at room temperature is considerably higher as compared to the O content in the interior of alloys deposited at 65 °C (Fig. 4b and c). According to the model proposed by V.
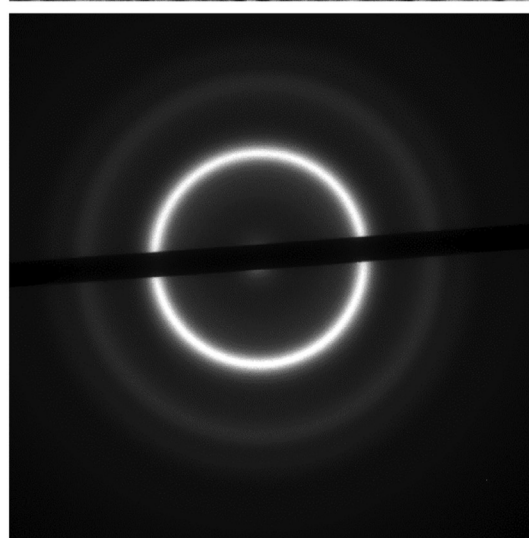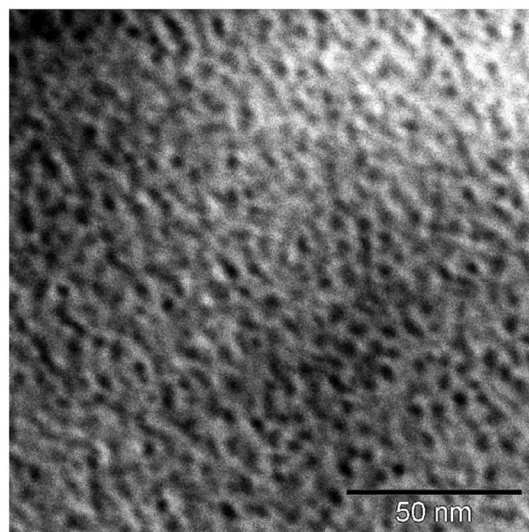

Fig. 6. TEM image of the electrodeposited sample with 24 at.% of W (a), and SAD pattern of the same sample (b).
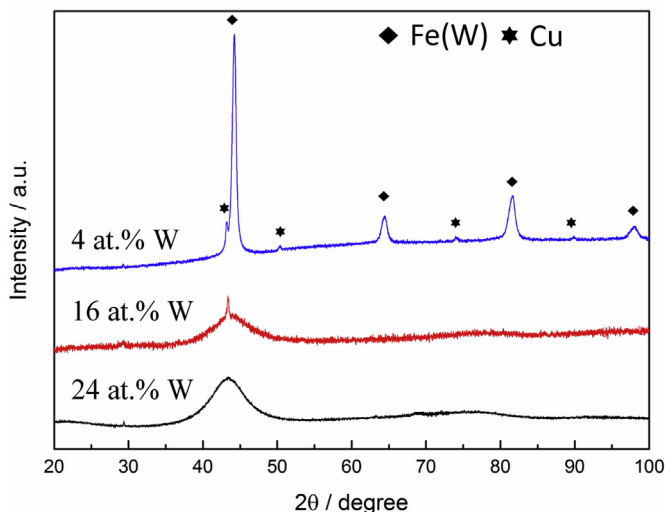

Fig. 5. X-ray diffraction profiles of the as-deposited Fe-W sample.
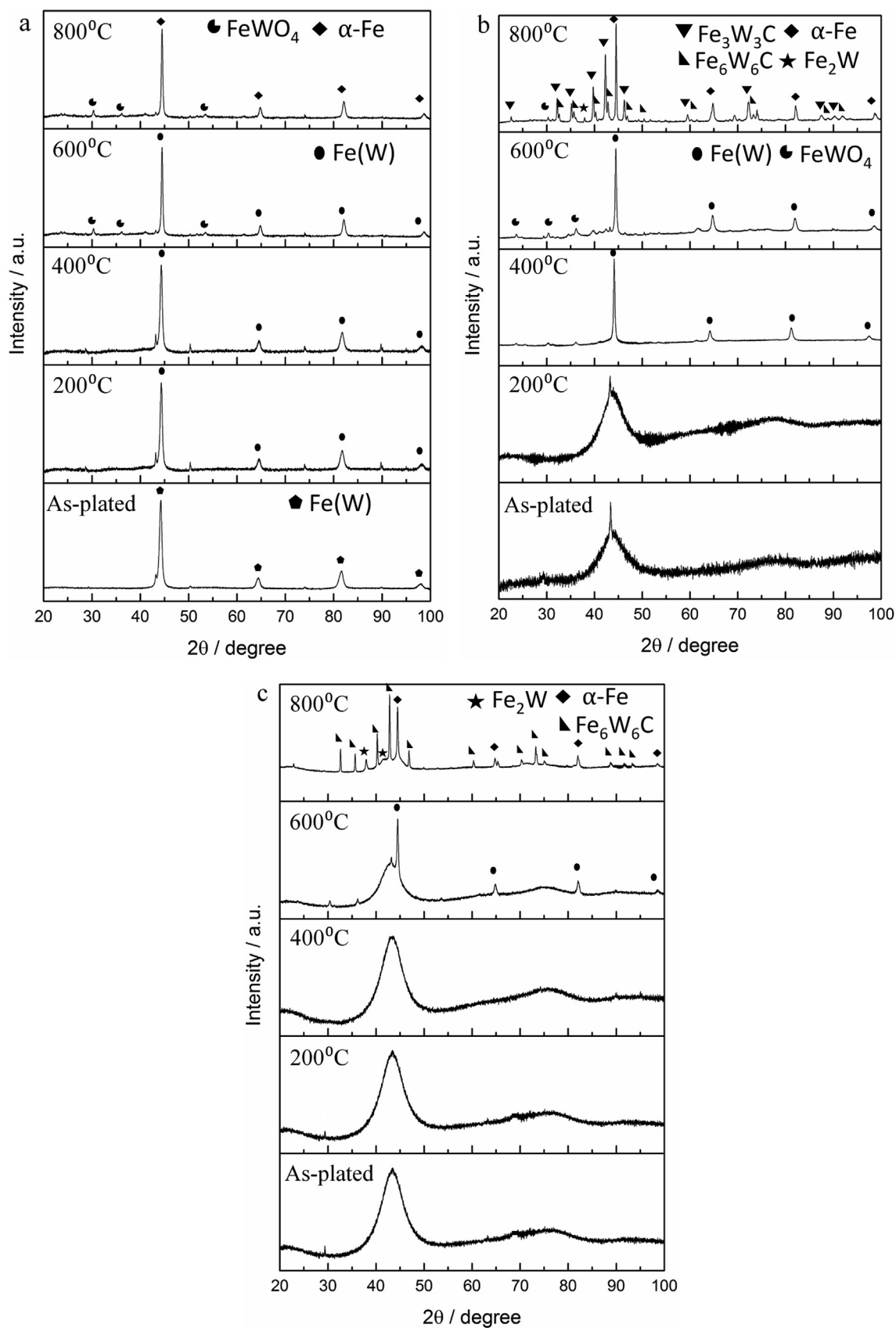
Fig. 7. X-ray diffraction patterns for Fe-W alloys with 4 at.% of W (a), 16 at.% of W (b), and 24 at.% of W (c) annealed at different temperatures.

Krasinov and A. Krasinov [44], the appearance of co-deposited O could be attributed to the interaction of intermediate particle of iron-group metal with absorbed refractory metal anion resulting in the formation of intermediate heterometallic cluster which is subsequently reduced. It can be supposed that at elevated temperatures the rate of the second step reaction is significantly higher, thus, formed intermediates are reduced faster without the formation of oxygen-containing admixtures [45].

XRD results of the as-plated Fe-W coatings are shown in Fig. 5. The X-ray diffraction profile of the sample deposited with 4 at.% W shows the presence of crystalline peaks which are indexed as an Fe(W) solid solution. This is in accordance with previous findings: with relative low W content, a solid solution is formed and the deposited alloys retain the structure of the base metal, in this case bcc-iron (Im3m), with an increased lattice parameter due to W substitution in the bcc lattice [12]. For W concentrations ranging from 11.5 at.% to 20 at.% Nishi et al. [46] have found that the Fe-W alloy could be deposited from simple citrate bath with either a crystalline, an amorphous or a mixed amorphous-crystalline structure. In this window of W composition they found that the pH of the electrolytic bath and the current density applied for the deposition had an influence on the as-deposited Fe-W structure. For a W content higher than 20 at.%, the deposited Fe-W alloys are instead fully amorphous [13,43,47], or possess a nanocrystalline structure [14,48]. Similar findings are observed from the X-ray diffraction patterns of the samples deposited with 16 at.% and 24 at.% W: a broad peak starts around 40° indicating the amorphous nature of both coatings. Though, a small crystalline peak appears at the top of the amorphous shoulder of the sample with 16 at.% W, indicating a certain degree of crystallinity to be present in this case. However, it is hard to distinguish solely by XRD measurements between a totally amorphous structure and a partially crystalline structure formed by the aggregation of crystals at the nanoscale. The presence of such nano-crystals would in fact as well cause a broad diffraction peak [49]. The Fe-W sample with 24 at.% W was analyzed with TEM to confirm the amorphous nature deduced from the XRD results. Fig. 6a shows the TEM bright-field image of the sample surface while Fig. 6b shows the selected area diffraction pattern (SAD). Both the TEM micrograph and the diffuse rings of the SAD pattern are typically observed in amorphous samples.

3.2. Characterization of annealed coatings

Vacuum annealing tests were performed on three selected samples, 4 at.%, 16 at.% and 24 at.% W, to study the thermal stability of the Fe-W coatings and the structural changes occurring at high temperature. The XRD profiles of the annealed samples with increasing W content are shown in Fig. 7. All the phases formed at their respective temperature, listed in Table 2, were compared with the phases expected from the binary equilibrium phase diagrams shown in Fig. 8. Fig. 8a corresponds to the binary Fe-W phase diagram, while Fig. 8b represents a Fe-W-C phase diagram as obtained by using Thermo-Calc software [50]. The amount of carbon was fixed to 2.5 at.%, which is the quantity found at a depth of 1.5 μm in both the sample with 4 at.% and 16 at.% of W.

There are minor changes in the XRD patterns acquired before and after the heat treatment for the coating deposited with 4 at.% of W. When increasing the temperature, the indexed Fe(W) solid solution peak of the as-deposited coating is shifted toward higher diffraction angles, approaching the diffraction angle of pure α-Fe. Small amounts of W probably remain dissolved in the crystal structure of the α-Fe phase because the maximum solubility of W in the α-Fe at 800 °C is 1.2 at.%, from the data acquired from Fig. 8a. The small peaks appearing at 600 °C are indexed as an iron-tungsten oxide phase and are also found at 800 °C. It can be excluded that this phase is formed during the annealing due to some oxygen contamination. Hence, phase formation can be inferred to the high level of oxygen co-deposited within the coating, as shown by GD-OES measurements (Fig. 4a).

The XRD profiles acquired at different temperatures of both 16 at.% W and 24 at.% W show that the samples are deposited in a metastable state and undergo phase transformation when exposed to elevated temperatures. Yet, the recrystallization process differs for these two samples (here and in the following the term recrystallization is used to describe the formation of crystalline phases upon annealing). The structure of the Fe-W sample having 16 at.% of W appears to be unaffected up to 200 °C. However, after heating at 400 °C recrystallization is observed. All crystalline peaks are identified and indexed as Fe(W) solid solution. Afterwards, the recrystallization proceeds similarly to what is seen in the 4 at.% W sample: the Fe(W) peak is approaching the diffraction angle of pure α-Fe and new stable phases are formed. At 600 °C small $FeWO_4$ peaks are visible, while at 800 °C two carbide phases, Fe_3W_3C and Fe_6W_6C, and the intermediate Fe_2W phase are also observed to occur. The formation of such carbides has been previously reported when performing annealing of electrodeposited Fe-W alloys [43,47] as well as for Ni-W alloys [19] because the presence of carbon in bulk is proved to be unavoidable in the electroplating process, and carbides begin to form at very low carbon concentrations. It has been shown that ~4 at.% of C is enough to form the carbide phase annealing at 800 °C. That amount of carbon can be easily co-deposited within the coating when organic complexing agents or additives are used [30]. Furthermore, the obtained phases α-Fe, Fe_2W and Fe_3W_3C at 800 °C are shown to be stable (see Fig. 8b). As a matter of fact, the M6C phase obtained by Thermo-Calc is a carbide with atomic ratio almost identical to the Fe_3W_3C phase.

The Fe-W having 24 at.% W annealed at 600 °C remains partially amorphous (the broad amorphous peak is still present), and the

Table 2
Phases forming at each respective temperature for the annealed samples.

Temperature	Phase		
	4 at.%W	16 at.%W	24 at.%W
As-deposited	$Fe_{0.96}W_{0.04}$ (PDF-04-006-3509) Cu (PDF-00-004-0836)	amorphous	amorphous
200 °C	$Fe_{0.98}W_{0.02}$ (PDF-04-004-2476)	amorphous	amorphous
400 °C	$Fe_{0.98}W_{0.02}$ (PDF-04-004-2476)	$Fe_{0.96}W_{0.06}$ (PDF-04-003-5513)	amorphous
600 °C	$Fe_{0.98}W_{0.02}$ (PDF-04-004-2476) $FeWO_4$ (PDF-01-074-1130)	$Fe_{0.98}W_{0.02}$ (PDF-04-004-2476) $FeWO_4$ (PDF-01-074-1130)	α-Fe (PDF-04-007-9753)
800 °C	α-Fe (PDF 04-007-9753) $FeWO_4$ (PDF-01-074-1130)	α-Fe (PDF 04-007-9753) $FeWO_4$ (PDF-01-074-1130) Fe_3W_3C (PDF 01-089-2579) Fe_6W_6C (PDF 04-003-9466) Fe_2W (PDF 01-075-7894)	α-Fe (PDF 04-007-9753) Fe_6W_6C (PDF 04-003-9466) Fe_2W (PDF 01-075-7894)
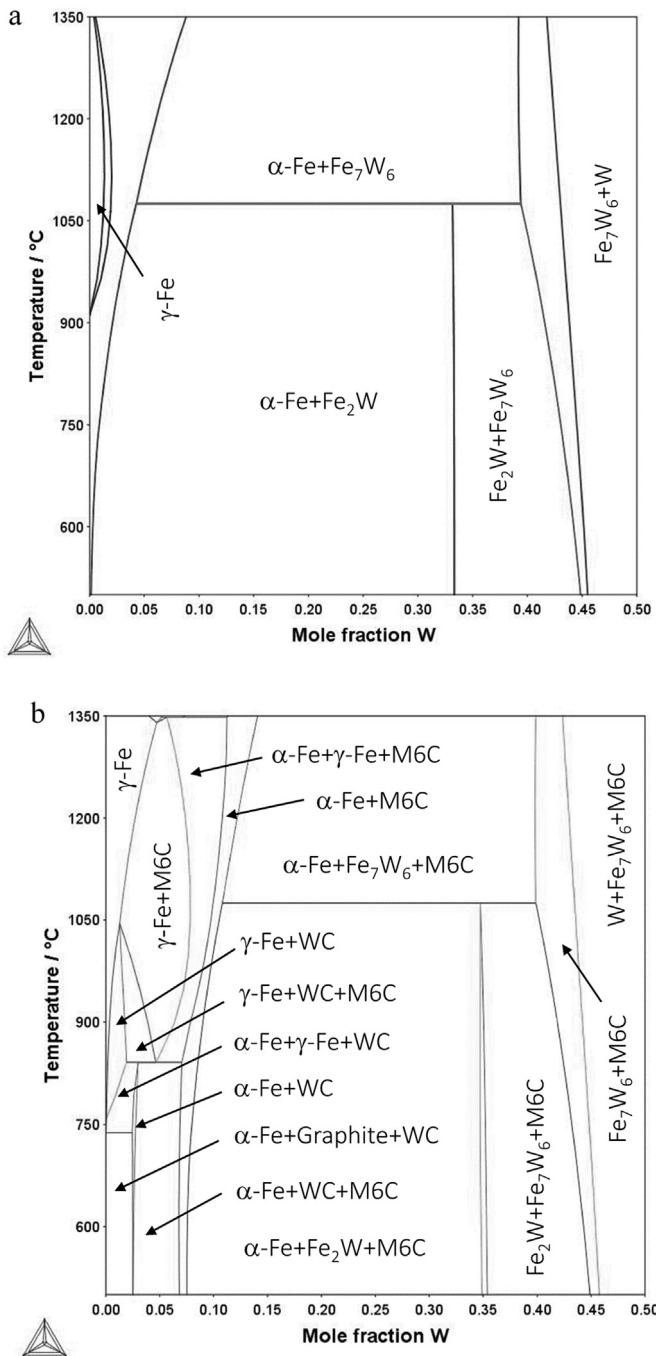
Fig. 8. Fe-W phase diagram (a) and Fe-W-C phase diagram (b) computed using Thermo-Calc software. M6C denotes a Fe-W-C phase with ~43 at.% Fe, 43 at.% W and 14 at.% C.

first crystalline phase formed is indexed as α-Fe. The amount of crystalline phase was estimated to be around 24%. This percentage was obtained by dividing the area of the crystalline peaks by the total area of the XRD spectrum. The same behavior was reported for Fe-W alloys with similar W content electrodeposited from Fe(II)-based citrate bath [43] and Fe(III)-based citrate-ammonia bath [14]. Remarkably, for Co-W alloys a well-developed polycrystalline structure appears already at 400 °C [15]. Thus, Fe-W alloys could be considered as more thermally stable coatings. At 800 °C, α-Fe formation is accompanied by two additional phase, i.e. Fe_6W_6C and Fe_2W, also found after heat treatment of the sample with 16 at.% W.

However, the Fe_3W_3C phase is not observed in the Fe-24 at.% W samples. Possible explanations to this behavior can be the following: the lower amount of carbon found within the sample with 24 at.% W, and the incomplete recrystallization after annealing for 1 h at 800 °C. As a matter of fact, for the samples with 4 at.% W and 16 at.% W, the carbon content is varying between 1.5 and 2.5 at.% at a distance of 5 μm below the surface. For the sample with 24 at.% W, in the same window of thickness, the carbon is ranging from 0.2 to 0.4 at.%. In addition, the Fe_3W_3C phase requires a higher amount of carbon to be formed with respect to the Fe_6W_6C phase. The other reason is concerning the incomplete recrystallization of the sample with 24 at.% W, since the broader amorphous peak is still partially visible in the XRD diffractogram acquired at 800 °C. The Fe_3W_3C peaks may be hidden within the remaining amorphous region. The reason for this incomplete recrystallization can be referred to the higher thermal stability of this sample. The higher thermal stability can be related to the lower rate of elemental diffusion obtained when adding a higher melting point element in the alloy, like in the case of W addition [3].

Heat treatment results can also be used to distinguish between a homogenous amorphous phase from a mixed amorphous-crystalline phase [49]. Thus, the different recrystallization process observed for the three annealed samples can help to define if the crystallographic state of the as-deposited sample with 16 at.% W is indeed not fully amorphous. As previously stated the structural changes upon heating of this sample are similar to those observed for the sample with 4 at.% W. With increasing annealing temperature, the small crystalline peak at the top of the broad amorphous shoulder sharpens and is indexed as a supersaturated Fe(W) solid solution which approaches the diffraction angle of pure α-Fe at 800 °C. This strengthens the hypothesis of the pre-existence of a crystalline phase in the sample in the as-plated state. The fully amorphous sample with 24 at.% W crystallizes instead by forming directly the equilibrium phases expected from the phase diagram: first α-Fe at 600 °C, and then the Fe_6W_6C carbide phase, and the Fe_2W laves phase at 800 °C.

The structural changes occurring in the samples upon annealing are observable from the morphology changes shown in Fig. 9. Here, the surface for each sample annealed at 800 °C is shown. After annealing, the morphology of the sample with 4 at.% W changes slightly: the globular structure observed in the as-plated state is still found, but it appears more compact with small crystallites on the top. Instead, major changes are visible for both the samples with 16 at.% W and 24 at.% W due to the recrystallization of the amorphous phase. Small crystallites homogeneously distributed appear on both surfaces as seen in Fig. 9b and c, where according to GD-OES the surface of both was contaminated with relatively high amounts of carbon (Fig. 4). At the surface of the sample with 16 at.% W the carbides formation is evident: see the clusters of round shape in Fig. 9b. Local EDS point analysis revealed that these features are W-rich clusters, reaching tungsten contents up to 45 at.%. Such contents fit with the W concentration present in the carbide phases. But the carbides appear to be also distributed along the surface of the 24 at.% W sample: small W-rich clusters are clearly visible when imaging with backscattered electrons.

4. Conclusions

In-depth characterization of composition and structure of electrodeposited Fe-W alloys from developed glycolate-citrate bath has been done. Annealing experiments were performed in order to estimate the thermal stability of Fe-W coatings and to trace the structural changes occurring in alloys of different composition. Based on the results presented in this study the following conclusions can be drawn:
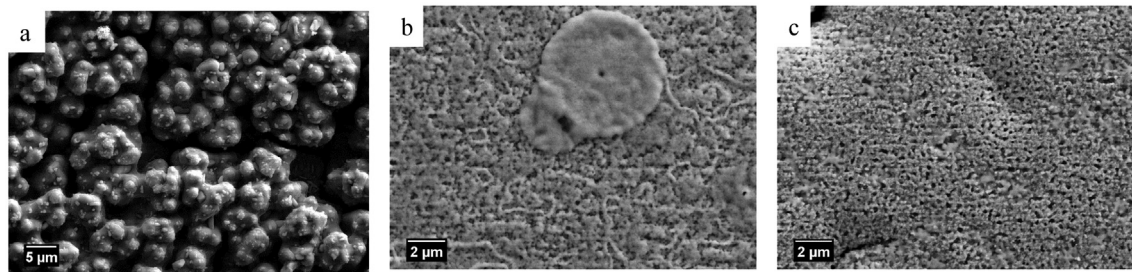
Fig. 9. SEM imaging of the surface morphology of the Fe-W alloy with 4 at.% W (a), 16 at.% W (b) and 24 at.% W (c) after annealing at 800 °C.

- According to the obtained GD-OES CDPs, electrodeposited Fe-W alloys contain up to 80 at.% of O, 10 at.% of C and few at.% of H at the top of the coatings, and the content of these elements decreases sharply within 0.5–0.7 μm. Only for an alloy with low W content we found ~7 at.% of O distributed along the entire film thickness. This correlates with intensive side reactions that occurred at room temperature deposition and caused the internal crack formation and increased the porosity of the coating. Carbon is present in three analyzed coatings in a lower concentration as compared to the surface: i.e. ~1–2 at.% for the samples with 4 at.% and 16 at.% W, and ~0.3 at.% for the sample with 24 at.% W.

- The XRD patterns acquired from the as-plated samples show how the crystallographic structure of the Fe-W coatings changes with increasing W content: a nanocrystalline structure is found for the 4 at.% W sample, a mixed nanocrystalline-amorphous structure for the sample with 16 at.% W, and a homogenous amorphous nature for the 24 at.% W sample. TEM analysis of the sample with 24 at.% W confirmed its amorphous structure.

- The thermal stability was evaluated in the range of 200 °C–800 °C. Annealing coupled with XRD analysis show that the thermal stability of Fe-W alloys increases with the W content. The Fe-W sample with 24 at.% W retains the amorphous structure up to 600 °C, where a partially crystalized structure was observed. Furthermore, the different recrystallization process observed for the three annealed samples helped to clarify the structural difference between the mixed nanocrystalline-amorphous phase of the sample with 16 at.% W and the homogenous amorphous phase of the 24 at.% W sample.

- The formation of carbide phases after annealing at 800 °C was noticed for alloys having 16 and 24 at.% of W. Two carbide phases, i.e. Fe_3W_3C and Fe_6W_6C, are observed after heat treatment of the 16 at.% W sample, while just the Fe_6W_6C phase is formed after heat treatment of the 24 at.% W sample. Possible explanations to this behavior are the lower amount of carbon found within the sample with 24 at.% W, and its incomplete recrystallization after annealing for 1 h at 800 °C.

Acknowledgements

References

[1] S.-J. Mun, M. Kim, T.-H. Yim, J.-H. Lee, T. Kang, Mechanical and structural characteristics of electrodeposited Ni–Fe–W alloy after heat-treatment, J. Electrochem. Soc. 157 (2010) D177–D180, https://doi.org/10.1149/1.3292282.

[2] M.X. Donten, H. Cesiulis, Z. Stojek, Electrodeposition and properties of Ni-W, Fe-W and Fe-Ni-W amorphous alloys. A comparative study, Electrochim. Acta. 45 (2000) 3389–3396, https://doi.org/10.1016/S0013-4686(00)00437-0.

[3] F. He, J. Yang, T. Lei, C. Gu, Structure and properties of electrodeposited Fe-Ni-W alloys with different levels of tungsten content: a comparative study, Appl. Surf. Sci. 253 (2007) 7591–7598, https://doi.org/10.1016/j.apsusc.2007.03.068.

[4] A. Chianpairot, G. Lothongkum, C.A. Schuh, Y. Boonyongmaneerat, Corrosion of nanocrystalline Ni-W alloys in alkaline and acidic 3.5wt.% NaCl solutions, Corros. Sci. 53 (2011) 1066–1071, https://doi.org/10.1016/j.corsci.2010.12.001.

[5] P. de Lima-Neto, G.P. da Silva, A.N. Correia, A comparative study of the physicochemical and electrochemical properties of Cr and Ni-W-P amorphous electrocoatings, Electrochim. Acta. 51 (2006) 4928–4933, https://doi.org/10.1016/j.electacta.2006.01.036.

[6] N. Tsyntsaru, H. Cesiulis, A. Budreika, X. Ye, R. Juskenas, J.P. Celis, The effect of electrodeposition conditions and post-annealing on nanostructure of Co-W coatings, Surf. Coatings Technol. 206 (2012) 4262–4269, https://doi.org/10.1016/j.surfcoat.2012.04.036.

[7] A. Nicolenco, N. Tsyntsaru, H. Cesiulis, Fe (III)-based ammonia-free bath from electrodeposition of Fe-W alloys, J. Electrochem. Soc. 164 (9) (2017) D590–D596, https://doi.org/10.1149/2.1001709jes.

[8] E.P. Barbano, I. Carlos, E. Vallés, Electrochemical synthesis of Fe-W and Fe-W-P magnetic amorphous films and Fe-W nanowires, Surf. Coat. Technol. 324 (2017) 80–84, https://doi.org/10.1016/j.surfcoat.2017.05.071.

[9] I.Y. Yermolenko, M.V. Ved, N.D. Sakhnenko, Y.I. Sachanova, Composition, morphology, and topography of galvanic coatings Fe-Co-W and Fe-Co-Mo, Nanoscale Res. Lett. 12 (1) (2017) 352, https://doi.org/10.1186/s11671-017-2128-3.

[10] G. Yar-Mukhamedova, M. Ved, N. Sakhnenko, A. Karakurkchi, I. Yermolenko, Iron binary and ternary coatings with molybdenum and tungsten, Appl. Surf. Sci. 383 (2016) 346–352, https://doi.org/10.1016/j.apsusc.2016.04.04.

[11] Y.D. Gamburg, E.N. Zakharov, G.E. Goryunov, Electrodeposition, structure, and properties of iron − tungsten alloys 37 (2001) 670–673.

[12] N. Tsyntsaru, H. Cesiulis, M. Donten, J. Sort, E. Pellicer, E.J. Podlaha-Murphy, Modern trends in tungsten alloys electrodeposition with iron group metals, Surf. Eng. Appl. Electrochem 48 (2013) 491–520, https://doi.org/10.3103/S1068375512060038.

[13] M. Donten, Bulk and surface composition, amorphous structure, and thermocrystallization of electrodeposited alloys of tungsten with iron, nickel, and cobalt, J. Solid State Electrochem 3 (1999) 87–96, https://doi.org/10.1007/s100080050133.

[14] N. Tsyntsaru, J. Bobanova, X. Ye, H. Cesiulis, A. Dikusar, I. Prosycevas, J.P. Celis, Iron-tungsten alloys electrodeposited under direct current from citrate-ammonia plating baths, Surf. Coat. Technol. 203 (2009) 3136–3141, https://doi.org/10.1016/j.surfcoat.2009.03.041.

[15] N. Tsyntsaru, H. Cesiulis, E. Pellicer, J.P. Celis, J. Sort, Structural, magnetic, and mechanical properties of electrodeposited cobalt-tungsten alloys: intrinsic and extrinsic interdependencies, Electrochim. Acta 104 (2013) 94–103, https://doi.org/10.1016/j.electacta.2013.04.022.

[16] R. Scully, A. Gebert, J.H. Payer, Corrosion and related mechanical properties of bulk metallic glasses, J. Mater. Res. 22 (2007) 302–313, https://doi.org/10.1557/jmr.2007.0051.

[17] A. Nicolenco, N. Tsyntsaru, J. Fornell, E. Pellicer, J. Reklaitis, D. Baltrunas, H. Cesiulis, J. Sort, Mapping of magnetic and mechanical properties of Fe-W alloys electrodeposited from Fe(III)-based glycolate-citrate bath, Mater. Des. 139 (2018) 429–438, https://doi.org/10.1016/j.matdes.2017.11.011.

[18] C.J. Marvel, D. Yin, P.R. Cantwell, M.P. Harmer, The influence of oxygen contamination on the thermal stability and hardness of nanocrystalline Ni-W alloys, Mater. Sci. Eng. A 664 (2016) 49–57, https://doi.org/10.1016/j.msea.2016.03.129.

[19] C.J. Marvel, P.R. Cantwell, M.P. Harmer, The critical influence of carbon on the thermal stability of nanocrystalline Ni-W alloys, Scr. Mater. 96 (2015) 45–48, https://doi.org/10.1016/j.scriptamat.2014.10.022.

[20] S. Hayata, S. Oue, H. Nakano, T. Takahash, Effect of annealing on the structure and hardness of electrodeposited Ni-W alloys, ISIJ Int. 5 (2015) 1083–1090, https://doi.org/10.2355/isijinternational.55.1083.

[21] Z. Gáliková, M. Chovancová, V. Danielik, Properties of Ni-W alloy coatings on steel substrate, Chem. Pap. 60 (2006) 353–359, https://doi.org/10.2478/s11696-006-0064-2.

[22] S. Oue, H. Nakano, S. Kobayashi, H. Fukushima, Structure and codeposition behavior of Ni–W alloys electrodeposited from ammoniacal citrate solutions, J. Electrochem. Soc. 156 (2009) D17–D22, https://doi.org/10.1149/1.3006389.

[23] T. Yamasaki, P. Schlossmacher, K. Ehrlich, Y. Ogino, Formation of amorphous electrodeposited Ni-W alloys and their nanocrystallization, Nanostruct. Mater. 10 (1998) 375–388, https://doi.org/10.1016/S0965-9773(98)00078-6.

[24] Y. Kimoto, A. Giga, T. Ohkubo, Y. Takigawa, K. Hono, K. Higashi, Ni-W amorphous/nanocrystalline duplex composite produced by electrodeposition, Mater. Trans. 48 (2007) 996–1000, https://doi.org/10.2320/matertrans.48.996.

[25] R. Juškenas, I. Valsiunas, V. Pakštas, R. Giraitis, On the state of W in electro-deposited Ni-W alloys, Electrochim. Acta 54 (2009) 2616–2620, https://doi.org/10.1016/j.electacta.2008.10.060.

[26] A.J. Detor, C.A. Schuh, Microstructural evolution during the heat treatment, J. Mater. Res. 22 (2007) 3233–3248, https://doi.org/10.1557/JMR.2007.0403.

[27] A.J. Detor, M.K. Miller, C.A. Schuh, Solute distribution in nanocrystalline Ni–W alloys examined through atom probe tomography, Philos. Mag. 86 (2006) 4459–4475, https://doi.org/10.1080/14786430600726749.

[28] E. Dislaki, J. Sort, E. Pellicer, Parametric aqueous electrodeposition study and characterization of Fe–Cu films, Electrochim. Acta 231 (2017) 739–748, https://doi.org/10.1016/j.electacta.2017.02.092.

[29] J. George, S. Elhalawaty, A.J. Mardinly, R.W. Carpenter, D. Litvinov, S.R. Brankovic, Oxide/hydroxide incorporation into electrodeposited CoFe al-loys - consequences for magnetic softness, Electrochim. Acta 110 (2013) 411–417, https://doi.org/10.1016/j.electacta.2013.06.097.

[30] Y.D. Gamburg, G. Zangari, Theory and Practice of Metal Electrodeposition, 2011, https://doi.org/10.1017/CBO9781107415324.004.

[31] J. Angeli, A. Bengtson, A. Bogaerts, V. Hoffmann, V.-D. Hodoroaba, E. Steers, Glow discharge optical emission spectrometry: moving towards reliable thin film analysis–a short review, J. Anal. At. Spectrom. 18 (2003) 670–679, https://doi.org/10.1039/B301293J.

[32] V. Hoffmann, S. Donath, H. Merker, Verfahren zur Herstellung von massiven Kalibrationsproben für die analytische Spektrometrie, DE 102013225940 B3.

[33] V. Hoffmann, Massive wasserstoffhaltige vakuumdichte Proben, Verfahren zu ihrer Herstellung und Verwendung, DE 102013225940 B3.

[34] L. Wilken, V. Hoffmann, K. Wetzig, Erosion rate measurements for GD-OES, J. Anal. At. Spectrom. 18.9 (2003) 1141–1145.

[35] C. Gonzalez-Gago, P. Smid, T. Hofmann, C. Venzago, V. Hoffmann, W. Gruner, The use of matrix-specific calibrations for oxygen in analytical glow discharge spectrometry, Anal. Bioanal. Chem. 406 (2014) 7473–7482, https://doi.org/10.1007/s00216-014-8186-9.

[36] M. Köster, Poster Presentation PW96 CSXXXVI, 2009.

[37] V. Hoffmann, 8th Nordic Conference on Plasma Spectrochemistry.

[38] L. Oniciu, L. Muresan, Some fundamental aspects of levelling and brightening in metal electrodeposition, J. Appl. Electrochem. 21 (1991) 565–574, https://doi.org/10.1007/BF01024843.

[39] O. Younes, E. Gileadi, Electroplating of Ni-W alloys. I. Ammoniacal citrate baths, J. Electrochem. Soc. 149 (2002) C100–C111, https://doi.org/10.1149/1.1433750.

[40] A. Kola, X. Geng, E.J. Podlaha, Ag–W electrodeposits with high W content from thiourea–citrate electrolytes, J. Electroanal. Chem. 761 (2016) 125–130.

[41] W. Cao, C. Marvel, D. Yin, Y. Zhang, P. Cantwell, M.P. Harmer, J. Luo, R.P. Vinci, Correlations between microstructure, fracture morphology, and fracture toughness of nanocrystalline Ni-W alloys, Scr. Mater. 113 (2016) 84–88, https://doi.org/10.1016/j.scriptamat.2015.09.030.

[42] P. Egberts, P. Brodersen, G.D. Hibbard, Mesoscale structure in electrodeposited nanocrystalline Ni-W alloys, Mater. Sci. Eng. A 441 (2006) 336–341, https://doi.org/10.1016/j.msea.2006.08.023.

[43] S. Wang, C. Zeng, Y. Ling, J. Wang, G. Xu, Phase transformations and electro-chemical characterizations of electrodeposited amorphous Fe–W coatings, Surf. Coat. Technol. 286 (2016) 36–41, https://doi.org/10.1016/j.surfcoat.2015.12.011.

[44] V. Krasinov, A. Krasinov, Mechanism for induced codeposition of alloys and some single refractory metals, Khimiya I Khimicheskaya Tekhnologiya 37 (2016) 8–14, https://doi.org/10.15217/issn1998984-9.2016.37.8.

[45] V. Krasinov, The role of electrochemical cobalt reduction intermediates in the formation of oxygen-containing admixtures, Khimiya I Khimicheskaya Tekh-nologiya 31 (2015) 40–46, https://doi.org/10.15217/issn1998984-9.2015.31.40.

[46] Y. Nishi, Y. Mogi, K. Oguri, T. Watanabe, Preparation of F e-W amorphous films by an electroplating method, J. Mater. Sci. Lett. 20 (1995) 1–3.

[47] M.C. Chou, C.F. Chu, S.T. Wu, Phase transformations of electroplated amor-phous iron-tungsten-carbon film, Mater. Chem. Phys. 78 (2003) 59–66, https://doi.org/10.1016/S0254-0584(02)00217-1.

[48] Z.I. Bobanova, A.I. Dikusar, H. Cesiulis, J.-.P. Celis, N.I. Tsyntsaru, I. Prosycevas, Micromechanical and tribological properties of nanocrystalline coatings of iron-tungsten alloys electrodeposited from citrate-ammonia solutions, Russ. J. Elec-trochem. 45 (2009) 895–901, https://doi.org/10.1134/S1023193509080096.

[49] F. Wang, K. Itoh, T. Watanabe, Relationship between the crystallographic structure of electrodeposited Fe – P alloy film and its thermal equilibrium phase diagram 44 (2003) 127–132, https://doi.org/10.2320/matertrans.44.127.

[50] J.O. Andersson, T. Helander, L. Höglund, P.F. Shi, B. Sundman, Thermo Calc and DICTRA, computational tools for material science, Calphad 26 (2002) 273–312, https://doi.org/10.1016/S0364-5916(02)00037-8.

Paper 4

Enhanced mechanical properties and microstructural modifications in electrodeposited Fe-W alloys through designed heat treatments

A. Mulone, A. Nicolenco, J. Fornell, E. Pellicer, N. Tsyntsaru,

H. Cesiulis, J. Sort, U. Klement

Enhanced mechanical properties and microstructural modifications in electrodeposited Fe-W alloys through controlled heat treatments

A. Mulone[a,*], A. Nicolenco[b], J. Fornell[c], E. Pellicer[c], N. Tsyntsaru[b,d], H. Cesiulis[b], J. Sort[c,e], U. Klement[a,*]

[a] Chalmers University of Technology, Department of Industrial and Materials Science, SE-412 96 Gothenburg, Sweden
[b] Vilnius University, Physical Chemistry Department, LT-03225 Vilnius, Lithuania
[c] Department de Física, Facultat de Ciències, Universitat Autònoma de Barcelona, E-08193 Bellaterra, Spain
[d] Institute of Applied Physics of ASM, Chisinau MD – 2028, Republic of Moldova
[e] Institució Catalana de Recerca i Estudis Avançats (ICREA), E-08010 Barcelona, Spain

ABSTRACT

Among W alloys, Fe-W has seen much attention recently, due to the need of moving toward the design of environmentally friendly materials. Coatings with 4, 16 and 24 at.% of W were electrodeposited from an environmental friendly Fe(III)-based glycolate-citrate bath. The samples were annealed in vacuum at different temperatures up to 800 °C. Different crystalline phases are formed upon annealing: α-Fe, Fe_2W, Fe_3W_3C, Fe_6W_6C, and $FeWO_4$. Their grain size and distribution within the coating was studied by means of Electron Backscattered Diffraction (EBSD) technique. The effect of annealing on the mechanical properties of the coatings was analyzed performing nanoindentation measurements. The results show a considerable increase of the hardness followed by a rapid decrease at higher temperatures. The highest hardness value, i.e. 16.5 GPa, is measured for the sample with 24 at.% of W after annealing at 600 °C owing to the precipitation of α-Fe crystallites. This study indicates the possibility to substantially increase the hardness of electrodeposited Fe-W coatings by optimization of the annealing treatment. In addition, the critical influence of the carbide and oxide phases on the mechanical properties of alloys is discussed. Hence, Fe-W coatings rich in W can be applied as a possible candidate for protective coating applications at elevated temperatures.

1. Introduction

In recent years, the attention toward electrodeposited W alloys has grown thanks to the remarkable properties of the alloys and their potential applications. W alloys exhibit good oxidation, mechanical and tribological resistance as well as good thermal stability [1–5]. Among W alloys, Fe-W has especially seen much attention recently, due to the need of moving toward the production of environmentally friendly materials. The Fe-W coatings have the prospect to be used as a replacement for coatings manufactured with environmentally hazardous processes such as the hard chromium coatings [3,6–9]. Typically, as-deposited Fe-W alloys with high W content (up to 30 at.%) show relatively high hardness, i.e. about 10–13 GPa, which is comparable to that of electrodeposited chromium [10,11]. Nevertheless, W-rich are alloys usually brittle due to higher internal stresses [12]. Thermal treatment can reduce the internal stress of the coatings and further improve their mechanical properties. However, most of the studies concerning the effect of heat treatments on hardness of electrodeposited W alloys have

been performed on Ni-W [8,13–18] and Ni-Fe-W [9,12] systems. Only a few studies have assessed the thermal stability and the phase transformations occurring upon annealing of Fe-W alloys [4,5,19]. However, the effects of the heat treatment on the mechanical properties of such alloys have been overlooked.

It is well known that the functional properties of an alloy are mainly determined by its composition and structure. In our previous study, Fe-W alloys with various W contents were electrodeposited from an environmentally friendly glycolate-citrate electrolyte and the structure development of the coatings at various annealing temperatures has been studied, as shown in Fig. 1 [20]. The crystallographic structure of the as-deposited samples changes with increasing the W content: a nanocrystalline structure was found for the sample with 4 at.% W, a mixed nanocrystalline-amorphous structure for the sample with 16 at.% W, and a fully amorphous structure for the sample with 24 at.% W. The amorphous structure of the sample with 24 at.% W was confirmed by the diffuse rings of the Selected Area Diffraction pattern (SAD) obtained by TEM analysis, see inset of Fig. 1c. The crystallographic
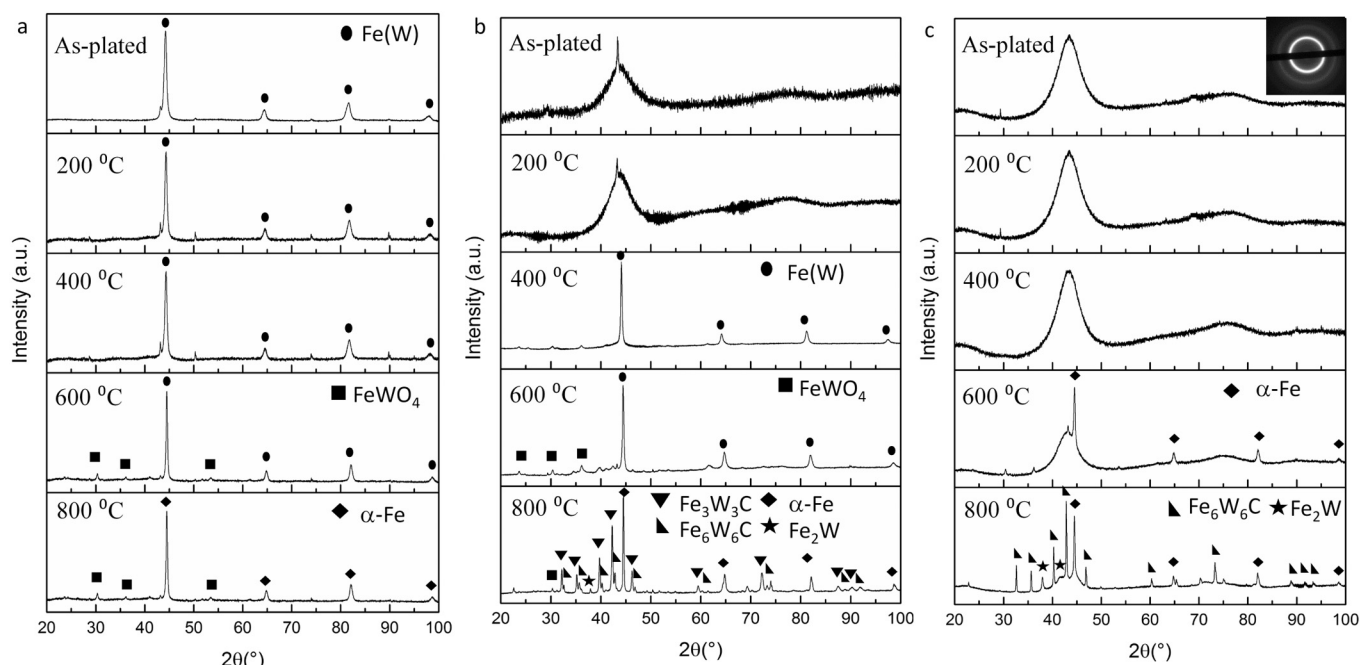

Fig. 1. X-ray diffraction patterns for Fe-W alloys with 4 at.% of W (a), 16 at.% of W (b), and 24 at.% of W (c) annealed at different temperatures. An insert of a Selected Area Diffraction pattern (SAD) acquired from the as-deposited Fe-W sample with 24 at.% of W is included [20].

evolution upon annealing differs for the Fe-W alloys, in correlation with their composition (i.e. W content and co-deposited impurities) and as-deposited crystal structure. The Fe-W alloy rich in W shows higher thermal stability. As a matter of fact, the as-deposited amorphous structure of the coating is partially retained after 1 h annealing at 800 °C. The formation of stable phases is also observed as expected from the Fe-W binary phase diagram [21,22], i.e. α-Fe and the intermetallic Fe_2W phase. The formation of W intermetallic phases during annealing is rather typical for this type of electrodeposits and it has been observed also for Ni-W and Co-W alloys [15,23]. In addition, different non-metallic elements (i.e. carbon, oxygen and hydrogen) co-deposited within the coating affect the microstructure development upon annealing leading to the formation of iron tungsten oxide $FeWO_4$ and iron tungsten carbide Fe_3W_3C, Fe_6W_6C phases, as observable in Fig. 1. The formation of tungsten carbides and tungsten oxides upon annealing has important consequences both for the thermal stability and the mechanical properties of the coating [24,25]. In particular, as shown by previous studies, Fe_3W_3C and Fe_6W_6C phases are characterized with high hardness and high elastic modulus [26–28].

The presence of co-deposited non-metallic elements in the Fe-W coatings was revealed by Glow Discharge Optical Emission Spectroscopy analysis and thoroughly discussed in a previous study [20]. The results showed that Fe-W electrodeposits normally contain up to 80 at.% of O, 10 at.% of C and few at.% of H in the subsurface, i.e. within 1 μm from the surface. In fact, the strongly bonded chemisorbed oxygen-containing layer is formed on the top of the tungsten alloys with almost no activation and the activation energy for oxygen desorption from the surface is high (269–480 kJ/mol) [23]. Moreover, water can act as an oxidizing agent to W [29]. Therefore, it is hard to avoid the surface oxidation of the Fe-W coatings in practice. The quantity of the light elements is strongly reduced in the bulk of the coatings and thus they can be considered as adsorbed surface impurities. Only for the alloy with 4 at.% of W it was found ~7 at.% of O distributed along the entire film thickness. In the bulk of the three analyzed coatings, the carbon content is lower than at the surface: i.e. ~1–2 at.% for the samples with 4 at.% and 16 at.% of W, and ~0.3 at.% for the sample with 24 at.% of W. The reduction of O, H and C is also depending on the W content of the deposits. Lower amounts of impurities were found for

the coating richer in W, which is probably related to the decrease in cathodic polarization and redistribution of the partial currents [20].

The aim of this study is to investigate the effect of annealing temperature on the mechanical properties, i.e. hardness and reduced elastic modulus, of Fe-W alloys electrodeposited with various W contents. The formation, distribution and orientation of sub-micro/nano sized oxides and carbides is evidenced by means of Electron Backscattered Diffraction (EBSD) technique. Furthermore, nanoindentation measurements are performed in order to correlate the differences in the microstructure to differences in the mechanical properties.

2. Experimental

2.1. Electrodeposition of Fe-W coatings

The electrodeposition of the Fe-W coatings was carried out from a bath with the following composition: 1 M glycolic acid, 0.3 M citric acid, 0.1 M $Fe_2(SO_4)_3$ and 0.3 M Na_2WO_4. The bath pH was adjusted by addition of either NaOH or H_2SO_4. The design of electrodeposition conditions leading to various tungsten content in Fe-W alloys was discussed elsewhere [3,20]. In order to study the heat treatment influence, Fe-W coatings with 4, 16 and 24 at.% of W were deposited applying a constant cathodic current density of 15 mA cm^{-2} [20]. The coating with 4 at.% of W was deposited at 20 °C, the coatings with 16 and 24 at.% were deposited at 65 °C. The electrodeposition was performed in a typical three-electrode cell and the electrolyte volume was kept at 250 mL. A pure copper sheet was used as the working electrode, platinized titanium was used as a counter electrode, and saturated Ag/AgCl/KCl$_{sat}$ was used as reference electrode. The thickness of electrodeposited coatings was ~10 μm. The values were calculated based on gravimetric and elemental analyses of the electrodeposited alloys and confirmed by measuring the thickness on the cross-section.

2.2. Coating characterization

Secondary Electrons (SE) and Back Scattered Electrons (BSE) were used for imaging of the as-plated and annealed samples in a Leo 1550 Gemini Scanning Electron Microscope (SEM) with field emission gun.

The instrument is equipped with Energy Dispersive X-ray Spectroscopy (EDS) and Electron Backscatter Diffraction (EBSD) technique. The EBSD measurements were performed using an HKL Channel 5 system and a Nordlys II detector. Transmission Electron Microscopy (TEM) investigations were performed with a Zeiss EM 912 OMEGA microscope operating at an accelerating voltage of 120 kV. The crystallographic structure and phase composition of the obtained coatings were identified by means of a Rigaku MiniFlex II diffractometer with Cu Kα radiation (λ = 1.54183 Å) operated at 30 kV and 30 mA. Vacuum annealing of the samples was performed in a controlled vacuum chamber (1×10^{-8} Pa) keeping the samples for 1 h at 200 °C, 400 °C, 600 °C and 800 °C. Afterwards, the samples were cooled down to room temperature inside the furnace. Moreover, the deposits with 16 at.% and 24 at.% of W were also annealed for 6 and 12 h at 800 °C.

The Fe-W cross-sections were investigated in the ordinary EBSD setup (70° tilt of sample toward the EBSD detector). For each cross-section three phase and band contrast maps of 4×3 μm were obtained applying an accelerating voltage of 20 kV and a step size of 20 nm. The maps were afterwards stitched together by using Map Sticher software. All the maps acquired were processed, i.e. wild spikes were removed and minor noise reduction (4 nearest neighbors required) was performed. In the phase maps, high angle grain boundaries are shown by black lines and are defined by a misorientation larger than 10°.

Metallographic preparation of the samples was performed by mechanical polishing with a 50 nm finishing using OP-S silica suspension as the last step. The mechanical tests on the as-plated and annealed coatings were performed on cross-section area using a NHT^2 Nanoindentation Tester from Anton-Paar equipped with a Berkovich pyramidal-shaped diamond tip under load control mode. A load of 10 mN was applied with a loading segment of 30 s followed by a load holding segment of 10 s and by an unloading segment of 30 s. The hardness and elastic modulus are reported as an average value of fifteen indentations, performed in the middle of the cross-section of each sample in order to avoid the influence from the resin. For the nanoindentation measurements the cross-sections were polished down to a 1 μm surface finishing.

3. Results and discussion

3.1. Structural characterization of Fe-W coatings: as-deposited and annealed

In our previous research, the structure development of the electrodeposited Fe-W coatings upon annealing at various temperatures was studied by means of XRD analysis [20] and it is here shown in Fig. 1. The evolution of the crystallization of the annealed samples was also studied by SEM imaging of the cross-sections of the samples. Metallographic preparation of the cross-sections was performed after the heat treatment at each investigated temperature. The corresponding images are shown in Fig. 2. The cross-section of the sample with 4 at.% of W reveals the presence of internal cracks. The cracks are probably caused by abundant hydrogen evolution during electrodeposition, which results in an increased internal stress of the coating obtained at room temperature. EDS point analysis revealed that the cracks occur in an O- and W-rich area and the brighter contrast in the surrounding indicates a chemical composition variation which is probably due to W segregation. The EDS results are presented elsewhere [20]. Upon annealing up to 600 °C, oxygen-rich areas grow in extension, and at 800 °C they appear to be replaced by the formation of bright grains. From EDS point analyses, these grains are identified as the FeWO$_4$ phase. The cross-section of the samples with 16 at.% and 24 at.% of W appear to be crack-free.

In both samples, a contrast variation in form of horizontally aligned lines is visible. The contrast can be inferred to small local variations of the chemical composition along the thickness of the samples which is however not revealed by the EDS line scan analyses performed along

both samples. Small composition fluctuations were found in the GD-OES measurements of the as-deposited samples [20]. Such fluctuations would resemble the composition variations aligned horizontally with respect to the substrate observed in the cross-section of the two samples with higher W content. Such composition variation appears more evident for the sample with 16 at.% of W, and it is still present after annealing at 800 °C and when the sample is fully crystalline. After annealing at 800 °C, the crystallization of the sample with 16 at.% of W is clearly visible in Fig. 2. Small bright grains appear distributed throughout the whole sample thickness and they are aligned horizontally with respect to the substrate similarly to the bright lines observed in the cross-sections annealed at lower temperatures. The bright contrast of these grains denotes that these are W-rich phases. Bigger round grains, with a diameter of ~2 μm, are also found and identified with EDS point analysis as FeWO$_4$. In the sample with 16 at.% of W the FeWO$_4$ grains appear to be located mostly in proximity of the surface of the coating. Formation of FeWO$_4$ phase in both the samples with 4 and 16 at.% of W due to eventual oxygen contamination during the annealing can be excluded. The formation of the oxides is thought to be related to the co-deposited oxygen within the coatings. As a matter of fact, the distribution of the oxide phases in the samples with 4 and 16 at.% of W is in well agreement with the co-deposited oxygen distribution, as observed from GD-OES analysis on the as-deposited samples [20]. As shown in Fig. 2, in the sample with 4 at.% W the FeWO$_4$ grains are visible throughout the whole thickness, whereas in the sample with 16 at.% W they are mostly located in proximity of the sample surface. GD-OES results show co-deposited oxygen distributed along the entire film thickness of the sample with 4 at.% W. For the sample with 16 at.% of W the oxygen is mostly co-deposited in the proximity of the surface of the coating.

The partial crystallization of the sample with 24 at.% of W is also clearly visible from the imaging of the cross-section after annealing at 800 °C. Here, islands of grains are present which are distributed mostly along the substrate-coating interface and in proximity of the surface of the coating. The brighter appearance together with EDS point analysis confirmed an enrichment of W within these grains. This finding suggests that these grains are the Fe$_6$W$_6$C carbides as observed by XRD analysis (Fig. 1). As reported in previous studies, the precipitation of carbides upon annealing of electrodeposited Fe-W coatings is caused by co-deposited carbon within the coatings [4,19,20]. The co-deposition of carbon is often related to the use of organic complexing agents and additives in the electrolyte [30]. However, the surface of the substrate might also serve as a source of carbon contamination, as suggested by the carbides formation along the substrate-coating interface.

The sample with 24 at.% of W was kept at 800 °C also for longer times, i.e. 6 and 12 h, in order to drive further its crystallization. However, for the alloy with 24 at.% of W after 12 h at 800 °C the amorphous peak appears unchanged, as can be seen in Fig. 3b. What appears clearly from the XRD spectra acquired after 6 and 12 h at 800 °C is a strong decrease of the presence of the carbide phase Fe$_6$W$_6$C. Already after 6 h heat treatment, most of the XRD peaks of the phase are absent or strongly reduced. On the other hand, an increase of the peaks intensity belonging to the Fe$_2$W phase is observed. The same trend is found for the sample with 16 at.% of W (Fig. 3a). Here the disappearance of the carbides is more gradual. As a matter of fact, after 6 h annealing at 800 °C the Fe$_6$W$_6$C phase is still stable and its peaks are present in the XRD spectra. Only after annealing for 12 h both carbides phases are strongly reduced, while the Fe$_2$W phase becomes more prominent.

The gradual disappearance of the carbides in both samples is also observed by BSE imaging of the surface of the samples after the annealing treatments at 800 °C (Fig. 4a–f). After annealing for 1 h at 800 °C, the carbide formation at the surface of both the samples with 16 at.% and 24 at.% W is evident and can be seen in form of the round clusters in Fig. 4a and d. As revealed by point EDS analysis, the tungsten content reach up to 45 at.% in these clusters, which fits with the W
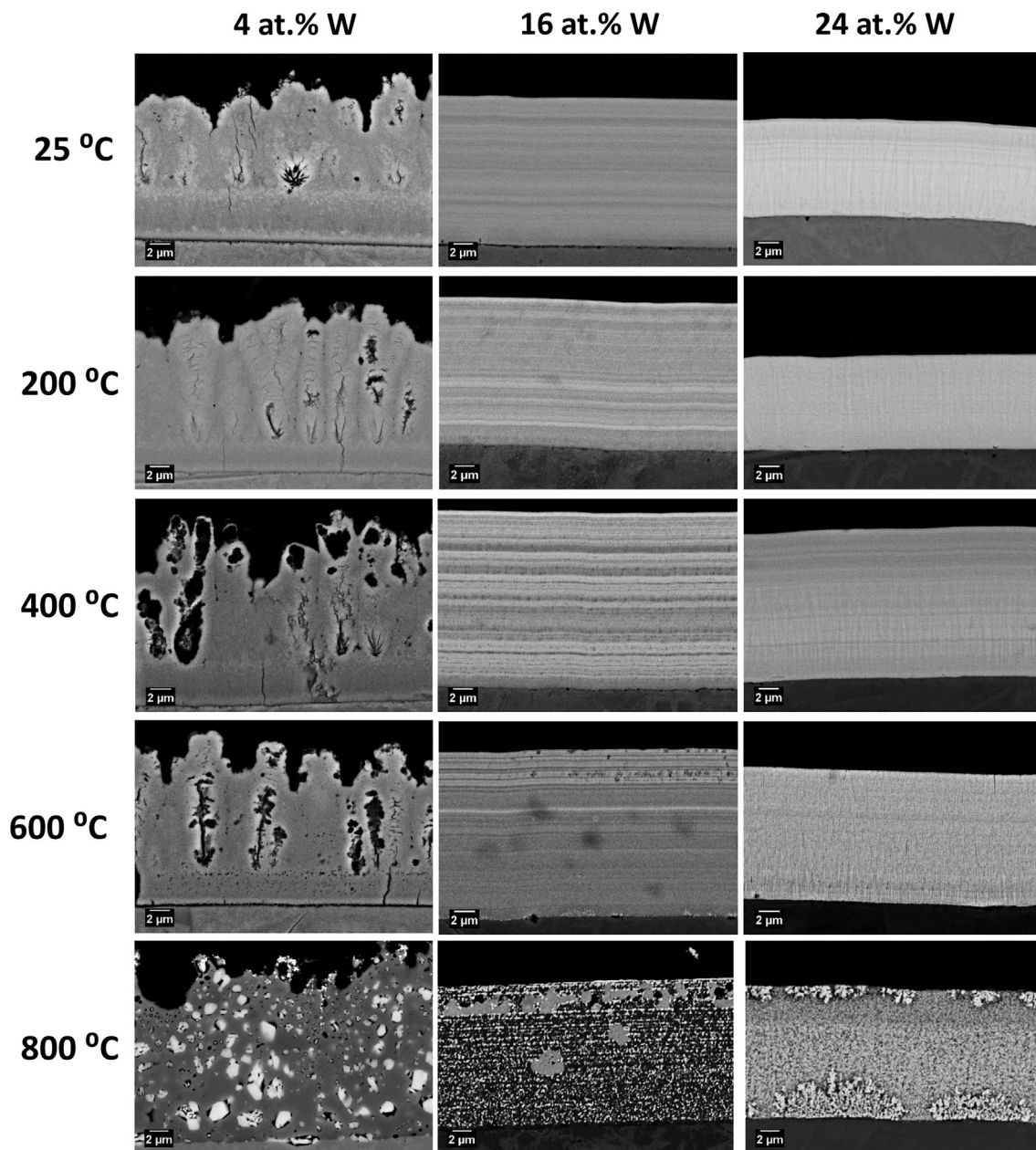
Fig. 2. BSE images of the Fe-W cross-sections with 4, 16 and 24 at.% of W content in the as-deposited state, and after 1 h annealing treatment at 200, 400, 600 and 800 °C, respectively.

concentration present in the carbide phases. These round clusters are still found in the sample with 16 at.% of W after annealing for 6 h (Fig. 4b) and when the Fe_6W_6C phase is still present in the XRD spectra. As anticipated by the XRD results, the carbides are not observed in the case of the sample with 16 at.% W after annealing for 12 h, and in the sample with 24 at.% W after annealing for 6 and 12 h, see Fig. 4c and e–f respectively.

3.2. EBSD analysis of annealed Fe-W coatings

To confirm the XRD findings and to further analyse the distribution of the crystalline phases, EBSD analysis was performed on some selected areas of the cross-sections of the samples annealed at 800 °C. Fig. 5a shows the BSE image of the sample with 4 at.% of W and the red dashed box defines the area where the EBSD phase map and band contrast map were acquired. Both maps are shown next to the BSE image (Fig. 5a). The cross-section image, the phase map and band

contrast map of the samples with 16 at.% and 24 at.% of W are shown in Fig. 5b and c, respectively. A band contrast map is providing information about the quality of the EBSD patterns acquired from the analyzed area. This map shows the material's microstructure in a grey scale image where areas providing poor quality patterns, e.g. grain boundaries, amorphous phase or deformed grains, will be shown as dark, while undeformed, crystalline regions which are easy to identify will appear bright [31]. The generated diffraction patterns are characteristic of the crystal structure of the sample and thus they can be used to discriminate between crystallographically different phases. The phases present in the sample need to be specified as a priori information in order for an EBSD software to index the acquired diffraction patterns [31]. The phases used as reference phase for the EBSD indexing were the phases acquired through XRD analysis: α-Fe, Fe_2W, Fe_3W_3C, Fe_6W_6C, and $FeWO_4$. However, when acquiring the diffraction patterns for the samples with 16 at.% and 24 at.% W, the fraction of indexed Fe_2W and Fe_3W_3C phase was very low, i.e. below 1%. For this reason
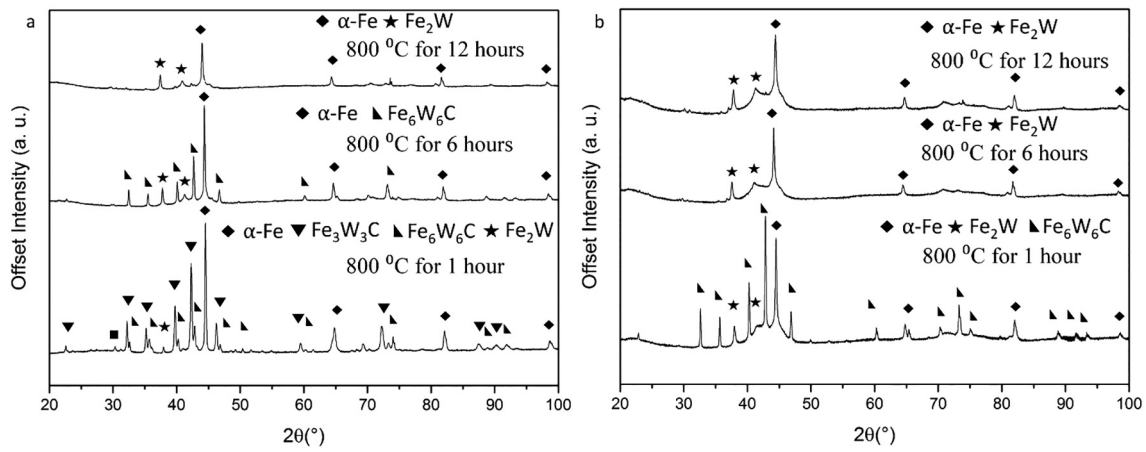
Fig. 3. X-ray diffraction patter evolution with increasing the annealing time (i.e. 1 h, 6 h and 12 h) at 800 °C for the sample with 16 at.% of W (a), and for the sample with 24 at.% of W (b), respectively.
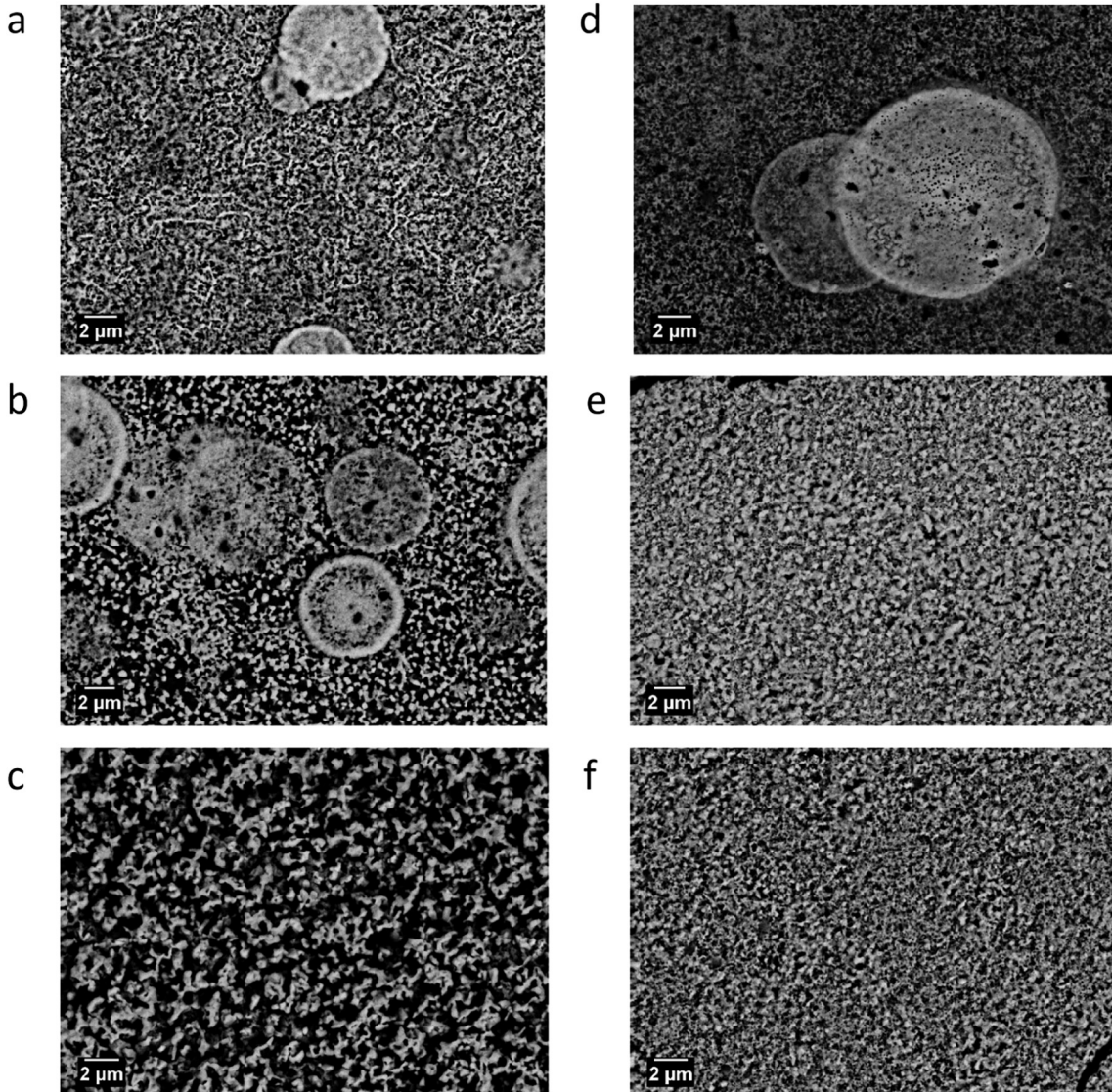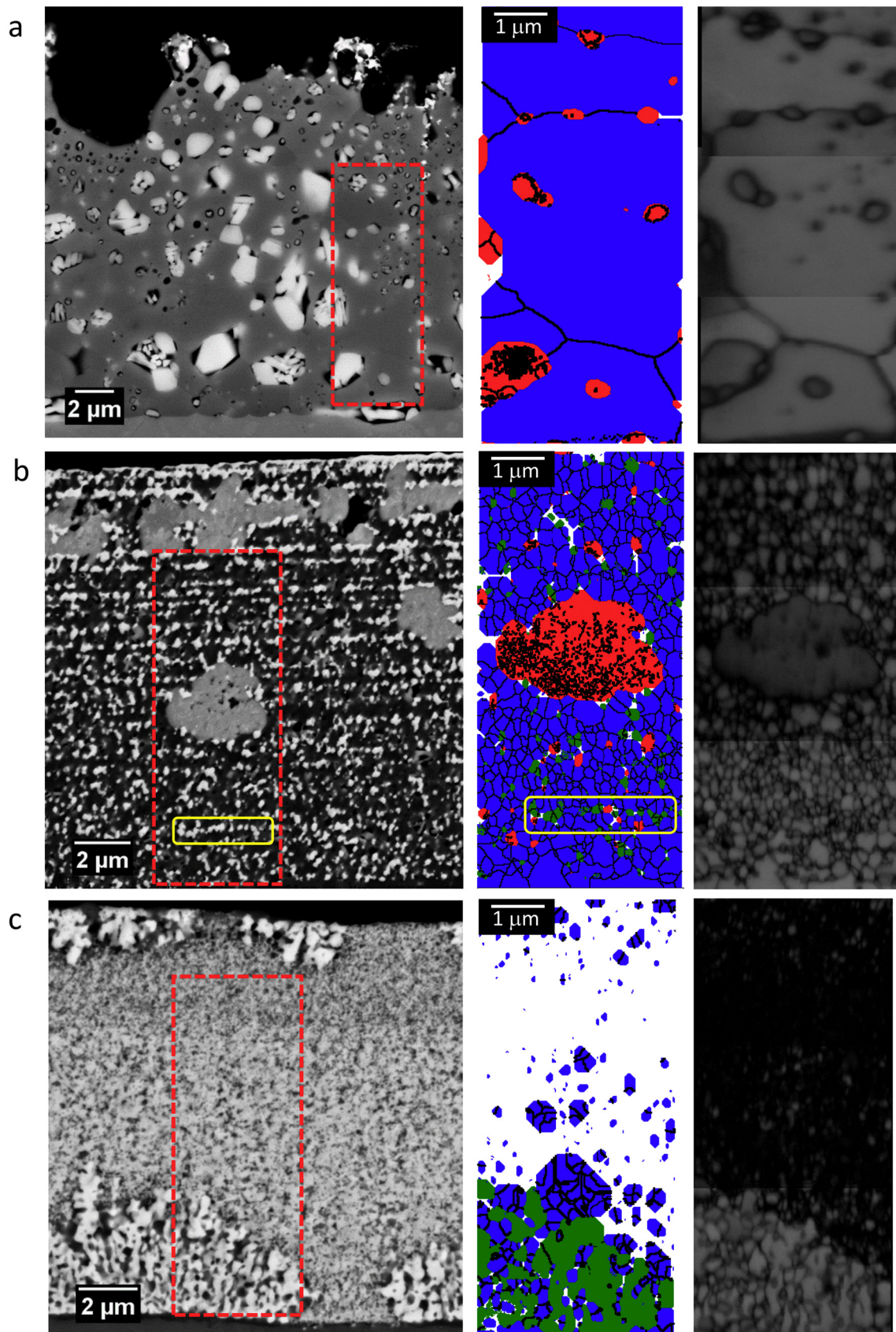

Fig. 4. BSE electron images of the surface morphology of the sample with 16 at.% W after annealing at 800 °C for 1 h (a), 6 h (b), and 12 h (c); BSE images of the surface morphology of the sample with 24 at.% W after annealing at 800 °C for 1 h (d), 6 h (e), and 12 h (f);

Fig. 5. BSE image, phase map and band contrast map of the cross-section of the 4 at.% W sample (a), 16 at.% W sample (b) and 24 at.% sample (c) annealed at 800 °C for 1 h; EBSD phase map and band contrast map are acquired from the red dashed box highlighted in each sample cross-section. The blue grains belong to α-Fe phase, the red grains to the FeWO$_4$ phase, and the green grains to the Fe$_6$W$_6$C phase. (For interpretation of the references to color in this figure legend, the reader is referred to the web version of this article.)
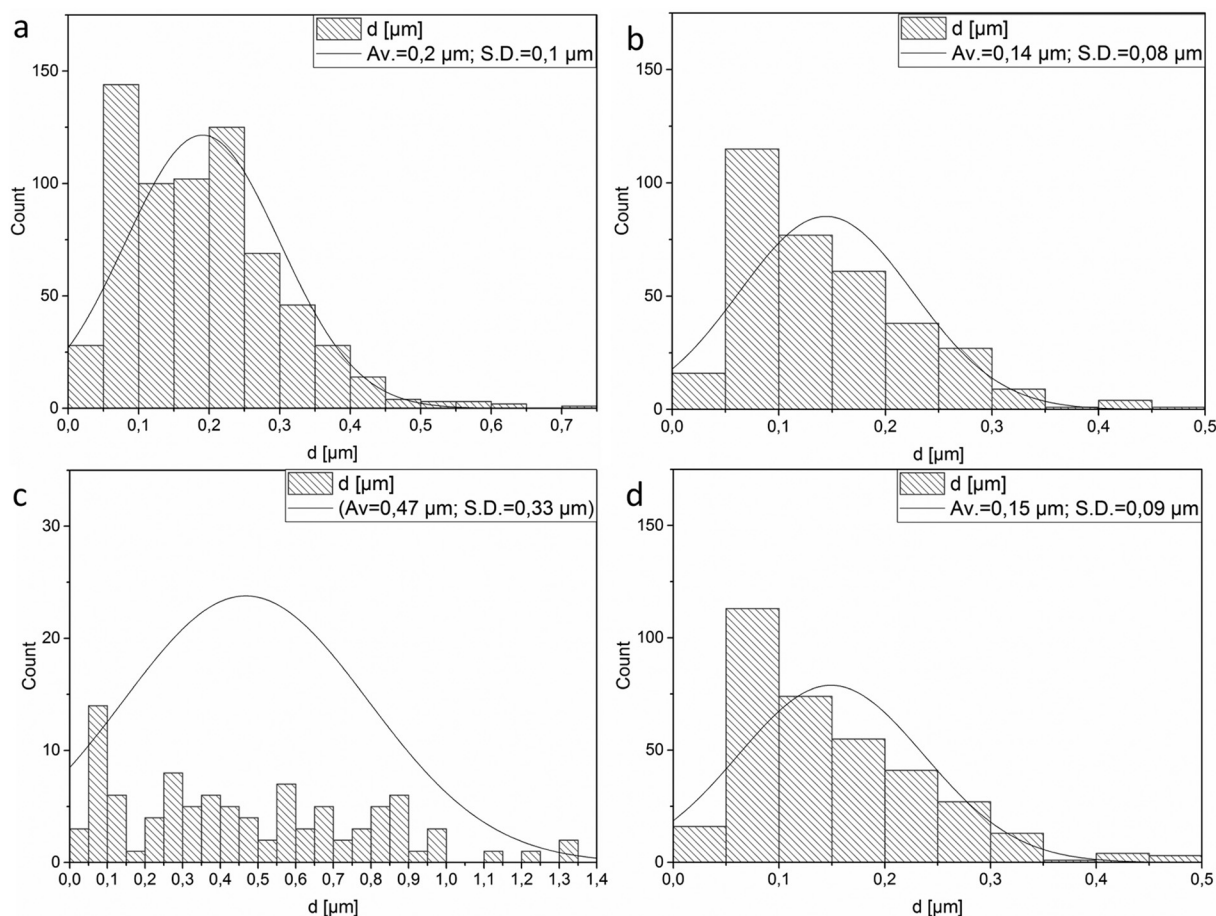
Fig. 6. α-Fe grain size histograms acquired from EBSD analysis of the sample with 16 at.% of W (a) and 24 at.% of W (b) after annealing for 1 h at 800 °C; grain size histogram acquired from EBSD analysis of the sample with 16 at.% of W (c) and 24 at.% of W (d) after annealing for 12 h at 800 °C.

both phases were excluded from the analysis and are not presented in the maps. For the three phase maps shown in Fig. 5 the same color code is used: the blue grains belongs to α-Fe phase, the red grains to the $FeWO_4$ phase, and the green grains to the Fe_6W_6C phase.

In the phase map of Fig. 5a, it is shown that the annealed 4 at.% W sample contains large α-Fe grains of a few micrometres in size and $FeWO_4$ grains which are distributed throughout the sample thickness. The fraction of zero solutions (appearing in the image as white pixels) is low, i.e. 2.2%, and it is due to retained porosity in the sample, concentrated mostly nearby $FeWO_4$ grains. Three phases are present in the phase map acquired from the 16 at.% W sample: α-Fe, Fe_6W_6C and $FeWO_4$. The bright grains horizontally aligned in the cross-section are indexed as the carbide phase Fe_6W_6C. This appears clearly by looking at the line of carbides situated approximately 2 μm from the substrate. This area is highlighted in the BSE image and in the corresponding phase map. Sub-micron oxide $FeWO_4$ grains (~200 nm in size) appear to be present across the entire coating thickness, while a bigger $FeWO_4$ particle (~3 μm) is present in the centre of the coating. Similar oxide grains are also visible in the SEM image in the proximity of the surface of the sample (Fig. 5b) but are not included within the phase map.

Different from the case of the 4 at.% W sample here the α-Fe grains are much smaller, as shown by the grain size histogram in Fig. 6a. Most of the grains are smaller than 250 nm, and the average α-Fe grain is 200 nm in size. The indexed α-Fe grains of the annealed sample with 24 at.% of W are also of submicrometer diameters, Figs. 5c and 6b. Here, the average grain size is 140 nm. The Fe_6W_6C carbide phase present in the vicinity of the substrate is also correctly indexed, see Fig. 5c. What appears clearly also from the maps acquired from the 24 at.% of W is the large fraction, i.e. 61%, of zero solutions (presented

in white in the phase map and in black in the band contrast map). The reason for such high fraction of zero solutions can be inferred to the nanocrystalline/amorphous nature of the sample which is preserved after the heat treatment and thus not possible to be indexed by EBSD technique. The broad amorphous peak still visible in the XRD spectrum acquired after annealing at 800 °C, see in Fig. 1, already indicated the presence of this retained nanocrystalline/amorphous structure in the sample.

EBSD analysis was also conducted for the 16 at.% and 24 at.% of W samples annealed at 800 °C for 12 h. The results are shown in Fig. 7. In the 16 at.% W sample, in Fig. 7a, bright grains are visible and distributed throughout the whole sample thickness. They are larger in size with respect to those observed in the same sample after annealing for 1 h. Furthermore, they are distributed more homogenously within the coating and are not aligned horizontally with respect to the substrate anymore, as in the case of the sample annealed for 1 h. As a matter of fact, the phase map acquired from the selected area shows that these bright grains are not the Fe_6W_6C carbides, as previously observed, but instead Fe_2W grains. $FeWO_4$ grains appear to be still present within the cross-section, also the average size of α-Fe grains has increased with respect of the sample annealed 1 h (Fig. 6c). After 12 h annealing, the α-Fe average grains is 0.5 μm. As revealed by the SEM image in Fig. 7b, the microstructure of the 24 at.% W sample is similar to what was seen after 1 h annealing (Fig. 5c). Also in this case, larger grains are visible at the substrate-coating interface, where the Fe_6W_6C carbides were previously located. However, after 12 h annealing the grains are indexed as Fe_2W, as shown from the phase map. These findings indicate that longer annealing times result in the crystallization of stable phases as expected from the Fe-W binary phase diagram [21,22]. This is observed with the
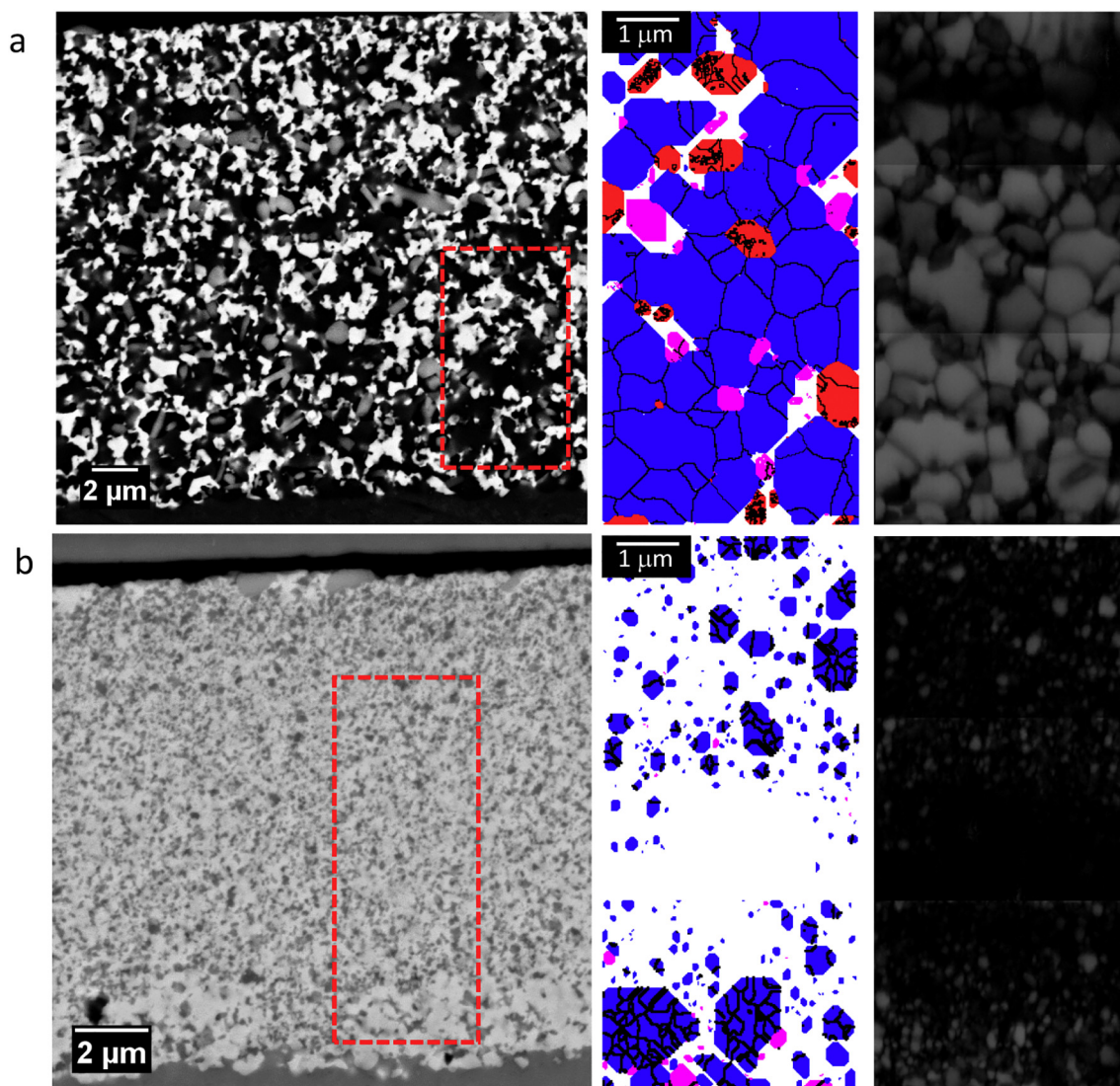
Fig. 7. BSE image, phase map and band contrast map of the cross-section of the 16 at.% W sample (a) and 24 at.% W sample (b) annealed at 800 °C for 12 h; EBSD phase map and band contrast map are acquired from the red dashed box highlighted in each sample cross-section. The blue grains belong to α-Fe phase, the red grains to the FeWO$_4$ phase, and the violet grains to the Fe$_2$W phase. (For interpretation of the references to color in this figure legend, the reader is referred to the web version of this article.)

gradual dissolution of the carbides phases and the crystallization of the Fe$_2$W phase. It is expected that the carbon coming from carbide phase dissolution segregates along the grain boundaries, as suggested by previous studies [32]. It is worth mentioning that according to the Fe-W-C phase diagram, both Fe$_6$W$_6$C and Fe$_3$W$_3$C carbides are expected to be stable at 800 °C [20,26]. The observed dissolution of the carbides is likely caused by the annealing perfomed in vacuum (1×10^{-8} Pa). Annealing treatments performed in other atmospheres (e.g. Ar atmosphere) will be performed to explain the observed mechanism. The average size of α-Fe grains is instead almost unchanged after the 12 h annealing treatment, see Fig. 6d.

3.3. Mechanical characterization of Fe-W coatings: nanoindentation

To study the effect of the thermal treatment on the mechanical properties of the Fe-W coatings, nanoindentation tests were performed on the as-deposited and annealed samples. The obtained values of the hardness and of the reduced elastic modulus (E$_r$), extracted from the load-displacement curves according to the method of Oliver and Pharr [33], are shown in Fig. 8. When working with electrodeposited W alloys with various W contents, an increase in the hardness of the material

with increasing its W content is commonly found in literature [3,12,13]. Different mechanisms play an important role with respect to the observed hardness increase, i.e. grain boundary strengthening, amorphization of the coating induced by W addition, and solid solution strengthening. In electrodeposited W alloys the first two mechanisms are thought to be more influent on determining the hardness increase, while a lower contribution is expected from the solid solution effect [34]. Both mechanisms are strongly correlated with the concentration of W deposited within the coatings. As a matter of fact, the addition of W content in the coatings is often associated with a continuous decrease in the crystallite size. The refinement of the microstructure is followed by an increase of the volume fraction of grain boundaries that are responsible for the hindering of dislocations motion and thus resulting in an higher mechanical strength of the material (Hall-Petch relationship) [14,34]. When reaching a certain co-deposited W content in the alloy, the crystallite size is so small that the long-range order is virtually lost and the material becomes amorphous [35]. Due to the lack of long-range order, conventional deformation mechanisms of crystalline materials (e.g., dislocation motion, creation of vacancies, planar defects like stacking faults, etc.) are not operative in amorphous alloys and, therefore, their hardness is larger.
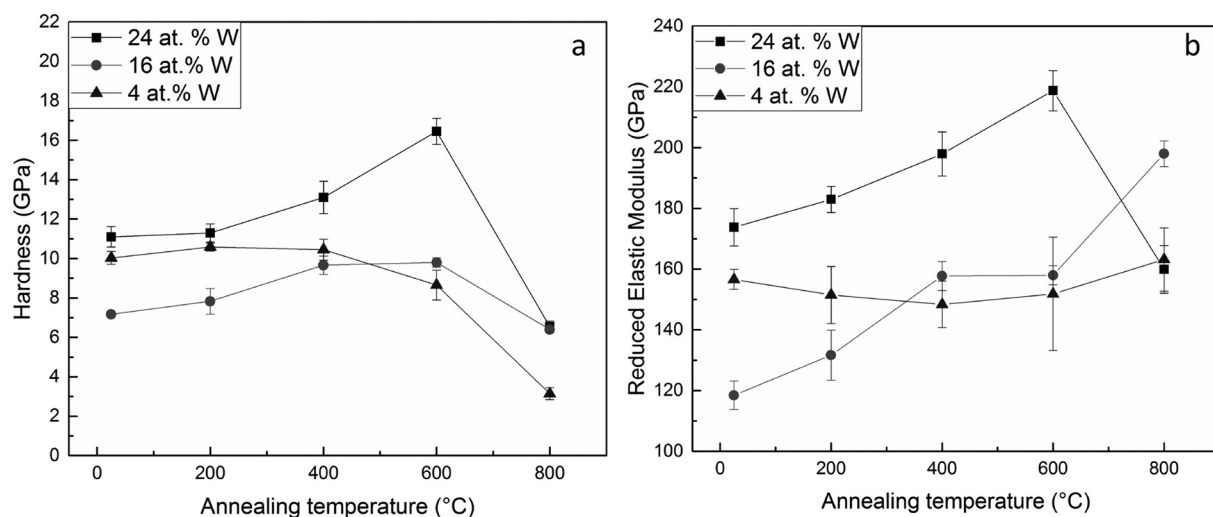
Fig. 8. Hardness and reduced elastic modulus of the Fe-W coatings with 4 at.%, 16 at.% and 24 at.% of W plotted as a function of the annealing temperature for 1 h heat treatment in figure (a) and (b), respectively.

The measured hardness of the as-deposited coatings shows that the sample deposited with 24 at.% of W is characterized with the highest hardness (Fig. 8a), confirming that the W-induced amorphization of the structure leads to a substantial increase of the hardness value. However, the hardness increase is not linear with the increase of the W content of the coatings. As a matter of fact, the sample with 4 at.% of W shows surprisingly high hardness, ~10 GPa. Namely, it is higher than the one measured for the sample with 16 at.% W which is ~7 GPa. The higher hardness value of the sample with 4 at.% of W could be explained by the presence of the oxygen rich areas observed in its cross-section, see Fig. 2, and as measured by GD-OES analysis [20]. The co-deposited oxygen could lead to the formation of nanoscale oxides distributed along the sample grain boundaries which are reported to increase the measured hardness [25]. Also, internal stresses in the coating due to the co-deposited oxygen can result in an increase in hardness. However, the strengthening mechanism caused by the oxide precipitation is thought to be the main factor influencing the increase in hardness [36]. As seen Fig. 8b, the reduced elastic modulus of the as-deposited samples shows a similar trend. The formation of these oxides can explain why the elastic modulus of the sample with 4 at.% W is higher than that with 16 at.% W.

Upon annealing, the samples with 16 and 24 at.% of W show the same hardness trend: an increase of the hardness up to 600 °C, where the maximum value is measured which is 16.5 GPa for 24 at.% W sample, followed by a strong decrease after annealing at 800 °C. The increase of hardness upon annealing can be explained by different mechanisms: grain boundary relaxation for the lower annealing temperatures [37], and the precipitation of fine crystallites [9,13]. For the sample with 16 at.% of W the phases responsible of the precipitation strengthening are both Fe(W) solid solution and FeWO$_4$, and α-Fe for the sample with 24 at.% of W. The hardness drop observed at 800 °C is related to the grain size increase of the mentioned phases, as observed both from the SEM images and EBSD analyses.

Thus, the hardness of the samples with 16 and 24 at.% of W appears to not be influenced by the presence of the hard Fe$_6$W$_6$C phase, whose hardness and the elastic modulus is reported to be ~15,6 GPa [26] and ~327 GPa [28], respectively. For the sample with 24 at.% of W, Fe$_6$W$_6$C phase is not expected to influence the hardness. As a matter of fact, the carbides are located at the substrate-coating interface and at the surface (Figs. 2 and 5c), and thus far from the area where the indents were performed. The SEM images of indent imprints are shown in Fig. 9. In the sample with 16 at.% of W, the Fe$_6$W$_6$C carbides are instead distributed throughout the whole sample thickness. However, as shown in

Fig. 9e and h, the carbides seem to follow the deformation of the softer α-Fe phase without hindering the penetration of the indenter. Hence, at 800 °C the detrimental effect of the α-Fe grain growth is the main factor influencing the hardness of the coatings. The average α-Fe grain size after annealing at 800 °C for 1 h is very similar in both coatings, see Fig. 6a and b, which is reflected in similar hardness values as seen in Fig. 8a.

The effects of the annealing treatments are less pronounced for the sample with 4 at.% of W. Only a slight increase in the hardness is revealed up to 400 °C, which is followed by a constant decrease at 600 °C and 800 °C. The decrease in hardness for the sample with 4 at.% W is due to grain growth that sets in at lower temperatures due the lower thermal stability of this sample.

The variation of the E$_r$ value of the three coatings upon annealing is shown in Fig. 8b. Here, the variation of E$_r$ with temperature differs for each sample. The trends can be related to the microstructural transformations occurring upon annealing of the three samples. For the sample with 4 at.% of W, E$_r$ remains almost constant with increasing temperature. The elastic modulus is an intrinsic property of the material which mainly depends on the bonding energy between the atoms. Hence, the elastic modulus is mostly not depending on grain size since variations typically occur when the grain size approaches the amorphous regime [38]. Upon annealing, the main microstructural change which occurs for the sample with 4 at.% of W is the grain growth of the as-deposited nanocrystalline Fe(W) solid solution, therefore E$_r$ remains almost constant with increasing temperature. The slight decrease in E$_r$ observed between 200 °C and 400 °C might be ascribed to the growth of internal cracks that occur before the crystallization of the FeWO$_4$, see Fig. 2. For the samples with 16 and 24 at.% of W, E$_r$ increases up to 600 °C. Here, the increase of E$_r$ is related to the structural relaxation and the density increase of the material, observed when annealing amorphous alloys [39,40]. Above 600 °C, the different crystalline phases found within the cross-section of the samples lead to the observed different trends for E$_r$. In particular, the precipitation of a secondary phase, i.e. F$_6$W$_6$C, contributed to the increase in the E$_r$ observed for the sample with 16 at.% of W. A precipitation strengthening effect on the elastic modulus of electrodeposited coatings was also observed on annealed NiW coatings [17]. In the sample with 16 at.% of W, the F$_6$W$_6$C phase is distributed throughout the whole sample thickness (see Figs. 5b and 9h). Hence, the stiff bonds of the F$_6$W$_6$C phase (caused by its high elastic modulus of ~327 GPa [28]) contribute to the measured E$_r$ and lead to the sharp increase of E$_r$ observed in Fig. 8b. For the sample with 24 at.% of W, the carbide phase is located at the substrate-
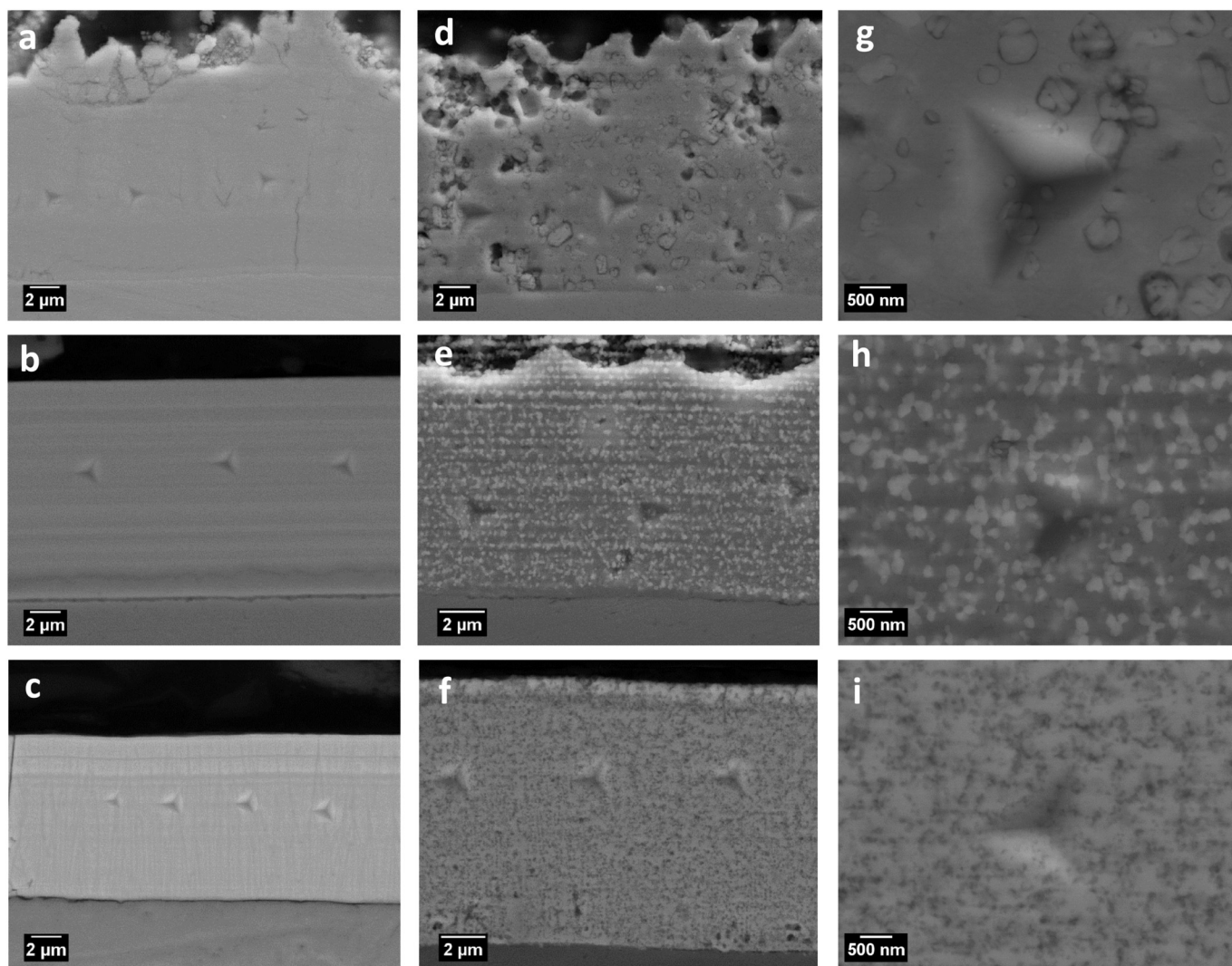
Fig. 9. SEM images of the indentation imprints on the cross-section of the Fe-W coating with 4 at.% (a–c), 16 at.% (b–f) and 24 at.% of W (g–i) in the as-deposited state (a–c) and after annealing for 1 h at 800 °C (d–f), respectively; the intends from (d–f) are also shown at higher magnification (g–i).

coating interface and in proximity of the surface of the coatings, thus it is not expected in the indent imprint (see Figs. 5b and 9i). Hence, the E_r value at 800 °C is related to the presence of the α-Fe crystalline phase. This is the same phase as found in the sample with 4 at.% of W annealed at 800 °C. Therefore, the measured E_r decreases (Fig. 8b) and approaches the value measured for the sample with 4 at.% of W.

The results here presented show that the microstructure of the Fe-W coatings influenced their mechanical properties both in the as-deposited condition and after heat treatments. In the as-deposited condition, the W-induced amorphization was found to be the main strengthening mechanism. The amorphous structure of the sample with 24 at.% of W substantially increased the hardness of the coating. Upon annealing, the observed increase in hardness is related to grain boundary relaxation and precipitation strengthening mechanism. In particular, the precipitation of α-Fe at 600 °C for the sample with 24 at.% of W leads to the maximum hardness value, i.e. 16.5 GPa. The precipitation of Fe_6W_6C phase contributed to a sharp increase in the E_r of the sample with 16 at.% of W after annealing at 800 °C. Finally, the grain growth mechanism of the α-Fe phase had detrimental effects on the hardness of the studied coatings.

4. Summary and conclusions

The influence of heat treatment on the microstructure and

mechanical properties of electrodeposited Fe-W alloys at various W contents has been studied. The structural changes occurring upon annealing have been observed through XRD and EBSD analysis. Nanohardness measurements on the cross-section of the Fe-W coatings have been performed to estimate the effect of annealing on the mechanical properties of the material. Based on the results presented in this study the following conclusions can be drawn:

- The crystallization of sub-micron/nano sized $FeWO_4$ phase occurs along the entire coating thickness upon annealing above 600 °C for the samples with 4 at.% and 16 at.% of W, respectively.
- Longer vacuum annealing treatments of 6 and 12 h of the samples with 16 and 24 at.% of W led to the formation of stable phases as expected from the Fe-W binary phase diagram. This occurs through gradual dissolution of the carbide phases and the crystallization of the Fe_2W phase.
- The results from EBSD and XRD analyses on the sample with 24 at.% of W highlight the outstanding thermal stability of that material. As a matter of fact, A partial broad amorphous shoulder is still observed in the XRD diffractogram acquired after the 6 and 12 h annealing, and the α-Fe average grain size also remained unchanged at both conditions. Furthermore, EBSD phase maps acquired from the sample with 16 at.% and 24 at.% of W after annealing for 12 h at 800 °C confirm the XRD findings regarding the process of a gradual

dissolution of the carbides phases followed by Fe$_2$W crystallization. In fact, Fe$_2$W grains are found in the areas where the Fe$_6$W$_6$C were located after 1 h annealing at 800 °C.

- The annealing treatments enable to improve considerably the hardness of the as-deposited Fe-W samples. A maximum hardness of 16.5 GPa was measured for the sample with 24 at.% of W after annealing for 1 h at 600 °C and was related to the precipitation of fine α-Fe crystallites. Upon annealing at 800 °C, the hardness decreased for all the samples due to grain growth.

- The hardness of the coatings appears to not be influenced by the presence of carbide phase. In fact, the α-Fe grain growth is the main factor influencing the hardness of the Fe-W coatings. However, the influence of the Fe$_6$W$_6$C phase is observed in the reduced elastic modulus of the sample with 16 at.% of W, i.e. at 800 °C the Fe$_6$W$_6$C phase formation leads to a sharp increase of the measured E$_r$.

Acknowledgements

References

[1] M.X. Donten, H. Cesiulis, Z. Stojek, Electrodeposition and properties of Ni-W, Fe-W and Fe-Ni-W amorphous alloys. A comparative study, Electrochim. Acta 45 (2000) 3389–3396, http://dx.doi.org/10.1016/S0013-4686(00)00437-0.

[2] A. Chianpairot, G. Lothongkum, C.A. Schuh, Y. Boonyongmaneerat, Corrosion of nanocrystalline Ni-W alloys in alkaline and acidic 3.5 wt.% NaCl solutions, Corros. Sci. 53 (2011) 1066–1071, http://dx.doi.org/10.1016/j.corsci.2010.12.001.

[3] A. Nicolenco, N. Tsyntsaru, J. Fornell, E. Pellicer, J. Reklaitis, D. Baltrunas, H. Cesiulis, J. Sort, Mapping of magnetic and mechanical properties of Fe-W alloys electrodeposited from Fe(III)-based glycolate-citrate bath, Mater. Des. 139 (2018) 429–438, http://dx.doi.org/10.1016/j.matdes.2017.11.011.

[4] S. Wang, C. Zeng, Y. Ling, J. Wang, G. Xu, Phase transformations and electrochemical characterizations of electrodeposited amorphous Fe–W coatings, Surf. Coat. Technol. 286 (2016) 36–41, http://dx.doi.org/10.1016/j.surfcoat.2015.12.011.

[5] N. Tsyntsaru, J. Bobanova, X. Ye, H. Cesiulis, A. Dikusar, I. Prosycevas, J.P. Celis, Iron-tungsten alloys electrodeposited under direct current from citrate-ammonia plating baths, Surf. Coat. Technol. 203 (2009) 3136–3141, http://dx.doi.org/10.1016/j.surfcoat.2009.03.041.

[6] U. Klement, E. Pellicer, J. Sort, Mid-term meeting of SELECTA: a European Training Network on smart electrodeposited alloys for environmentally sustainable applications, Trans. IMF. 95 (2017) 124–125, http://dx.doi.org/10.1080/00202967.2017.1299307.

[7] P. de Lima-Neto, G.P. da Silva, A.N. Correia, A comparative study of the physicochemical and electrochemical properties of Cr and Ni-W-P amorphous electrocoatings, Electrochim. Acta 51 (2006) 4928–4933, http://dx.doi.org/10.1016/j.electacta.2006.01.036.

[8] N. Imaz, J.A. Díez, E. Pellicer, J. Sort, H. Grande, E. Garcia-Lecina, Thermal treatment effect on the mechanical, tribological and corrosion properties of Ni–W alloy obtained by direct and pulse plating electrodeposition, Int. J. Surf. Eng. Coat. 2967 (2017), http://dx.doi.org/10.1080/00202967.2017.1260885.

[9] S.-J. Mun, M. Kim, T.-H. Yim, J.-H. Lee, T. Kang, Mechanical and structural characteristics of electrodeposited Ni–Fe–W alloy after heat-treatment, J. Electrochem. Soc. 157 (2010) D177–D180, http://dx.doi.org/10.1149/1.3292282.

[10] N. Tsyntsaru, A. Dikusar, H. Cesiulis, J.P. Celis, Z. Bobanova, S. Sidel'Nikova, S. Belevskii, Y. Yapontseva, O. Bersirova, V. Kublanovskii, Tribological and corrosive characteristics of electrochemical coatings based on cobalt and iron superalloys, Powder Metall. Met. Ceram. 48 (2009) 419–428, http://dx.doi.org/10.1007/s11106-009-9150-7.

[11] A. Nicolenco, N. Tsyntsaru, H. Cesiulis, Fe (III)-based ammonia-free bath from electrodeposition of Fe-W alloys, J. Electrochem. Soc. 164 (9) (2017) D590–D596, http://dx.doi.org/10.1149/2.1001709jes (D1).

[12] F. He, J. Yang, T. Lei, C. Gu, Structure and properties of electrodeposited Fe-Ni-W alloys with different levels of tungsten content: a comparative study, Appl. Surf. Sci. 253 (2007) 7591–7598, http://dx.doi.org/10.1016/j.apsusc.2007.03.068.

[13] K. Hou, Y. Chang, S. Chang, C. Chang, The heat treatment effect on the structure and mechanical properties of electrodeposited nano grain size Ni – W alloy coatings, Thin Solid Films 518 (2010) 7535–7540, http://dx.doi.org/10.1016/j.tsf.2010.05.041.

[14] N. Sunwang, P. Wangyao, Y. Boonyongmaneerat, The effects of heat treatments on

[15] S. Hayata, S. Oue, H. Nakano, T. Takahash, Effect of annealing on the structure and hardness of electrodeposited Ni-W alloys, ISIJ Int. (5) (2015) 1083–1090, http://dx.doi.org/10.2355/isijinternational.55.1083.

[16] C. Borgia, T. Scharowsky, A. Furrer, C. Solenthaler, R. Spolenak, A combinatorial study on the influence of elemental composition and heat treatment on the phase composition, microstructure and mechanical properties of Ni–W alloy thin films, Acta Mater. 59 (2011) 386–399, http://dx.doi.org/10.1016/J.ACTAMAT.2010.09.045.

[17] M.V.N. Vamsi, N.P. Wasekar, G. Sundararajan, Influence of heat treatment on microstructure and mechanical properties of pulse electrodeposited Ni-W alloy coatings, Surf. Coat. Technol. 319 (2017) 403–414, http://dx.doi.org/10.1016/j.surfcoat.2017.03.074.

[18] L. Jinlong, W. Zhuqing, L. Tongxiang, K. Suzuki, M. Hideo, Effect of tungsten on microstructures of annealed electrodeposited Ni-W alloy and its corrosion resistance, Surf. Coat. Technol. 337 (2018) 516–524, http://dx.doi.org/10.1016/j.surfcoat.2018.01.070.

[19] M.C. Chou, C.F. Chu, S.T. Wu, Phase transformations of electroplated amorphous iron-tungsten-carbon film, Mater. Chem. Phys. 78 (2003) 59–66, http://dx.doi.org/10.1016/S0254-0584(02)00217-1.

[20] A. Mulone, A. Nicolenco, V. Hoffmann, U. Klement, N. Tsyntsaru, H. Cesiulis, In-depth characterization of as-deposited and annealed Fe-W coatings electrodeposited from glycolate-citrate plating bath, Electrochim. Acta 261 (2018) 167–177, http://dx.doi.org/10.1016/j.electacta.2017.12.051.

[21] A. Jacob, C. Schmetterer, L. Singheiser, A. Gray-Weale, B. Hallstedt, A. Watson, Modeling of Fe-W phase diagram using first principles and phonons calculations, Calphad 50 (2015) 92–104, http://dx.doi.org/10.1016/j.calphad.2015.04.010.

[22] A. Antoni-Zdziobek, T. Commeau, J.M. Joubert, Partial redetermination of the Fe-W phase diagram, Metall. Mater. Trans. A Phys. Metall. Mater. Sci. 44 (2013) 2996–3003, http://dx.doi.org/10.1007/s11661-013-1658-2.

[23] N. Tsyntsaru, H. Cesiulis, A. Budreika, X. Ye, R. Juskenas, J.P. Celis, The effect of electrodeposition conditions and post-annealing on nanostructure of Co-W coatings, Surf. Coat. Technol. 206 (2012) 4262–4269, http://dx.doi.org/10.1016/j.surfcoat.2012.04.036.

[24] C.J. Marvel, P.R. Cantwell, M.P. Harmer, The critical influence of carbon on the thermal stability of nanocrystalline Ni-W alloys, Scr. Mater. 96 (2015) 45–48, http://dx.doi.org/10.1016/j.scriptamat.2014.10.022.

[25] C.J. Marvel, D. Yin, P.R. Cantwell, M.P. Harmer, The influence of oxygen contamination on the thermal stability and hardness of nanocrystalline Ni-W alloys, Mater. Sci. Eng. A 664 (2016) 49–57, http://dx.doi.org/10.1016/j.msea.2016.03.129.

[26] W. Barona Mercado, J. Cuevas, I.Y. Castro, M. Fajardo, G.A. Pérez Alcázar, H. Sánchez Sthepa, Synthesis and characterization of Fe6W6C by mechanical alloying, Hyperfine Interact. 175 (2007) 49–54, http://dx.doi.org/10.1007/s10751-008-9587-y.

[27] D.V. Suetin, I.R. Shein, A.L.Ã. Ivanovskii, Structural, electronic and magnetic properties of η carbides (Fe3W3C, Fe6W6C, Co3W3 C and Co6W6C) from first principles calculations, Phys. B Phys. Condens. Matter. 404 (2009) 3544–3549, http://dx.doi.org/10.1016/j.physb.2009.05.051.

[28] X.Y. Chong, Y.H. Jiang, R. Zhou, H. Zhu, J. Feng, Electronic structure, anisotropic elastic and thermal properties of the η phase F6W6C, Comput. Mater. Sci. 108 (2015) 205–211, http://dx.doi.org/10.1016/j.commatsci.2015.06.037.

[29] E. Lassner, W.-D. Schubert, Tungsten: Properties, Chemistry, Technology of the Element, Alloys and Chemical Compounds, Kluwer Academic/Plenum, New York, 1999.

[30] Y.D. Gamburg, G. Zangari, Theory and Practice of Metal Electrodeposition, (2011), http://dx.doi.org/10.1017/CBO9781107415324.004.

[31] T. Maitland, S. Sitzman, Electron backscatter diffraction (EBSD) technique and materials characterization examples, Scanning Microsc. Nanotechnol. Tech. Appl. (2007) 41–76 (doi:0387396209).

[32] P. Choi, T. Al-Kassab, F. Gärtner, H. Kreye, R. Kirchheim, Thermal stability of nanocrystalline nickel–18 at.% tungsten alloy investigated with the tomographic atom probe, Mater. Sci. Eng. A 353 (2003) 74–79, http://dx.doi.org/10.1016/S0921-5093(02)00670-6.

[33] W.C. Oliver, G.M. Pharr, Measurement of hardness and elastic modulus by instrumented indentation: advances in understanding and refinements to methodology, J. Mater. Res. 19 (2004) 3–20, http://dx.doi.org/10.1557/jmr.2004.19.1.3.

[34] C.A. Schuh, T.G. Nieh, H. Iwasaki, The effect of solid solution W additions on the mechanical properties of nanocrystalline Ni, Acta Mater. 51 (2003) 431–443, http://dx.doi.org/10.1016/S1359-6454(02)00427-5.

[35] Y. Nishi, Y. Mogi, K. Oguri, T. Watanabe, Preparation of F e-W amorphous films by an electroplating method, J. Mater. Sci. Lett. 20 (1995) 1–3.

[36] A. Brenner, P. Burkhead, C. Jennings, Physical properties of electrodeposited chromium, J. Res. Natl. Bur. Stand. 40 (1948) 1–11 http://technic.com/apac/sites/default/files/assets/pdfs/literature/PhysicalProperties of Electrodeposited Nickel.pdf.

[37] T.J. Rupert, J.R. Trelewicz, C.A. Schuh, Grain boundary relaxation strengthening of nanocrystalline Ni–W alloys, J. Mater. Res. 27 (2012) 1285–1294, http://dx.doi.org/10.1557/jmr.2012.55.

[38] U. Erb, K.T. Aust, G. Palumbo, Electrodeposited nanocrystalline metals, alloys, and composites, Nanostruct. Mater. (2007) 235–292, http://dx.doi.org/10.1016/B978-081551534-0.50008-7 (Second Ed.).

[39] H.S. Arora, A.V. Aditya, S. Mukherjee, Structural relaxation driven increase in elastic modulus for a bulk metallic glass, J. Appl. Phys. 117 (2015), http://dx.doi.org/10.1063/1.4905145.

[40] C.A. Schuh, T.C. Hufnagel, U. Ramamurty, Mechanical behavior of amorphous alloys, Acta Mater. 55 (2007) 4067–4109, http://dx.doi.org/10.1016/j.actamat.2007.01.052.

Paper 5

Wear resistance of electrodeposited Fe-W alloy coatings under dry conditions and in the presence of rapeseed oil

A. Nicolenco, N. Tsyntsaru, T. Matijošius, S. Asadauskas,

H. Cesiulis

Green Tribology 1 (2018) 17-23

Reprinted with permission from *Green Tribology*

WEAR RESISTANCE OF ELECTRODEPOSITED Fe-W ALLOY COATINGS UNDER DRY CONDITIONS AND IN THE PRESENCE OF RAPESEED OIL

A. Nicolenco*, N. Tsyntsaru*,**[1], T. Matijošius***, S. Asadauskas***, H. Cesiulis**[1]
* Physical Chemistry Department, Vilnius University, Vilnius, Lithuania
**Institute of Applied Physics of ASM, Chisinau, Moldova
***Institute of Chemistry, Center for Physical Sciences and Technology, Vilnius, Lithuania
* Corresponding authors

Abstract: Amorphous Fe-W alloys with 25 at.% of W were electrodeposited under direct and pulse modes from glycolate-citrate bath with and without addition of polyethylene glycol. The tribological behavior of the coatings was studied at 1, 2 and 5 N loads under dry friction and in the presence of rapeseed oil films of 0.2-5.0 μm thickness. The tribological behavior of obtained coatings at dry friction reveals their severe tribo-oxidation resulting in a high wear depth and coefficient of friction. Observed groove like surface with well-adhered particles inside the wear track point out on abrasive-adhesive wear mechanism of Fe-W alloys. In the presence of rapeseed oil films the wear mechanism changes, and values of coefficient of friction decrease up to 10 times compared to dry friction conditions. The optimum thickness of rapeseed oil film was 1 μm. This film has the satisfactory adhesion and uniform distribution on the surface, and could withstand up to 2 000 cycles.

Keywords: iron alloys, tungsten alloys, tribooxidation, abrasive wear, rapeseed oil

1. INTRODUCTION

Recently, electrodeposited tungsten alloys with iron group metals (Fe, Co, Ni) become the subject of extensive studies due to their attractive properties: high hardness [1], corrosion and wear resistance [2, 3]; thermal stability [4]; catalytic activity for hydrogen evolution reaction [5], methanol oxidation [6] and reduction of NO_x [7]. This makes these alloys appealing alternative materials for different industrial branches, including the fabrication of protective coatings for Cr replacement, barrier layers for Cu- and Sn-containing interconnects [8] and different microelectromechanical systems (MEMS) [9]. In addition, recent works show that the magnetic properties of these alloys can be tuned by fine control of the deposition parameters. Thus, indicating that owing a certain combination of the properties, these alloys could be potential candidates for the biomedicine application [10]. Furthermore, the usage of Ni for devices that might be in contact with human skin was currently restricted (European Union directive EN 1811), since it was recognized to be highly allergenic. Also, in 2007 the Cobalt REACH Consortium Ltd. was created with the purpose of preparing the registration dossiers for cobalt and cobalt compounds which may cause long lasting harmful effects on humans. Taken this into account, electrodeposition of Fe-based coatings is of great interest for "green" manufacturing of advanced materials for targeted applications.

Fe-W is more eco-friendly material and it has higher hardness and thermal stability than Co- and Ni-based alloys. Thus, the hardness of electrodeposited Fe-W coatings can reach up to ~13 GPa (at low loads) which is comparable to that of electrodeposited chromium [3, 10]. Usually, Fe-W alloys with higher W content (up to 30 at.%) have better mechanical properties due to grain boundary strengthening, solid solution strengthening and nanostructurization processes. Thus, increasing the percentage of W in alloys leads to the significant grain size refinement and hence the structure transforms form nanocrystalline to amorphous. Remarkable, the electrodeposited Fe–W alloys containing high amount of tungsten retain their structure even after annealing up to 800 °C [4].

Many researchers report over the years the importance of high hardness for the good wear resistance and show the strong linear relationships between these two properties for different polycrystalline materials like Ni-W [11], Ni-Fe-W [11], Ni-P [12] and other [13]. However, this is not always the rule.

---

[1] Author for contacts: N. Tsyntsaru, H. Cesiulis.
E–mail: tintaru@phys.asm.md, henrikas.cesiulis@chf.vu.lt.

The hardness is an intrinsic parameter, i.e. it depends on the composition and structure of the material only, while the wear resistance is an extrinsic property and depends on the certain tribo-system used. Therefore, for the alloys which undergo abrasive wear the resistance remains relatively unaffected with increasing the hardness and, in some cases, even decreased. For instance, the wear resistance of hard electrodeposited Fe-W alloys at dry friction is rather low, due to severe oxidation of the coating during fretting (tribooxidation) [1]. Formed oxides act as the third body, thus leading to the increase of coefficient of friction (COF) and larger wear volume, as compared to Co-W alloys evaluated at similar conditions.

Furthermore, it was shown that lubricants can reduce the oxygen penetration into the sliding pairs, thus lowering the tribooxidation and improving the tribological performance of the coating (N. I. Tsyntsaru et al., 2010). Different types of liquid lubricants were investigated, e.g. vegetable oils, mineral oils, ionic liquids, etc. As the metallic surfaces generally are hydrophilic, it is of particular importance to ensure the ability of the lubricant to penetrate into the area of the wear and remain there. The use of sugar films as a solid lubricant for the Co-W alloy was discussed in [15]. As a different approach, the co-deposition of solid lubricants (like graphene, WS_2, MoS_2) into the metallic matrix was also reported [16]. In this case, the second phase soft particles can reduce the asperity contact between the coating and the counter body, therefore reduce the wear. However, the electrodeposition conditions should be optimized carefully in order to achieve uniform particles distribution, low porosity and appropriate microstructure of the coating.

In this work, the rapeseed oil was used as a lubricant, as it is known to be potential candidate to replace some of mineral oils. The investigation of the lubricating properties of the rapeseed oil is recently actively studied due to its inherent biodegradability, non-toxicity (as compared to motor oils) and good lubricity of metallic surfaces [17]. It also has some advantages in terms of sustainability. Among all other oil plants, the rapeseed gives more oil per unit of land area compared to other oil sources, such as soybeans and canola. Across the Europe, in Germany, France and Poland around 15 millions of tons of rapeseed are grown every year mostly for the production of biodiesel and cooking oils (according to Food and Agriculture Organization (FAO)).

For this study, the Fe-W alloys have been electrodeposited from the recently developed [10, 18] glycolate-citrate bath based on Fe(III)-salt. The bath is considered as environmentally-friendly one, while Fe-W deposits are considered as green and sustainable materials. This study aimed to investigate the tribological behavior of obtained coatings under dry and lubricating conditions keeping the main concepts of green tribology.

2. MATERIALS AND METHODS

Fe-W samples having 25 at.% of W were electrodeposited onto Si wafer with sputtered Cu conductive layer from glycolate-citrate electrolytes of the following composition: 1 M glycolic acid, 0.3 M citric acid, 0.1 M $Fe_2(SO_4)_3$ and 0.3 M Na_2WO_4 (bath 1), and with addition to the bath 1 of 0.25 g polyethylene glycol (PEG) (bath 2). Fe-W alloys were electrodeposited under direct current (DC) and pulse current (PC) modes and the coating thickness was cca 10 μm. The corresponding baths and deposition conditions are given in Table 1.

In the case of pulse current, the average current density was calculated from:

$$i_{avg} = \frac{i_p d.c.}{100\%} \qquad (1)$$

$$d.c. = \frac{\tau_{pulse}}{\tau_{pulse} + \tau_{pause}} 100\% \qquad (2)$$

where i_p is the pulse current density, *d.c.* is the duty cycle, t_{pulse} and t_{pause} is the duration of pulse and pause periods, respectively.

Table 1. Electrodeposition conditions for Fe-W alloys.

| Sample	Bath	pH	T°C	$-i_{avg}$, mA/cm^2	d.c., %	t_{pulse}, s	t_{pause}, s
1_DC	1				100	-	-
2_PEG	2	6.5	65	15	100	-	-
3_PC	1				95.2	1	0.05

For the investigation of tribological behavior of Fe-W electrodeposited coatings the pin-on-disc Tribometer (Anton Paar TriTec SA, Switzerland) was employed by using a ball-on-flat configuration. The corundum ball of 6 mm diameter was the counter-body that oscillated against rigidly fixed coated samples for 2 000 cycles at 2 Hz frequency of reciprocating motion, resulting in a track length of 1 mm and the total distance of 2 mm for one reciprocal friction cycle. All the tests were performed in ambient air at 23±2 °C and 48 % relative humidity. After the sliding tests, the samples were cleaned in acetone and ethanol in order to remove debris before measuring the wear track profiles. Scanning electron microscope (SEM) imaging was performed using Hitachi TM3000 instrument and elemental analysis of the wear tracks was determined with the energy dispersive X-ray spectroscopy (EDS) analysis tool attached to the SEM.

Rapeseed oil was used as a lubricant, and films of fixed thickness (0.2, 0.5, 1.0, 2.0 and 5.0 μm) were applied on Fe-W coatings before tribological tests. In order to obtain the oil film of particular thickness, the corresponding amount (10÷250 μL/cm^2) of oil stock solution (100 μL oil in 50 mL of diethyl ether) was applied on electrodeposited samples and kept until full evaporation of ether.

3. RESULTS AND DISCUSSIONS

All investigated Fe-W coatings were electrodeposited under conditions elaborated earlier (Nicolenco et al., 2018) in order to assure 25 at.% of W in deposits; this tungsten content leads to amorphous structure and high hardness revealed for these alloys. The typical SEM images of the Fe-W surface are shown in Fig. 1. The surfaces are free of cracks and smooth. It was expected that the addition of PEG to the plating bath should assists hydrogen release from the surface, thus lowering the imbedded stress into electrodeposited coatings. Indeed, as it is seen from Fig. 1b, the surface of the alloy deposited from the bath containing PEG appears with some small globules, which probably indicates the different nucleation and growth of the coating. Also, it was expected, that deposition under PC mode should result in essential improvement of tribological behavior of tungsten alloys due to the microstructural changes, as it was shown for Co-W alloys [19]. However, in the case of Fe-W alloys deposition, the corrosion processes occur during the pause, thus resulting in a higher oxidation and porosity of Fe-W coating (Fig. 1 c). Nevertheless, three Fe-W coatings are bright and mirror-like in appearance, and the average roughness of the coatings is less than 100 nm (Fig. 2).
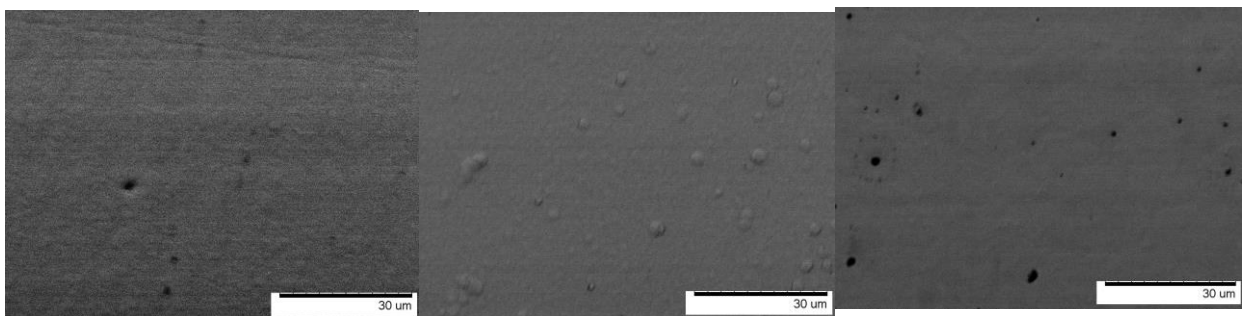

Figure 1. SEM images of Fe–W alloys deposited under conditions stated in Table 1: 1_DC (a); 2_PEG (b) and 3_PC (c).
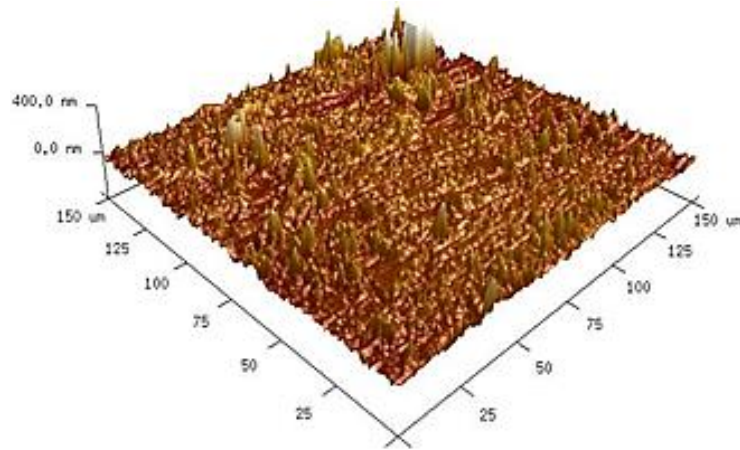
Figure 2. Typical AFM image of Fe–W alloy, sample 1_DC.

The evaluation of tribological behavior of Fe-W coatings deposited at different conditions was carried out under dry friction conditions applying 1, 2 and 5 N normal loads. As it can be seen from the Fig. 3, the COF increases sharply at the first 50–100 cycles, then reaches the maximum and remains constant. Furthermore, the maximum of the COF decreases with an increase in applied load (Fig. 3). The COF reaches the similar values between 0.8 and 1.2 after run-in period for all of three investigated coatings independently from deposition conditions. This could be associated with the tribooxidation of Fe-W alloys at the early stages of fretting test, as it was noticed earlier [1]. Abrasive particles –iron oxides, may act as the third body particles that slide against the hard corundum counter body and result in high values of COF. These particles form independently on the deposition conditions applied, apparently, due to the direct contact of Fe-W coatings with the ambient air, which contains the molecules of water and oxygen.
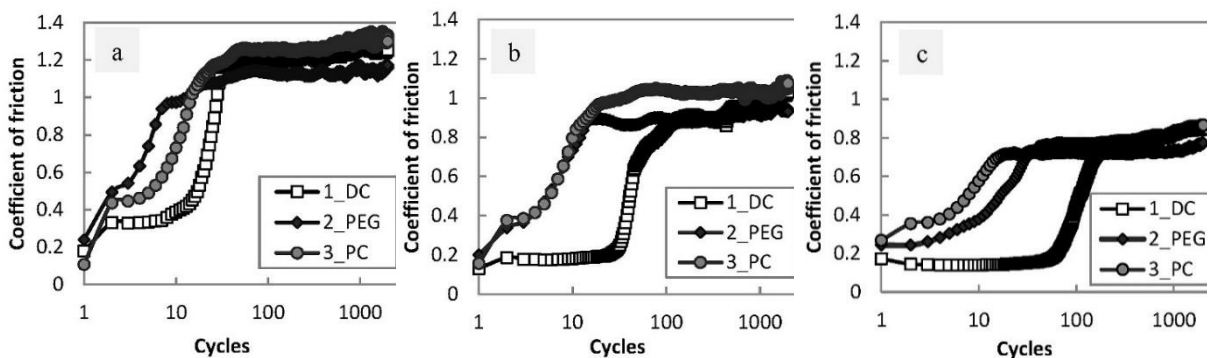

Figure 3. Evolution of COF of Fe-W samples at dry friction under applied loads: 1 N (a), 2 N (b), 5 N (c).
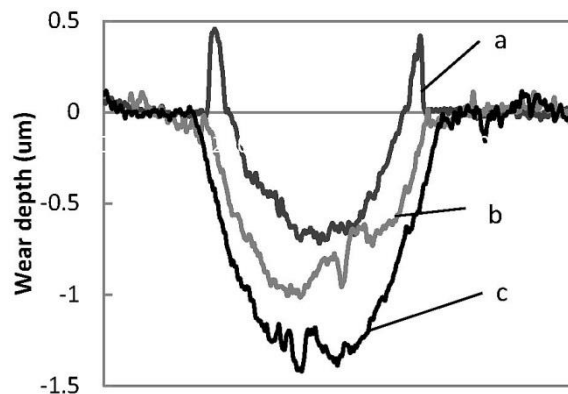
Figure 4. Depth profiles of wear tracks of Fe-W alloys (sample 1_DC) after dry friction at 1 N (a), 2 N (b) and 5 N (c).

In order to understand the nature of wear mechanism involved, the wear tracks were examined by 2D profilometer, SEM and EDS analysis after 2 000 fretting cycles performed at different loads. Depth profiles presented in Fig. 4 show that despite the COF was decreasing with increase of the applied load, the severe wear propagation was noticed at higher loads. The lowest COF and maximum wear depth of ~1.4 μm were obtained at 5 N load. The profiles of Fe-W worn surfaces are rather sharp, denoting the abrasive type of wear.
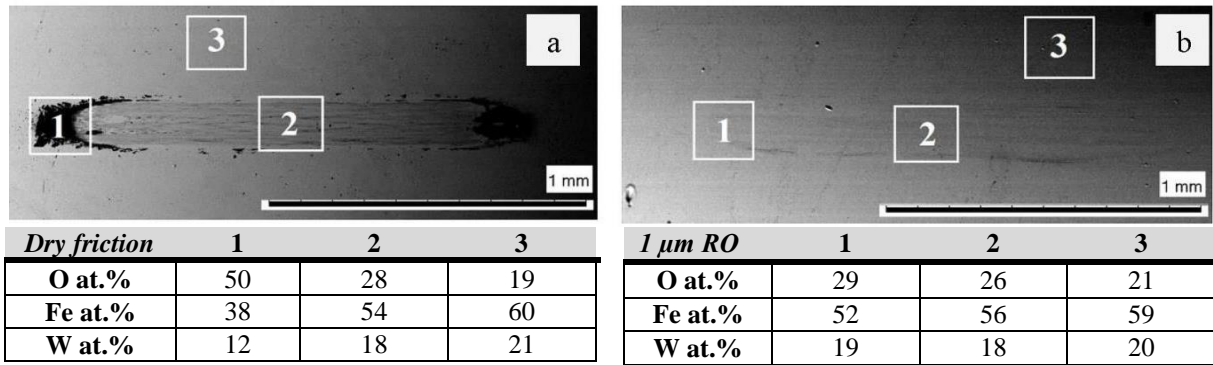
SEM images (Fig. 5) are attesting the results discussed above on COF and the important role of third body particles on tribological behavior of Fe-W coatings. When sliding against the hard corundum counter body, these abrasive particles leave deep grooves, which eventually increase the wear volume. Indeed, freshly formed debris are agglomerated in piles at low loads and distributed on the surface of the wear track. Thus, resulting asperities lead to a high COF (up to 1.2) at these conditions (Fig. 5 a, b). While at higher loads, abrasive particles could be incorporated inside the wear track therefore reducing the COF, but causing cracks propagation (Fig. 5 c). The diminishing of cracks propagation was noticed while using PEG for Fe-W deposition (Fig. 5 d). However, for the investigated system, pulse deposition mode did not improve the tribological behavior (Fig. 5 e), in the contrary to Co-W alloys [19], probably due to the corrosion processes occurring during the pause.
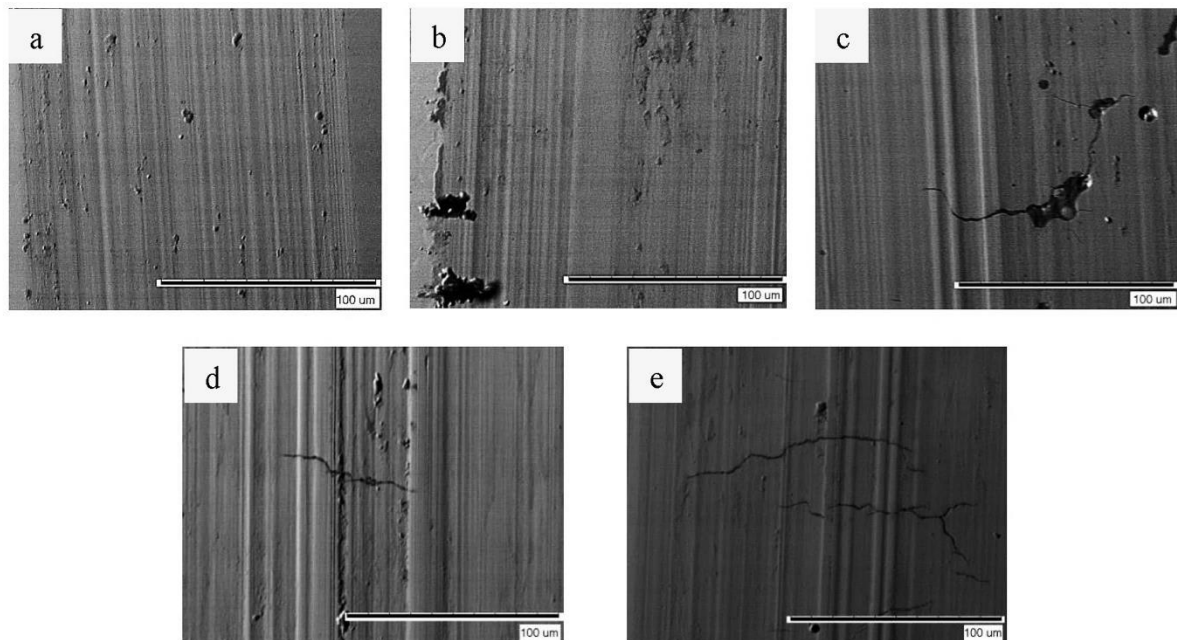
Figure 5. SEM images of wear tracks on Fe-W alloys at dry friction applied on sample 1_DC: 1 N (a), 2 N (b) and 5 N (c); and sample 2_PEG (d) and sample 3_PC (e) tested both at 5 N load.

It is noticeably seen from SEM images that some of wear particles remain adhered to the surface even after cleaning. Therefore, we could suggest that the wear mechanism of Fe-W alloys at dry friction can be ascribed to a combination of abrasive and adhesive wear.

In order to clarify the chemical content of the debris and confirm whether the high wear is caused by the tribooxidation or not, the EDS analysis on three different areas was performed (Fig. 6). Chemical analysis shows that the oxygen content in debris is increased up to 50 at.% after dry friction, which corresponds to the atomic fraction of oxygen in the mixed iron oxide Fe_3O_4 (Fig. 6 a). The oxygen content is also increased inside the wear track, due to the presence of adhered oxide particles. Moreover, the clear brown particles were observed on the surface of Fe-W samples after the fretting, thus attesting that tribooxidation under dry friction is indeed the driving factor which influence on the wear propagation.

Dry friction	1	2	3
O at.%	50	28	19
Fe at.%	38	54	60
W at.%	12	18	21

1 μm RO	1	2	3
O at.%	29	26	21
Fe at.%	52	56	59
W at.%	19	18	20

Figure 6. SEM images and EDS analysis of wear tracks on sample 1_DC after fretting test at 2 N: dry friction (a); in the presence of 1 μm rapeseed oil (b); 1, 2 and 3 denote corresponding EDS analyzed zones.

In order to diminish the Fe-W tribooxidation the surface was covered with thin film of the lubricant. Previously, the reduction of Fe-W tribooxidation was achieved by using the M-10 G2K engine oil [20]. In this study, the rapeseed oil was used as a lubricant in order to increase the environment sustainability of the process.
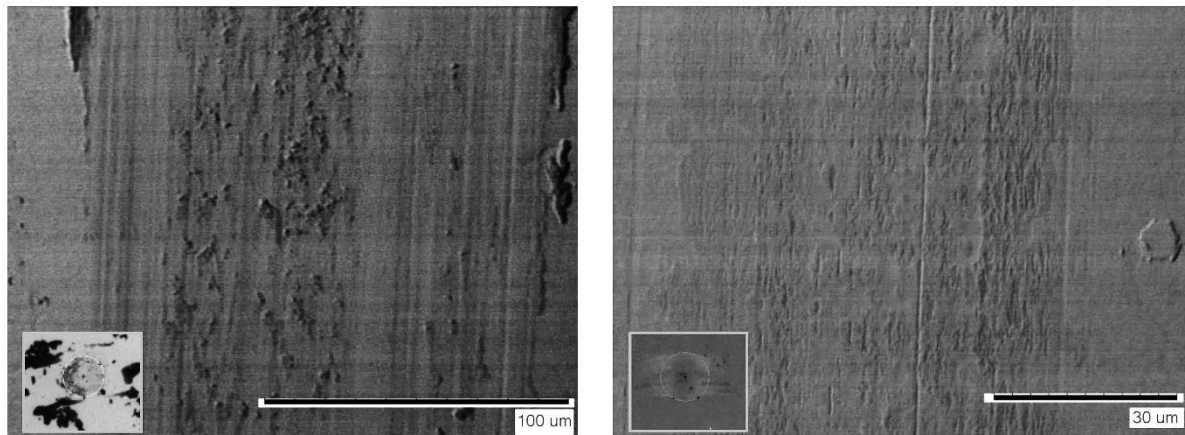
Figure 7. SEM images of the wear track after 2 N applied on Fe-25W sample after dry friction (a) and in the presence of 1 μm thick layer of rapeseed oil (b). In insert is the microscopic image of the corundum ball after the test.

Indeed, EDS analysis of the wear track on the sample 1_DC under lubricated conditions showed only slight increase in the oxygen content, while after dry friction it was increased more than 2 times on the edges (Fig. 6 b). The use of lubricant significantly reduces the contact of the Fe-W surface with aggressive medium, i.e. ambient air, which in fact is of special importance for Fe-based alloys. Due to substantial lowering of tribooxidation, the wear depth decreases significantly in comparison to dry friction and the surface becomes only slightly "polished" (Fig. 7). It was reported [15] that the oxidation can occur even when the oil film is applied, but in significantly smaller extent. Thus, no oxide particles neither adhered at the worn surface nor on the counter body were observed, while the average roughness after the test with the rapeseed oil was comparable to the roughness of as-deposited alloy. Therefore, it could be proposed that the wear mechanism changes from adhesive-abrasive at dry friction to abrasive under lubricating conditions, where produced fretting debris acts as an "in-situ" polishing agent.

In order to estimate the minimum thickness of rapeseed oil that should be applied on Fe-W coatings, the interval from 0.2 to 5.0 μm was evaluated. Obviously, the values of COF will decrease in the presence of lubricating films. Under lubricating conditions, the COF has been reduced by approximately five times for Fe-W coatings covered with rapeseed oil films on top compared to the dry friction conditions (Fig. 8). The minimal thickness of oil film when COF begins to decrease is 0.2 μm, but it could not withstand more than 50 cycles and therefore, 0.5 μm should be applied in order to retain the experiment for 2 000 cycles (Fig. 8 a). Moreover, the optimal thickness of rapeseed oil film
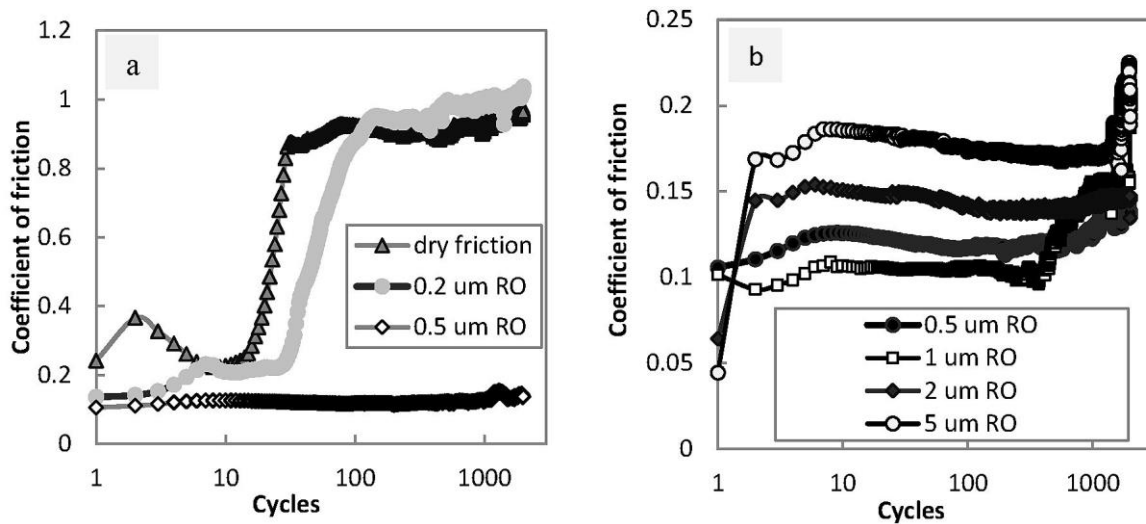
Figure 8. Evolution of the coefficient of friction at 2 N load applied on Fe-W sample 1_DC in the presence of rapeseed oil (RO) film of 0÷0.5 μm (a) and 0.5÷5.0 μm (b) thickness. Lubricating conditions are indicated on the graph.

that provides the lowest COF is 1 μm. That could be related to the better adherence of such film to the Fe-W coating and its uniform distribution on the surface, what ensure the ability of the lubricant to penetrate into the area of the wear and remain there during the test.

4. CONCLUSIONS

The wear resistance of electrodeposited Fe-W alloys having 25 at.% of W obtained under direct and pulse current modes was studied under dry and lubricating conditions using rapeseed oil. It has been shown that high COF obtained under dry friction can be linked to the combination of abrasive and adhesive wear. Abrasive particles are generated during early stages of sliding as a result of Fe-W tribooxidation.

The tribooxidation has been revealed to be the driving factor which influences on the wear propagation, which was inhibited by covering the surface with thin rapeseed oil film. Thus, the coefficient of friction was reduced by ten times from ~1.0 at dry friction to ~ 0.1, when the surface was covered with rapeseed oil film. It has been shown, that the optimum film thickness of rapeseed oil that has satisfactory adhesion to the surface and could withstand up to 2 000 cycles was 1 μm.

The roughness of the wear track after friction under lubricated conditions was found to be at the range of the initial surface roughness and no adhered particles on the worn surface were observed. Hence, the wear mechanism changes from adhesive-abrasive at dry friction to abrasive under lubricating conditions.

Taking into account the green and sustainable origin of produced Fe-W coatings they could be considered for engineering applications, where lubricating conditions can be applied. Particularly, the rapeseed oil can be used as a lubricant increasing the sustainability of the process.

ACKNOWLEDGMENTS

REFERENCES

[1] Z.I. Bobanova, A.I. Dikusar, H. Cesiulis, J.-P. Celis, N.I. Tsyntsaru, I. Prosycevas, Micromechanical and tribological properties of nanocrystalline coatings of iron-tungsten alloys electrodeposited from citrate-ammonia

solutions, Russ. J. Electrochem. 45 (2009) 895–901. doi:10.1134/S1023193509080096.

[2] K.R. Sriraman, S. Ganesh Sundara Raman, S.K. Seshadri, Corrosion behaviour of electrodeposited nanocrystalline Ni-W and Ni-Fe-W alloys, Mater. Sci. Eng. A. 460–461 (2007) 39–45. doi:10.1016/j.msea.2007.02.055.

[3] N. Tsyntsaru, A. Dikusar, H. Cesiulis, J.P. Celis, Z. Bobanova, S. Sidel'Nikova, S. Belevskii, Y. Yapontseva, O. Bersirova, V. Kublanovskii, Tribological and corrosive characteristics of electrochemical coatings based on cobalt and iron superalloys, Powder Metall. Met. Ceram. 48 (2009) 419–428. doi:10.1007/s11106-009-9150-7.

[4] N. Tsyntsaru, J. Bobanova, X. Ye, H. Cesiulis, A. Dikusar, I. Prosycevas, J.P. Celis, Iron-tungsten alloys electrodeposited under direct current from citrate-ammonia plating baths, Surf. Coatings Technol. 203 (2009) 3136–3141. doi:10.1016/j.surfcoat.2009.03.041.

[5] S.E. Fosdick, S.P. Berglund, C.B. Mullins, R.M. Crooks, Evaluating electrocatalysts for the hydrogen evolution reaction using bipolar electrode arrays: Bi- and trimetallic combinations of Co, Fe, Ni, Mo, and W, ACS Catal. 4 (2014) 1332–1339. doi:10.1021/cs500168t.

[6] A. Bodaghi, J. Hosseini, Corrosion resistance and electrocatalytic properties of Co−W alloy coatings, Surf. Eng. 28 (2012) 632–635. doi:10.1179/1743294412Y.0000000024.

[7] H. Wang, Z. Qu, S. Dong, H. Xie, C. Tang, Superior Performance of Fe$_{1-x}$W$_x$O$_\delta$ for the Selective Catalytic Reduction of NO$_x$ with NH$_3$: Interaction between Fe and W, Environ. Sci. Technol. (2016) acs.est.6b03589. doi:10.1021/acs.est.6b03589.

[8] N. Tsyntsaru, G. Kaziukaitis, C. Yang, H. Cesiulis, H.G.G. Philipsen, M. Lelis, J.P. Celis, Co-W nanocrystalline electrodeposits as barrier for interconnects, J. Solid State Electrochem. 18 (2014) 3057–3064. doi:10.1007/s10008-014-2488-x.

[9] C. Su, M. Ye, L. Zhon, J. Hou, J. Li, J. Guo, Oxidation of Fe−W alloy electrodeposits for application to anodes as lithium ion batteries, Surf. Rev. Lett. 23 (2016) 1550100. doi:10.1142/S0218625X15501000.

[10] A. Nicolenco, N. Tsyntsaru, J. Fornell, E. Pellicer, J. Reklaitis, D. Baltrunas, H. Cesiulis, J. Sort, Mapping of magnetic and mechanical properties of Fe-W alloys electrodeposited from Fe(III)-based glycolate-citrate bath, Mater. Des. 139 (2018) 429–438. doi:10.1016/j.matdes.2017.11.011.

[11] K.R. Sriraman, S.G. Sundara Raman, S.K. Seshadri, Synthesis and evaluation of hardness and sliding wear resistance of electrodeposited nanocrystalline Ni-W alloys, Mater. Sci. Eng. A. 418 (2006) 303–311. doi:10.1016/j.msea.2005.11.046.

[12] D.H. Jeong, U. Erb, K.T. Aust, G. Palumbo, The relationship between hardness and abrasive wear resistance of electrodeposited nanocrystalline Ni-P coatings, Scr. Mater. 48 (2003) 1067–1072. doi:10.1016/S1359-6462(02)00633-4.

[13] A. Leyland, A. Matthews, On the significance of the H/E ratio in wear control: A nanocomposite coating approach to optimised tribological behaviour, Wear. 246 (2000) 1–11. doi:10.1016/S0043-1648(00)00488-9.

[14] N.I. Tsyntsaru, Z.I. Bobanova, D.M. Kroitoru, V.F. Cheban, G.I. Poshtaru, A.I. Dikusar, Effect of a Multilayer Structure and Lubrication on the Tribological Properties of Coatings of Fe-W Alloys, Surf. Eng. Appl. Electrochem. 46 (2010) 538–546. doi:10.3103/S1068375510060025.

[15] N. Tsyntsaru, Tribological Behaviour of Co-W Under Dry and Lubricating Conditions, Proc. 8th Int. Sci. Conf. "BALTTRIB 2015." (2015). doi:10.15544/balttrib.2015.15.

[16] E. García-Lecina, I. García-Urrutia, J.A. Díez, J. Fornell, E. Pellicer, J. Sort, Codeposition of inorganic fullerene-like WS2 nanoparticles in an electrodeposited nickel matrix under the influence of ultrasonic agitation, Electrochim. Acta. 114 (2013) 859–867. doi:10.1016/j.electacta.2013.04.088.

[17] K.S. Brajendra, B. Girma, Environmentally Friendly and Biobased Lubricants, Boca Raton: CRC Press, Taylor & Francis Group. UK, 2017.

[18] A. Nicolenco, N. Tsyntsaru, H. Cesiulis, Fe (III)-based ammonia-free bath from electrodeposition of Fe-W alloys, J. Electrochem. Soc. 164(9), D1 (2017) D590–D596. doi:10.1149/2.1001709jes.

[19] N. Tsyntsaru, S. Belevsky, a. Dikusar, J.-P. Celis, Tribological behaviour of electrodeposited cobalt–tungsten coatings: dependence on current parameters, Trans. Inst. Met. Finish. 86 (2008) 301–307. doi:10.1179/174591908X371131.

[20] N.I. Tsyntsaru, Z.I. Bobanova, D.M. Kroitoru, V.F. Cheban, G.I. Poshtaru, A.I. Dikusar, Effect of a Multilayer Structure and Lubrication on the Tribological Properties of Coatings of Fe-W Alloys, Surf. Eng. Appl. Electrochem. 46 (2010) 538–546. doi:10.3103/S1068375510060025.